# Sustainable Synthesis of Two-Dimensional Materials via Liquid Phase Exfoliation: Graphene and Beyond

Kai Ling Ng

Linacre College

University of Oxford

A thesis submitted for the degree of

*Doctor of Philosophy*

Michaelmas 2023

# Acknowledgements

I commence this acknowledgment with profound gratitude towards my supervisor, Prof. Nicole Grobert, and my co-supervisor, Dr Barbara Maciejewska, who not only granted me the privilege to involve in this interesting research project but also provided support, motivation, and guidance throughout my doctoral journey. I extend my appreciation to Dr Maciejewska for her invaluable guidance in the characterisation of 2D materials at the onset of this project, and also her help in the XPS analysis of graphene.

Beyond my esteemed supervisors, I extend heartfelt thanks to the members of the Nanomaterials by Design (NbD) group, who not only supported my research endeavours but also became a source of camaraderie. Special gratitude to my batch mates, Dillon, John, and Eoin, for evolving and "growing" together within the NbD group. I am indebted to Ruth, Koen, Shiling, Ping-Yuan, Nayantara, Tongshan, Bianca, George, Ryan, and the entire NbD group for their steadfast support and insightful discussions. A particular acknowledgment to Maya Landis for her expertise in chemistry and assistance with the preliminary NMR characterisations of my solvent samples. I would also like to thank Alex Xu Zhicheng for his help and advice on various aspects of chemistry and the number of layer calculations based on the results from Raman Spectroscopy. Profound thanks to Prof. Hazel Assender and Dr Enzo Liotti for their valuable advice on my project during our regular joint-group meeting presentation sessions.

In addition to my research colleagues, I express gratitude to individuals from other groups, including Ruining Jin, Xiaohang Cai, Justin Limkaichong, Zheng Wu, Yun Deng, Yige Sun, Marveh Forghani, Sean Zhang, Harry Potter, Sean Telford, Botao Hao, Weixin Song, Michael Metzler, Insung Han, Zhonghua Ren, Julia, Maureen, Xuefei Liang, Zeyang Geng, Indrajeet, Shengpan Zhang, Jacob Brandler, Tianyi Chen and many more, who have become cherished friends enriching my experience at Oxford.

I am thankful for the support provided by Linacre College, especially during the challenging times of the Covid-19 pandemic. My interactions with individuals from diverse academic backgrounds in the college have significantly broadened my perspectives in life. My sincere thanks are also to Linacre College Principal, Dr Nick Brown, and Senior Tutor, Dr Jane Hoverd, for fostering the college environment that I felt like home away from home.

The success of my research project owes much to the collaboration with external partners. I express my gratitude to the Henry Royce Institute for granting me the access to the KRUSS K100 Force Tensiometer equipment, a crucial asset in evaluating the surface energy of graphite powder. Special thanks to Dr Ling Qin for his assistance with shear force simulation, uncovering the key insights into the high exfoliation efficiencies of green solvents.

I extend my appreciation to members of the Oxford Materials Characterisation Service (OMCS): Dr Colin Johnston, Dr Phil Holdway, Dr Wai Man Chan, and Nicola

Flanagan for their training on the characterisation equipment and providing the characterisation services. I am particularly grateful to Nicola Flanagan for her patience during AFM training sessions and to Dr Colin Johnston for managing equipment access and training, especially during the challenging period of the Covid-19 pandemic. Thanks also to the department administrative staffs: Samantha Pearce, Sharmaine Ijada, and Lorraine Laird for their support and care. Special thanks to Greg Cook and Richard Turner for technical support, and the casual chat and jokes that help in alleviating my work stress.

Lastly, I extend heartfelt thanks to my parents and sister for being the pillars of motivation, encouragement, and support throughout my challenging Ph.D. journey. A special acknowledgment to my father for proofreading my thesis.

While I may inadvertently overlook names in this acknowledgement, my sincere gratitude extends to all who contributed to my research life at Oxford.

# Abstract

The discovery of graphene, a single layer of graphite, is a game changer that has revolutionised the field of materials science due to the superior properties it owns; ranging from high electrical conductivity, high mechanical strength to large surface area. All these attributes make graphene a promising material for diverse applications in flexible electronic and photonic devices, as well as concrete additives and renewable energy technologies. While the prospects of graphene seem boundless, the challenges for increasing its yield and lowering its production costs persist. These limit its widespread industrial applications. Furthermore, the synthesis processes of graphene often involve the use of toxic chemicals, calling for sustainability concerns. Hence, there is a critical need for the search of a scalable, efficient, and sustainable graphene production method.

Liquid Phase Exfoliation (LPE) synthesis technique emerges as a cost-effective approach, producing graphene dispersions compatible to electronic device printing technologies. However, the reliance on toxic solvent like 1-Methyl-2-pyrrolidinone (NMP) in the LPE processes hampers the progress of LPE. Despite the efforts to replace NMP with greener alternatives like ethanol and isopropanol, graphene yield remains significantly lower than that in NMP. The main advantage of using green solvents with low boiling points and low toxicity, is that they can be easily removed by low temperature evaporation without degrading the graphene quality. The commonly used methods to enhance the graphene yields in green solvents often involve functionalisation of graphene and the use of chemical surfactants/dispersants. These processes degrade graphene quality and require additional treatment steps to remove the surfactants/dispersants.

The present work focuses on the shear mixing technique, one of the LPE techniques used in graphene production. The potential of using green solvents to replace the currently state-of-art NMP is addressed. The main problem associated with low graphene yields in green solvents has been identified and revealed, for the first time, by the NMP-redispersion technique. Subsequently, a pioneering yield enhancement method was developed. This method can achieve a remarkable 90-fold increase in graphene yield, negating the use of dispersants, surfactants, and functionalisation. The efficacy of this technique extends beyond graphene, as may be evident from its ability to enhance the yield of hexagonal Boron Nitride (a layered material sharing the same hexagonal lattice structure as graphite). Each of the experimental chapters unfolds the new dimensions and research insights into the scalability, efficiency, and sustainability of graphene production and of other two-dimensional materials.

# Publications and Conferences

## Peer-Reviewed Publication

Kai Ling Ng, Barbara M Maciejewska, Ling Qin, Colin Johnston, Jesus Barrio, Maria-Magdalena Titirici, Iakovos Tzanakis, Dmitry G Eskin, Kyriakos Porfyrakis, Jiawei Mi, and Nicole Grobert, *"Direct Evidence of the Exfoliation Efficiency and Graphene Dispersibility of Green Solvents toward Sustainable Graphene Production"*, ACS Sustainable Chemistry and Engineering, 2022, 11 (1), pp 58-66. DOI: 10.1021/acssuschemeng.2c03594. (the work was selected to be highlighted as the journal cover image)

*The content of this publication is partly reproduced in Chapter 2.

## Conferences

- Kai Ling Ng, "*Sustainable Productions of High-Yield and High-Quality Graphene in Green Solvents",* Royce Student Summit organised and sponsored by Henry Royce Institute (2022)

- Kai Ling Ng, B. M. Maciejewska, L. Qin, I. Tzanakis, D. G. Eskin, K. Porfyrakis, J. Mi, N. Grobert, "*New Routes to Assessing and Enhancing the Yield of Hexagonal Boron Nitride using Sustainable Liquid Phase Exfoliation",* MRS Fall Meeting 2021.

- Kai Ling Ng, B. M. Maciejewska, L. Qin, Z. Xu, D. McGurty, D. G. Eskin, I. Tzanakis, K. Porfyrakis, J. Mi, N. Grobert, "*Sustainable Solvents for Graphene Production: Yield and Structural Defect Analysis*", NT21 conference (June 6-11, 2021).

# Declaration

I, Kai Ling NG, hereby affirm that the research and content presented in this thesis are the result of my own efforts. In instances where contributions have been made by others or information has been derived from external sources, their contribution has been appropriately acknowledged, and the respective sources have been duly referenced.

Signature:

Date: 1st January 2024

# Contents

# List of Abbreviations

| | |
|---|---|
| **2 US** | Two-Minute Ultrasonication |
| **2D** | Two-Dimensional |
| **Ace** | Acetone |
| **AFM** | Atomic Force Microscopy |
| **BET** | Brunauer–Emmet–Teller |
| **BNNS** | Boron Nitride Nanosheets |
| **D.I.** | Deionised Water |
| **EA** | Ethyl Acetate |
| **EtOH** | Ethanol |
| **G** | Graphite |
| **GR** | Graphene |
| **GS-R** | Green Solvent-Re-Dispersion |
| **HSP** | Hansen Solubility Parameters |
| **hBN** | Hexagonal Boron Nitride |
| **IPA** | Isopropanol |
| **LPE** | Liquid Phase Exfoliation |
| **MeOH** | Methanol |
| **$MoS_2$** | Molybdenum Disulphide |
| **NMP** | NMP-Re-Dispersion |
| **NMP-R** | N-methyl-2-pyrrolidone |
| **OWRK** | Owens–Wendt–Rabel and Kaelble |
| **PEUS** | Post-Exfoliation Ultrasonication |
| **SEM** | Scanning Electron Microscopy |
| **US** | Ultrasonication |
| **$WS_2$** | Tungsten Disulphide |
| **XPS** | X-Ray Photoelectron Spectroscopy |
| **XRD** | X-Ray Diffraction |

# List of Figures

# List of Tables

# Thesis Chapters Summary

## Chapter 1: Introduction

The basic principles and backgrounds involving in the LPE of 2D materials are discussed, with a particular emphasis on graphene production. These include the theory and background of the solubility parameters, commonly used in solvent selection in LPE. The rationales and criteria behind the selection of solvents as the "green solvents" in this work are reviewed and discussed. Towards the end of this chapter, attentions are drawn to the existing gaps and challenges faced for a sustainable production of 2D materials by LPE. The unresolved research challenges were identified as the main research focus and as my aspirations for the well-beings of mankind.

## Chapter 2: Solvent Exfoliation Efficiency and Graphene Dispersibility Studies

The design of N-Methyl-2-pyrrolidone (NMP)- redispersion technique to precisely quantify the amount of graphene produced in green solvents is reported in this chapter. This technique allows a precise determination of the graphene content in the dispersion after the exfoliation process (the exfoliation efficiency). The redispersion of NMP-exfoliated graphene into various green solvent media also serves as direct "evidence" and a reliable experimental way to assess their dispersibilities in these solvents. The redispersion technique enables the independent study of two crucial factors that influence the final graphene yield, namely, exfoliation efficiency and graphene dispersibility of green solvents.

The key insight gained from this study is: green solvents, particularly IPA, can achieve higher exfoliation efficiencies than NMP. The primary reason for low graphene yield in green solvents was attributed to their low dispersibility. This finding has led to the introduction of post-exfoliation ultrasonication (PEUS) method with the duration as short as two minutes, to enhance the graphene dispersibility and improve the yield in green solvents (Chapter 3).

## Chapter 3: Graphene Yield Enhancement by Post-Exfoliation Ultrasonication (PEUS)

This chapter covers the development of a simple PEUS method, on which a brief two-minute ultrasonication (2 US) step was imposed at room temperature after shear mixing exfoliation, aiming to enhance graphene dispersibility in green solvents. This method negates the need for functionalisation and the use of surfactants or dispersants. Interestingly, the results obtained show a 90-fold increase in the graphene concentration without compromising its quality. For this, the microstructures, morphologies and chemistry of the as-produced graphene and the dispersion stability were studied using a range of imaging and spectroscopic techniques. This newly introduced shear mixing-PEUS method resulted in high-quality leaf-like graphene flakes in green solvent with an average thickness of less than 10 layers. This establishes the potential of the method as a transformative approach for advancing graphene production and applications.

## Chapter 4: Beyond Graphene-Exfoliation of Hexagonal Boron Nitride

Building upon the success of the PEUS yield enhancement method for graphene in green solvents, this chapter covers the area of hexagonal Boron Nitride (hBN), a 2D layered material sharing the same hexagonal lattice structure as graphene. Renowned for its challenging exfoliation attributed to stronger van der Waals forces between the layers, hBN becomes the next frontier for the application of PEUS method. The yield of hBN has a remarkable enhancement of up to 12 times in IPA solvent through the application of PEUS method. Similar set of physiochemical characterisation techniques used on graphene was used to assess the properties of the hexagonal Boron Nitride Nanosheets (BNNSs) produced. The production of BNNS- graphene using the shear mixing exfoliation technique with PEUS is also discussed.

## Chapter 5: Outlook

This chapter provides an overview of the key findings from the present research, alongside with proposed areas for future exploration. The future work mentioned here are underpinned by the preliminary experimental evidence from the present work. One of the proposed future works involve the development of theoretical model for selecting the optimum solvent for each of the exfoliation and dispersion steps for 2D materials production. Other potential future works include identifying the crucial solvent parameters that influence the size and thickness of the 2D materials for bandgap tuning, designing a solvent recovery and materials recycling system for sustainable LPE process, and the development of large-scale printing based on 2D materials dispersion in green solvent for energy and flexible devices.

# 1

# Introduction

## 1.1 Overview

In this chapter, the process, background, and mechanism of LPE technique for graphene production and other 2D materials such as hexagonal Boron Nitride (hBN), Molybdenum Disulphide ($MoS_2$) and Tungsten Disulphide ($WS_2$), in the form of dispersion are discussed. Emphasizing on the background of LPE of graphene, this chapter ends with an insightful summary on the extension of LPE to cover the production of a broader spectrum of 2D materials.

The LPE process for graphene and other 2D materials production involves "peeling off" the graphite layers from a 2D material or exfoliation in a solvent medium from its bulk counterpart.[1,2] In this case, the solvent serves as both the exfoliating and stabilising media. Good solvents for LPE are those that could provide high exfoliation efficiency and dispersibility; the two crucial factors influencing the graphene yield in LPE.[3] Exfoliation efficiency refers to the effectiveness or ability of separating individual graphene layers from bulk graphite during the exfoliation process.[3,4] It quantifies the extent to which multilayered graphene structures are successfully reduced to few-layer or monolayer graphene sheets. Dispersibility, on the other hand, is the ability of the exfoliated graphene layers to remain stably suspended and well-separated in a suitable solvent, preventing re-aggregation and ensuring a uniform dispersion of the nanosheets over time.[5,6] Reviews on the graphene production through LPE mainly explores those factors affecting the graphene yield and conventional theories and challenges guiding solvent selection in LPE.[7–9] In this respect, there is generally lacks a direct and reliable method to accurately determine the quantity of the exfoliated materials produced.

Centrifugation plays a pivotal role in isolating the exfoliated 2D materials from other aggregates of bulk materials to yield the final dispersions of 2D materials. The process of centrifugation also affects the quantity and quality of the graphene produced.[10,11] Despite its importance, literatures often overlook the impacts of centrifugation conditions and parameters on the graphene's yield and quality. In this work, the theory of centrifugation is investigated on the ground that it has an important bearing on graphene production in LPE.

In a scale-up production of graphene and other 2D materials by LPE, the increase in yield of the materials produced is often achieved at the expense of its quality, by adopting commonly used yield-enhancing techniques like functionalisation, solvent-exchange and the use of surfactants or dispersants. This chapter explores these widely adopted yield enhancement techniques in more details and concludes by identifying the research gaps and challenges in the LPE to produce graphene and other 2D materials.

## 1.2 Two-Dimensional Materials: Graphene and Hexagonal Boron Nitride

Two-Dimensional (2D) materials are nanomaterials having a single dimension, their thickness, in the nanoscale range.[12] The thickness of 2D materials is typically at one- or two- atom thick.[13] There are two primary methods for producing 2D materials: bottom-up and top-down techniques.[14,15] The bottom-up approach involves constructing a 2D material layer from its molecular precursors, often using chemical vapour deposition (CVD).[16,17] In contrast, the top-down approach involves overcoming the van der Waals forces between layers to exfoliate or "peel off" sheets of 2D materials from the bulk material, which can be accomplished through mechanical, electrochemical, or chemical exfoliation methods.[18–20]

Compared to their bulk forms, 2D materials have a higher surface area-to-volume ratio, offering more surface area for functionalisation, sensing, and chemical reactions. This characteristic is advantageous for various applications, such as catalysis and sensors.[21,22] The bottom-up technique allows for precise control over the number of layers, making it possible to synthesize materials close to a monolayer. Despite of yielding 2D materials with controlled thickness and near-monolayer uniformity, bottom-up technique often come at the cost of lower yields and higher production costs. On the other hand, top-down synthesis is more cost-effective and produces 2D materials at a higher yield, but controlling the quality of the material can be challenging. The quality of 2D materials is assessed based on attributes such as lateral size, thickness, defect types, defect density, and oxidation level, all of which are selected depending on the intended application.[23–25]

In this thesis, two types of 2D materials are discussed: graphene and hexagonal Boron Nitride Nanosheets (BNNSs).

### 1.2.1 Graphene

Graphene is a 2D material composed of a single layer of carbon atoms arranged in a hexagonal, honeycomb-like lattice.[26] Each carbon atom in graphene forms three $sp^2$ hybridised orbitals, creating strong sigma (σ) bonds, and a π-bond that is delocalised across the entire graphene sheet. This unique structure gives graphene its remarkable properties. However, in practical applications, the top-down production approach often results in the creation of few-layer graphene (FLG) rather than monolayer or bilayer graphene.[27] FLG consists of stacked graphene layers ranging from two to ten layers, as defined by ISO/TS 80004–13:2017.[28] FLG are usually stacked in Bernal (AB) or Rhombohedral (ABC) stacking orders Figure 1.1a.[29] While FLG retains many of the advantageous properties of monolayer graphene, the increase in thickness affects its overall surface area, which, in turn, influences its chemical and catalytic properties.[30,31] Additionally, the transition from monolayer graphene to FLG leads to changes in its electronic structure, particularly in the bandgap and the mobility of charge carriers, such as electrons and holes.[32,33]

Monolayer graphene exhibits a linear dispersion of its electronic band structure around the Dirac cone, meaning that the energy of the electrons varies linearly with their momentum.[34–36] This linear relationship results in a very low effective mass for the electrons, leading to exceptionally high electron mobility. However, as the number of layers increases in FLG, the band structure begins to bend (Figure 1.1b),[37] causing a reduction in electron mobility and, consequently, a change in its optical and electronic properties. Hence, controlling the number of layers is critical for electronic and optoelectronic applications.

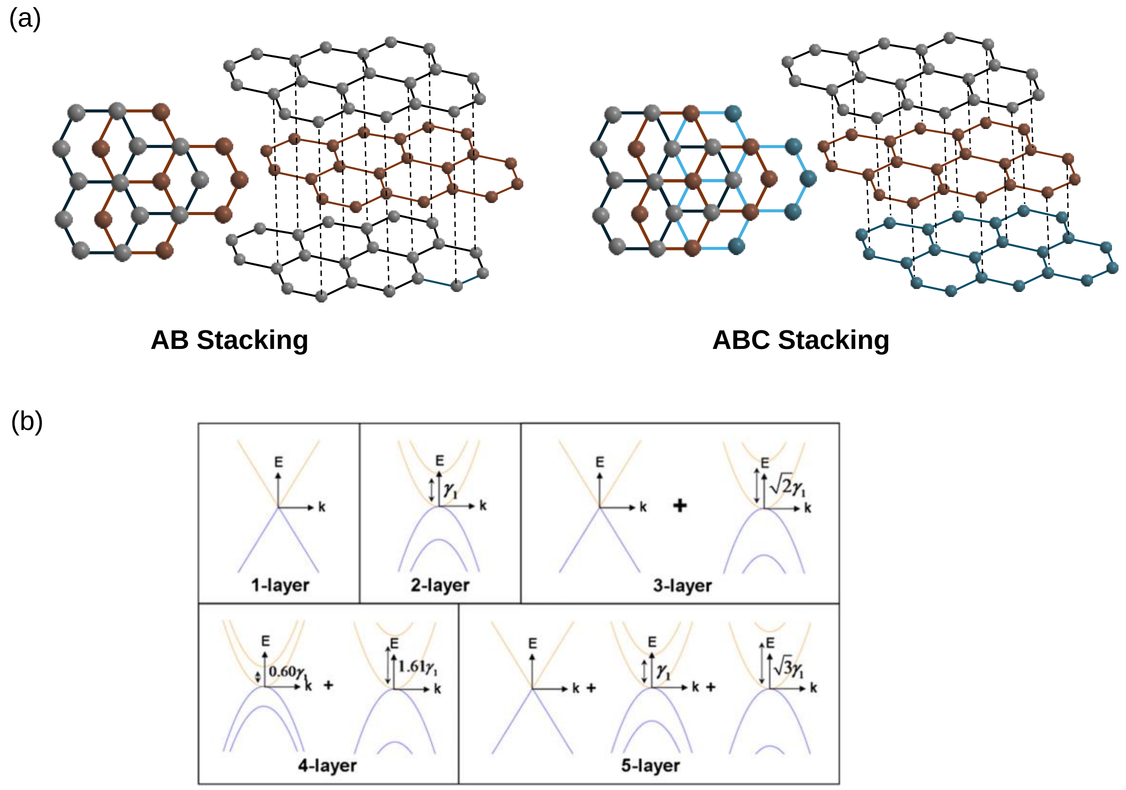

**Figure 1.1:** (a) The possible stacking orders of graphene layers. (b) Schematic diagram showing the bending of the band structure to hyperbolic bands near the Dirac cone as the number of layers increases beyond a single layer, deviating from linear dispersing band. Adapted from Mak K. F. et al. (2010) "The evolution of electronic structure in few-layer graphene revealed by optical spectroscopy." *PNAS,* 107 (34), 15002. © 2010 National Academy of Sciences.

The synthesis of graphene varies depending on the specific application requirements. Electronic and optoelectronic applications typically require graphene that is close to a monolayer due to its superior electronic and optical properties,[38–40] such as high electron mobility and transparency. In contrast, for applications like catalysis and energy storage, FLG is often sufficient.[41,42] FLG offers a good balance between performance and cost, as it retains many of the desirable properties of monolayer graphene while being less expensive and easier to produce in higher yields.

FLG is commonly synthesized using top-down approaches, which involve exfoliating graphene layers from bulk graphite materials.[43] These methods are versatile, allowing for the use of various graphite sources for exfoliation, including carbon-based waste materials such as plant waste, food waste, and graphite electrodes from used batteries.[44] One popular top-down technique for producing FLG is Liquid Phase Exfoliation, which enables direct exfoliation of graphene in a solvent medium.[45] This process not only produces graphene at a lower cost but also allows the resulting graphene dispersion, or "graphene ink," to be readily used for coating or printing onto substrates. This makes it particularly suitable for applications in sensors, energy devices, and other areas requiring functional coatings. Further details on this synthesis technique will be discussed in Section 1.3.

### 1.2.2 Hexagonal Boron Nitride Nanosheets

Hexagonal boron nitride nanosheets (BNNSs) share a similar hexagonal lattice structure to graphene, which is why they are often referred to as "white graphene."[46,47] The layer of hexagonal boron nitride (hBN) consists of alternating boron (B) and nitrogen (N) atoms, bonded by strong sigma (σ) bonds formed through the overlap of $sp^2$ hybrid orbitals from both B and N atoms, unlike graphene, which is composed of carbon atoms. Despite this structural similarity, BNNSs exhibit significantly different electronic properties. Graphene is a zero-bandgap material and an excellent conductor, in contrast, BNNSs have a wide bandgap ranging from 5.9 to 6.1 eV,[48] making them electrically insulating. This is due to the uneven electron distribution between B and N atoms in hBN. The more electronegative nitrogen atoms attract the shared electrons more strongly, resulting in partial ionic character in the B-N bonds. Consequently, the π electrons in hBN are less delocalised compared to graphene, leading to its insulating behaviour. In addition to their insulating properties, BNNSs possess high in-plane thermal conductivity of ~ 550 $W\ m^{-1}\ K^{-1}$.[49] Figure 1.2 illustrates the different stacking orders of hBN layers and how the band structure evolves with the number of layers. The AA′ stacking order is the most observed stacking configuration in hBN.

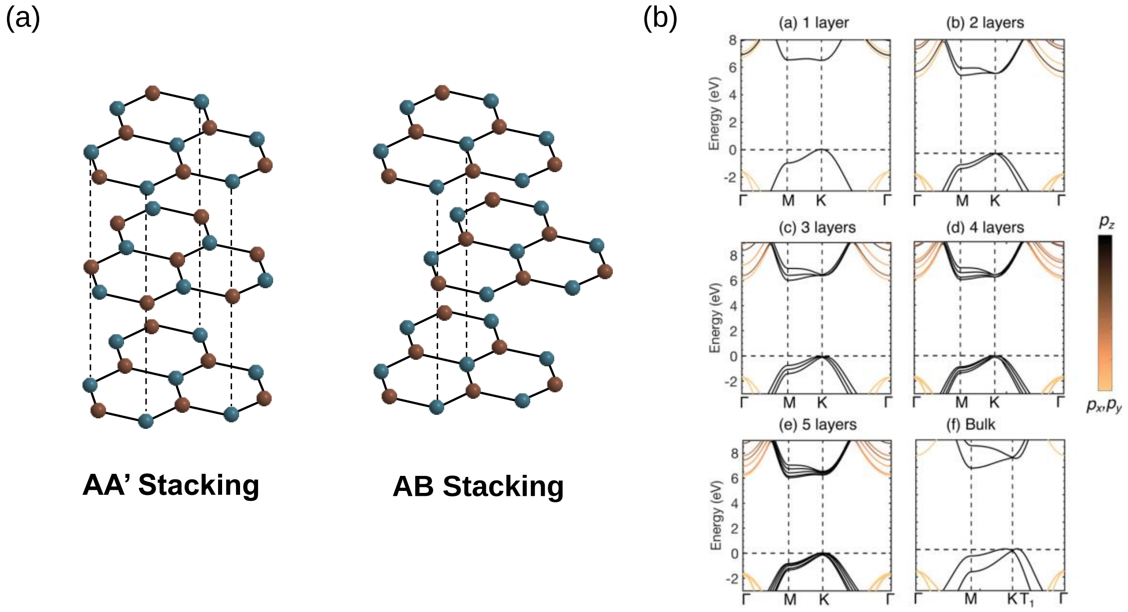

**Figure 1.2:** (a) Stacking orders of hBN. Red and blue represent Boron and Nitrogen atoms, respectively. (b) Evolution of the hBN band structure in AA' stacking as a function of the number of layers. Adapted with permission from Wickramaratne, D. et al. (2018), "Monolayer to Bulk Properties of Hexagonal Boron Nitride," *The Journal of Physical Chemistry C*, 122(44), 25525. © 2018 American Chemical Society.

The synthesis of BNNSs can be achieved using methods similar to those employed for graphene. Bottom-up techniques, such as CVD,[50] allow for the controlled growth of BNNSs, while top-down approaches, including exfoliation, involve peeling off layers from bulk hBN.[51] Functionalisation can assist in weakening the van der Waals forces between layers, facilitating exfoliation. However, due to the chemical inertness of BNNSs, functionalisation is challenging.[52,53] To aid exfoliation, high temperatures and pressures are often required.[54,55] Besides this, the chemical inertness and electrical insulating properties of BNNSs make them unsuitable for chemical and electrochemical exfoliation methods.[56] Currently, there is still a lack of cost-effective and high-yield production methods for BNNSs.

Despite these challenges in synthesis, BNNSs have promising applications due to their tunable bandgap, high thermal stability, and excellent dielectric properties. These characteristics make them suitable for use in optoelectronic devices, sensors, fillers for thermal interface materials, photocatalysis, heterogeneous catalysis and thermal management systems.[57–61]

As the importance of achieving net-zero emissions and advancing decarbonisation grows, 2D materials such as graphene and BNNSs are finding applications in energy storage and conversion devices, including batteries, supercapacitors, and fuel cells, where they enhance performance. However, the widespread adoption of these materials in large-scale manufacturing has been limited by high production costs. Consequently, there is a critical need for sustainable and cost-effective methods to produce high-quality 2D materials, optimising the balance between performance and production cost. By improving the efficiency and sustainability of these production techniques, 2D materials could play a significant role in the global transition to a low-carbon economy.

## 1.3 Liquid Phase Exfoliation (LPE)

The common methods for graphene synthesis are LPE, Chemical Vapour Deposition (CVD) and electrochemical techniques.[62–64] CVD is a bottom-up synthesis technique which is well-known for its ability to produce high-quality monolayer graphene on a catalyst substrate under well-controlled temperature and gas pressure. Frequently used substrates for CVD synthesis of graphene include polycrystalline nickel and copper.[65,66] On-going investigations focus on understanding how substrate type and crystallinity impact the resulting graphene quality.[67–69]

On the contrary, LPE is a mechanical and top-down approach for graphene synthesis. LPE yields graphene in the form of dispersion and is compatible to the printing and coating technologies like, roll-to-roll printing. Unlike CVD, where the graphene layer is grown and supported on a solid substrate, graphene produced by LPE is suspended or dispersed in liquid phase. This inevitably leads to some restacking of exfoliated graphene in the solvent medium. Consequently, achieving the synthesis of a few-layer graphene becomes challenging in LPE. Moreover, the use of toxic and high-boiling-point solvents, such as NMP and Dimethylformamide (DMF), presents a notable drawback.[70] This would require the search for alternative green solvents and surfactants. It is also necessary to have an in-depth understanding of the mechanism involved in LPE for graphene production. Figure 1.3 shows the comparisons of the advantages and limitations of CVD and LPE techniques in graphene production. There are two main techniques in LPE, which are ultrasonication and shear mixing. Ultrasonication, while widely employed, is hindered by the challenges in controlling the quality and morphology of the resultant graphene.[71] Probe sonication, in particular, is associated with elevated defect generation due to the substantial cavitation bubbles and the shock waves produced, creating localised "hot spots."[72] Addressing these issues is vital for advancing the effectiveness and scalability of the graphene synthesis.

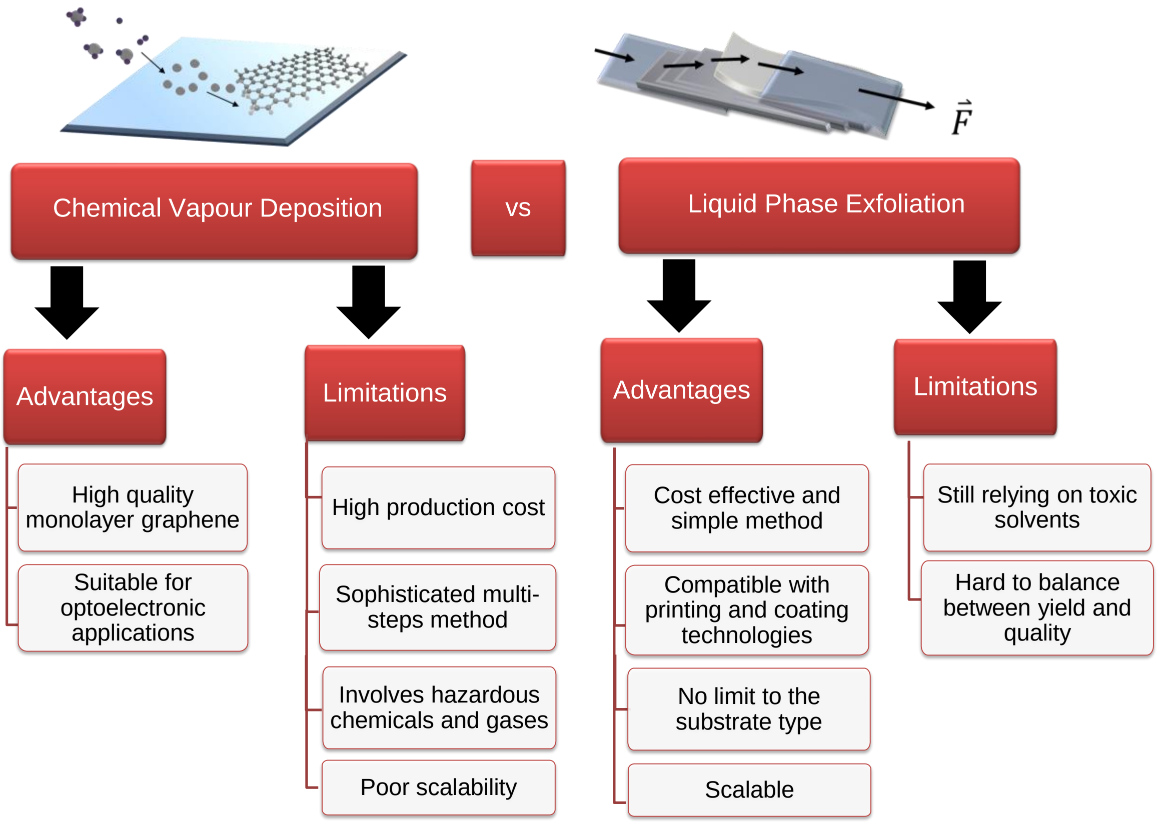

**Figure 1.3:** Comparison between the advantages and limitations of chemical vapour deposition (CVD) and liquid phase exfoliation (LPE).

Shear mixing technique was investigated as a potential alternative to ultrasonication within the framework of LPE.[45,73,74] Shear mixing in LPE is more viable for large-scale synthesis of graphene based-materials due to the ease of scalability.[75] This claim was supported by comprehensive studies conducted by Paton et al. in 2014,[76] elucidating the scalability of shear mixing in the synthesis of graphene with minimal defects. A scaling-up model that relates and estimates the exfoliated graphene concentrations with processing parameters has been established and experimentally tested.[45] Given its demonstrated efficacy and scalability, this synthesis technique is the selected technique in this work and will be discussed in more details in the subsequent sections.

In graphene synthesis using LPE, various experimental factors play a crucial role in determining its quality and quantity. These factors can be classified into different categories based on the solvent type, graphite source, and operating conditions employed. [62,77] In this section, these factors are discussed, emphasizing on graphene-solvent interaction by considering the solubility parameters or surface tension for both the solvent and graphene. The graphene produced is typically evaluated based on the number of graphene layers, presence of crystal defects and occurrence of oxygen-containing species. A key guideline for achieving high concentration or yield of graphene in LPE is to select a solvent with surface tension, as close as possible, to the surface energy of the graphene.[78, 79] This choice aims to minimise the enthalpy of mixing, $\Delta\overline{H}_{mix}$ to reduce and achieve negative Gibbs free energy of mixing, $\Delta\overline{G}_{mix}$ for a more feasible dispersion of graphene in solvent, leading to high graphene yield.[80, 81] Gibbs free energy of mixing, $\Delta\overline{G}_{mix}$ is given by the following equation formulated by Gibbs, J. W.:[82]

$$\Delta\overline{G}_{mix} = \Delta\overline{H}_{mix} - T\Delta\overline{S}_{mix} \tag{1.1}$$

Where $\Delta\overline{G}_{mix}$, $\Delta\overline{H}_{mix}$ and $\overline{S}_{mix}$ are the free energy, enthalpy, entropy and volume of the mixing, respectively. $T$ is the absolute temperature.

Entropy represents the randomness or disorder of a system.[83] In the case of graphene, which is a rigid, flat 2D material with limited configurational freedom, the entropy contribution is minimal.[84] The temperature term indicates the significance of entropy effect at higher temperature. However, the exfoliation and dispersion processes are normally carried out at room temperature where entropy, $\overline{S}_{mix}$ has negligible impact.

Enthalpy of mixing, $\Delta\overline{H}_{mix}$ which plays critical role in achieving efficient dispersion of graphene is given by the equation below:[85]

$$\frac{\Delta\overline{H}_{mix}}{V_{mix}} \approx \frac{2}{t_{flake}}(\delta_G - \delta_{sol})^2 \Phi \qquad 1.2$$

Where $V_{mix}$, $t_{flake}$ and $\Phi$ are the volume of the mixing, the flake thickness and the volume fraction of dispersed graphene, respectively. Surface energy of graphene and surface tension of solution is represented by $\delta_G$ and $\delta_{sol}$, respectively.

The equation indicates to minimise $\Delta\overline{H}_{mix}$, $\delta_G$ and $\delta_{sol}$ should be as close matched as possible. This concept can also be applied to the exfoliation of other 2D materials.

## 1.3.1 Experimental Approaches for LPE

Shear mixing is a mechanical exfoliation technique that utilises mainly the high shear forces to "peel off" layers of a 2D material from its bulk counterpart. This method applies mechanical stress, typically through rotating blades, to overcome the van der Waals forces holding the layers together.[45,86] In ultrasonication, the energy needed to separate graphene layers from graphite and overcome the interlayer van der Waals forces comes from the collapse of cavitation bubbles and the resulted shock wave that generated in the solvent.[87,88] In the context of LPE for both ultrasonication and shear mixing, the solvent medium assist in separating the layers or exfoliation and providing a stabilising environment for the exfoliated material. The efficacy of exfoliation relies on the solvent's properties, particularly, the viscosity and surface tension. Surface tension of a solvent determines the enthalpy of mixing and efficiency of graphene production, as can be evident from Equation 1.2. This holds true regardless of the exfoliation technique employed, whether it is shear mixing or ultrasonication. However, the impact of viscosity on exfoliation efficiency depends on the exfoliation technique used and the exfoliation mechanism involved. In the case of shear mixing, the exfoliation efficiency increases with solvent viscosity at a fixed shear rate.[89] Conversely, for ultrasonication, lower solvent viscosity impedes the generation and subsequent collapse of cavitation bubbles. Consequently, this hindrance leads to a reduction in exfoliation efficiency under such applied conditions.[90]

Theoretically, exfoliating graphite with larger lateral sizes would incur a higher energy cost than that of smaller lateral sizes. [91,92]As a result, the process of "scission" or breaking up graphite flakes into smaller sizes occurs before exfoliation, and the extent of size reduction would depend on the intralayer bonding energies of the graphene layers.[92,93] Smaller sizes are achieved with bulk materials exhibiting lower intralayer bonding energies. Size reduction of the scission process relies upon the intralayer bonding energies. It is worth noting that there was research finding suggesting a different scenario, in which the concentration or yield of graphene is independent on the sizes of the graphite starting materials.[94] Close examination reveals that this study involved different type of graphite (from what has been used in this work), which is the expanded graphite with weaker interlayer binding energy.

### Ultrasonication Technique

Ultrasonication stands out as the predominant technique for 2D materials synthesis. It involves dispersing, breaking down, agitating, and (in the case of layered materials) exfoliating the layers of 2D materials through the generation of vacuum bubbles induced by ultrasonic waves with a frequency exceeding 20 kHz.[95–97] This process creates alternating high- and low-pressure regions corresponding to contraction and rarefaction, respectively. Cavitation bubbles form when the hydrodynamic pressure drops below the vapour pressure of the solvent and subsequently collapse when reaching a saturation level. The growth and collapse of these cavitation bubbles generate shock waves, releasing mechanical energy that facilitates the fragmentation and exfoliation of layered materials. Additionally, the bubbles colliding with the graphite surface also contribute to shear forces, further aiding in the exfoliation of the layers.[96, 98]

There are two typical types of ultrasonication exfoliation methods; the probe sonication and bath sonication.[99, 100] Probe sonication operates by the direct insertion of an ultrasonic probe into the sample dispersion, while bath sonication involves the propagation of ultrasonic waves through a water medium to the sample dispersion in a container. Bath sonication offers the advantages of minimising sample contamination and sample loss, as in the probe sonication. While probe sonication exhibits a higher efficiency for graphene, it comes at the cost of inducing more defects in the final material produced. A choice between these two methods would involve a trade-off between exfoliation efficiency and the quality of the resulting 2D material produced.

**Shear Mixing Technique**

A standard high shear mixer is composed of a rotor and a stator with holes as illustrated in Figure 1.4. The gap between the rotor and stator (a stationary ring surrounding the moving rotor) is small, typically ranging from 0.1 to 3 mm. This minimal gap serves to induce a velocity gradient, acting as the source of shear force crucial for the exfoliation process.[101] The high shear region, situated between the rotor and stator, is the focal point where most of the exfoliation events happen. In order to meet the minimum shear rate,

$\dot{\gamma}_{min}$, essential for graphene production, a high shear rate of 20 000 – 100 000 $s^{-1}$ is generated.[76, 102] It should be noted that any mixer, including commonplace kitchen blenders capable of achieving this minimum shear rate can be used for graphene production.[103] The exfoliation mechanisms involved in shear mixing include the generation of shear force resulting from fluid velocity gradients, jet cavitation occurring when the fluid is propelled through the stator holes under high pressure differentials, random collisions between graphite particles, and the collisions of graphite particles at the edges of stator.[104]

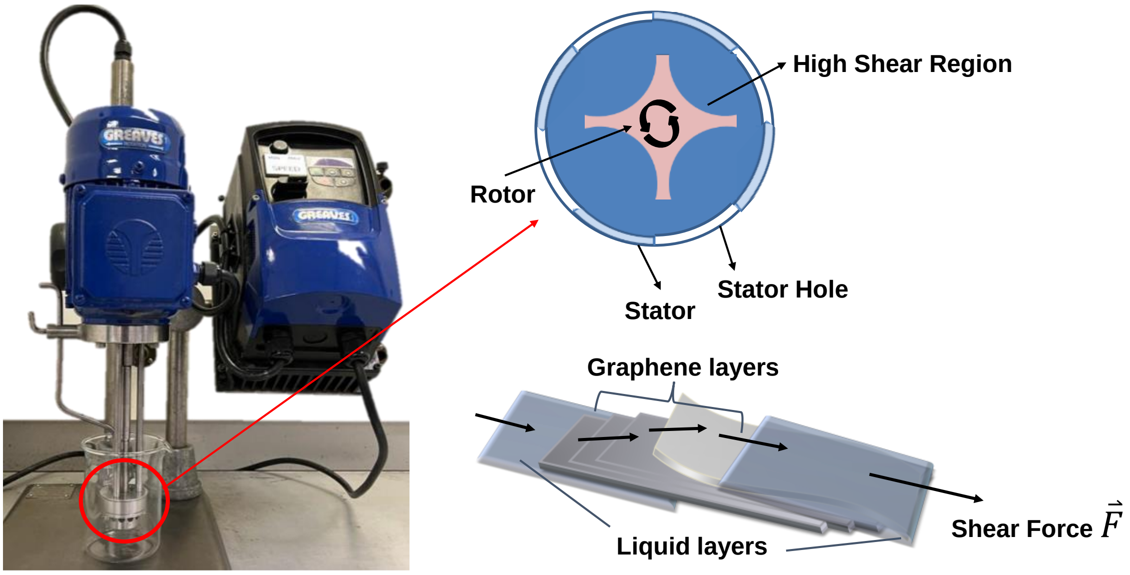

**Figure 1.4:** Lab-scale high shear mixer and the schematic depicting the rotor-stator compartment. The shear force arises from the velocity gradient within the space between the rotor and stator. This shear force causes the "sliding" of liquid layers, which facilitates the peeling-off of graphene layers from graphite.

The Reynolds number (Re) is used to distinguish between turbulent (Re > $10^4$) and laminar flow during shear mixing (Equation 1.3a).[105] Shear rate of shear mixing exfoliation, $\dot{\gamma}$, can be calculated from Equation 1.3b,[45] using operator parameters of shear mixer: rotor speed ($N$) and rotor diameter ($D$). Paton et al. conducted a study using various combinations of $N$ and $D$ to generate data points for different shear rates and Re values.[45] The effectiveness of graphene exfoliation was evaluated based on these parameters. The study demonstrated that turbulent flow is not necessary for graphene production, as long as the minimum shear rate required to initiate exfoliation is achieved. Equation 1.3c displays the minimum shear rate, $\dot{\gamma}_{\min}$,[76, 80] which is the shear rate required to initiate the exfoliation. The shear rate required is low if the graphene surface energy matches with the solvent surface tension. This concept is shown in Equation 1.2.

$$\mathrm{Re}_{mixer} = \frac{\rho N D^2}{\eta} \tag{1.3a}$$

$$\dot{\gamma} = \frac{\pi D N}{\Delta R} \tag{1.3b}$$

$$\dot{\gamma}_{\min} = \frac{\left[\sqrt{E_{s,G}} - \sqrt{E_{s,L}}\right]^2}{\eta L} \tag{1.3c}$$

Where $E_{s,G}$, $E_{s,L}$, $\eta$ and $L$ are the graphene surface energy, solvent surface tension, solvent viscosity and flake length respectively.

The shear rate equation can be rewritten to give the average flake size, which is the mean of the minimum and maximum flake sizes retained after centrifugation, $L_{CF}$ of the graphene produced by shear exfoliation as a function of rotor-stator gap, $\Delta R$, rotor speed, $N$ and rotor diameter, $D$ (Equation 1.4).[76, 102]

$$\langle L \rangle \approx \frac{\Delta R\left[\sqrt{E_{s,G}} - \sqrt{E_{s,L}}\right]^2}{2\eta\pi N D} + \frac{L_{CF}}{2} \tag{1.4}$$

The scaling up model for the shear mixing process is as follows (Equation 1.5):

$$C \propto C_i^{\chi} t^{\tau} N^{n} D^{d} V^{v} \tag{1.5}$$

Series of experiments are carried out by varying the processing parameters, one at a time, to work out the values of the exponents. The graphene concentration, $C$ can be scaled-up with the processing parameters. $C_i$ is the initial graphite concentration use for exfoliation.

$$C \propto C_i t^{0.66} N^{1.13} D^{2.28} V^{-0.68} \tag{1.6}$$

$$C \propto C_i t N^{0.53} V^{-0.16} \tag{1.7}$$

While the first model in Equation 1.6 was created based on the shear mixing of exfoliated graphite flakes in NMP solvent using rotor and stator,[76] the second model Equation 1.7 was constructed based on the exfoliation of graphite powder in Fairy washing-up liquid (as surfactant) and water, using a kitchen blender. [103] These models in equation 1.6 and 1.7 are specific to particular set-up of the shear mixing system that used to create the models. Parameter $D$ cannot be varied if a kitchen blender is used. The rotor speed, $N$, obeys the power-law only when it is beyond the minimum rotor speed due to the minimum shear rate requirement. These scaling up models also work quite well for the shear mixing exfoliation of another 2D material, $MoS_2$.

Besides the operating parameters of the shear mixer, previous study has shown that the stator geometry (shape and opening number) can affect the strain rate, shear stress, drop size and flow characteristic of solvent in a high shear mixer.[106] The drop size decreases with increasing rotor speed due to the droplet breaking effect under high rotor speed. This droplet breaking effect is more prominent for the solvent with low viscosity.[75]

## 1.3.2 Graphene Extraction by Centrifugation

Centrifugation is a crucial step after the exfoliation process to separate graphene from the residual graphite, which may include partially exfoliated graphite or graphene restacked into graphite agglomerates. This process not only determines the quantity of graphene obtained but also influences its quality in the final dispersion.[107, 108] The centrifugation speed is one of the parameters that determines the characteristics of the graphene collected, including quantity, size, and thickness. Higher speeds result in the collection of fewer, smaller, and thinner graphene.[10,109]

The commonly adopted minimum centrifugation speed is 500 rpm.[78, 80, 110] This speed was typically chosen for comparing graphene yields in different solvents. The rationale behind this selection lies in the fact that higher centrifuge speeds lead to very low graphene concentrations in the green solvents, making the concentration differences among solvents less apparent for comparison. Two key properties, solvent density and viscosity, significantly influence the amount of graphene collected during centrifugation, as described by Stokes' Law.[111] While Stokes' Law applies to spherical particles, its principles still affect non-spherical graphene flakes. Higher viscosity solvents exert greater drag on the flakes,[112] slowing their sedimentation and retaining more material after centrifugation. As a result, more viscous solvents retain greater quantity of material after centrifugation.[113] This important consideration is often overlooked in literature, leading to inaccuracies when comparing the quantity of graphene exfoliated in different solvents. This oversight also contributes to the error in solvent exfoliation efficiency, particularly when the solvent with poor exfoliation efficiency but high viscosity tends to retain more materials as the supernatant after centrifugation. Hence, standardising the solvent used in centrifugation is crucial for studying the solvent exfoliation efficiency, and this will be explored in detail in Chapter 2.

### 1.3.3 Surface Tension and Solubility Parameters

Solubility parameters and surface tension of a solvent are the fundamentals for studying the interactions between graphite or graphene and the exfoliating solvent medium.[78, 114, 115] These solubility parameters, based on the like-dissolve-like theory, indicate that if a solvent shares similar solubility parameters with graphene, it is more likely to effectively disperse graphene. Various solubility parameters, including Florry-Huggins, Hansen Solubility Parameters (HSP), and Hildebrand Parameters, have been developed primarily for investigating polymer-solvent interactions.[116, 117] These parameters are used to study the interactions involving nanomaterials, for instance, graphene and carbon nanotubes.[81]

Hildebrand solubility parameter is the basic parameter that measures the cohesive energy of the molecules.[118] It can be more accurately applied to non-polar materials with insignificant hydrogen bonding.[119, 120] In 2010, Hernandez et al. first used Hildebrand parameters to select suitable solvent for LPE and found that high graphene yield was achieved when the solvent had Hildebrand parameters close to that of graphene.[78] It had also been found that the Hansen Solubility Parameters (HSP) was more precise in explaining the high graphene yield.[121–123] HSP takes into consideration of three types of interactions; dispersive (D), polar (P) and hydrogen (H) interactions. Hansen space is a three-dimensional (3D) space representing these three forces of interactions. High graphene yield is achieved when the HSP distance in 3D Hansen space between graphene and the solvent is minimised, or when graphene and the solvent exhibit similar HSP (Figure 1.5).[123, 124] Given the significance of surface tension and solubility parameters in determining graphene yield, the following section covers the determination of these parameters for solvents and graphene. The equation for the enthalpy of mixing, $\Delta \overline{H}_{mix}$, has been written to incorporate dispersive ($\delta_D$), polar ($\delta_P$) and hydrogen ($\delta_H$) forces (Equation 1.8),[81] where, $\phi$ is the volume fraction of the solute (e.g.: graphene). A and B in the subscript of cohesive energy, $\delta$ denote the cohesive energy of solute and solvent, respectively.

$$\Delta \overline{H}_{mix} = \phi(1-\phi)\left[(\delta_{D,A}-\delta_{D,B})^2+(\delta_{P,A}-\delta_{P,B})^2+(\delta_{H,A}-\delta_{H,B})^2\right] \qquad 1.8$$

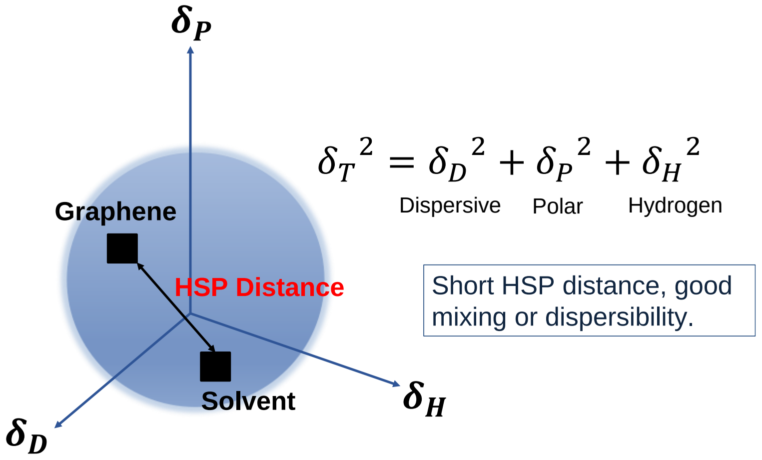

**Figure 1.5:** Hansen space depicting three fundamental forces of interaction: dispersive, polar, and hydrogen bonding. According to the Hansen Solubility Parameters theory, the total cohesive energy is deconvoluted into these distinct forces. The Hansen space can use to elucidate the Hansen Solubility Parameter distance governing the interaction between two components. Figure modified from Hansen, C. M. (2007). *Hansen solubility parameters: A user's handbook* (2nd ed.). CRC Press.

The determination of solubility parameter and surface tension are important for selecting an appropriate solvent in graphite exfoliation and dispersion of the exfoliated graphene. The surface tension of s solvent assesses the wetting behaviour of the graphite surface by the solvent, which correlates to the exfoliation efficiency. The better the wetting of graphite surface, the higher is the exfoliation efficiency. Solubility parameters determine the graphene-solvent compatibility and interactions, aiding the assessment of the dispersibility for graphene layers in the solvent after exfoliation.[125]

Surface tension is a property of liquid, while for solids such as graphite and graphene, surface energy is used instead. Solvent surface tension can be measured using pendant drop and capillary methods, by extracting surface tension information from the capillary action and the shape of a hanging droplet.[126–128] Solubility parameters of liquid or solvent are deduced from the cohesive energies between the molecules and it is related to the intermolecular interactions.[129] Since solubility parameters are a measure of cohesive energies, they are obtained by measuring the energy of vaporisation. Deconvolution of surface tension into polar and non-polar components would require the measurement of the contact angle between a liquid and a purely non-polar (dispersive) solid surface (typically Teflon).[130] The polar and dispersive components can then be determined through Owens, Wendt, Rabel and Kaelble (OWRK) model (Equation 1.9).[131] Traditionally, the polar component was derived by subtracting the vaporisation energy of a solvent from that of its non-polar homomorph. Homomorph of a polar molecule is its non-polar counterpart with the same size and shape (e.g.: homomorph of a straight-chain polar molecule is paraffin).[132]

$$\sigma_{sl} = \sigma_s + \sigma_l - 2\sqrt{\sigma_s{}^d \sigma_l{}^d} - 2\sqrt{\sigma_s{}^p \sigma_l{}^p} \tag{1.9}$$

Where $\sigma_{sl}$ is the solid-liquid interfacial surface tension, $\sigma_s$ is the solid surface tension and $\sigma_l$ is the liquid surface tension. The superscripts “d” and “p” represent dispersive and polar components of surface energy, respectively.

The data for surface tension or solubility parameters of common solvents used for LPE are readily accessible. However, it should be noted that the surface energy or solubility parameters of a solid material, such as graphite or graphene, are specific to its type. Solvent exfoliation efficiency is determined by the surface energy of graphite and NOT graphene. It is the surface energy of graphene that influences its dispersibility after exfoliation.

The surface energy of graphite is the energy per unit area that is required to overcome the van der Waals force to "peel" two graphite sheets apart.[133] The easiest way to measure the surface energy or surface wettability of graphite and graphene is by contact angle measurement. Two types of contact angle measurement methods are commonly used, i.e. the drop-shape analysis and the Washburn methods.[134–136] Drop-shape analysis is suitable for macroscopically flat and homogenous surface, such as the CVD-synthesized graphene films. This technique is used to measure the wettability of graphene for selecting the suitable solvents for LPE.[137] However, the wettability of the substrate-supported CVD-grown graphene does not represent that of graphite or graphene in powder form used in LPE. Attempts to adapt drop-shape analysis for powder materials, like coating them on a substrate or pressing them into pellets,[138] are hindered by their uneven surfaces, thus making this method unviable for powder materials.

The Washburn method serves as an alternative for directly measuring the surface energies of powder materials in their raw, unaltered states, avoiding the need for coating, or pressing into pellets. Pellet pressing can introduce surface irregularities which affect the accuracy of the measurement. The Washburn method determines the surface energy of powder materials based on the capillary force that flows through the bed of densely packed powder.[139]

$$\frac{m^2}{t} = \frac{c \cdot \rho^2 \cdot \sigma \cdot \cos\theta}{\eta} \qquad 1.10$$

Equation 1.10 is the Washburn equation,[140] showing the increase in the mass of tube ( $m$ per unit time, $t$) caused by the capillary action of the liquid used. $\rho$ ,$\sigma$, and $\eta$ are the density, surface tension and viscosity of liquid respectively. A liquid exhibiting total wetting on the powder (zero-degree contact angle) is chosen as the test liquid to determine the geometric factor, denoted by '$c$', which is a function of the sample dimensions and packing density. To extract the polar and dispersive surface energy components based on OWRK model, the contact angle must be measured using at least four different liquids.

Other methods for measuring surface energy include Atomic Force Microscopy (AFM) and Inverse Gas Chromatography (IGC) methods.[141, 142] IGC was used to determine surface energy of layered materials such as Graphene Oxide (GO), graphene and $MoS_2$, in powder form.[143, 144] IGC operates by assessing the interaction between specific functional groups on the sample powder and vaporous probe molecules.[145] The retention time of the vaporous probe molecules allows the calculation of surface energy. Both the non-polar and polar components of surface energy can be determined via the corresponding non-polar and polar probe molecules in the IGC method.

The Washburn method with OWRK model used in this work is most suitable for surface energy measurements for powder materials. Washburn method allows direct measurement of surface energy of the material in its raw powder form. This is suitable for the case of graphite and graphene powders. Although the IGC method can also be used on powder samples, it requires the solvent to be in vapour form. Washburn method allows direct measurement of surface energy or wettability of a sample surface using a solvent in liquid form.

Although solubility parameters or surface energies matching between graphene and solvent is commonly used to select the suitable solvent for Liquid Phase Exfoliation (LPE), it comes with limitations. Surface energies or solubility parameters can vary depending on the measurement technique used. Additionally, other physical parameters like density and viscosity can also influence the yield of graphene.[137]

### 1.3.4 Quality of the Bulk Starting Materials Used for Exfoliation

Graphite, the starting material for producing graphene via LPE, is evaluated based on several factors such as its oxidation level, lateral size, thickness, and defect density.[146–148] These characteristics are crucial for determining the quality of the resulting graphene produced, and the quality requirements, in turn, vary according to the intended applications. For electronic applications, graphene with low number of layers, large lateral size, low degree of oxidation and low defect density is desired for achieving good electronic conductivity.[149,150] Since the quality of graphene is strongly influenced by the properties of its graphite starting material, the selection of the right graphite, besides the exfoliation method and conditions used, is key to achieving the desired graphene quality. The properties or quality of graphite not only affect the quality of graphene produced, but also its yield. It is worth noticing that only the effect of graphite size on graphene yield is widely investigated in most published works,[151, 152] although the surface energy of graphite provides deeper insight into its effects on graphene yield.[80, 153] Graphene yield depends on the difference in the surface energies between graphite or graphene, and the solvent used.[154,155] This surface energy varies with the quality of graphite and graphene,[156,157] including the types of defects present, e.g.: defects on basal plane, point or edge defects. Therefore, we need to consider the types of graphite and graphene involved while selecting the suitable solvent to exfoliate and disperse them.

Graphene quality is evaluated based on the International Organization for Standardisation (ISO) specifications [SOURCE:ISO/TS 80004-3:2010]. Although the ideal requirement for graphene is a single layer, few-layer graphene (FLG) can range from two to ten layers. Obtaining a significant amount of single-layer graphene through LPE is challenging due to graphene restacking in the solvent. LPE often produces FLG. Single-layer graphene is typically synthesized on a substrate using the CVD method.[158] It is important to produce single layer graphene or at least nanosheets with thickness of less than 10 layers for graphene to maintain its linear or near-linear band structure to give high electron mobility for its unique electronic properties. (see Introduction, Section 1.2.1). Beyond ten layers, the electronic properties become similar to bulk graphite. Techniques such as Raman spectroscopy and Atomic Force Spectroscopy are recognised for analysing the thickness of 2D materials like graphene.

### 1.3.5 Green Solvents and Sustainability

Green solvents are environmentally friendly solvents that have minimal environmental impacts throughout their entire life cycles, from production to usage.[159] These solvents are chosen for their low inherent risk, energy consumption, waste generation, and emissions.[160] For LPE of graphene, green solvents with low boiling points (below 82°C) such as ethanol and isopropanol are preferred. This is because these solvents can be easily removed by low-temperature evaporation and recycled for reuse (Table 1.1).

Despite the advantages of green solvents, the yield of graphene produced in these solvents is approximately ten times lower than that obtained with the commonly used, but toxic, NMP solvent with a high boiling point of 202°C. [161, 162] To justify the use of green solvents, factors such as the amount of solvent required and operational energy cost, in comparison to that of NMP, need to be considered. Besides this, it is crucial to either improve the yield of graphene or develop methods to recover and reuse the solvent for repeated exfoliation processes. The advantages of the low-boiling-point solvents lies in their easy evaporation, recovery, and reuse, thus minimising emission, and disposal concerns. In contrast, high-boiling-point solvent like NMP requires more energy for removal through evaporation. Vacuum filtration is an alternative method for removing high-boiling-point solvents, but it requires filtration membranes, leading to the problems of material loss and additional membrane maintenance.

To make the use of green solvents economically and environmentally beneficial, efforts are needed to enhance the yields of 2D materials like graphene and hexagonal boron nitride. The optimisation methods for improving yield will be explored in Chapters 3 and 4.

**Table 1.1:** Solvent classification based on environmental impacts.

| Hazardous | Between Hazardous and Problematic | Recommended |
|---|---|---|
| Dimethylformamide (DMF) | Acetone | Water |
| N-Methyl-2-pyrrolidone (NMP) | Methanol | Ethanol |
| | | Ethyl Acetate |
| | | Isopropanol |

*Data adapted from Byrne, F. P. et al. Tools and techniques for solvent selection: green solvent selection guides. Sustain. Chem. Process. (2016). doi:10.1186/s40508-016-0051-z*

# 1.4 Current Research on LPE in Green Solvents

Over the last decade, the effects of solvent solubility parameters on graphene yields are being actively investigated for LPE to select the suitable solvent that can give high graphene yield. However, most of these studies focused on the sonication exfoliation technique.[78, 163] Two main approaches were used to enhance the graphene yields in LPE. First, researchers often examine the interaction between solvent and graphene by considering their solubility parameters. Second, efforts are being made to enhance the graphene yield through techniques such as surface modification or functionalisation. The following sections discuss these two approaches in greater detail. After the graphene yield has been optimised, tuning of the operational parameters (i.e.: shear mixing exfoliation speed and time) is carried out to further scale-up the production. Figure 1.6 summarises the development of the yield enhancement strategies used for LPE over the last decade.

## 1.4.1 Solvent-Graphene Interaction Study

The interaction between the solvent and graphene is investigated by examining either surface energy, surface tension or solubility parameters. This interaction plays a crucial role in influencing two key factors: exfoliation efficiency and dispersibility. These factors directly impact the yield of graphene. Exfoliation efficiency refers to the solvent's capacity to efficiently exfoliate or peel-off the graphene layers, essentially determining the quantity of graphene produced. On the other hand, solvent dispersibility refers to the solvent's effectiveness in “separating and distributing” the exfoliated graphene, ensuring it is well-dispersed. Both aspects are integral to the understanding and optimisation of graphene production.

It is widely acknowledged that a high yield of graphene is attained when the solvent's surface tension or solubility parameters closely match those of graphene, aiming to minimise the enthalpy of mixing ($\Delta H_{mix}$). [76] This principle not only guides the selection of solvents in Liquid Phase Exfoliation (LPE) but is also employed as a method to deduce the surface energy or solubility parameters of graphene by conducting exfoliation in various solvent media. The solubility parameters of graphene were taken to be similar to that of the solvent which gave the highest graphene yield.[78] Optimisation of graphene yield by tuning its solvent mixture composition based on Hansen Solubility Parameters (HSP) was carried out using low boiling point and low toxicity green solvents.[164, 165] Commonly used value from literatures for graphene surface energy is 68 mJ/m$^2$ (or the HSP of $\delta_D$=18 MPa$^{1/2}$, $\delta_P$=9.3 MPa$^{1/2}$, $\delta_H$=7.7 MPa$^{1/2}$). This value is frequently employed in selecting the effective solvents for LPE.[165, 166] NMP stands out as a well-known and efficient solvent for LPE due to its surface energy of 69 mJ/m$^2$, which closely aligned with the literature surface energy value of graphene. [76, 80]

Green solvents, which are less toxic and have lower boiling points than NMP (such as acetone, water, and ethanol), are generally considered poor solvents for LPE due to the significant difference between their surface tensions and that of graphene. According to surface tension or solubility parameters theory, these green solvents are typically excluded from the list of effective solvents for LPE. To explore the potential of green solvents in achieving high graphene yield or concentration, various theories, including modified HSP and potential mean force, are being developed.[165, 167] These theories formed the basis for the formulation of solvent mixtures using green solvents. Studies on acetone: water and ethanol: water solvent mixtures had demonstrated significantly higher graphene yields compared to the case where individual pure solvent was used. For instance, there was at least a tenfold increase in graphene concentration for the ethanol: water solvent mixture with 70% volume ethanol compared to pure ethanol and pure water.[166] Comparable results were observed for water: acetone mixture with 75% volume acetone.[168] The tuning of acetone: water was based on modified HSP, which considered the dispersed graphene concentration. Recent molecular dynamics simulations exploring the surface-solvent interface have indicated that 2-pyrrolidone had the potential to replace NMP for highly efficient exfoliation.[169] This was attributed to the well-aligned solvent molecules on the graphene surface, contributing to the stabilization of exfoliated graphene layers and enhanced dispersibility.

Current literature tends to focus on and emphasize the final yield of graphene when developing theories that relate solvent properties to the yield. However, the yield is influenced by both the efficiency of the exfoliation process and the dispersibility of the graphene. There is a lack of investigation into how solvent properties specifically impact each of these two processes: exfoliation and dispersion. Understanding how the solvent properties affect each process is crucial and necessary for unravelling the mechanisms involved and enabling the selection of effective solvent or the formulation of an ideal solvent mixture to meet the demands of exfoliation and dispersion.

### 1.4.2 Yield Enhancement Technique for LPE in Green Solvents

Despite extensive research on solvent-2D material interactions and the quest for sustainable, low-boiling-point, and less toxic green solvents for LPE, the yield of graphene and other 2D materials in these solvents remains relatively low. To overcome this challenge, the additions of surfactants, dispersants, or other additives to the solvent have been studied.[170, 171, 172] These additives introduce steric or electrostatic repulsion forces, counteracting the attractive van der Waals forces that cause restacking of graphene layers. In doing so, they enhance the dispersibility of graphene in the solvent, leading to higher yield. Other commonly adopted yield enhancement techniques for LPE of 2D materials are also covered in this section, with a particular focus on graphene.

*Solvent Exchange technique:* In order to implement the use of sustainable solvents in LPE, Zhang et al. redispersed graphene which was initially exfoliated in the less sustainable NMP solvent into ethanol (one of the green solvents). This process yielded graphene of concentration up to 0.04 mg $mL^{-1}$.[173] Although the final storage of graphene was in the ethanol (green solvent), the use of NMP in the initial exfoliation step was inevitable. Attempts have been made by the same research group to redisperse NMP-exfoliated graphene into other solvents like methanol, dichloromethane (DCM), and toluene, but these solvents resulted in poor dispersibility. Interestingly, direct exfoliation in ethanol led to an unstable dispersion compared to redispersion of NMP-exfoliated graphene into ethanol. The underlying mechanism behind this phenomenon is still unclear at this moment. In the light of the above argument, there is a pressing need for a deeper and renewed understanding of the exfoliation and dispersion mechanisms. Another similar solvent exchange approach was investigated by Li et al., who initially exfoliated graphite in DMF and then redispersed the resulting exfoliated graphene into terpineol solvent. Terpineol was found to be effective in stabilising graphene, resulting in a final concentration of 0.39 mg $mL^{-1}$.[174] However, the solvent exchange method has seen limited use in recent years due to its reliance on toxic solvents for the initial exfoliation step. This underscores the ongoing challenge of finding solvent systems that are both effective for exfoliation and environmentally sustainable.

*Intercalant- and Salt- assisted exfoliation:* Sodium ($Na^+$), potassium ($K^+$), and lithium ($Li^+$) ions, alongside with anions from acid species, serve as intercalants in the process of expanding the interlayer spacing of 2D materials. This expansion weakens the van der Waals forces between layers, facilitating the exfoliation and stabilisation of these materials.[175–177] Apart from these cations, intercalants can also be the anions from acid species.[178–180] This intercalation method is typically carried out using either electrochemical or hydrothermal techniques and is not limited to graphene but can be extended to other layered materials like $MoS_2$.[181] Intercalating $NaNO_3$ crystals with strong sulfuric acid can expand $MoS_2$ layers, easing the subsequent exfoliation process.

A cost-effective and sustainable technique known as salt-assisted exfoliation was also employed as part of the intercalation approach.[182, 183] This method utilises easily available and water-soluble salts, such as sodium chloride (NaCl), potassium chloride (KCl), and sodium carbonate ($Na_2Co_3$).[184, 185] Salt and water-assisted exfoliation can significantly enhance the exfoliation process, resulting in a graphene concentration of up to 0.71 mg/mL, which is two to three times higher than without salt assistance.[186]

Using intercalants has its drawbacks, including the generation of defects during ion intercalation and the necessity for harsh conditions, such as elevated temperatures and strong oxidative environments, to introduce intercalants into the layers.[187] Despite these challenges, the concept of intercalation provides an avenue to expand graphite layers, thus open an opportunity to exfoliate graphene from used batteries where graphite layers are already expanded.[188, 189]

*Surfactant or Dispersants:* The more commonly used yield enhancement techniques are by using surfactant or dispersant, and this technique has ever been used since before

2010.[190] Dispersants play a key role in preventing graphene flakes from aggregating by relying on electrostatic repulsion and adsorption on their surfaces because of the differences in polarity. Examples of dispersants used include the pyrene species (e.g.: sodium pyrene sulfonate (Py-SASS), sodium pyrene- butane- 1- sulfonate (Py- $C_4$-SASS),1- Pyrenesulfonic acid, Sodium Dodecyl Sulphate (SDS), and Poly (2-butylaniline)).[62, 161, 191, 192] Polymers also serve as dispersants by providing steric stabilisation through their polymer chains.

Surfactants function by reducing the surface energies of the material. This reduction weakens the π=π interaction between graphene flakes, improving the interaction between graphene and the solvent and thereby stabilising graphene in the solvent. Popular surfactants used for LPE include sodium dodecylbenzene sulfonate (SDBS), polyvinylpyrrolidone (PVP) and sodium cholate (NaC).[76, 193] However, using surfactants introduces an additional step for their removal, since insulating surfactants can impact the electronic properties of graphene. In addition, surface modification and functionalisation methods are also employed to enhance graphene dispersibility in green solvents.[194] It is important to note that these methods often introduce a high defect density and $sp^3$ defects, which can degrade the electronic properties of graphene.

*Operating Parameter Optimisation:* In addition to the theoretical study on graphene-solvent interaction, the effect of each of the equipment operating parameter on the graphene yield has been well-studied in a scale-up model.[76] This scale-up model has demonstrated the scalability of the shear mixing exfoliation technique, achieving a notable production rate of 5.3 g $h^{-1}$ and a high graphene concentration up to 0.07 mg $mL^{-1}$ in a water-surfactant solvent via the operating parameter tuning. The effectiveness of this model has been verified in a large-scale trial facility with a volume capacity of up to

300 L. It is important to note that the model can vary depending on the type of solvent and exfoliation equipment used. Similar scale-up models have also been successfully applied to exfoliate $MoS_2$ in the same solvent.[195]

The choice of an appropriate yield enhancement technique depends on the specific properties desired for the target applications. In the context of optimising yield in green solvents, there is often a trade-off between achieving higher yield and potentially compromising the quality of the graphene produced. This underscores the need for a careful balance and consideration of application requirements when selecting and optimising these techniques.

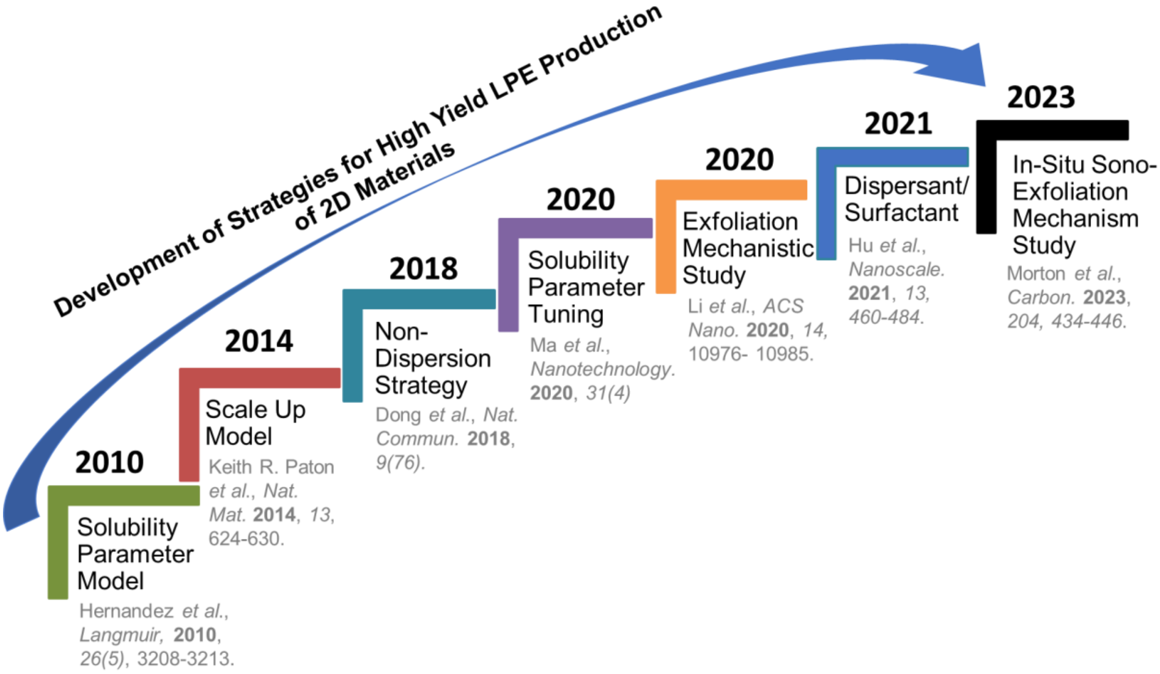

**Figure 1.6:** Selected highlights of the strategies used to enhance the yield of graphene and other 2D materials produced via LPE over the past decade.

### 1.4.3 Beyond Graphene

Following the successful production of graphene through LPE, this method has been widely adopted for the exfoliation of other 2D materials or layered substances, including hBN, $MoS_2$ and $WS_2$.[122, 196] These materials, extending beyond graphene, find applications in catalysis, sensors, and energy conversion devices.[197, 198] The LPE production of these diverse 2D materials enables the creation of inks that can be coated on substrates or membranes, particularly advantageous in flexible electronics.[199] The solvent selection approach in LPE, as reported in the literature, remains consistent for these 2D materials, relying on factors such as surface energy, surface tension, and solubility parameters. The guiding principle is to match the surface energy or surface tension between the 2D materials and the solvent. Dispersants and surfactants such as polyvinyl pyrrolidone (PVP) and sodium chlorate (NaC) are used to enhance the yields of these 2D materials, beyond graphene, in green solvents.[200, 201]

Among all the 2D materials, hBN stands out due to its structural similarity with graphene. It often serves as a substrate for graphene, forming heterostructures and finding applications in optoelectronic devices.[202, 203] Unlike graphene, hBN is electrically insulating but thermally conductive, making it suitable for applications in nanoelectronic devices and high-speed machinery that demand for effective heat dissipation.[204] hBN, however, presents challenges in exfoliation due to stronger interlayer forces resulting from ionic interactions.[205] Interestingly, hBN can be well- dispersed in IPA (a green solvent).[122, 206] Molecular dynamic simulations indicated that IPA could intercalate into hBN layers, acting as an effective dispersing agent.[207] Solvothermal and hydrothermal exfoliation methods are used to facilitate the exfoliation process of hBN under elevated temperature and pressure in IPA, or aqueous medium that consists of IPA, hydrazine hydrate ($N_2H_4 \cdot H_2O$) and water.[208, 209] Given LPE's versatile applicability to a range of 2D materials, using graphene as a well-studied model provides a foundation for the development of the fundamentals and relevant methodologies that extend beyond graphene.

## 1.5 Research Gap and Challenges

NMP has emerged as the preferred solvent for LPE in graphene production owing to its ability to yield a high graphene output. Consequently, it serves as the reference solvent for studying factors that govern graphene yield, e.g.: solubility parameters and the surface tension differential between graphene and the solvent. The efficacy of NMP as a solvent is attributed to its surface tension that closely matches that of graphene. However, the practice of predominant reliance on surface tension as a determining factor may prematurely eliminate various green solvents from consideration, given their substantial deviation in surface tension from the literature surface energy values of graphene, typically cited as 40 mN/m. Before dismissing green solvents, it is imperative to address two often-overlooked points in literatures:

**1. Lack of a reliable method for surface energy measurement of graphite powder.**

> The surface energy of graphite, a precursor to graphene, exhibits notable variability based on factors such as morphology, size, chemical composition, and defect density. Consequently, a one-size-fits-all approach, epitomised by universal application of NMP as the suitable solvent medium in LPE, may potentially lead to misleading conclusions. A critical need exists for a robust and standardised method to experimentally evaluate the surface energy of graphite, particularly in powder form, rather than adopting its value from literatures.

Knowing the surface energy of graphite starting materials used for exfoliation would help in selecting and formulating suitable exfoliation solvent medium.

**2. Absence of an independent study on the exfoliation efficiency and dispersibility.**

The efficiency of a solvent in exfoliating graphite does not inherently correlate with its ability to disperse graphene, and vice versa. It is essential to recognise the effectiveness of a solvent in the exfoliation to produce graphene (solvent exfoliation efficiency) is affected by the surface energy of the precursor material, graphite, rather than the resultant graphene. The surface energy of graphene determines the dispersibility of graphene in each solvent after the exfoliation. Solvent exfoliation efficiency and graphene dispersibility involves two distinct mechanisms. Therefore, it becomes imperative to investigate these two aspects independently. The current challenge lies in determining whether the low graphene yield in green solvents, compared to the state-of-the-art NMP solvent, is attributed to their poor exfoliation efficiency, or poor dispersibility, or both.

In light of these research gaps and challenges, it is crucial to address the methodological limitations in surface energy measurement, conduct independent studies on exfoliation efficiency and dispersibility, and seek innovative approaches to enhance graphene yield without compromising on its quality. Addressing these overlooked aspects helps in paving the way for a more comprehensive evaluation of solvent suitability for exfoliating and dispersing 2D materials in LPE. This would subsequently lead to the formulation of a suitable green solvent or solvent mixture for each of the exfoliation and dispersion steps to optimise the 2D materials production. This is essential not only for advancing graphene production but also for other 2D materials.

# 2

# Solvent Exfoliation Efficiency and Graphene Dispersibility Studies

## 2.1 Overview

Green solvents are the low boiling point and low toxicity solvents ideal for exfoliating layered materials into 2D materials due to their ease of removal from the material surfaces to give pristine products. However, the believe that green solvents are generally not as efficient in exfoliating layered materials as the commonly used toxic solvent, NMP, prevails in the research community of graphene production using LPE. Exfoliation efficiency is the number of layered materials being “peeled off” in a given time while dispersibility is the ability of the solvent to isolate and stabilise the exfoliated materials. This misconception on graphene’s low exfoliation efficiency in green solvents arises due to the lack of a reliable method to determine the actual amount of graphene produced in green solvents.

Centrifugation is used to separate the graphene from the un-exfoliated graphite after the exfoliation process. However, because the green solvents are incapable of stabilising the exfoliated graphene, restacking of the latter occurs. The restacked graphene eventually sink to the bottom of the centrifuge tube as sediment after centrifugation and not be collected as the final graphene dispersion. This causes the amount of graphene collected in the dispersion to be much lower than the amount of exfoliated graphene produced. This makes the solvent dispersibility the “limiting factor” in determining and comparing the actual amount of graphene exfoliated, especially for the green solvents with low graphene dispersibilities.

To reveal the true exfoliation efficiency of the green solvents, graphene exfoliated from the green solvents was redispersed into NMP, which is a solvent with high graphene dispersibility. This method helps in the determination of the actual amount of graphene produced, or the exfoliation efficiency. Interestingly, by using this method, it has been found that green solvents exhibit high exfoliation efficiencies and are capable of exfoliating graphene as much as that exfoliated in NMP. Among all the green solvents, IPA exhibits the highest exfoliation efficiency. This redispersing process is the key to experimentally “deconvolute” the overall graphene yield into the contributions from exfoliation efficiency and dispersibility, the two factors affecting the final graphene yield. This enables the understanding of the mechanisms involved in the exfoliation and dispersion processes, which in turn helps in selecting the right solvent for each of the two processes.

## 2.2 Materials and Methods

### 2.2.1 Materials

**Solvents:** 2-propanol (Sigma Aldrich, ≥99.8 %, GC grade), Acetone (Sigma Aldrich, ≥99.5 %, GC grade), Ethanol (Sigma Aldrich, ≥99.8 %, GC grade), Ethyl Acetate (Sigma Aldrich, ≥99.5 %, GC grade), Methanol (Sigma Aldrich, ≥99.9 %, HPLC grade), 1-Methyl-2-Pyrrolidinone (Sigma Aldrich, ≥ 99.5 %, anhydrous), 1-Methyl-2-

Pyrrolidinone (Sigma Aldrich, ≥99.0 %, non-anhydrous), and 1-Methyl-2-Pyrrolidinone (Alfa Aesar, ≥99.0 %, non-anhydrous).

**Graphite:** Sigma Aldrich 100-mesh graphite flakes (denoted as G150) and Alfa Aesar 300-mesh graphite powder (denoted as G50). The graphite purchased is used in its raw form for exfoliation, without any additional treatment. G150 has larger flake size of 150 µm and G50 has smaller size of 50 µm (Figure 2.1a,b). G50 has expanded structure as shown in the inset of Figure 2.1b, with seven times higher Brunauer–Emmet–Teller (BET) surface area than G150 (Figure 2.1f). The peak at 26.50° of the X-Ray Diffraction (XRD) spectra of both G150 and G50 is the most prominent peak generated by the diffraction of (002) plane of graphite which corresponds to the graphite interlayer (d-spacing) of 0.34 nm (Figure 2.1c,d). The XRD peaks are indexed according to the reference from the powder diffraction file database PDF 00-041-1487 C. XRD spectra of G50 shows another significant peak at lower angle of 11.58° degree, which corresponds to a larger d-spacing of 0.76 nm. This can be caused by the expanded structure of G50. In term of crystal defect, G50 has more defects as can be evident from the higher D peak from Raman spectrum at around 1350 cm$^{-1}$ (Figure 2.1e).

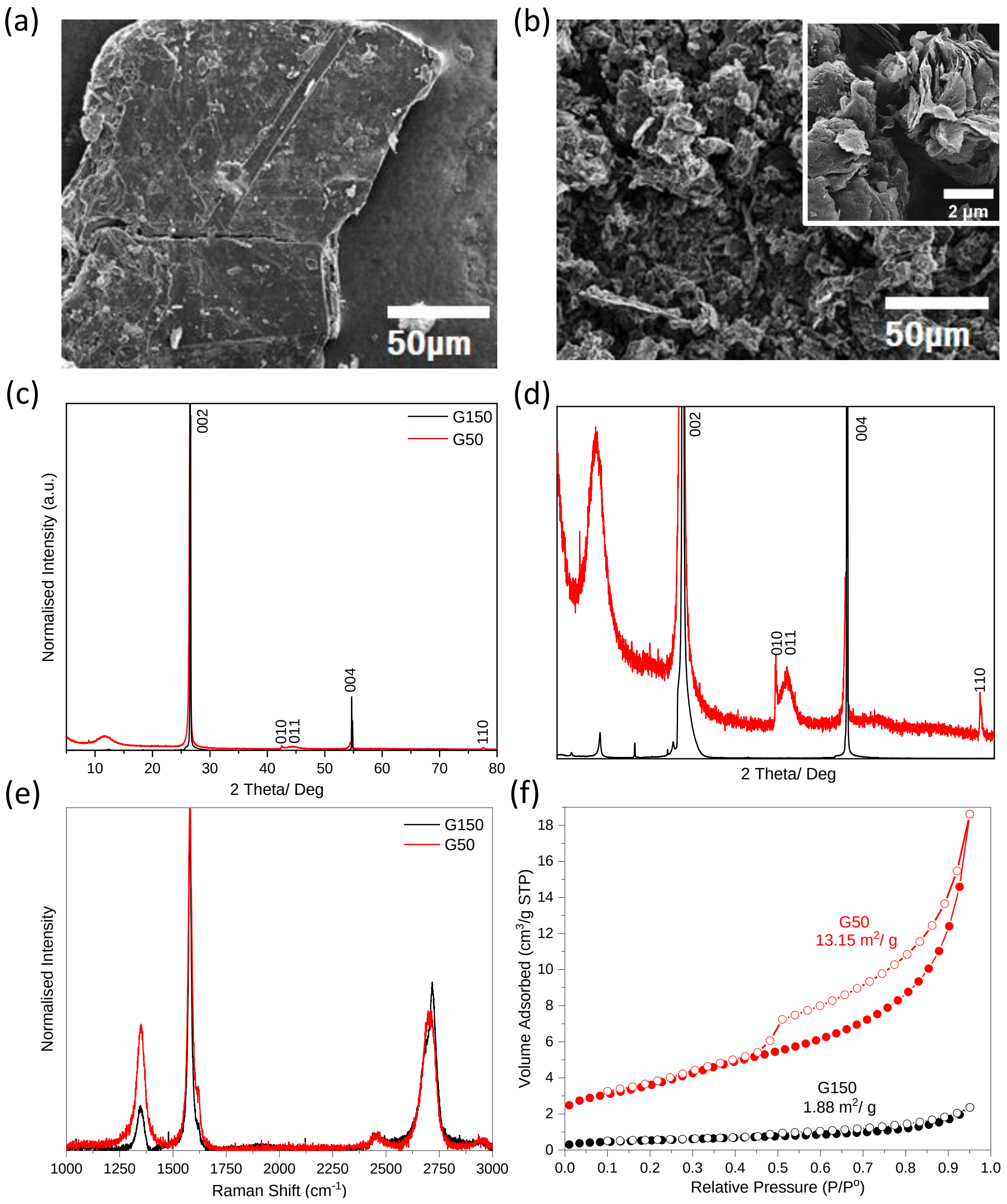

**Figure 2.1:** SEM images of (a) G150 graphite and (b) G50 graphite. Inset: Enlarged image showing the expanded structure of G50; (c) XRD spectrum comparison of G150 and G50 with the enlarged peaks shown in (d); (e) Raman spectrum (normalised to the highest peak) comparison of G150 and G50; (f) BET surface area measurements of G50 and G150. Adapted from Ng *et al.*, 2022, Ref. [210].

## 2.2.2 Methods

### 2.2.2.1 Shear Mixing Exfoliation

Two different graphite sources, Sigma Aldrich 100 mesh (G150) and Alfa Aesar 300 mesh (G50) were used as the starting materials for exfoliation. A range of different low toxicity and low boiling point solvents (D.I., EtOH, MeOH, EA, Ace, IPA) and solvent mixtures [EtOH:D.I. (1:1 vol. %) and IPA:Ace (1:1 vol. %)] were used as the exfoliation solvent media. High shear mixer model used is Greaves Model D lab mixer. The dimension of stator and rotor are shown in Figure 2.2. Graphite samples were exfoliated, with an initial concentration of the graphite dispersion of 25 mg/mL in 150 mL of solvent, under a shear mixing speed of 5000 rpm for three hours. To compensate for the lost in the volatile solvents due to evaporation, the solvents were constantly added throughout the exfoliation process. After exfoliation, the graphene produced was separated from the graphite aggregates by centrifuging the dispersions at 500 rpm or 52 rcf for one hour. The conversion of rpm to rcf is shown in equation 2.1.[211] The speed of 500 rpm was used unless otherwise specified. The supernatant after centrifugation at 500 rpm (Su_500) was taken as the final graphene dispersion and was used for UV-Vis spectroscopy concentration analysis and other characterisations (i.e.: Raman, XPS, AFM) for quality evaluation.

$$RCF = 1.118 \times 10^{-5} \times r \times (RPM)^2 \tag{2.1}$$

Where $RCF$ is the relative centrifugal force, $RPM$ is the revolutions per minute and $r$ is the rotor radius in cm.

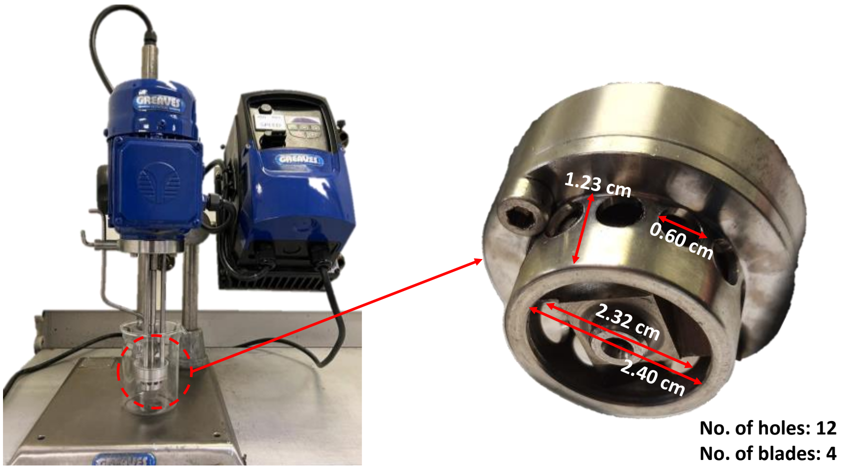

**Figure 2.2:** The lab-scale high shear mixer used for liquid phase exfoliation. The dimensions of the rotor-stator unit are also shown in the figure.

### 2.2.2.2 NMP- and Green Solvent- Redispersion (NMP-R and GS-R)

For NMP-redispersion (NMP-R), the exfoliation products* produced after the exfoliation in green solvents (D.I., EtOH, MeOH, EA, Ace, IPA, EtOH:D.I. and IPA:Ace) were dried at 100 °C in a vacuum oven to evaporate the solvent after exfoliation. NMP (equal volume as the evaporated amount) was added to maintain the concentration**.** The samples were centrifuged at 500 rpm for one hour and the supernatant was taken for concentration analysis.

For green solvent-redispersion (GS-R), the exfoliation products* produced after the exfoliation in NMP were washed with ethanol using vacuum filtration with 0.22-micron PTFE membrane before drying them in a vacuum oven at 100 °C to evaporate the remaining solvent. Same volume of green solvents was added to disperse the NMP exfoliation products*. For both NMP-R and GS-R, a vortex mixer was used to homogenise the samples after redispersion to eliminate the effects from ultrasonic cavitation. This is to prevent additional exfoliation from redispersion, ensuring accurate quantification of the graphene produced by shear mixing. Cavitation bubbles are generated from the compression and rarefaction cycles when high-frequency ultrasonic wave propagates through liquid.[212] The collapse of the cavitation bubbles creates shock wave to exfoliate the graphene layers.[213] Vortex mixer is the mechanical agitation to stir the liquid and there are lacks the high-frequency acoustic forces needed for cavitation bubbles generation.[214] Hence, it does not have the exfoliation effect. After homogenisation using vortex mixer, the samples were centrifuged at 500 rpm (52 rcf) for one hour and the supernatant was taken for concentration analysis.

Note: **Exfoliation products are the graphene-containing products with graphite aggregates obtained after exfoliation and before centrifugation.*

## 2.2.3 Characterisations

### 2.2.3.1 Raman Spectroscopy

**Sample preparation:** All the graphene dispersions used for Raman spectroscopy characterisation were obtained from 500 rpm centrifugation. For low-concentration graphene dispersions (appearing clear), the dispersion was further centrifuged at 4000 rpm for one hour to concentrate and collect the graphene as sediment, ensuring sufficient material for a strong Raman signal. The concentrated graphene dispersion was then drop-cast onto a Si/$SiO_2$ wafer. For high-concentration dispersions (appearing greyish), a dilution of at least five times was performed to enhance the dispersion of graphene flakes on the wafer and minimise aggregation. This was typically necessary for IPA- and NMP-exfoliated graphene dispersions. The graphene-coated wafers were left to dry under ambient conditions for characterisation. In the case of NMP-based dispersions, the drop-casting was done on Si wafers preheated to 200°C on a hot plate to evaporate and remove NMP before Raman characterisation. [76]

Raman Spectroscopy was performed using the Horiba Scientific LabRAM ARAMIS. An objective lens of x50, laser wavelength of 532 nm, diffraction grating density of 1800 lines/mm (spectra resolution of ~2cm$^{-1}$), and laser power of <2 mW was used to acquire the Raman spectra.

**Data Analysis:** The D and G peaks in the Raman spectrum of graphene typically appear at around 1350 cm$^{-1}$ and 1580-1600 cm$^{-1}$, respectively.[215] D' peak often occurs as the "shoulder" of the G peak. The Lorentzian peak fitting function is used to fit the D, G and D' peaks, including the deconvolution of G and D' peaks. D' peak appears as the overlapped "shoulder" of the G peak.[216–218] Background subtractions and peak fitting were performed using Origin 2019 graph plotting software. Peak fitting was done with the reduced $\chi^2$ value of at least 0.99. Reduced $\chi^2$ indicates the goodness of fit. Value of Reduced $\chi^2$ close to one indicates good fitting/ match between the experimental and fitted data (spectra).

D to D' peak intensity ($I_D/I_{D'}$) provides the information on the types of defects present in the graphene samples.[219, 220] D to G peak intensity ratio ($I_D/I_G$) provides information on defect density. High $I_D/I_G$ implies high degree of defects. The typical range of $I_D/I_G$ in non-oxidised graphene is <0.6,[221, 222] whereas for oxidised graphene, $I_D/I_G$ is >1.[223, 224] However, care must be taken when using $I_D$ to analyse the defects on graphene crystal structure because the exposed edges of small graphene flakes give high $I_D$ despites having almost no defect on the crystal structure. If two graphene samples have the same defect density, the one with smaller lateral size (more exposed edges) will give higher $I_D$. $I_D$ can be used to compare the defect densities of different graphene samples only if they have the same lateral size. The $I_D/I_G$ ratio is commonly used in defect density analysis, with D peak intensity ($I_D$) varies according to the types and amounts of the edges present as well as the laser polarisation direction.[225, 226] Therefore, there is a possibility that a perfect graphene with low disorder may exhibit high $I_D$. In this case, the FWHM of G peak is a more accurate feature for the analysis of lattice disorders.[219] Disordered graphene should show a broad G peak FWHM despite its low $I_D/I_G$ ratio. For the Raman Spectroscopy analysis, at least six measurements were taken at randomly selected spots on each graphene sample.

The use of a x50 objective lens with a numerical aperture (NA) of 0.55 and a 532 nm laser wavelength produces a laser spot size of approximately 1 μm. Since this spot size is larger than the exfoliated graphene flakes in my study, which range from 400 to 800 nm, it effectively captures the edges of the flakes, allowing for the detection of edge defects. However, the drop-casting method used for sample preparation often results in unavoidable re-aggregation of graphene flakes. In these re-aggregated flakes, it becomes more challenging to distinguish between edge and basal plane defects compared to well-dispersed individual flakes. Consequently, defect analysis on re-aggregated graphene primarily provides information about the dominant defect type present in the sample, rather than enabling detailed analysis of specific defect types. This approach is still acceptable for comparing dominant defect types and defect density among different samples, and for observing broader trends rather than precise, localised defect analysis.

### 2.2.3.2 UV-Vis Spectroscopy

UV-Vis characterisation was used mainly to calculate the concentration of dispersion produced and to qualitatively determine the thickness and oxidation level based on the position and intensity of $\pi - \pi^*$peak. The UV-Vis characterisation was conducted using Cary 5000 UV-Vis-NIR (Agilent) in dual-beam mode, with the scan rate of 100 nm/ min in the range of 200 nm to 700 nm or 250 nm to 700 nm (for NMP-dispersed samples due to the UV cut-off wavelength).

**Sample Preparation:** After the centrifugation of the exfoliation product dispersion, the top 1/3 of the dispersion, which is the supernatant, was taken for the UV-Vis analysis, leaving behind the large graphite aggregates that collected at the bottom of the tube as sediment. Quartz cuvette of 1cm thickness (or also known as the optical path length) was used for the UV-Vis measurements.

**Data Analysis:** The concentration of graphene dispersion produced was calculated based on the Lambert-Beer Law (Equation 2.2).

$$A = \varepsilon l c \tag{2.2}$$

Where A is the absorbance, $\varepsilon$ is the absorptivity (in mL mg$^{-1}$ m$^{-1}$), $l$ is the optical path length (in m) and $c$ is the concentration (in mg mL$^{-1}$) of the attenuating species (graphene). All the concentrations were determined from the supernatant of graphene dispersions after centrifugation at 500 rpm for 1 hour, unless stated otherwise.

The absorbance at 660 nm wavelength is taken for the concentration calculation using (Equation 2.2) This wavelength lies outside the absorption edge of graphene (~250-270nm), hence, the absorbance depends solely on the quantity of graphene presence and not its electronic transition which is affected by the dimensions and thicknesses of the graphene flakes.[227] Backes et al. also claimed that the absorbance at this high wavelength region was independent of the size of the graphene flakes.[227]

The absorptivity value, $\varepsilon$ in (Equation 2.2) was determined by the gradient/slope of the calibration curve. This was done by calibrating the measured UV-Vis absorbance with a series of graphene dispersions with known concentrations (Figure 2.3a,b) The absorptivity varies with the solvent medium of the graphene dispersions used for the calibration curve, as shown in Figure 2.3. Given that the same mass of graphene has been dispersed in the same volume of different solvents, the measured concentration value using UV-Vis is different.

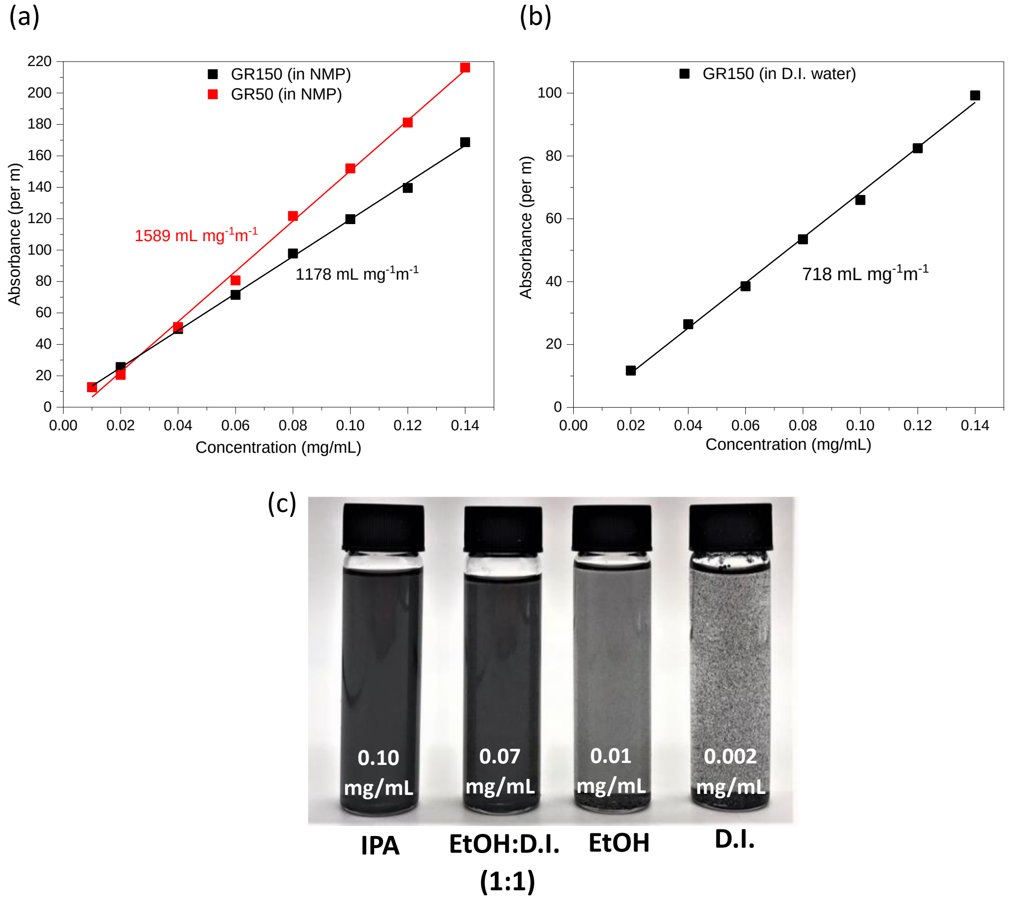

**Figure 2.3:** (a) UV-Vis spectroscopy calibration curve of GR150 and GR50 in NMP for absorptivity determination through graph gradient. (b) Calibration curve of GR150 in D.I. water. (c) Digital photograph of same mass of graphene dispersed in different solvents, resulted in different measured concentration. Adapted from Ng *et al.*, 2022, Ref. [210].

The absorptivity value, $\varepsilon$ used in the literature is obtained from other published works.[6,228,229] However, there is a variation in the literature value of $\varepsilon$, which range from 2460 to 6600 mL mg$^{-1}$m$^{-1}$.[86,154,230] The is due to the incomplete removal of surfactant/dispersant from the graphene sample being analysed and which also accounted for the measured mass of graphene.[227] Furthermore, the value of $\varepsilon$ also depends on the dispersing solvent medium used and this fact is often overlooked in the literature. Therefore, selecting the right dispersing medium for calibration curve is important to ensure the accuracy in the $\varepsilon$ value obtained.

The preparation of graphene dispersion for the determination of the absorptivity from calibration curve should involve dispersing graphene in a solvent with good graphene dispersibility, such as the NMP. When solvent with poor graphene dispersibility such as deionised water was used, the graphene was not well-dispersed in the solvent, causing the absorbance detected to be much lower than the actual absorbance. This underestimated the absorptivity, as shown in Figure 2.3, which the absorptivity of GR 150 determined by dispersing GR 150 in deionised water was much lower compared to that dispersed in NMP. When absorptivity is underestimated, the concentration will be overestimated (based on Equation 2.2). With this consideration, the absorptivity measured in NMP (solvent with high graphene dispersibility) was adopted. The absorptivity of **GR 150 was 1178 mL mg$^{-1}$ m$^{-1}$** and that for **GR 50 was 1589 mL mg$^{-1}$ m$^{-1}$**, as determined from the gradient of the calibration curves shown in Figure 2.3a.

### 2.2.3.3 Atomic Force Microscopy (AFM)

An Agilent 5400 AFM was used to evaluate the sample morphology and graphene flakes thicknesses. The samples were prepared by drop casting graphene solutions onto a Si/SiO$_2$ wafer placed on a hot plate, heated to 80 °C (for green solvents) and to 150 °C (for NMP). This was to evaporate the solvents and disperse the materials on the substrate. The probe used was MikroMasch HQ:NSC35/AI BS (silicon tips) with resonance frequencies of between 150 and 300kHz. The scanning mode used was the tapping mode. Compares to the contact mode, the tapping mode causes less damage to soft samples like graphene and offers higher lateral resolution. Relative to non-contact mode, this operation mode can achieve higher scanning speed, and is less sensitive to the adsorbed fluid when operates under ambient atmosphere.

### 2.2.3.4 Brunauer-Emmett-Teller (BET)

Brunauer Emmet Teller (BET) measurements were performed under nitrogen atmosphere (nitrogen adsorption-desorption isotherm at 77K) using a Micromeritics' Gemini Vll . The powder samples were degassed at 225 ˚C overnight under nitrogen prior to the measurements. A sample mass of 0.3228 g was used for all the measurements.

### 2.2.3.5 Scanning Electron Microscopy (SEM)

The graphite was sparingly sprinkled onto a sticky copper tape for SEM analysis of the raw materials. SEM micrographs were taken at 5 kV, using JEOL JSM-840F with cold cathode field emission gun.

### 2.2.3.6 Contact Angle Measurement for Graphite Powder

Interfacial contact angle measurements at the interfaces between graphite powder and test solvents (exfoliation solvents used in this work) were performed using KRUSS K100 tensiometer (in collaboration with Henry Royce Institute) based on Washburn method. The solid sample was packed in a glass tube with a filter base. The liquid drawn up by the capillary action and capillary force caused an increase in the mass of tube. The increase in mass of tube over time was detected by a force sensor. The interfacial contact angle was determined based on the change in mass of tube over time based on Washburn equation (Equation 2.3).[213]

$$\frac{m^2}{t} = \frac{c \cdot \rho^2 \cdot \sigma \cdot \cos\theta}{\eta} \qquad 2.3$$

*m* [g] mass of the tube and sample; *t* [s] flow time; *c* [mm$^5$] capillary constant of the sample ($c_{G150}$ = 2.76847335 mm$^5$; $c_{G50}$ = 0.6138338 mm$^5$; *ρ* (g/ml) density; *σ* (mN/m) surface tension; *η* (mPa·s) viscosity; and *θ* (deg) contact angle of the test liquid.

The capillary constant, c, reflects the physical characteristics of the capillary system, such as the geometry of the material or the packing tube. It is determined by performing measurements with hexane, which achieves complete wetting (θ = 0°, cos θ = 1) on the material. This allows the determination of c using the known variables in the Washburn equation. The values for other parameters are provided in Table A1.

### 2.2.3.7 X-Ray Diffractometry (XRD)

Bruker D8 ADVANCE Eco and Siemens D5000 X-ray diffractometer (XRD). The XRD was operated at 40 kV, and 40 mA using Cu Kα radiation, with step size of 0.02° and scan rate of 5s per step. To correct for the instrumental broadening, a value of 0.06° for instrumental broadening was determined from the Full Width at Half Maximum (FWHM) of the spectrum obtained in the same measurement range, using Lanthanum Hexaboride ($LaB_6$) (SRM 660) as the standard.

# 2.3 Background

## 2.3.1 Exfoliation Efficiency and Dispersibility

To date, there is purportedly no experimental method to study the exfoliation efficiency and dispersibility independently. Dispersibility depends on the solubility parameters of graphene and solvent (graphene-solvent interaction),[85,154,231] while the exfoliation process depends on the solvent equipment operating parameters such as rotating speed, shear mixing time, mixing head diameter, rotor-stator gap, initial graphite concentration and liquid volume.[45,86,232] More details on the exfoliation efficiency and dispersibility can be found in Section 1.4.1. Most of the published works only emphasize on determining the final graphene yield, which is the combined effect of the exfoliation efficiency and dispersibility, and to find method for achieving highest possible graphene yield.[233–235] Extensive studies have been conducted to understand the effects of graphene surface energy on its yield.[81, 121] However, bearing in mind that for exfoliation efficiency, it is the surface energy of graphite that should be considered rather than that of graphene. This is because the exfoliation process starts from graphite. Dispersibility, on the other hand, depends on the surface energy of graphene.

Designing an experimental method to study the exfoliation efficiency and dispersibility independently would help to identify the right solvent for each of the exfoliation and dispersion processes for improved yield (Figure 2.4). Properties of graphite staring materials such as oxygen content, morphology, size and surface energy could also affect the yields and qualities of the graphene produced.[236, 151] The "deconvolution" method used in this work can potentially be applied on different types of graphite starting materials and even other layered materials such as hBN and $MoS_2$.

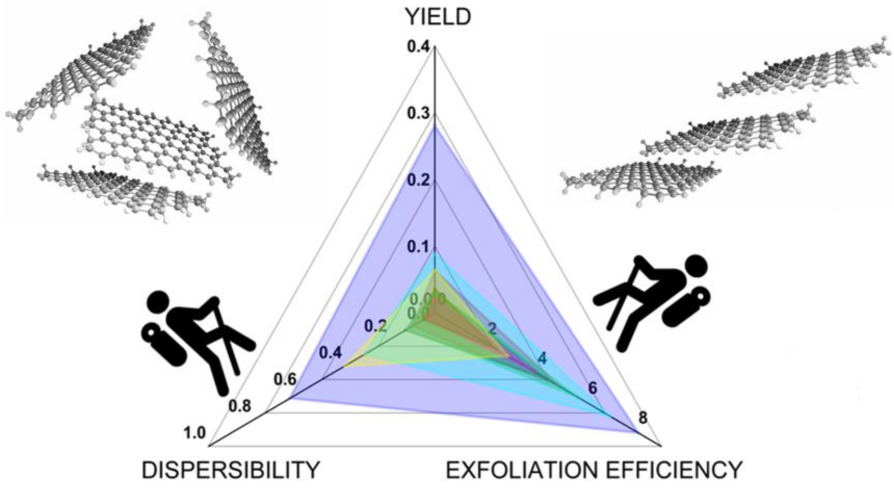

**Figure 2.4**: "Deconvolution" of the overall graphene yield into exfoliation efficiency and dispersibility unveils the high exfoliation efficiency of green solvents. Each number on the scale is a quantitative representation of the yield, dispersibility and exfoliation efficiency, according to the concentration of graphene obtained. Adapted from Ng *et al.*, 2022, Ref. [210].

### 2.3.2 Conventional vs. NMP-R Technique for Exfoliation Efficiency Study

The product after shear mixing exfoliation typically contains well-dispersed graphene (with well-separated layers), and other graphite aggregates such as stacked graphene flakes and partially exfoliated graphite. Figure 2.5 shows an equal amount of graphene dispersed in NMP, which has high dispersibility, and IPA, which has low dispersibility. In IPA, the lower dispersibility causes much of the exfoliated graphene to restack and settle as sediment after centrifugation, leaving less graphene collected in the supernatant compared to NMP. This is the main problem associated with the conventional method for the determination of the total amount of graphene exfoliated in green solvents with low graphene dispersibilities.

To reliably quantify and compare the amount of graphene exfoliated in different solvent media, it is important to use a standardised solvent with good graphene dispersibility to redisperse the exfoliated graphene for centrifugation. The reasons of using one standardised solvent with good graphene dispersibility are as follows:

1. To eliminate the effect of solvent density while comparing the amount of graphene produced (or the exfoliation efficiency) in different solvents because solvent density also affects the amount of graphene extracted from the exfoliation products via centrifugation.[237] Hence, for a fair comparison of amount of graphene exfoliated in different solvents, it is crucial to use only one standardised solvent medium for the centrifugation process.
2. To prevent the restacking of the exfoliated graphene in the green solvents. This is because the measured graphene concentration is constrained by the amount of unstacked or well-dispersed graphene flakes in the dispersion, which does not represent the total amount of graphene produced from the exfoliation process.
3. Using the same solvent medium environment for dispersing graphene to ensure the dispersed graphene flakes have identical surface conditions for concentration analysis.

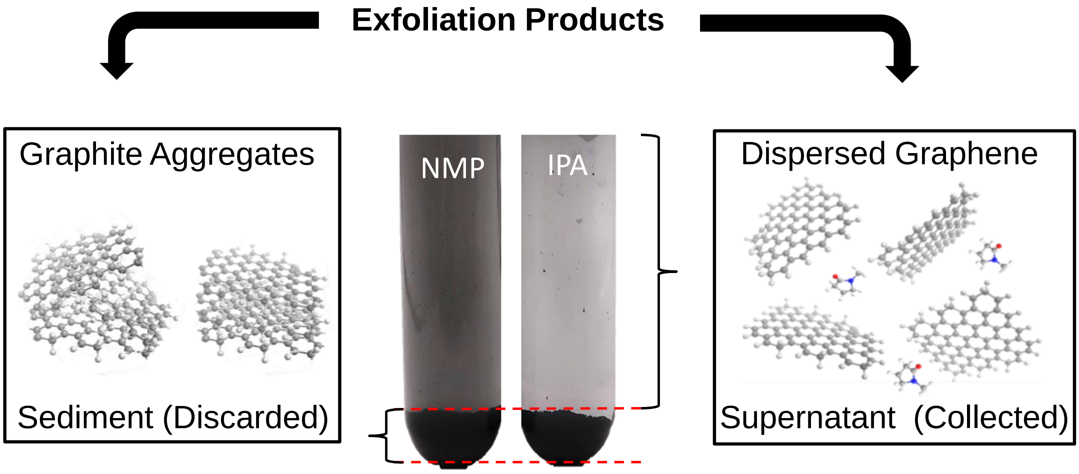

**Figure 2.5:** The exfoliation products in NMP and IPA solvent media with different graphene dispersibility after centrifugation. The exfoliation products consist of graphite aggregates and well-dispersed graphene. Well-dispersed graphene was collected as the supernatant after centrifugation. Two centrifuge tubes shown contains similar amount of graphene. IPA has low graphene dispersibility that causes the graphene produced to restack into graphite aggregates resulted in little amount of graphene being collected as the supernatant after centrifugation, as compared to that collected in NMP. Adapted from Ng *et al.*, 2022, Ref. [210].

The schematic diagram in Figure 2.6 is the conceptual illustrations on how the proposed NMP-Redispersion (NMP-R) method could overcome the problem faced by the conventional method in determining the quantity of graphene exfoliated in a solvent with low graphene dispersibility. Same volume of solvent A and B containing equal amounts of graphene, with solvent A having lower graphene dispersibility. It follows naturally that the concentration of graphene measured using UV-Vis spectroscopy from the supernatant of solvent A, was lower than that of solvent B (“conventional method” in Figure 2.6). This is because the measured graphene concentration in solvent A was limited by its low graphene dispersibility. This causes the discrepancy in the measured concentration of the same amount of graphene in solvent A and B. The measured concentrations using the conventional method was the combined contribution from both the exfoliation efficiency and graphene dispersibility of the solvent. In short, it is impossible to isolate the influence of dispersibility on the measured graphene concentration for the exfoliation efficiency analysis across different solvent.

For the exfoliation efficiency study using the proposed NMP-R method, the solvent medium used to disperse the exfoliated graphene was standardised; whereas for the dispersibility study through the proposed GS-R method, the solvent medium used to exfoliate the graphene was standardised. The proposed NMP-R and GS-R methods, allow the accurate and independent evaluations of the exfoliation efficiency (NMP-R method) and graphene dispersibility (GS-R method) of the green solvents.

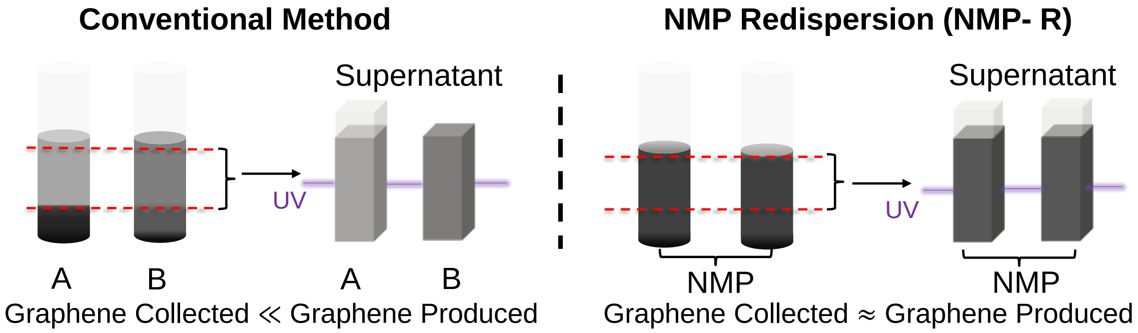

**Figure 2.6**: In the conventional method, for the same amount of graphene exfoliated/produced in both solvent A and B, lower amount of graphene was collected and characterised from solvent A due to its lower graphene dispersibility than solvent B. The NMP-redispersion (NMP-R) method exploits the high graphene dispersibility nature of NMP so that the amount of graphene collected is not limited by the graphene dispersibility of the solvent. This enables fair comparison of amount of graphene exfoliated in different solvents. Adapted from Ng *et al.*, 2022, Ref. [210].

## 2.4 Results and Discussions

### 2.4.1 NMP-R Technique for Exfoliation Efficiency Study

As discussed in Section 2.3.2, graphene's low dispersibility in green solvents often results in stacking and re-aggregation, leading to an underestimation of the amount produced when using conventional concentration analysis methods. To address this, NMP was used in this study as a standardised dispersing solvent for graphene exfoliated in various green solvents. The results of the concentration analysis after redispersion the exfoliated graphene in NMP are presented Figure 2.7.

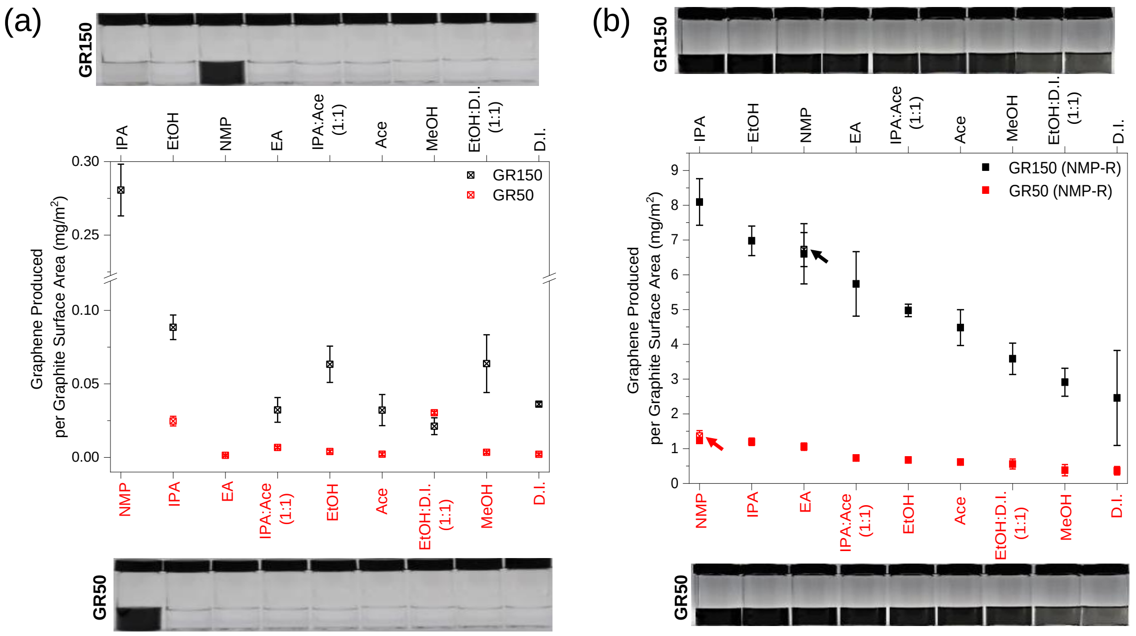

**Figure 2.7**: Mass of GR150 and GR50 graphene produced per surface area of G150 and G50 graphite respectively, exfoliated in various exfoliation solvent media (x-axis), determined by the (a) conventional method (without redispersion) and (b) NMP-redispersion (NMP-R). The solvents on the x-axes of the graphs (a) and (b) are arranged in the order of decreasing solvent exfoliation efficiency. The data points for NMP-exfoliated graphene in (a) are shown in (b) instead, to compare with the NMP-R of the NMP-exfoliated graphene. Error bars showed the standard deviations obtained from at least 3 sets of repeated experiments. Digital images of graphene dispersion are shown above/below the respective axes and arranged according to the solvent sequence along the x-axis of the graphs. The NMP-R graphene dispersions shown in (b) is diluted five times for better contrast. Adapted from Ng *et al.*, 2022, Ref. [210].

By redispersing the graphene in NMP, significantly higher masses were observed, which is up to 29 times more graphene for IPA-exfoliated GR150 and 48 times more for IPA-exfoliated GR50, as compared to conventional concentration analysis (Figure 2.7a vs. Figure 2.7b) This NMP-R concentration analysis approach enables a more accurate "capture" of the graphene produced in green solvents, as compared to the conventional analysis method. This unveils the high exfoliation capability latent in green solvents that has not been realised before, particularly IPA.

For accurate comparison of exfoliation efficiency across different graphite samples, the amount of graphene produced is normalised to the surface area of the starting graphite, as confirmed by BET surface area analysis. GR50 was found to have seven times the surface area of GR150 at the same mass (Figure 2.1f). Hence, the amount of graphene produced is reported here as "mass of graphene produced per surface area of graphite (mg/m$^2$)", instead of the commonly used "concentration (mg/mL)" unit (Figure 2.7).[238] The results reported in concentration is shown in (Figure A1 and Figure A2). (Please refer to Section 2.2.3.2 for the concentration calculations). To show that NMP-R technique used does not further exfoliate the material, but merely helped in dispersing the exfoliated graphene, the NMP-exfoliated GR150 and GR50 containing exfoliation products were redispersed back into the NMP. The concentration remained the same after NMP-R (data marked with red and black arrows in Figure 2.7b) confirming the NMP-R step did not impose further exfoliation effects.

From the study of exfoliation efficiency using NMP-R technique, IPA shows the highest exfoliation efficiency among the green solvents being studied for both GR150 and GR50. The black and red graphs show the data for G150/GR150 and G50/GR50 respectively. Interestingly, the exfoliation efficiencies of both, IPA and EtOH, have exceeded that of NMP for GR150 (Figure 2.7b), whereas for GR50, the exfoliation efficiencies of IPA and EA are comparable to that of NMP. This finding has led to the proposal of a new technique for studying the solvent dispersibility of graphene in this work.

## 2.4.2 GS-R Technique for Dispersibility Study

Graphene dispersibility is one of the main factors affecting the overall graphene yield in LPE, besides exfoliation efficiency. The evaluation and comparison of graphene dispersibility of the selected solvents were conducted by the Green Solvent-Redispersion (GS-R) method (Section 2.2.2.2), in which the G150 and G50 graphite were first shear-mixed in NMP. NMP was adopted as the standard exfoliation solvent medium. The graphene-containing exfoliation product was then filtered and washed with EtOH to remove any NMP residues, dried and redispersed in selected green solvents shown on the x-axis of Figure 2.8. From the dispersibility study in Figure 2.8, IPA has the best graphene dispersibility among the selected green solvents for GR150, followed by the EtOH:D.I., whereas for GR50, EtOH:D.I. possesses better dispersibility than IPA. The fact that EA is a good solvent to disperse GR150 but not GR50 implies the dissimilar potentials of a given solvent towards dispersing different graphene types produced from different graphite sources. D.I., Ace and MeOH are recognised as poor solvents for exfoliation and dispersion of both, GR150 and GR50. EtOH:D.I. solvent medium has the highest dispersibility towards GR50, and this contributes to the high overall graphene concentrations (Figure 2.8a and Figure A1b). Please refer to Figure A2b for the dispersibility study reported in “concentration (mg/mL)” unit.

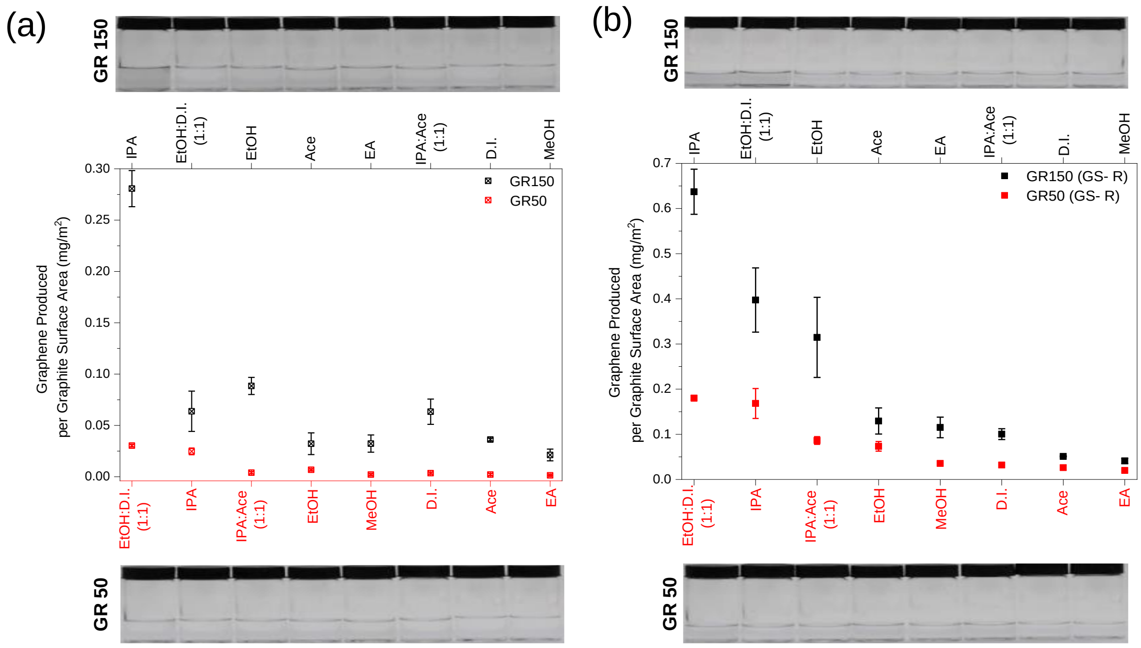

**Figure 2.8:** Mass of GR150 and GR50 graphene produced per surface area of G150 and G50 graphite respectively, exfoliated in various exfoliation solvent media (x-axis), determined through the (a) conventional method (without redispersion) and (b) Green solvent-redispersion (GS-R). The solvents on the x-axes of the graphs (a) and (b) are arranged in the order of decreasing solvent graphene dispersibility. Error bars showed the standard deviation obtained through at least 3 sets of repeated experiments. Digital images of graphene dispersion are shown above/below the respective axes and arranged according to the solvent sequence in the x-axis of the graphs. Adapted from Ng *et al.*, 2022, Ref. [210].

In order to prove the reliability of the exfoliation efficiency and dispersibility study, graphene exfoliated in EA, which is the solvent identified to have low GR50 dispersibility but high exfoliation efficiency, was redispersed into the green solvents identified with high GR50 dispersibility *i.e.* IPA and EtOH:D.I. The yield was enhanced by 16 times when redispersed in IPA (from 0.0005 mg/ml to 0.0077 mg/ml), and 60 times (from 0.0005 mg/ml to 0.0298 mg/ml) when redispersed in EtOH:D.I. (Figure 2.9). The UV-Vis spectra of EA-exfoliated GR50 in IPA and EtOH:D.I. are shown in Figure 2.9b. The more intense peak near 250 nm is the peak caused by $\pi$–$\pi$* transitions of the conjugated carbon network in graphene,[239] and the second peak at higher wavelength near 280 nm might be caused by either the presence of oxygen-containing functional groups, or larger and more aggregated sheets.[239–241] The higher absorbance reflects higher concentrations based on Beer-Lambert's law (refer to Section 2.2.3.2 for more details on UV-Vis data analysis).

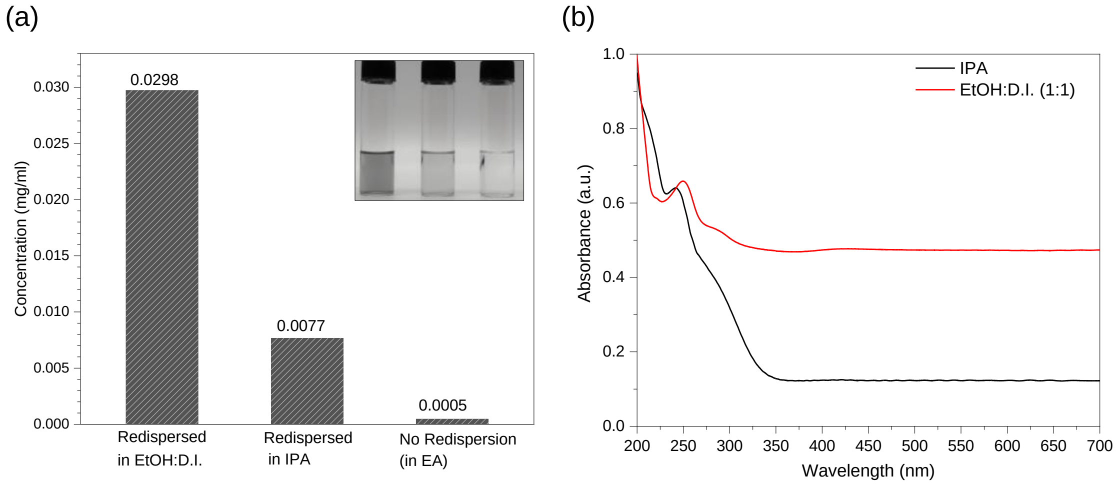

**Figure 2.9:** (a) The concentration of GR50 exfoliated in EA and dispersed in the same solvent (no redispersion), in comparison to the redispersion of EA-exfoliated GR50 in IPA and EtOH:D.I. (1:1). Inset: Digital images of dispersions correspond to the x-axis arrangement. (b) Normalised UV-Vis spectra of EA-exfoliated GR50 dispersed in IPA and EtOH:D.I. (1:1). Adapted from Ng *et al.*, 2022, Ref. [210].

## 2.4.3 Solubility Parameters and Surface Energy Analysis

The findings from the exfoliation efficiency study ponder the question as what the reason behind the high exfoliation efficiency of green solvents is, especially IPA. In order to understand the exfoliation efficiency, the correlation between graphite surface energy and solvent surface tension was studied. One should bear in mind that exfoliation efficiency is based on graphite-solvent interaction whereas dispersibility is based on graphene-solvent interaction. Washburn method was employed to evaluate the interfacial contact angle between G50 and G150 graphite and the selected solvents, without the need of compressing the graphite powder into pellet or coating the powder on a flat substrate, which is often required for a conventional drop-cast contact angle measurement approach.

The contact angle was calculated based on Equation 2.3, using parameters listed in Table A1. Graphite surface energy was calculated through the interfacial contact angle obtained, from the gradient and y-intercept of the Owens-Wendt-Rabel & Kaelble (OWRK) plot (Figure A3). The solvents surface tension components data used for surface energy calculations are listed in Table A2. It is worth noticing that G50 and G150 graphite exhibit different surface energies, which are 19.44 and 23.93 mN/m respectively (Figure A3). Therefore, the solvent ranking for exfoliation efficiency and dispersibility for the LPE of these two graphite materials are difference. The K100 force tensiometer, with a resolution of 0.001 mN/m, enables detection of small differences in surface energy between materials. Measuring the surface energy of graphite helps guide the selection of solvents with appropriate surface tension for exfoliation. The smallest surface tension difference among the solvents used in this study is 2 mN/m (Table A1), so the 4.49 mN/m difference in surface energy between G150 and G50 is considered significant for solvent selection.

The interfacial contact angles between all tested solvents and graphite is lower than 90$^{o}$ (Figure 2.10a,b), showing that both graphite are wettable. However, not all solvents with similar wettability/ interfacial contact angle/ surface tension contribute to the exfoliation efficiency of graphite materials in the same way. For example, NMP, which is known as the best solvent for LPE of graphene, has poorer wettability (larger interfacial contact angles) than the green solvents tested besides water. NMP also has much higher surface tension than the surface energies of both G150 and G50 graphite. The reason why IPA wets graphite surface (G50 and G150) better than NMP, can be explained by the low interfacial contact angle between IPA and graphite surface. This again proves that the NMP is superior to IPA in producing high yield graphene mainly because of its high dispersibility rather than the exfoliation efficiency. Green solvents (besides D.I.), have the magnitude of the surface tension close to the surface energies of both graphite used, which is close to 20 mN/m. However, the exfoliation efficiencies of green solvents toward graphite varies. Polar to dispersive component ratio of surface tension, $\sigma_p/\sigma_d$, is another possible way to explain the trend in exfoliation efficiency.[138, 242]

OWRK model was used to calculate the polar component, $\sigma_s{}^p$, and dispersive component, $\sigma_s{}^d$, of graphite (Section A.2.2). The difference in $\sigma^p/\sigma^d$ between graphite and the solvent ($\Delta\sigma_{(p/d)}$) media was used to evaluate the exfoliation efficiency (Figure 2.10c,d). $\Delta\sigma_{(p/d)}$ for NMP is lower than that for green solvents despite its large surface tension difference with G150 and G50 graphite. This explains its high exfoliation efficiency. Similarly, IPA, the solvent having exfoliation efficiency close to that of NMP, shows low $\Delta\sigma_{(p/d)}$ as well. On the other hand, acetone and D.I. which show high $\Delta\sigma_{(p/d)}$, have low exfoliation efficiencies.

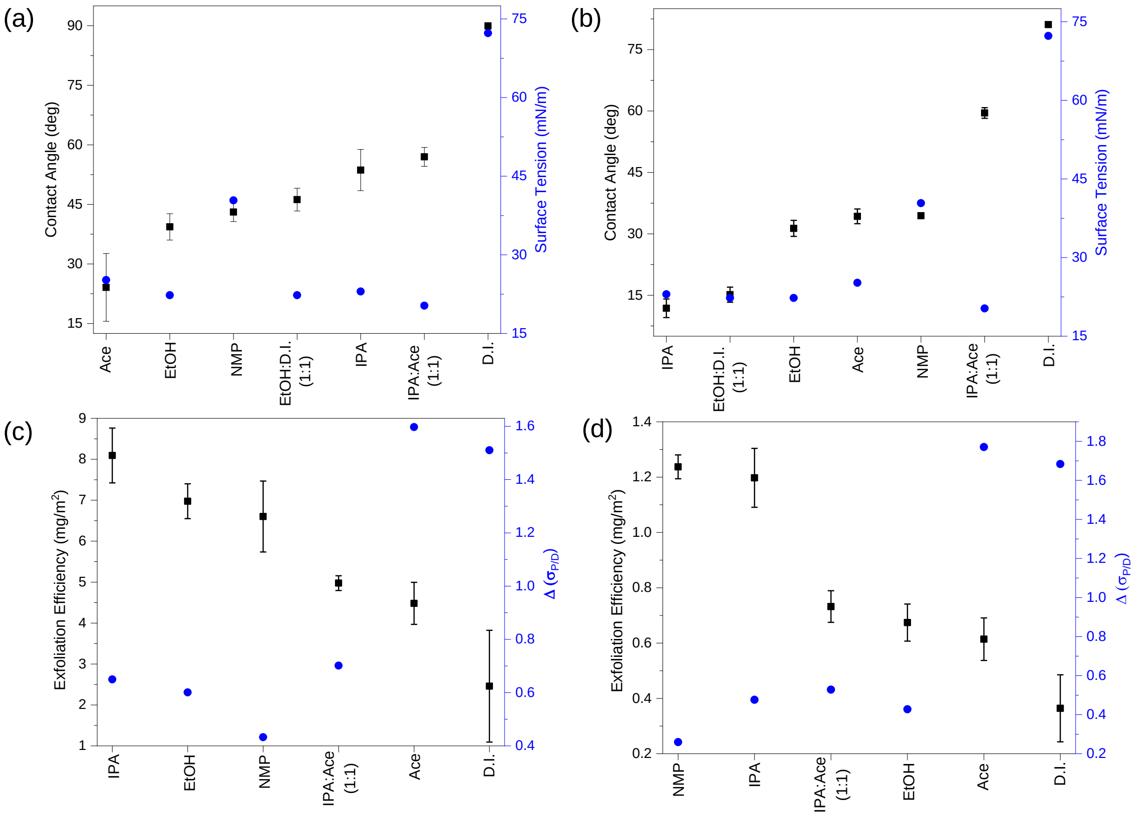

**Figure 2.10:** (a) and (b) The interfacial contact angle between the graphite starting materials (G150 and G50) and the exfoliation solvent media listed on the x-axis, and its relationship with the solvent surface tension. The data for G150 and G50 are shown in (a) and (b) respectively. (c)

and (d) show the exfoliation efficiencies of (c) G150 and (d) G50 graphite, and its relationship with the difference in polar to dispersive ratio of surface tension $\Delta\sigma_{(p/d)}$ between solvents and graphite. Adapted from Ng *et al.*, 2022, Ref. [210].

## 2.4.4 The "Mystery" of NMP

It should be noted that although NMP is a well-known solvent for graphene dispersion, certain types of NMPs, such as the non-anhydrous Alfa Aesar (AA) NMP used in this work, have poor graphene dispersibilities similar to those of the green solvents being tested. Exfoliation in non-anhydrous AA NMP produced a final graphene dispersion of concentration 0.006 mg mL$^{-1}$, which was substantially lower than that produced from exfoliation in anhydrous Sigma Aldrich (SA) NMP (0.164 mg mL$^{-1}$ (Figure 2.11). The graphene in non-anhydrous AA NMP also had poor stability. In most of the published works on LPE, graphene was exfoliated under the anhydrous NMP (99.5%).[76, 80] The effect of the presence of a trace amount of water in NMP on its graphene dispersibility has rarely been discussed in the literatures. Gupta et. al found that a trace amount of water in NMP (0.1 mole fraction) resulted in up to ~0.9 mg ml$^{-1}$ concentration enhancement of $MoS_2$.[243] High-density of water molecules localised at the Mo-terminated edges of $MoS_2$ sheets helped in stabilising the dispersion. TMU-water mixture was reported to have a higher performance than NMP in LPE due to the formation of water aggregates and solvent molecules.[244] Nevertheless, the NMP used for comparison in this case was 99% pure with poor dispersibility that only produce a graphene concentration of 0.029 mg/mL. It is ironic that although the type of NMP used has an important bearing on graphene dispersibility, has rarely been discussed in the literatures.

To investigate whether the presence of water in non-anhydrous AA NMP influences its graphene dispersibility, water was removed from non-anhydrous AA NMP using a molecular sieve (mole sieve) prior to exfoliation. There was a 28-fold increase in the graphene concentration after the removal of water from the NMP and 4.7 folds more in concentration after 3 weeks. Interestingly, the dispersion with the mole-sieved AA NMP stayed more stable and did not settle to a complete sedimentation after three- week period of stability test (Figure 2.11). Nevertheless, water has been widely used as an environmental-friendly solvent medium for LPE and also to form mixtures with other solvents for tuning and optimising solvent HSP or surface tension for better graphene dispersibility.[165, 245] To further check whether the poor graphene dispersibility of non-anhydrous AA NMP was caused by the presence of water, 4wt% of water was added into the SA anhydrous NMP, which was the "good" NMP. Surprisingly, the results from Figure 2.11 shows that the addition of water to anhydrous NMP had negligible effect on its graphene dispersibility and this did not prevent it from producing a stable dispersion with high graphene concentration. Same result was recorded with the non-anhydrous SA NMP. Hence, the poor graphene dispersibility of non-anhydrous AA NMP might be caused by the presence of other chemical compound (which still remains unknown at this stage) that might have been removed by the process of molecular sieving, rather than due to the presence of water.

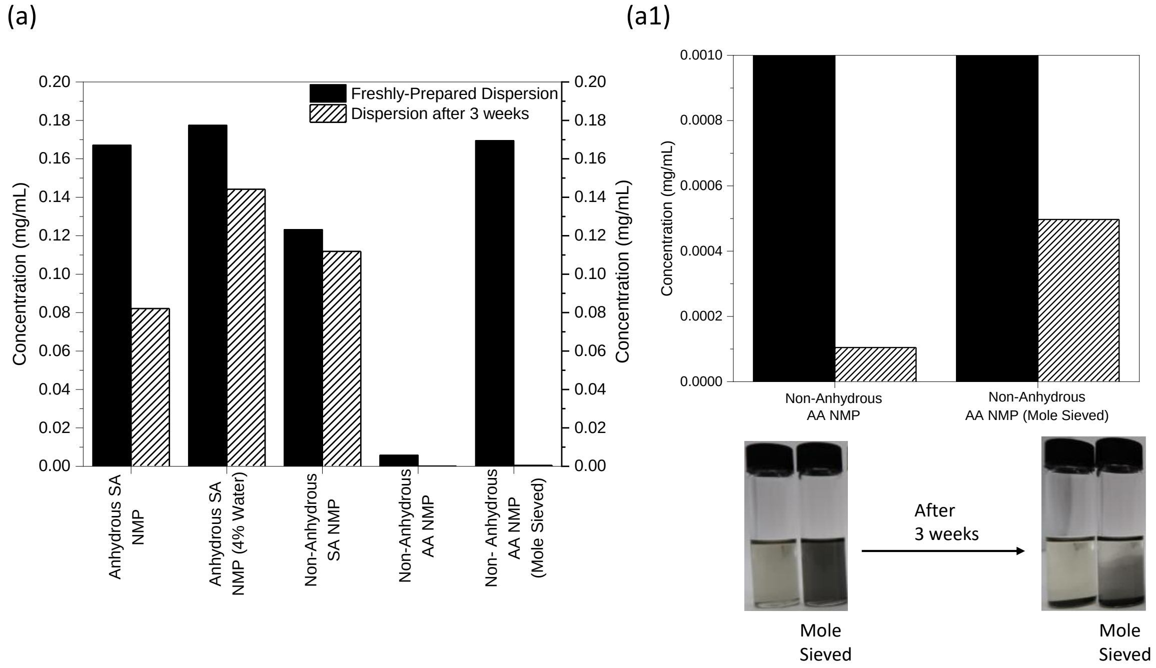

**Figure 2.11:** (a) Concentration of freshly-prepared graphene dispersions and the dispersions after 3 weeks in different types of NMP solvent. (a1) Enlarged graph to compare the concentration after 3 weeks of non-anhydrous AA NMP with and without mole-sieved. Digital images shown are the graphene dispersions in non-anhydrous AA NMP with and without mole-sieved.

## 2.4.5 Graphene Quality Assessment

Besides graphene yield, graphene quality is also a key factor to consider, and it is usually characterised using UV-vis spectroscopy, Raman Spectroscopy, XPS and AFM. The UV-Vis spectra of GR150 and GR50 in different solvents are shown in Figure A4a,b. UV-Vis spectra of NMP-exfoliated GR150 and GR50 redispersed in different green solvents (GS-R) are shown in Figure A4c,d The UV-Vis spectra of GR150 and GR50 are different. GR150 have prominent pristine graphene peak at 270 nm whereas this peak is not prominent for GR50. This indicates that GR50 has been oxidised more, with peak near 230 nm.[246, 247] The peak at ~230 nm which indicates the presence of oxygen species in graphene, is absent in GS-R of both GR150 and GR50. For GS-R, all the graphene is exfoliated in NMP but redispersed in different green solvents. This shows that to a large extent, the degree of oxidation is mainly affected by the exfoliation step due to the presence of cavitation bubbles. The UV-Vis spectra of graphene in NMP (e.g.: NMP-exfoliated and NMP-R graphene) are not suitable for quality analysis since the UV cut-off wavelength is at 285 nm,[248] meaning that graphene signature peaks, 270 and 230 nm for pristine and oxidised graphene respectively, that occur below 285 nm are not detected. Ace and EA also have the UV cut-off wavelength of 330 nm and 260 nm respectively,[248,249] which are near to the graphene signature peaks (Figure A5).

The ratio $I_D/I_{D'}$ observed in Raman spectra can be used to identify defect types in graphene.[220] $I_D/I_{D'}$ value of ~3.5 is characteristic of edge defects with a high density of exposed boundaries, serving as a fingerprint for liquid-phase exfoliated graphene flakes with edge defects.[250] To study the variation of $I_D/I_{D'}$ with different defect types, $sp^3$ and vacancy defects were intentionally introduced via plasma treatment and ion bombardment.[251] Corresponding $I_D/I_{D'}$ values of ~7 and ~13.5 were observed for vacancy and $sp^3$ defects, respectively.[219,251,252] It is important to note that the intensity ratio and positions of the defect-activated D and D' peaks vary with excitation energy, which is dependent on the wavelength of the Raman laser used.[251] To ensure reliable comparison of defects across all graphene samples, a consistent laser wavelength of 532 nm (2.33 eV excitation energy) was used for characterisation.

The results show that the type of defects with and without the NMP-redispersion is similar, except for the EA-exfoliated GR150 (Figure 2.12a). G150 graphite exhibits predominantly vacancy defect whereas G50 graphite exhibits predominantly edge defects, due to its smaller size and more exposed edges. The graphene exfoliated from G150 and G50 also exhibit predominantly vacancy and edge defects respectively, in all the selected solvents. After redispersing the exfoliated graphene from each of the selected solvents into NMP (refer to the NMP-R results), the type of defects for GR50 shift from edge defects to vacancy defect. This shows NMP disperses graphene with larger lateral size (less exposed edges). This is due to the higher density of NMP as compared to other green solvents studied.

FWHM of G peak is a more accurate way to determine the lattice disorder as compared to the commonly used D to G peak intensity ratio ($I_D/I_G$).[219, 225] This is because D peak intensity ($I_D$) does not fully represent lattice disorders, because it is affected by the amount and types of edges (armchair or zig-zag) in relative to the laser polarisation direction. GR50 has a higher lattice disorder than the GR150 due to the higher G peak FWHM (Figure 2.12b). For GR50, the NMP-R GR50 has higher lattice disorder and defect density than without NMP-R. This is due to the higher density of NMP as compared to other green solvents, it disperses wider range of graphene which includes highly disordered graphene. The Raman spectra of GR150 and GR50 with and without NMP-redispersion is shown in Figure A6.

The quality of the graphene produced is compared to the commercial graphene by Raman Spectroscopy. The Raman spectra of GR150, which is the graphene with less disorder and defect is chosen for comparison with the commercial graphene (Figure A7). GR150 exfoliated in IPA and NMP, which are the solvents with high exfoliation efficiency, are compared with the commercial graphene. The spectra were normalised to the highest intensity G peak. There is no obvious difference in both, the defect density (D peak) and the number of layers (2D peak) between in-house fabricated GR150 and commercial graphene.

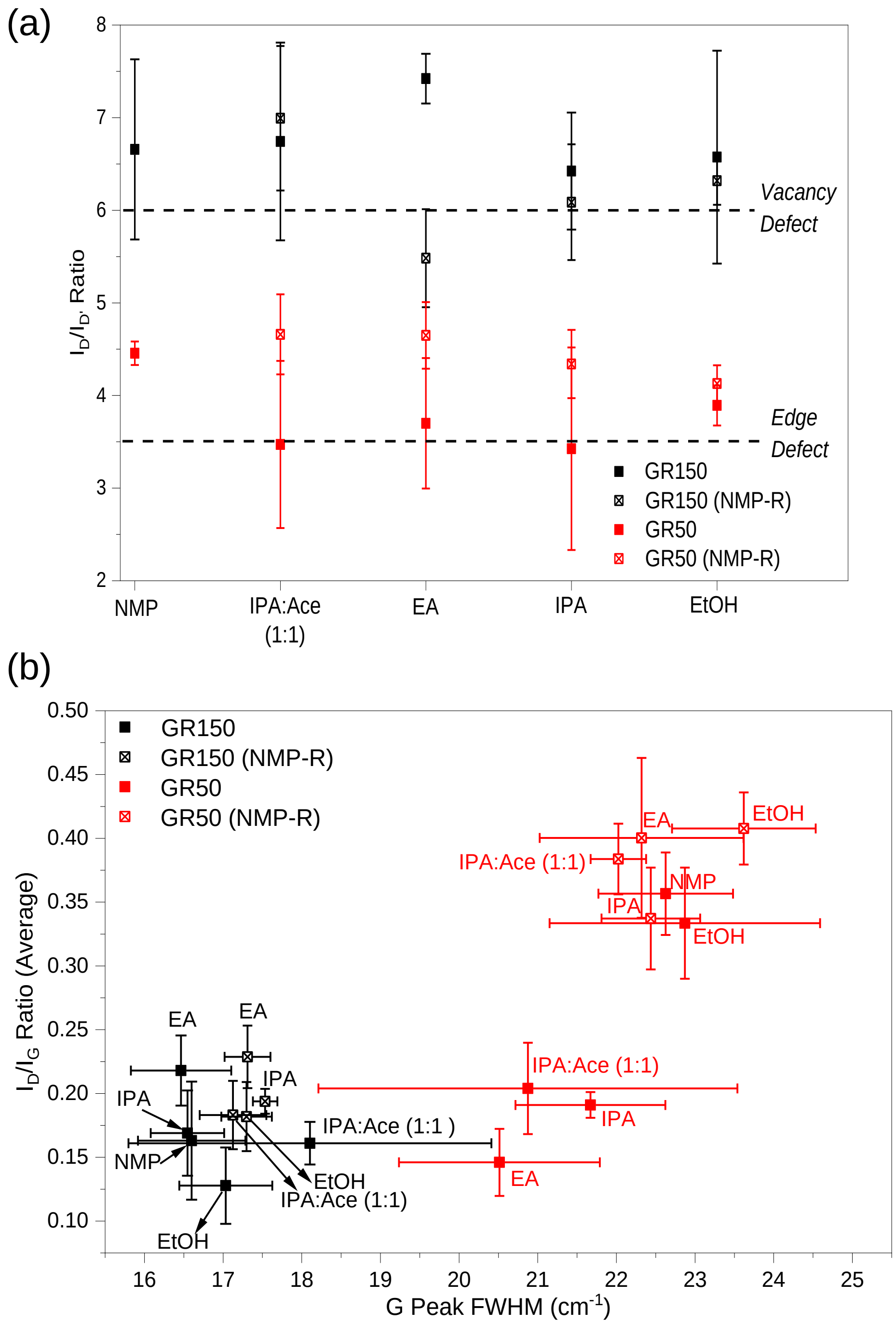

**Figure 2.12:** Raman spectroscopy analysis for GR150 and GR50 before and after NMP redispersion (NMP-R) on (a) the type of defects (D/D' intensity ratio) and (b) the defect density (D/G intensity ratio) against disorder (G peak FWHM). Error bars are constructed from the standard deviation of measurements at a minimum of six randomly selected points on the sample. Adapted from Ng *et al.*, 2022, Ref. [210].

The thickness of for GR150 and G50 exfoliated in IPA, which is the best-performed green solvent, is analysed with AFM. The exfoliated GR150 in IPA shows very homogenous leaf-like structure with lateral sizes approaching the micron scale, and with thickness ranging from five to nine layers (Figure 2.13a). GR50 exfoliated in IPA are smaller in lateral sizes but thicker than the IPA-exfoliated GR150 (Figure 2.13b). This shows the structure and morphology of the initial graphite materials influences the quality and lateral size of the graphene produced, while the solvents affect more on the quantity or yield of the graphene produced. Since NMP was used as the standard dispersing medium and tool to investigate the amount of graphene produced, additional AFM data was also obtained to confirm the presence of graphene for the samples after NMP-R. To prove the reliability of NMP in NMP-R technique only dispersed graphene and not graphite, additional AFM characterisations on the IPA-exfoliated GR150 graphene which has been redispersed in NMP was carried out. The AFM image (Figure A8) shows GR150 graphene exfoliated from IPA and redispersed in NMP still retaining its original leaf-like structure (shown in Figure 2.13a) of less than 10 layers thick. The “spots” in the AFM image are the remaining NMP residue, despite thorough cleaning with ethanol. This also shows the difficulty in getting rid of NMP completely.

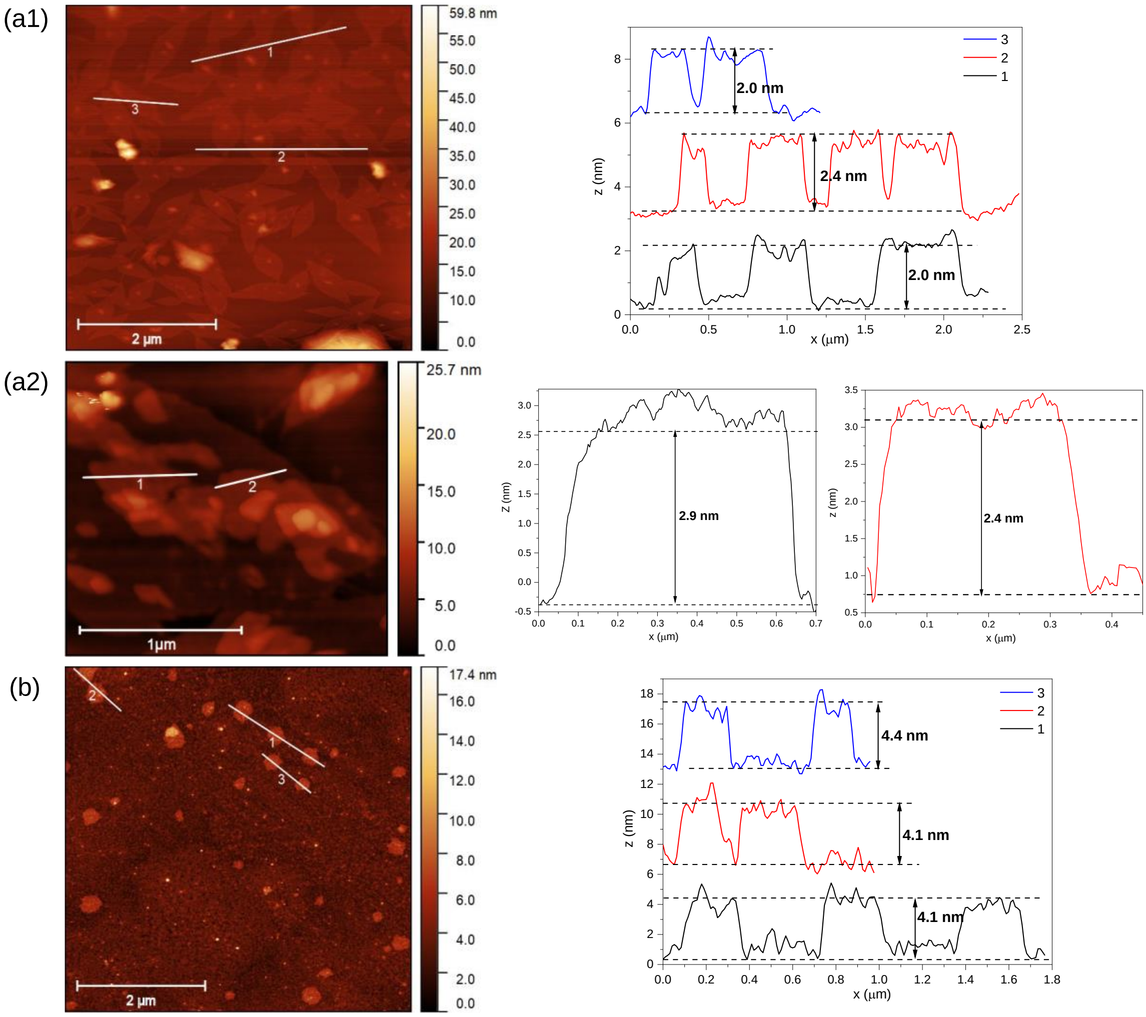

**Figure 2.13**:Atomic Force Microscopy thickness analysis performed on (a1and a2) GR150 and (b) G50 exfoliated in IPA. Adapted from Ng *et al.*, 2022, Ref. [210].

## 2.5 Conclusion

The conventional LPE method is unable to "unfold" the actual amount of graphene exfoliated in green solvents with low graphene dispersibility because the amount collected is constrained by the "incomplete" graphene dispersibility of the solvent media. Therefore, NMP-R and GS-R methods have been established for a reliable and independent investigation of the exfoliation efficiency and dispersibility of a given solvent in LPE of graphene. The main outcomes of this chapter are summarised as follows:

1. The NMP-R method designed in the present work has enabled the reliable determination of the actual amount of graphene exfoliated from each solvent, or the exfoliation efficiency. Besides this, the GS-R method also allows the determination of the solvent dispersibility.
2. By independently studying the exfoliation efficiency and dispersibility, it has been found out that IPA solvent has high exfoliation efficiency, close to the that of the state-of-art NMP solvent, despite of its low graphene dispersibility.
3. By "deconvoluting" the overall graphite yield into exfoliation efficiency and dispersibility, the right green solvent can be selected for each of the exfoliation and disperse process. Graphene concentration can be enhanced up to 16 times, by dispersing the graphene exfoliated in the solvent with high exfoliation efficiency but low graphene dispersibility, into solvent with high dispersibility.
4. The surface energy analysis by Washburn method showed that green solvents like IPA and EtOH have surface tension close to the surface energy of G150 and G50. This explains the high exfoliation efficiency of green solvents.

# 3

# Graphene Yield Enhancement by Post-Exfoliation Ultrasonication (PEUS)

## 3.1 Overview

Previous chapter focused on the exfoliation efficiency and dispersibility, and how these could be evaluated independently. This chapter will focus on optimising the final graphene yield through concentration analysis for the graphene dispersions in green solvents.

Hansen Solubility Parameters (HSP), which is known as the rule-of-thumb for selecting a suitable solvent for LPE in order to achieve high graphene yield, based on the like-dissolve-like principle. To obtain a high graphene yield, the solvent and graphene need to have the similar HSPs. This theory of solvent-graphene interactions is more suitable for describing the dispersibility of graphene in solvent, where no external exfoliation mechanism is involved. Graphite (not graphene)-solvent relationship needs to be considered in the exfoliation process. Up to date, most of the studies on the solubility parameters are limited to the ultrasonication exfoliation technique only. This ponders a question as whether the relationship between solvent HSP and graphene yield varies with the exfoliation technique or mechanism used? In this case, will the HSP theory still apply if different exfoliation mechanisms and graphite type is involved? To elucidate this question, the study on graphene yield vs. solvent HSP for the graphene exfoliation using both ultrasonication and shear mixing technique was performed here. Two different graphite starting materials (Figure 2.1) were used for the exfoliation process.

Besides solvent HSP, the shear force generated by solvent during exfoliation will also affect the graphene yield. The shear force for graphite exfoliation is the force from the liquid layers that acts parallel to the graphite surface causing its surface layer to “slide” over the layer underneath. As such, this shear force has the solvent-dependent properties. The work on shear force generation in different green solvents, especially, the shear mixing parameters used in this study were carried out in collaboration with Dr. Qin Lin from University of Wyoming. This helped in the selection of the right green solvent to fulfil both the requirements of the shear force and surface tension (discussed in previous chapter) for achieving high graphene yield.

From the study in previous chapter, IPA, which is one of the green solvents, has high graphene exfoliation efficiency similar to the state-of-art NMP. This is due to the high shear forces it generates during the exfoliation process (as will be discussed in this chapter). The main concern of low graphene yields in green solvents is low graphene dispersibility. This is a need to search for an improved method to increase the graphene dispersibility in green solvents for high graphene yield. The new yield optimisation method introduces in the present work is a quick, simple, and scalable physical approach for enhanced dispersion of graphene, negating the needs of NMP, surfactant and functionalisation. This yield optimisation method is denoted as “Post-Exfoliation Ultrasonication (PEUS)” method. This PEUS method incorporates a quick ultrasonication step after shear mixing exfoliation and before the centrifugation, to enhance the dispersion of the exfoliated graphene flakes. The yield increase of up to 90 times was achieved without degrading the graphene quality. The quality of graphene produced was examined and assessed in the aspects of the degree of oxidation, thickness, and crystallinity. This simple idea on yield optimisation resolves the drawback of green solvents and paves the way for sustainable production of high quality and high yield graphene in green solvents.

# 3.2 Materials and Method

## 3.2.1 Materials

**Solvents:** 2-propanol (Sigma Aldrich, ≥99.8 %, GC grade), Acetone (Sigma Aldrich, ≥99.5 %, GC grade), Ethanol (Sigma Aldrich, ≥99.8 %, GC grade), Ethyl Acetate (Sigma Aldrich, ≥99.5 %, GC grade), Methanol (Sigma Aldrich, ≥99.9 %, HPLC grade), 1-Methyl-2-Pyrrolidinone (Sigma Aldrich, ≥99.5 %, anhydrous)

**Graphite:** Two types of graphite detailed in Section 2.2.1 were used.

## 3.2.2 Method

### 3.2.2.1 Shear Mixing Exfoliation

The method used to produce graphene is the same as the shear mixing exfoliation method described in Section 2.2.2.1.

### 3.2.2.2 Post-Exfoliation Ultrasonication (PEUS) Yield Enhancement

After three-hour shear mixing exfoliation, the graphene-containing exfoliation product* was ultrasonicated in a bath sonicator (50-60 kHz and 700 Watts) for two minutes, unless stated otherwise. This was followed by the centrifugation at 500 rpm (or 52 rcf) for one hour to obtain the final graphene dispersion. This yield optimisation method is denoted as the PEUS method, and 2 US is the associated ultrasonication step in PEUS. The graphene dispersion produced with this PEUS method by using 2 US was denoted by GR150 (2 US) or GR50 (2 US).

The controlled experiment was carried out to study the effect of two-minute ultrasonication in PEUS. This was done by two-min ultrasonication (2 US) directly on the graphite starting materials (without the shear mixing exfoliation), followed by the centrifugation to obtain the final dispersion. This dispersion is denoted by C-GR150 (2 US) or C-GR50 (2 US).

Three-hour ultrasonication exfoliation technique was also used as the comparison with three-hour shear mixing. The temperature of the ultrasonication bath is controlled at room temperature (22 °C) throughout the entire process. Ultrasonication exfoliation was carried out by exfoliating 3.75 g of graphite in 150 mL of solvent (25 mg/mL concentration) in a glass beaker, which is the same as in shear mixing (Section 2.2.2.1). The beaker was covered using a film and lid to keep the solvent from evaporating away. The graphene dispersion produced using this method was labelled as US-GR150 or US-GR50. The abbreviations for each type of graphene dispersion, along with their corresponding production routes, are illustrated in Figure 3.1.

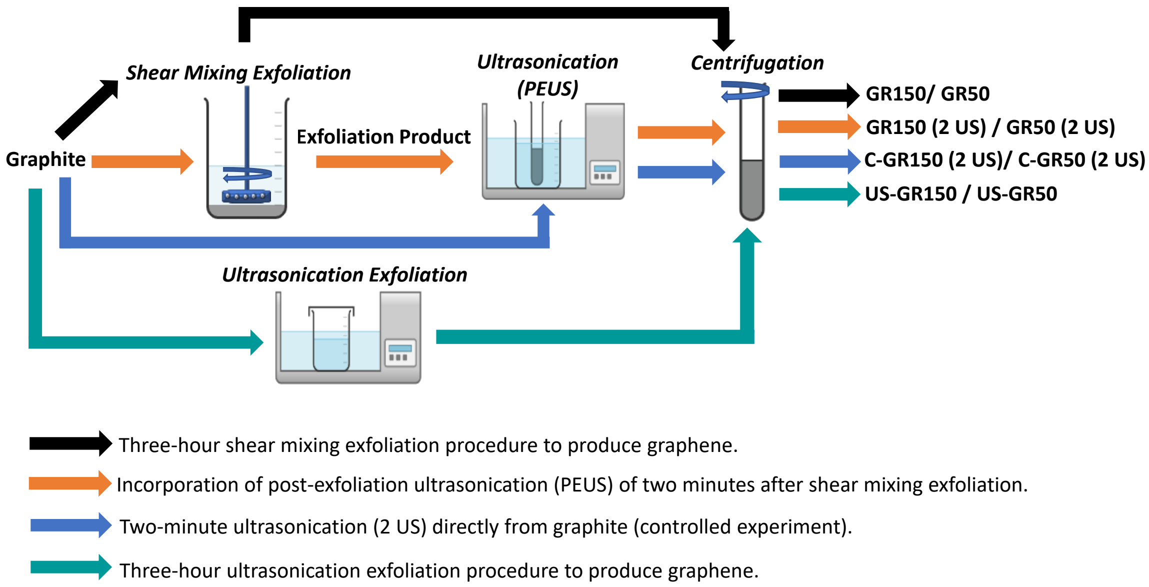

**Figure 3.1:** Schematic diagram showing the procedures and routes to produce different graphene-containing dispersions in this work.

**Exfoliation products: the graphene-containing products with graphite aggregates obtained after exfoliation and before centrifugation.*

## 3.2.3 Characterisations

### 3.2.3.1 Raman Spectroscopy

The sample preparation method, Raman operating conditions and acquisition parameters used were the same as those in Section 2.2.3.1. Besides the defect density and the defect type analysis mentioned in Section 2.2.3.1, in this chapter, Raman Spectroscopy was also used to estimate the number of layers.

The number of graphene layers was calculated from an empirical formula based on the analysis of 2D peaks.[76] The thickness of few-layer graphene nanosheets were reflected by the shape of the 2D bands (~2700 $cm^{-1}$). Two variables in this formula are $\omega_{p,G'ite}$, the wavenumber of the graphite 2D band peak; and $\omega_{s,G'ite}$, the wavenumber of the graphite 2D band shoulder. Since the peak for $\omega_{\mathrm{p,G'ite}}$ is well defined and can be identified easily and the shoulder is poorly defined, therefore, $\omega_{\mathrm{s,G'ite}} = \omega_{\mathrm{p,G'ite}} - 30\ \mathrm{cm}^{-1}$ was established. However, the peak-to-shoulder intensity ratio ($\mathrm{I}_{\mathrm{G'ene}}(\omega = \omega_{\mathrm{p,G'ite}})/\mathrm{I}_{\mathrm{G'ene}}(\omega = \omega_{\mathrm{s,G'ite}})$) alone is not an effective metric. It varies according to the graphite source. Hence, the graphene intensity ratio is normalised to that of graphite. This gives a metrics, M, in Equation 3.1,[76] which varies with flake thickness:

$$M = \frac{I_{G'ene}(\omega = \omega_{p,G'ite}) / I_{G'ene}(\omega = \omega_{s,G'ite})}{I_{G'ite}(\omega = \omega_{p,G'ite}) / I_{G'ite}(\omega = \omega_{s,G'ite})} \qquad 3.1$$

Flake layers, $N_G$ can be described empirically by $\mathrm{N_G} = 10^{0.84\mathrm{M}+0.45\mathrm{M}^2}$. They estimated the error to be ±1.5 layers.[76]

All spectra for the graphene were collected under the same acquisition parameters as the graphite starting materials used. This is because the results are sensitive to any shift in the 2D band of the graphene spectrum being analysed in relative to the spectrum of the graphite used.

### 3.2.3.2 UV-Vis Spectroscopy

The UV-Vis characterisation was conducted using Cary 5000 UV-Vis-NIR (Agilent) in dual-beam mode, with the scan rate of 100 nm/ min in the range of 200 nm to 700 nm or 250 nm to 700 nm (NMP-dispersed samples due to the UV cut-off wavelength). The sample preparation steps and data analysis are as detailed in Section 2.2.3.2.

### 3.2.3.3 X-Ray Photoelectron Spectroscopy (XPS)

The XPS analysis was performed using Thermo Scientific K-Alpha XPS with microfocused monochromated Al Kα X-ray source at 12 keV with 400 μm spot size. The analyser operated at a constant analyser energy (CAE) of 200 eV for survey scans and 50 eV for detailed (high resolution) scans. Charge neutralisation was applied using a combined low energy / ion flood source.

Data acquisition and analysis were performed with Thermo Scientific Avantage software. Normalised atomic percentages were determined from peak areas of the elemental main peaks detected using the survey scan following background subtraction and the application of Thermo sensitivity factors.

### 3.2.3.4 X-Ray Diffraction (XRD)

Bruker D8 ADVANCE Eco and Siemens D5000 X-ray diffractometer (XRD). The XRD was operated at 40 kV, and 40 mA using Cu Kα radiation, with step size of 0.02° and scan rate of 5s per step.

### 3.2.3.5 Atomic Force Microscopy (AFM)

The procedure for AFM is the same as detailed in section 2.2.3.3. Briefly, an Agilent 5400 AFM was used. The samples were prepared by drop casting graphene solutions on a Si/SiO2 wafer placed on a hot plate, heated to 80 °C (for green solvents). The probe used was MikroMasch HQ:NSC35/AI BS (silicon tips) with resonance frequencies between 150 and 300kHz and the scanning mode used was the tapping mode.

## 3.3 Background

### 3.3.1 Hansen Solubility Parameters (HSP) Distance

The concept of HSP, which is closely related to surface energy, was introduced and explained in Section 1.3.3, Chapter 1. HSP distance between graphene and solvent (Equation 3.2) is normally being used to access the suitability of the solvent for LPE. However, instead of using the solvent HSP distance with respect to (w.r.t.) graphene to access the solvent suitability, HSP distance w.r.t. NMP is selected to be used. This is because different types of graphite exhibit varying surface energies (refer to Section 2.4.3), and same applies to graphene. Graphene's surface energy ranging from 37 mJ/m² to 180 mJ/m², depending on the size, defect and measurement technique.[253,254]As a result, using HSP or surface energy of graphene as a reference is challenging unless measured with high accuracy. In contrast, the HSP and surface tension of commonly used solvents like NMP are well-established.[248] NMP's proven ability to disperse a range of 2D materials with varying surface energies suggests its broad compatibility.[255,256] Therefore, NMP can serve as a useful benchmark for evaluating solvent effectiveness for graphene, despite variations in graphene's surface energy, simplifying the comparison of other solvents based on their HSP distances to NMP.

The work by Yi et al. involved the tuning of solvent HSP using the acetone and water solvent mixture in mimicking the HSP of NMP.[165] The closer the solvent HSP distance w.r.t. NMP, theoretically, the higher the graphene concentration. The study on the effect of solvent HSP on graphene yield is usually done using ultrasonication exfoliation technique. Shear mixing was the selected exfoliation technique used in this work whereas ultrasonication is the more widely used technique. It is questionable whether the HSP distance w.r.t. NMP theory is applicable if different exfoliation method/mechanism (e.g.: shear mixing) and different graphite starting materials are used. In this aspect, the HSP study was performed using two different exfoliation methods (shear mixing and ultrasonication) and two different graphite (G150 and G50) are used in this study.

The calculation for each of the of dispersive, polar and hydrogen bond components of the solvent that represented by $\delta_D$, $\delta_P$ and $\delta_H$ respectively, is shown as followed:

$$\delta_{DM'} = \frac{(a\delta_{D1} + b\delta_{D2})}{a+b} \tag{3.2a}$$

$$\delta_{PM'} = \frac{(a\delta_{P1} + b\delta_{P2})}{a+b} \tag{3.2b}$$

$$\delta_{HM'} = \frac{(a\delta_{H1} + b\delta_{H2})}{a+b} \tag{3.2c}$$

The subscript 'M' refers to the HSP components of the mixture, while subscripts '1' and '2' denote the HSP components of the two solvents used to form the mixture. The values for $\delta_D$, $\delta_P$ and $\delta_H$ of the solvents are shown in Table 3.1. $a$ and $b$ are the volume fractions of Solvents 1 and 2 (indicated by subscripts 1 and 2) respectively.

The HSP distance, $R_a$ between the solvents or solvent mixtures used in this work with that of NMP solvent was calculated from Equation 3.3:

$$R_a = \sqrt{(4(\delta_D - \delta_{D(NMP)})^2 + (\delta_P - \delta_{P(NMP)})^2 + (\delta_H - \delta_{H(NMP)})^2} \tag{3.3}$$

$\delta_D$, $\delta_P$ and $\delta_H$ are the HSP components of the solvents, or the solvent mixtures calculated from Equation 3.2a,b,c.

**Table 3.1**: Solvents HSP and calculated HSP distance w.r.t. NMP.[154,257,258]

| Solvent/ Solvent Mixture | δD [MPa$^{1/2}$] | δP [MPa$^{1/2}$] | δH [MPa$^{1/2}$] | Distance to NMP [MPa$^{1/2}$] |
|---|---|---|---|---|
| NMP | 18 | 12.3 | 7.2 | **0** |
| Acetone | 15.5 | 10.4 | 7 | **5.35** |
| IPA: Acetone (1:1) | 15.65 | 8.25 | 11.7 | **7.66** |
| Ethyl Acetate | 15.8 | 5.3 | 7.2 | **8.27** |
| 2-propanol (IPA) | 15.8 | 6.1 | 16.4 | **11.93** |
| Ethanol | 15.8 | 8.8 | 19.4 | **13.43** |
| Methanol | 15.1 | 12.3 | 22.3 | **16.18** |
| Ethanol: Deionised Water (1:1) | 15.7 | 12.4 | 30.85 | **24.09** |
| Water | 15.6 | 16 | 42.3 | **35.62** |

## 3.3.2 Shear Force Simulation

Shear force is also one of the factors that affects the exfoliation efficiency, besides the interfacial surface tension between graphite and solvent (as discussed in Section 2.4.3 Chapter 2). The shear force is calculated as followed:

$$\tau = \mu \frac{d\gamma}{dt} \tag{3.4}$$

$\tau$ is the shear stress, $\frac{d\gamma}{dt}$ is the rate of strain and $\mu$ is the dynamic viscosity. According to Equation 3.4,[259] high viscosity gives more effective shearing (or exfoliation) of graphene layers. The organic solvents used in this research are Newtonian fluids, which means the viscosity remains unchanged with the strain rate.[260] For the shear mixing exfoliation technique that was used in this research, the strain/shear rate was determined by the speed of shear mixer rotor, which was fixed in this work. For Newtonian fluid with higher viscosity, the shear stress was higher at a given strain rate. The shear force was simulated by Dr Ling Qin, using "Ansys Fluent 14", specific to the dimensions of the rotor and stator used for the shear mixing exfoliation in this work. Solvent properties used in the simulation include density, viscosity, saturated vapor pressure, surface tension, heat capacity and sound speed. Schneer and Sauer (2001) cavitation model was used to check the formation of the cavitation bubbles,[261] and there were no significant cavitation bubbles generated at the mixing speed used in this work, which is 5000 rpm. Hence, the main exfoliation mechanism is still by the shear force instead of the shock wave generated by the cavitation.

## 3.4 Results and Discussions

### 3.4.1 Shear Force Study

Shear force generated by the solvent during shear mixing exfoliation process is one of the factors that determines the exfoliation efficiency, besides the difference in polar and dispersive components of surface energy ($\sigma^p/\sigma^d$) between graphite and solvent (Section 2.4.3). Despite of its high HSP distance w.r.t. NMP, the shear force produced from the exfoliation in water is sufficient for the exfoliation of graphene layers from graphite. The main problem of the low graphene concentration in green solvents is due to their inabilities to stabilise or disperse the exfoliated graphene. This fact is evident and discussed in Chapter 2. From the shear force simulation results in Figure 3.2 (a1 and a2), although D.I. water can generate high shear force compatible to that of NMP, its exfoliation efficiency is low. This is a consequent of the significant difference in $\sigma^p/\sigma^d$ between graphite and D.I. solvent. Being able to generate large shear force comparable to that of D.I., IPA has the advantage in exfoliation efficiency due to the small difference between its $\sigma^p/\sigma^d$ to that of graphite. Since, MeOH and Ace solvents possess low shear force and large difference in $\sigma^p/\sigma^d$ compared to graphite, they have low exfoliation efficiency (Figure 3.2b). Results from shear force simulation show that the exfoliation efficiency is governed by the interplay between the shear force and the difference in $\sigma^p/\sigma^d$, between graphite and solvent. Shear force can be increased by increasing the rotor speed of the shear mixer. This results from simulation of shear forces at different rotor speeds also presented in Figure 3.2(a2). The differences in the magnitudes of the shear forces produced from different solvents shows increased significance at high rotor speeds of between 8000 to 12000 rpm.

*Note: Black and red graphs shown in the results and discussion section represent the data for G150/GR150 and G50/GR50, respectively.

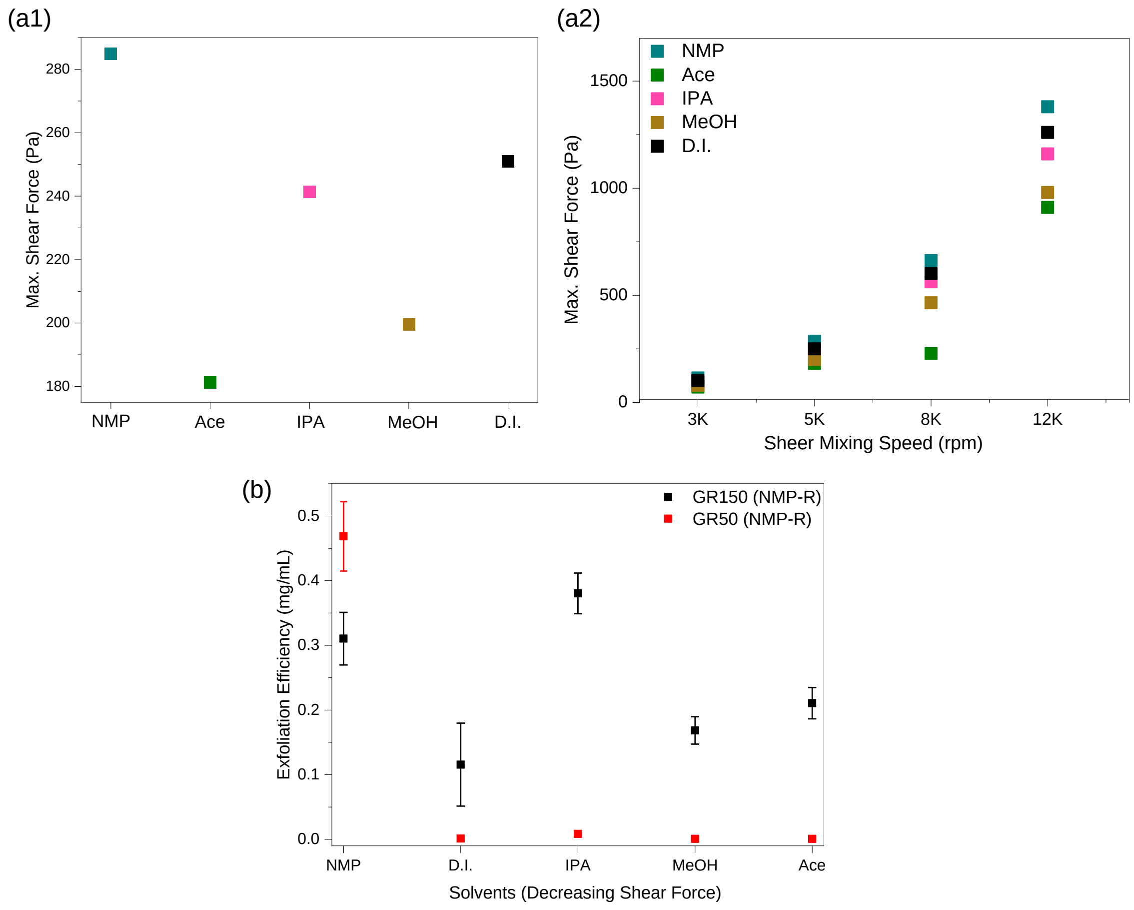

**Figure 3.2:** (a1) Maximum shear forces of different solvents at speed of 5K rpm and (a2) Comparison of maximum shear forces generated at different shear mixing rotor speeds. (b) The correlation between solvent exfoliation efficiency and shear force in the productions of GR150 and GR50. Error bars showed the standard deviation obtained through at least three sets of repeated experiments.

## 3.4.2 Solvent HSP Distance w.r.t. NMP

Figure 3.3 show the correlations between solvents' HSP distance w.r.t. NMP and graphene concentrations obtained with different exfoliation mechanisms (shear mixing and ultrasonication) on G150 and G50 graphite. The UV-Vis spectra from graphene dispersions in selected solvents, with UV cut-off beyond the main absorption peak at 270 nm are shown in Figure B1. The synthesis procedures for all the graphene samples can be found in Figure 3.1. The data points for GR150 and GR50 are generated based on the average of three repeated experiments. Data points for US-GR150 and US-GR50 are based on a single experiment, as all exfoliation containers, containing G150 and G50 graphite dispersed in different solvents, were processed simultaneously in the same sonicator. This standardised setup gives reliable comparison of US-GR150 and US-GR50 concentrations across different solvent media.

Solvents on the x-axis of the graphs are arranged in an increasing order of the HSP distance w.r.t. NMP. Theoretically, high graphene concentration is achieved when the solvent has close HSP distance w.r.t. that of NMP. This implies that concentration should decrease across the x-axis. However, this trend is not generally observed in Figure 3.3. Ace, the solvent with closest HSP distance w.r.t. NMP has the lowest concentrations of GR150 and GR50 from the shear mixing exfoliation of G150 and GR50 graphite. But, it yields the highest concentration of ultrasonication exfoliation of G150 graphite (US-GR150). This shows that the trend in solvent HSP vs. graphene yield varies with both the graphene/graphite types and the exfoliation method used (mechanisms involved). For graphene produced by shear mixing (GR150 and GR50), the trend in graphene concentration vs. solvent HSP is similar for both GR150 and GR50. However, for graphene produced via ultrasonication (US-GR150 and US-GR50), the trend varies with graphene type. The solvent requirement for the exfoliation of larger size G150 graphite depends greatly on the exfoliation technique used (shear mixing or ultrasonication). Shear mixing exfoliation "peels-off" the graphene layer from graphite surface while ultrasonication involves fragmentation as the first step to create active edges before peeling-off the layers through the intercalation of cavitation bubbles.[262, 263] The smaller size G50 graphene reduces the fragmentation event during ultrasonication. Therefore, the solvent requirement for shear mixing and ultrasonication exfoliation for G50 are the same.

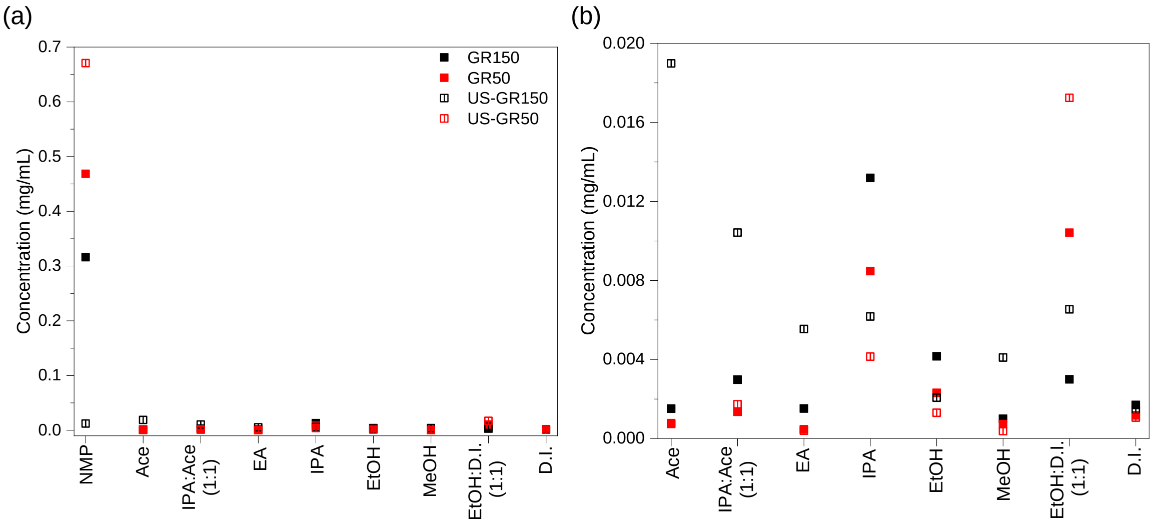

**Figure 3.3:** (a) The concentration of graphene obtained using different exfoliation technique (shear mixing and ultrasonication). Graphene obtained through shear mixing is labelled as GR150 and GR50; graphene obtained through ultrasonication is labelled as US-GR150 and US-GR50. (b) Enlarged graph to show the green solvents region (excluding NMP). The solvents in x-axis are arranged in the increasing order of solvent HSP distance w.r.t. NMP.

Since, solvent selection for high graphene yield/concentration is specific to the exfoliation technique used and graphene type, the effective solvents for GR150 exfoliation using ultrasonication are the acetone-containing solvents (Ace and IPA:Ace*) whereas for GR50, it is the EtOH:D.I.* solvent mixture. IPA is the effective solvent for shear mixing exfoliation of both GR150 and GR50, but not for the ultrasonication exfoliation. By analysing the graphene concentration produced from different graphite sources using shear mixing and ultrasonication exfoliation techniques, we can select the right solvent specific to the graphite type and the exfoliation technique used.

**IPA:Ace and EtOH:D.I. are the solvent mixtures with 1:1 volume ratio.*

## 3.4.3 PEUS Method for Yield Enhancement

### 3.4.3.1 Graphene Concentration Analysis with PUES (2 US)

Graphene yields in green solvents are usually low (only about half of the concentration produced in NMP under same operating condition).[78, 163] Methods to improve graphene yields in green solvents include surface functionalisation, use of surfactant or increase the exfoliation time and temperature.77, 152, 153 All these methods inevitably impose defects on graphene and increase its oxidation level. To date, the production of high yield and high-quality pristine graphene in green solvents remains as a formidable challenge. Ultrasonication technique is the most fundamental and common technique used in LPE. However, its major drawbacks include long ultrasonication time of more than 2 hours, which is necessary for exfoliation. This causes the heating of the solvent medium, leading to the generation of defect and oxygen-containing species on graphene.[266] Defects and oxidation of graphene lower its electrical conductivity.[267] On top of this, there is also a lack of consistency in the qualities of the graphene produced via ultrasonication. This hinders its scalability. Shear mixing is an alternative method to ultrasonication for graphene exfoliation and its scalability has been proven.[76]

Although ultrasonication is not a preferred exfoliation technique used in this work, it is effective for dispersing the exfoliated graphene-containing products. In search of a way to improve graphene dispersibility in green solvents, two-minute ultrasonication (2 US) was imposed on the graphene-containing product obtained right after shear mixing exfoliation and before the centrifugation have been found to increase the graphene concentrations in all the solvents tested. This post-exfoliation ultrasonication (PEUS) method helped to disperse the exfoliated graphene, enabling more well-dispersed exfoliated graphene to be collected as the supernatant after centrifugation. This combination of shear mixing (exfoliation)-ultrasonication (dispersion) approach has been demonstrated for the first time, to be the key to the production of high-yield pristine graphene with minimum defects and oxidation levels. The schematic diagram of the experimental procedures involved in the graphene productions and the details on the abbreviations used for the graphene products are shown in Figure 3.1.

Figure 3.4b shows the enhancement in graphene concentration after PEUS-2 US to disperse the exfoliated graphene. In general, the introduction of the 2 US step in the PEUS method causes an increase in graphene concentration, regardless of the solvent and graphite types. This shows that the 2 US step is effective in dispersing the exfoliated graphene. Nevertheless, the amount increased depends on the solvent and graphene type. The UV-Vis spectra of the graphene dispersions produced in the respective solvents with and without 2 US step are shown in Figure B2. In the light of the above arguments, solvents less effective in shear mixing exfoliation of graphene could otherwise be effective for dispersing the exfoliated graphene through ultrasonication (2 US). Shear mixing exfoliation and dispersion of graphene via ultrasonication are two distinct mechanisms with different characteristics of solvent requirements. In this respect, shear mixing exfoliation requires high viscosity to generate shear force to exfoliate the graphene layers,[76] while the process of ultrasonication requires low viscosity to generate cavitation bubbles to disperse the exfoliated graphene.[95] For example, IPA:Ace and EA both lead to significant increase in the concentration of the exfoliated GR50 (up to 90 times in EA) after the 2 US step, despite being a less effective solvent for shear mixing and ultrasonication exfoliation compared to EtOH:D.I. and IPA. In the case of GR150, EtOH shows the highest increase in graphene concentration after the 2 US treatment, followed by IPA:Ace. IPA:Ace can disperse both GR50 and GR150 well upon ultrasonication.

The enhancement in graphene concentration after the introduction of 2 US step in PEUS depends on (i) the shear mixing exfoliation efficiency and, (ii) the effectiveness of solvent to disperse the exfoliated graphene by ultrasonication. The effectiveness of solvent to disperse the exfoliated graphene by 2 US step is reflected in the concentrations of US-GR150 and US-GR50 exfoliated from three-hour ultrasonication. IPA:Ace and Ace both show a high concentration of US-GR150, despite of its lower shear mixing exfoliation efficiency than EtOH (Figure 3.3b). This suggests that Ace and IPA:Ace are effective in generating cavitation bubbles upon ultrasonication to disperse the exfoliated GR150 graphene because of its low viscosity. Despite of the good ability in dispersing GR150 through 2 US, the overall concentration of GR150 (2 US) in IPA:Ace and Ace are still lower than IPA because of its low shear mixing exfoliation efficiency (low amount of graphene produced after shear mixing exfoliation), as shown in (Figure 2.7, Chapter 2). EtOH gives the highest concentration increase for GR150 and high concentration for GR150 (2 US) mainly due to its high shear mixing exfoliation efficiency. For GR50, EA has high exfoliation efficiency towards GR50, and its low viscosity facilitates the ultrasonication dispersion. Therefore, it gives one of the highest concentrations increase upon 2 US step to produce GR50 (2 US).

The degree of materials dispersibility through ultrasonication is depending on physical properties of solvents such as viscosity and vapour pressure, rather than the solubility parameters. This is based on the study of ultrasonication dispersion process on Single-Walled Carbon Nanotubes (SWCNT).[268] This also explains why there is no clear trend between graphene concentration and solvent HSP distance w.r.t. NMP as observed in Figure 3.3. Study elsewhere showed that the sonochemical effect of 120-minute sonication on NMP has caused the polymerisation of NMP, giving steric stabilisation effect to disperse the SWCNTs.[269] However, for the case of the green solvents in the present study, the reasons behind the improved graphene dispersibility after applying a short post-exfoliation ultrasonication remain unclear at this moment. This might be merely due to the physical process for ultrasonication to disperse the exfoliated graphene.

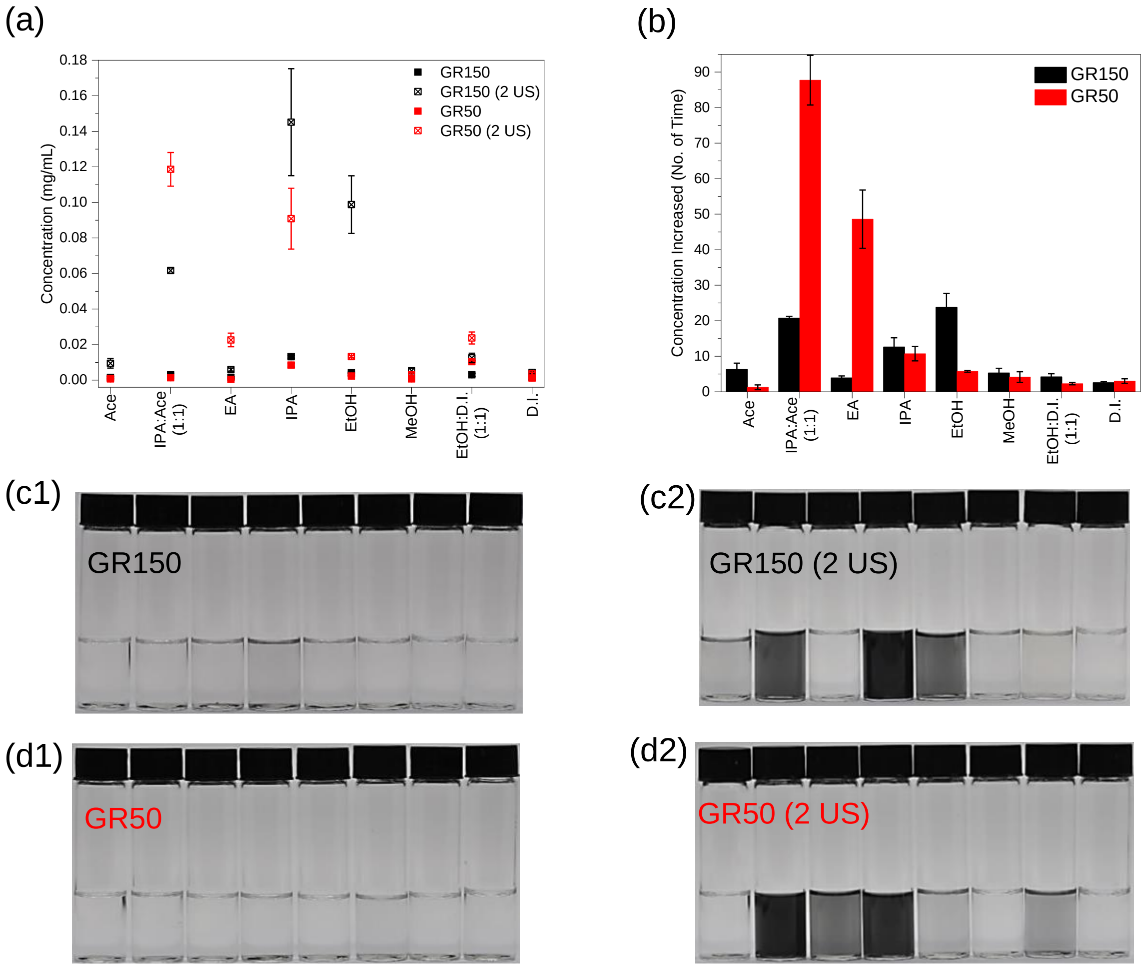

**Figure 3.4:** (a) The concentration of graphene produced from three-hour shear mixing (GR150 and GR50) and three-hour shear mixing followed by PEUS (2 US) (GR150 (2 US) and GR50 (2 US)). (b) The enhancement in graphene concentration after two-minute ultrasonication (2 US) step from PEUS. The error bars are constructed based on at least three repeated experiment data points. (c1& c2) Digital image of GR150 and (d1& d2) GR50 dispersion before and after applying PEUS (2 US) process. The solvents in the vials are arranged corresponding to the solvent sequence on the x-axis for (a) and (b).

The effect of the durations of post-exfoliation ultrasonication on graphene concentration are reported here (Figure 3.5). For both GR150 and GR50, graphene concentration increases with the increase in the duration of PEUS from two to ten minutes, before it starts to plateau off at a PEUS duration beyond ten minutes. Please note that the two-minute duration (2 US) of PEUS that used in this work is just a standardised duration used to investigate the effect of PEUS on different solvents. The intention is to ensure consistency and comparability in the assessment of PEUS effects across different solvents by employing a uniform and well-defined time of two minutes.

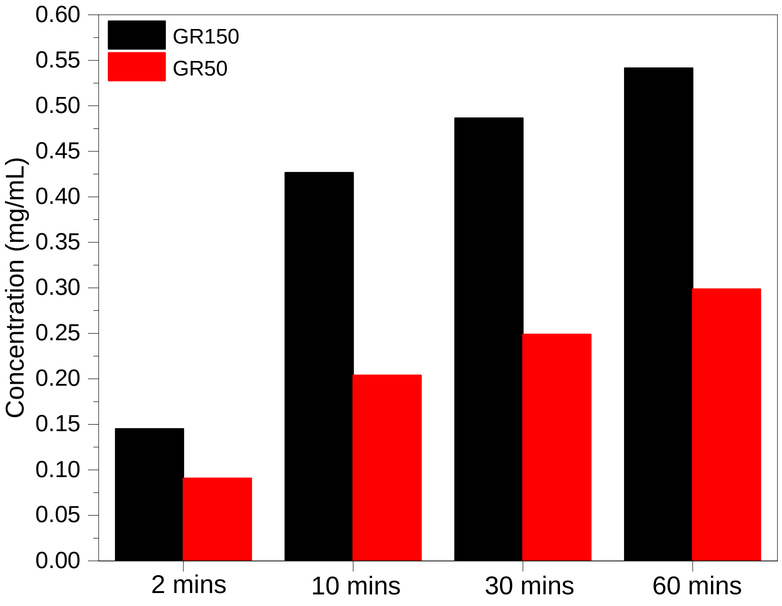

**Figure 3.5**: The concentration of GR150 and GR50 graphene obtained with different post-exfoliation ultrasonication (PEUS) times.

### 3.4.3.2 Ability of PEUS in Dispersing Graphene

In order to verify that the role of 2 US step from PEUS is solely to facilitate the dispersion of the exfoliated graphene but not the exfoliation process itself, two-minute ultrasonication was performed directly on the graphite starting materials (C-GR150 or C-GR50) as a control experiment. This is to check if there is any exfoliated graphene produced (Figure 3.6 and Figure B3). The difference in graphene concentration before and after introducing 2 US step (GR150 (2 US)- GR150 or GR50 (2 US)- GR50) in Figure 3.6 indicates the amount of graphene disperse through 2 US. For GR150 graphene, the graphene concentration produced from the control (C-GR150 (2 US)) is insignificant as compared to the concentration of graphene dispersed through 2 US step in PEUS. This implies that the 2 US mainly helped in enhancing the dispersion of GR150 graphene but not exfoliating the graphite. However, this is not the case for GR50 graphene in Ace, EtOH:D.I. and D.I. solvent media. The concentration of the C-GR50 (2 US) dispersion in these solvent media collected from two-minute ultrasonication on G50 graphite starting material is higher than the concentration increase resulted from the 2 US. Interestingly, the concentration of C-GR50 (2 US) in EtOH:D.I. is also higher than the US-GR50 and GR50 graphene produced in EtOH:D.I., through three-hour ultrasonication and three-hour shear mixing, respectively. This finding led to another question: Is EtOH:D.I. more effective in dispersing graphite than graphene?

To answer this, a two-minute vortex mixing (to exclude any exfoliation effect) was used to homogenise the G50 graphite powder in EtOH:D.I.. This sample is denoted as C-GR50 (2 Vortex). This is to ensure that C-GR50 (2 Vortex) in EtOH:D.I. contains only graphite and not exfoliate into graphene. Surprisingly, C-GR50 (2 Vortex) in EtOH:D.I. solvent showed higher concentration (higher UV-Vis absorbance in Figure B2) than the GR50 graphene produced from three-hour shear mixing in the same solvent. This implies EtOH:D.I. shows preferentially dispersion of graphite. A reason for this is the expanded layered structure of G50 graphite allows the effective trapping of cavitation bubbles produced in EtOH:D.I. (1:1). The trapping of cavitation bubbles between graphite layers is possible.[270] This lowers the density of the graphite, which causes larger amount of these bubble-trapped layered-graphite collected after centrifugation. Contact angle measurement using Washburn method showed that EtOH:D.I. solvent mixture has high affinity (low contact angle) towards G50 graphite (Figure 2.10, Chapter 2). The UV-Vis analysis of C-GR50 (2 Vortex) showed a prominent peak at 270 nm, which is typically known as the of $\pi - \pi^*$absorption peak of graphene (Figure B2). However, this does not mean that C-GR50 (2 Vortex) is graphene. It should be noted that G50 graphite powder used is the expanded graphite (Figure 2.1b), which causes it to have the graphene characteristics (e.g.: symmetry Raman 2D peak as in Figure 2.1e). The UV-Vis peak at 270 nm was also observed for the pristine graphite (not graphene) dispersed in EtOH in a study done by Wang et al. and Fauzi et al..[185,271]

A study by Morton et al. on the acoustic pressure produced in water, EtOH and EtOH:D.I. (50:50 vol%) over a fixed time of 40 ms and the formation of cavitation bubbles was captured by high-speed camera. Their study showed that EtOH:D.I. solvent mixture with volume of 150 ml at 50:50 v/v composition (same as the volume and composition used in the present study), showed high stability up to at least 6 months with ~78% of graphene retained.[272] On the other hand, through the controlled experiments, the present study has shown that EtOH:D.I. can disperse graphite better than graphene. Nonomura et al. found the acetone:water mixture is effective for dispersing graphite, not graphene, as no centrifugation step was used to separate graphene from graphite aggregates after the dispersion step, and electron microscopy confirms the material is graphite.[273] However, this acetone:water mixture has used by another research group to produce high concentration of graphene.[165] Hence, it is crucial to verify the selectivity of a solvent towards graphene dispersion.

The results of G50 graphite and GR50 graphene dispersed in EtOH:D.I. shows that control experiments, either by applying two-minute ultrasonication or two-minute vortex mixing, directly on graphite starting material are important in checking the selectivity of the solvent towards graphene. Unlike EtOH:D.I., in IPA, two-minute ultrasonication or vortex mixing directly on both G150 and G50 graphite (C-GR150 and C-GR50) yields much lower concentration (or UV-Vis absorbance) than that of GR150 and GR50 graphene, produced with three-hour shear mixing (Figure B2). This shows that IPA has high selectivity towards dispersing graphene instead of graphite.

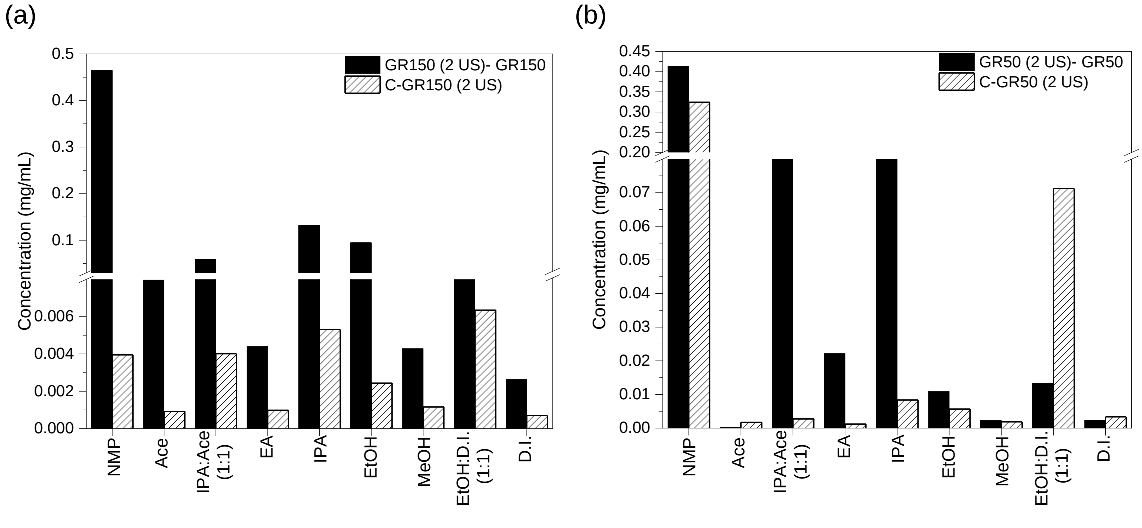

**Figure 3.6**: The comparison of (a) GR150 and (b) GR50 graphene concentration increase caused by two-minute post-exfoliation ultrasonication (PEUS), with the concentration obtained through direct two-minute ultrasonication from their respective graphite starting materials (C-GR150 (2 US) or C-GR50 (2 US)).

### 3.4.3.3 The Effect of PEUS Temperature on Graphene Concentration

Temperature is a crucial factor affecting the cavitation bubbles generation in ultrasonication besides the properties of the solvent medium used. While two-minute ultrasonication (2 US) step in PEUS is effective in dispersing exfoliated graphene to enhance its concentration/yield, such a short ultrasonication at 70°C significantly lower the concentration of the dispersed graphene in solvents (Figure B4). This finding is contradicted to the study by Kim et al. that showed the yields of graphene exfoliated in water increased with increasing temperature of the bath sonicator from 30°C to 60°C.[274]

This is because the sonic pressure in water increases upon heating, and this favours the formation of cavitation bubbles. Morton et al. did the study on acoustic pressure and shock wave generated in water at temperature range from 10°C to 70°C for graphite exfoliation by sonotrode (probe sonicator). According to their finding, low temperature favours the dispersion of graphene because bubble implosion decreases with increasing temperature.[275] This finding is contradict to Kim et al. who proved high temperature favours the graphene exfoliation in water. Kim et al. used bath sonication instead of probe sonication technique that used by Morton et al. It is worth noticing that Kim et al. measured the graphene concentration produced whereas Morton et al. measured the acoustic pressure generation during exfoliation under different temperatures. We must be aware that measurement of graphene concentration combined the effect of exfoliation temperature on both exfoliation and stabilisation of graphene, while measurement of acoustic pressure during exfoliation indicates the effect of temperature on just the exfoliation efficiency. Combining the study by Kim et al. and Morton et al., it can be deduced that high temperature favours graphene stabilisation and low temperature favours the exfoliation. There is a study by Lund et al. showed the graphene concentration increases with decreasing temperature using shear exfoliation technique in water-surfactant solvent system. The explanation of this is the high temperature does not favour the physisorption of sodium cholate (NaC) surfactant on graphene. This affects the stabilisation of graphene by the surfactant.[276]

The contradictory results reported from the above-mentioned literatures regarding how sonication temperature affects the yield of graphene could be attributed to the temperature at which the graphene dispersion is maintained during the centrifugation process. Centrifugation is the method used to separate the exfoliated graphene after the initial exfoliation process. Results from the present study shows that apart from the heated sonication, centrifugation at a slightly heated temperature of 30ºC after exfoliation lowering the graphene concentration (Figure B4). This implies that the decrease in graphene yield upon heated sonication might be due to the centrifugation of the warm dispersion after sonication, rather than the sonication process itself. This observation has never been discussed in the literatures. This is because the increase in temperature causes the decrease in solvent density and hence, the increase in the sedimentation rate.

In order to eliminate the influence of centrifugation conditions and gain a clearer insight into how sonication temperature impacts the graphene yield, the dispersion obtained after PEUS (2 US) at 70ºC was left to cool down to the room temperature before centrifugation. In this case, the graphene yield obtained through PEUS (2 US) at 70ºC is higher than that obtained at room temperature (Figure B4). As 2 US step in PEUS is used just to disperse the exfoliated graphene, this shows that 2 US under heat enhances graphene dispersibility, which is well-agreed with the finding by Kim et al.. Besides the concentration, the effect of heated 2 US at 70ºC on the graphene defect is also assessed by the Raman spectroscopy. Figure B5 shows examples of peak fitting from the Raman spectra of GR150 and GR50 graphene. Lorentzian-based peak fitting was used to analyse defects by evaluating the intensities and FWHM of the fitted peaks. See also section 2.2.3.1 for peak fitting description. 2 US short ultrasonication under heat at 70ºC introduced insignificant defect and disorder on the graphene despite of having significant effect on the graphene yield. There is also insignificant variation in the type of defect from 2 US at room temperature to 2 US at 70ºC (Figure B6).

### 3.4.4 Quality Assessment of the Graphene Dispersions

#### 3.4.4.1 Oxidation Analysis by XPS and UV-Vis Spectroscopy

The oxidation level of graphene affects its electronic properties (e.g.: the presence of oxygen species on graphene lowers its electrical conductivity).[277,278] Long ultrasonication duration can also lead to the oxidation of graphene besides introducing crystal defects. A short ultrasonication duration of two minutes (2 US) in PEUS was introduced here to facilitate the dispersion of exfoliated graphene to avoid the oxidation caused by long ultrasonication. XPS analysis in Figure 3.7 was carried out to investigate the oxidation level after shear mixing exfoliation (sample GR150 and GR50), and after introducing 2 US (sample GR150 (2 US) and GR50 (2 US)). The XPS peak fitting (shown in Figure B7) done by CasaXPS with reference to established literatures.[279–281] The oxygen species of C=O, C-O and O-C=O occur in the graphite starting materials G150 and G50, from which the graphene has been exfoliated. C=O is the dominant oxygen species. The oxygen content of GR50 and GR50 (2 US) are similar, meaning that the effect from oxidation caused by PEUS (2 US) is negligible. Interestingly, the oxygen content of GR150 (2 US) is around 10%, lesser than that of GR150 (14%). This indicates that 2 US step stripped off the oxygen species. Ultrasonication duration as short as two minutes is sufficient to generate the shock waves required to strip off the oxygen functional groups. It has been proven that longer ultrasonication duration could reduce the oxygen content of the exfoliated graphene at the expense of increasing the defective $sp^3$ carbon atoms.[282] Given that only one XPS measurement was taken per sample, the observed decrease in oxygen content may be due to measurement variability. However, the key point is to demonstrate that no additional oxidation occurred during the short sonication period. The $sp^3$ did not increase after 2 US step for GR150, instead, $sp^3$ content decreases. For GR50 (2 US), $sp^3$

increases with slight increase in the oxygen content (from 8% to 10%) after applying PEUS (2 US). Increasing in the disorders and sp$^3$ content also had been observed upon ultrasonication of graphene oxide from 2 to 11 mins.[283]

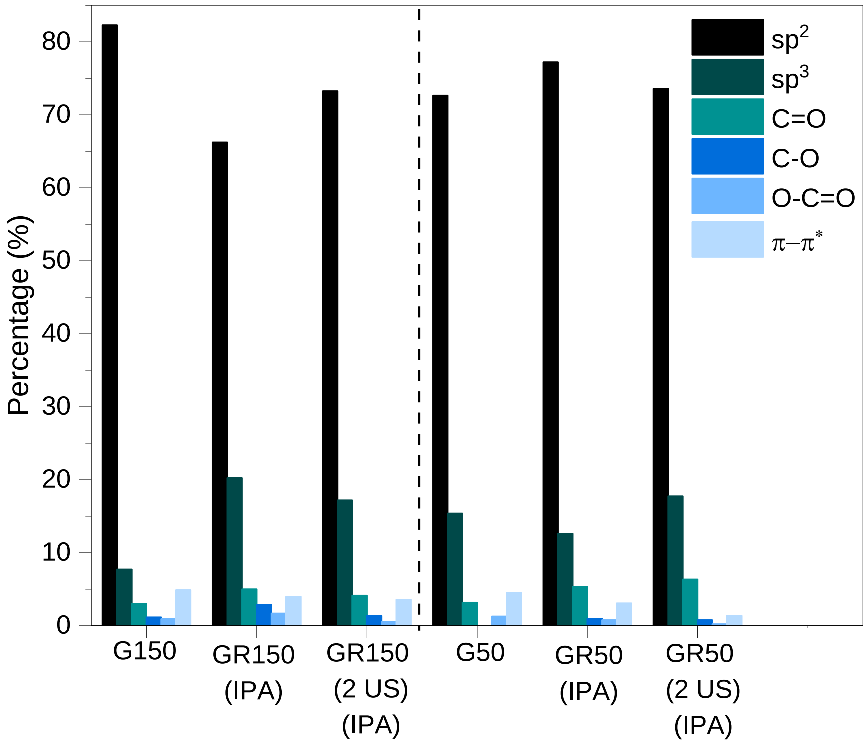

**Figure 3.7**: The comparison of the XPS-analysed composition of oxygen groups and defects from the graphite starting materials (G150 and G50), the exfoliated graphene (GR150 and GR50), and the exfoliated graphene with post exfoliation ultrasonication (PEUS) of two minutes (2 US).

While the absorbance at the featureless region of UV-Vis spectra towards 700 nm is used to calculate the concentration of graphene (Equation 2.1), the absorption peak shift (at 270 nm for pristine unoxidised graphene) of UV-Vis spectrum after applying PEUS (2 US) is used to evaluate the degrees of oxidation in graphene.[284] Peak shifts in IPA and EtOH:D.I. solvents are analysed because they are promising exfoliation solvent for the production of GR50 (2 US) and GR150 (2 US). Although IPA:Ace gives the highest concentration of GR150 (2US), the absorption peak is obscured by the UV-Vis cut off wavelength of Ace at 330 nm. EtOH:D.I. works the best in exfoliating GR50 using both shear mixing and sonication technique (Figure 3.3). There is no significant peak shift after PEUS (2 US) in IPA for both GR150 and GR50 (Figure B1). This showed that 2 US step from PEUS does not lead to the oxidation of the graphene, which is in good agreement of the XPS results (Table B1 and Figure B7).

### 3.4.4.2 Graphene Quality Obtained at Different Centrifugation Speed

Centrifugation is mandatory for the extraction of graphene from the dispersion after exfoliation. If PEUS (2 US) really help in dispersing more graphene, the concentration of graphene dispersion produced with PEUS (2 US) obtained at high centrifugation speeds should be higher than that without PEUS (2 US). This is because well-dispersed graphene should be able to overcome the gravitational force exerted by the effect of centrifugation and remained dispersed, especially at high centrifugation speeds. IPA is a promising solvent for yielding high graphene concentration for both GR150 and GR50 after PEUS (2 US). Therefore, GR50 and GR150 produced in IPA are selected for centrifugation at different speeds (Figure 3.8a,b) Besides IPA, concentration of GR50 in EtOH:D.I. at different centrifugation speeds has also been investigated (Figure 3.8c) following the effectiveness of EtOH:D.I. in exfoliating GR50 through three-hour shear mixing. The results show that the concentration of graphene obtained after PEUS (2 US) is higher than that obtained without the 2 US treatment even at higher centrifugation speeds. This demonstrates the effectiveness of PEUS (2 US) in dispersing more graphene in the solvent.

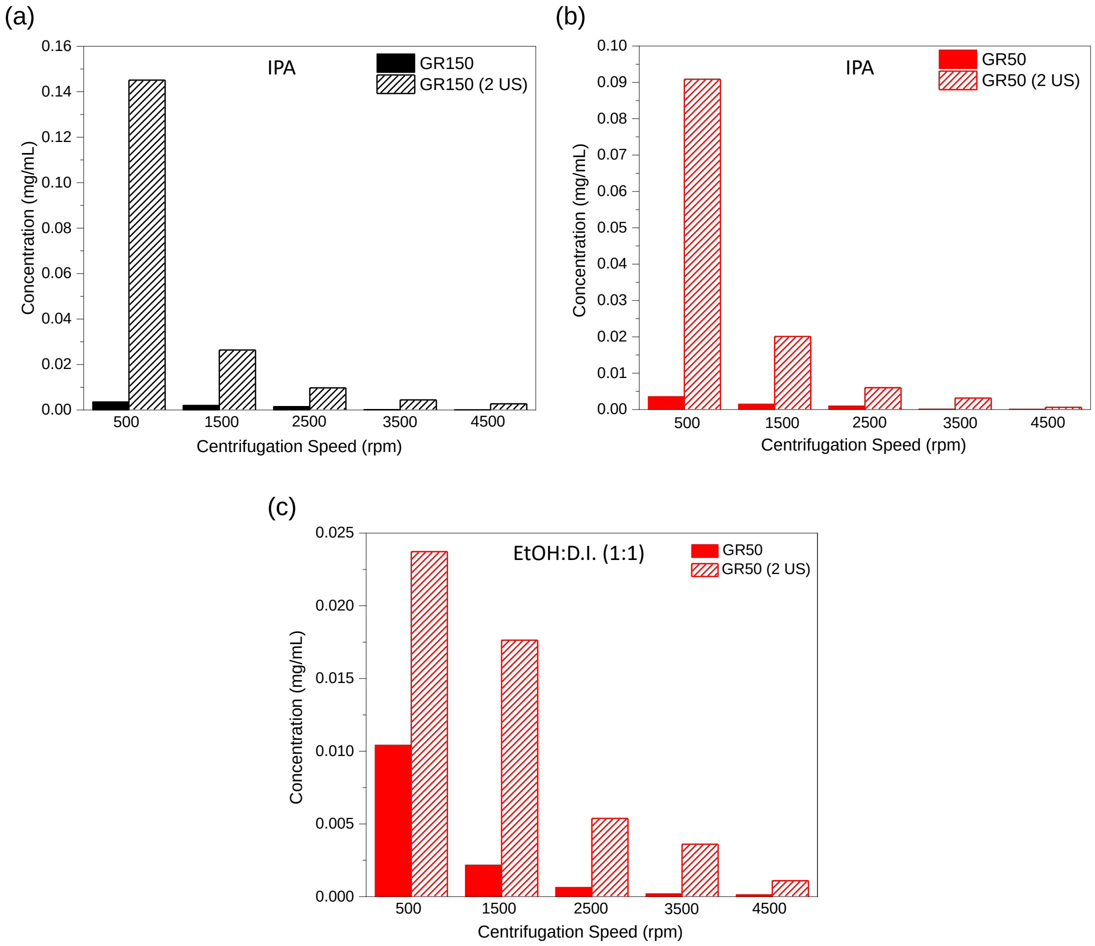

**Figure 3.8:** Concentration of (a) GR150 in IPA, (b) GR50 in IPA and (c) GR50 in EtOH:D.I. (1:1) obtained from different centrifugation speeds.

Thinner graphene flakes can be collected at the higher centrifugation speed (Equation 1.8). However, the chemistry aspect which is not included in the equation also needs to be considered. Since graphene with higher oxidation level disperse better in polar solvent, hence, high speed centrifugation for polar solvent might yield the graphene with higher oxidation level as compared to the centrifugation at lower speed. Will higher centrifugation speed yield thinner but more oxidised graphene? To answer this, the oxidation level of GR150 in IPA produced from different centrifugation speeds is assessed using UV-Vis spectroscopy and XPS. GR150 in IPA is selected because GR150 has lesser defect as compared to GR50, and IPA is the most effective solvent for exfoliating and dispersing GR150. Besides this, the expanded structure of GR50 makes the analysis of oxidation level based on $\pi - \pi^*$absorption peak position from UV-Vis spectrum difficult because the peak also shifts away from the 270 nm position of pristine/ un-oxidised graphene due to the interlayer expansion. Expanded graphite, intercalated graphite and oxidised graphene have the UV absorption peak lesser than 250 nm.[185] Hence, the peak shifting due to the oxidation is hard to judge from GR50. The UV-Vis spectra of GR150 in IPA obtained at different centrifuge speeds are shown in Figure 3.9. A shift of the $\pi - \pi^*$absorption peak from 270 nm to the lower wavelength at higher centrifuge speed (> 500 rpm) implies the expansion of interlayer caused by the oxygen species. The peak around 230 nm, which is caused by the oxygen species, is also more prominent at higher centrifuge speed. Hence, in general, graphene collected at higher centrifugation speed contain more oxygen species, which is also proven by the XPS analysis in Figure 3.10.

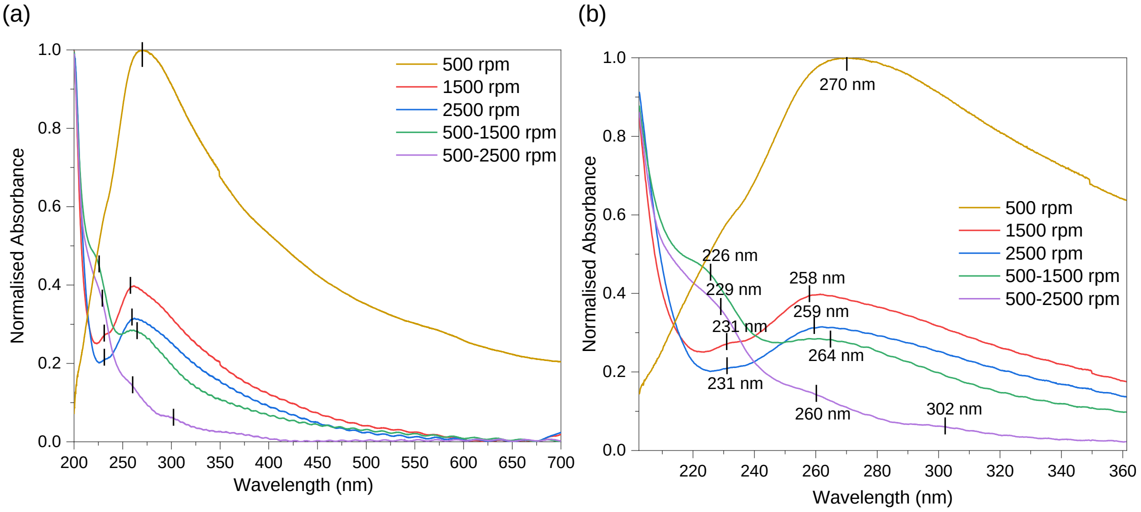

**Figure 3.9:** (a)The absorption peaks for GR150 (2 US) in IPA collected at different centrifuge speeds. (b)The enlarged of (a) showing the wavelength of each absorption peak. The shift in absorption peak positions indicates the difference in quality of graphene (in the aspect of oxidation level and layer number) collected at different centrifuge speeds. 500-1500 rpm and 500-2500 rpm are the GR150 (2 US) collected from 1500 rpm and 2500 rpm centrifugation, respectively, after the centrifugation at 500 rpm.

The XPS analysis on the GR150 (2 US) in IPA obtained from different centrifugation speeds showed the percentage of oxygen species (C-O=C, C-O and C=O) increases with the increasing centrifugation speeds. Therefore, higher centrifugation speeds not only yield thinner and smaller graphene, but also the more oxidised graphene. This is because oxidised graphene can disperse better in polar solvent such as IPA and will not sediment even at the high centrifugation speeds.

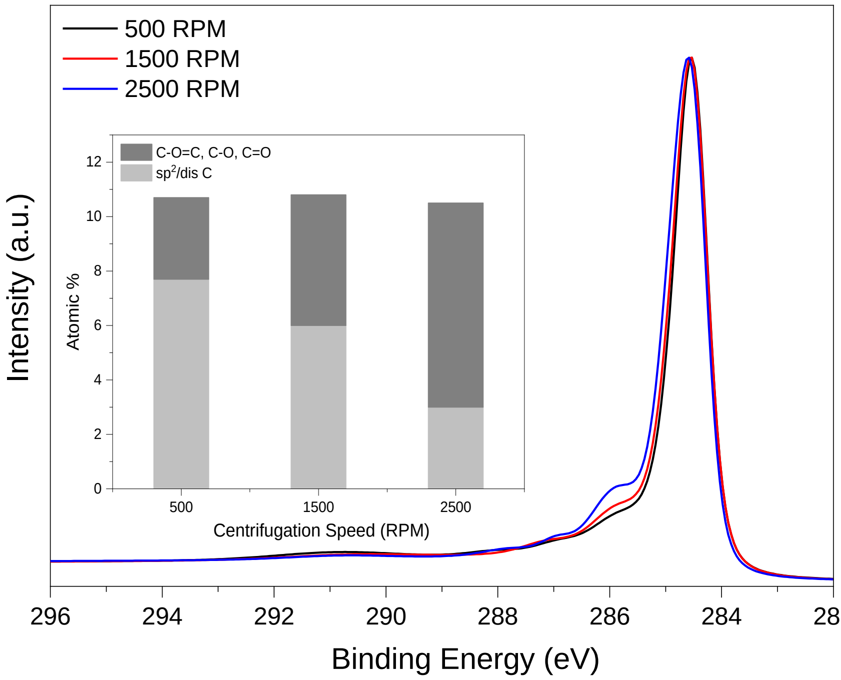

**Figure 3.10:** XPS analysis showing the percentage of oxygen groups and disorder carbon (dis C) on GR150 (2 US) in IPA produced from different centrifugation speed.

It has been reported that the intensity ratio of $\pi - \pi^*$absorption peak at short wavelength (~270nm) to the long wavelength plateau (~550-800 nm) can be used to determine the graphene thickness.[285] However, will the concentration of dispersion also affect this ratio? In order to investigate if the concentration of the dispersion is affecting the ratio, the dispersions have been diluted (Figure B8). Slight decrease in the ratio after dilution is observed. Backes et al. claimed the decrease in the ratio indicates thinner graphene.[227] However, thinner graphene was obtained using higher centrifuge speed that gives lower graphene dispersion concentration. Apart from the graphene thickness. the decrease in graphene concentration can also contribute to the decrease in the ratio. Hence, the metric can only be used for thickness comparison among the graphene dispersion with same concentration, which is not suitable to be used to compare the graphene thickness produced at different centrifugation speeds.

### 3.4.4.3 Defect and Disorder Analysis by Raman Spectroscopy

Raman spectroscopy is used to study the defect density, defect types and disorder of graphite and graphene. G peak FWHM gives the information on the lattice disorder (unaffected by the edges) whereas D to G peak intensity ratio ($I_D/I_G$) provides the information on defect densities which is affected by the edges.[225] High $I_D/I_G$ with low G peak FWHM indicates the defect density is mainly from the edges (caused by the discontinuity of crystal structure) rather than the lattice disorder of the graphene. The Raman laser spot size of 1μm used is sufficient to capture the edges for both GR150 and GR50 produced (see Section 2.2.3.1). Disordered graphene should show a large G peak FWHM despite of its low $I_D/I_G$. Hence, the $I_D/I_G$ against G peak FWHM is plotted to give the information on whether the defect is from the edges.

Figure 3.11 showed the comparison of defect density ($I_D/I_G$), crystal disorder (G peak FWHM) and type of defect ($I_D/I_{D'}$) of GR50 and GR150 graphene produced through three-hour shear mixing. All the graphene produced exhibit low defect density, as evidenced by low $I_D/I_G$, which is below 0.4 (Figure 3.11a). $I_D/I_G$ of reduced graphene oxide with high defect density is ~0.8,[286] or even > 1.[287] For graphene generated from pre-treated partially-oxidised graphite, the value is 0.22- 0.55.[288] The $I_D/I_G$ value reported for the exfoliation in NMP using shear mixing of the graphite type similar to G150 that we used, was 0.18,[76] which is in close agreement with the $I_D/I_G$ value of GR150 obtained in the present work. The disorder and type of defect in graphene is dependent on the properties of the graphite starting materials used. From Figure 3.11a, G50 graphite shows higher disorders with larger G peak FWHMs and $I_D/I_G$ ratio than that of G150 graphite. Similarly, GR150 graphene that exfoliated from G150 (black data points) also show larger G peak FWHM than that of GR50 graphene (red data points). Given the Raman spectral resolution of 2–3 cm$^{-1}$, a difference in G peak FWHM is expected between GR50 and GR150. However, no significant variation is likely within samples of the same type of graphene.

The defect of exfoliated graphene is affected by the graphite starting materials. D to D' peak intensity ratio ($I_D/I_{D'}$) analysis in Figure 3.11b showed G150 and GR150 exhibit predominantly vacancy defect, whereas G50 and GR50 exhibit predominantly edge defect. The exfoliation in NMP and EtOH:D.I. for G50 showed high $I_D/I_G$ and G peak FWHM, which means high in both defect density and disorder, as compared to most of the green solvents used. For G150, the exfoliation in NMP showed quite low defect density and disorder. NMP and EtOH:D.I. are more effective LPE solvent for G50 than for the G150, as can be evidenced by the higher G50 concentration produced. However, the high disorder of NMP- and EtOH:D.I.- exfoliated G50 showed that the high exfoliation efficiency and dispersibility were achieved at the expense of creating the disorder on the graphene.

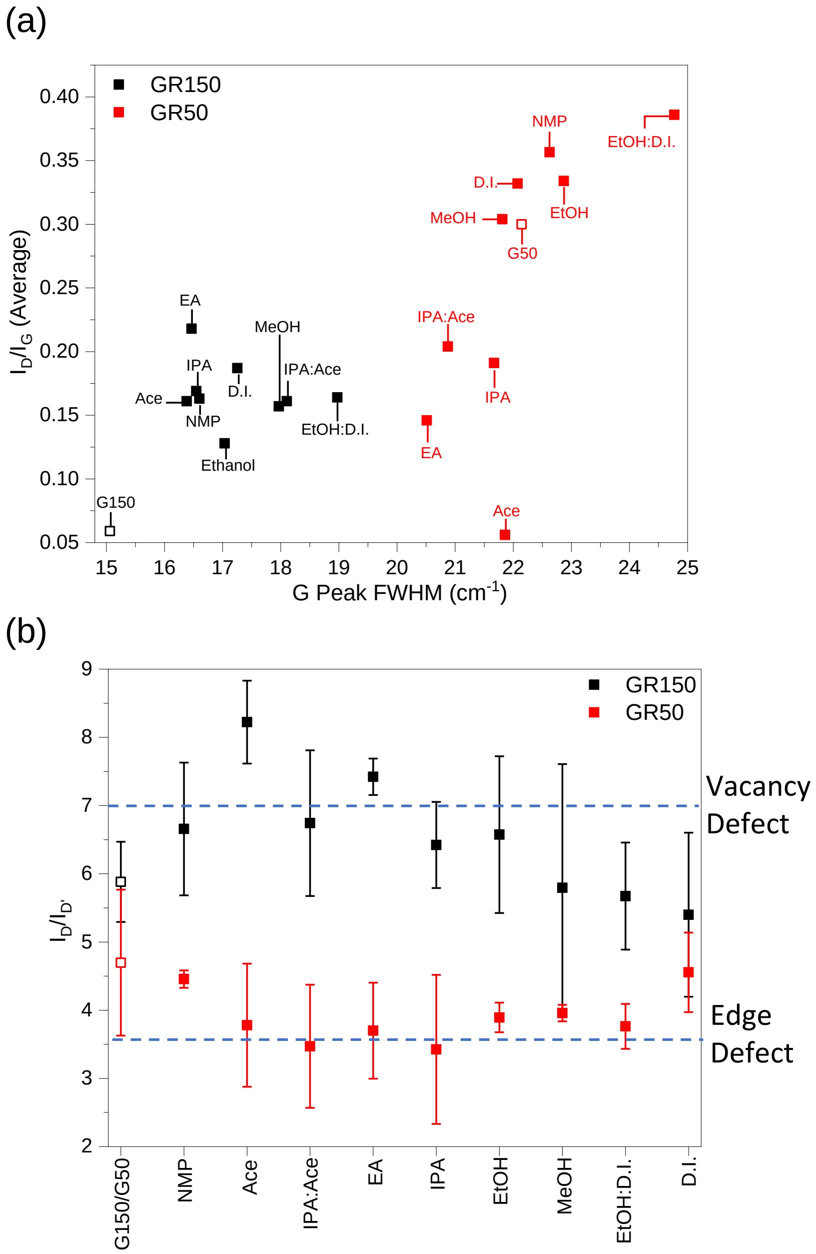

**Figure 3.11:** (a) The average D to G intensity ratio (average from at least six Raman spectra) and G peak FWHM analysis from Raman spectra, which gives the information on the defect density and crystal disorder respectively, for GR150 and GR50 graphene. (b) The D to D’ intensity ratio analysis from Raman spectra that gives the information on the type of graphene defect. Error bars are constructed from the standard deviation of measurements at a minimum of six randomly selected points on the sample. Peak fitting examples are shown in Figure B5, while the original spectra are in Figure A6 and Figure B9.

It is important to ensure the PEUS (2 US) yield enhancement technique used here does not give significant defects on the graphene. Figure 3.12 shows the comparison of the defects of graphene before and after PEUS (2 US) for the selected solvents (see Figure

B6 and Figure B9). Since PEUS (2 US) with short ultrasonication time was used as the yield enhancement technique, the defect of US-GR150 and US-GR50 graphene produced by purely three-ultrasonication method is also analysed.

IPA is one of the selected solvents because it gives high yield for both GR50 and GR150. For GR50 in IPA, the disorders (broadening of G peak FWHM) and defect density ($I_D/I_G$) increase after PEUS (2 US). Further increase in graphene yield was achieved when PEUS (2 US) is done at 70°C (Figure B6). The same trend is observed for GR150 in IPA with less significant defect density and disorder created by PEUS (2 US). For GR150 in IPA:Ace solvent mixture, there is no significant increase in disorder (G peak FWHM) has been observed as the error bar of its G peak FWHM without PEUS (2 US) covers the range of G peak FWHM with PEUS (2 US). In general, defect and disorder imposed by such short ultrasonication time of two minutes on graphene is still insignificant.

The defect analysis of graphene produced from three-hour ultrasonication (US-GR150 and US-GR50) is compared to that of GR150 and GR50, which produced from three-hour shear mixing (without ultrasonication). For GR150 in IPA and IPA:Ace, $I_D/I_G$ increases from GR150 to GR150 (2 US) to US-GR150. This shows that $I_D/I_G$ increases with the ultrasonication time. Ultrasonication introduces mainly edge defect (caused by the reduction in flake size) as the increase in G peak FWHM, which represents the crystal disorder, is not significant. For GR50, the defect trend is out of expectation, especially for the case of EtOH:D.I. (Figure 3.12b). The G peak FWHM and $I_D/I_G$ reduced upon ultrasonication (2 US). For IPA, both GR50 (2 US) and US-GR50 with ultrasonication increased $I_D/I_G$ and FWHM, as compared to GR50 produced from pure shear mixing without ultrasonication.

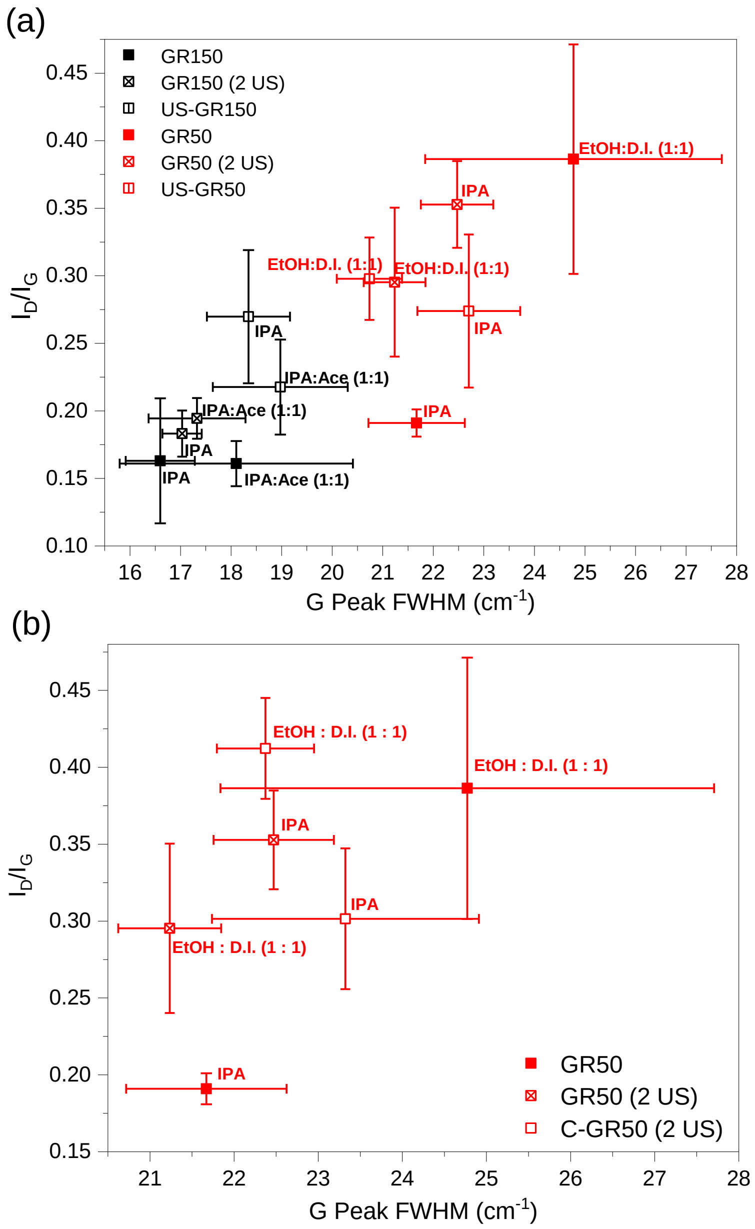

**Figure 3.12**: The comparison of defect density ($I_D/I_G$) and crystal disorder (G peak FWHM) of Raman Spectra between (a) the graphene produced with only shear mixing (GR150 and GR50), shear mixing with PEUS (GR150 (2 US) and GR50 (2 US)), and only ultrasonication (US-GR150 and US-GR50) in the selected solvents; (b) between the GR50 and GR50 (2 US) graphene in EtOH:D.I. (1:1) solvent produced, in comparison to the controlled experiment, which is the 2-minute ultrasonication directly from the G50 graphite (C-GR50 (2 US)). Error bars are constructed from the standard deviation of measurements at a minimum of six randomly selected points on the sample. Peak fitting examples are shown in Figure B5, while the original spectra are in Figure B9 and B12.

Thinner and smaller graphene can be collected at higher centrifuge speed.[289] However, the analysis on the oxygen content through UV-Vis and XPS in Section 3.4.4.2

show that more oxidised graphene is also collected at higher centrifuge speed. Defect analysis on the graphene collected for GR150 (2 US) in IPA at different centrifuge speeds is also performed. From Figure 3.13a, the defect density $I_D/I_G$ increases with the centrifugation speed. This might be due to the smaller size of GR150 (2 US) is collected at increasing centrifugation speed that increases D peak intensity due to edge defect, which agree with $I_D/I_{D'}$ analysis (Figure 3.13c). The Raman spectra used for Figure 3.13 are shown in Figure B10 and Figure B11.

PEUS has proven to increase the concentration of graphene significantly and the concentration increases with the increasing PEUS time and eventually plateauing (Figure 3.5). It is crucial to understand whether the increase in PEUS time increases the defect as well and to what extent the defect being introduced. From Raman spectroscopy defect analysis in Figure 3.13b the PEUS time affect more on GR50 than GR150, especially on the $I_D/I_G$. For GR50, $I_D/I_G$ increases slightly with the increase in PEUS time beyond two minutes. The increase in defect density is due to the formation of new edges as not much change observed in G peak FWHM, which represents the crystal disorder. For GR150, the increasing ultrasonication time does not affect much on the defect density and disorder, but the type of defect is shifting towards the edge defect based on $I_D/I_{D'}$ analysis (Figure 3.13d) indicating that the flakes size has turned smaller with more edges formed under longer ultrasonication. The decrease in lateral size with ultrasonication time is also proven by the literature.[290]

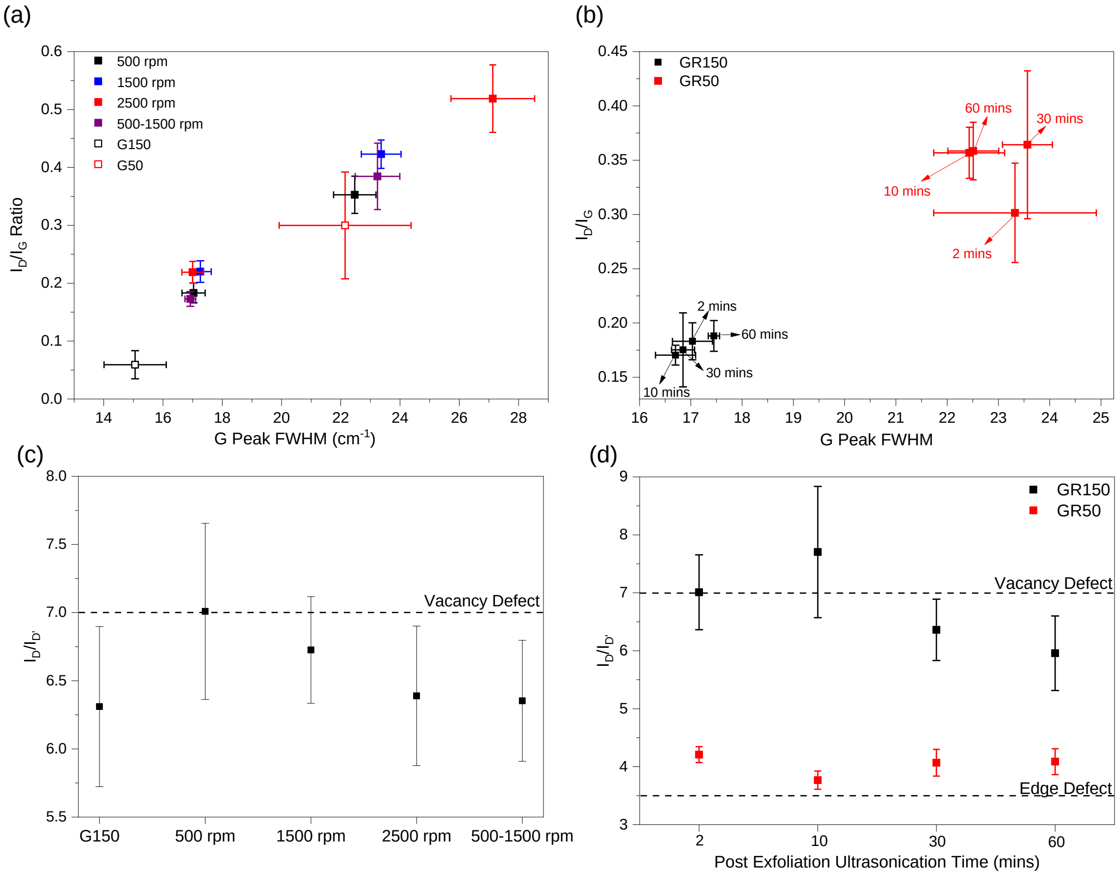

**Figure 3.13:** The comparison of defect density ($I_D/I_G$) and crystal disorder (G peak FWHM) of Raman Spectra between (a) GR150 (2 US) collected at different centrifugation speeds, with the type of disorder $I_D/I_{D'}$ shown in (c); and (b) GR150 and GR50, synthesized using different PEUS time, with $I_D/I_{D'}$ shown in (d). Error bars are constructed from the standard deviation of measurements at a minimum of six randomly selected points on the sample. Peak fitting examples are shown in Figure B5, while the original spectra are in Figure B10 and B11.

### 3.4.4.4 Number of Layers Analysis by Raman Spectroscopy and AFM

Although number of graphene layers can be evaluated from the information obtained from the 2D peak of Raman spectrum, deconvolution of this peak might impose significant error in calculations. The number of layers more than 10 cannot be evaluated from the 2D peak.[291] It also varies with the type of graphene produced.[76] Instead of deconvoluting of 2D peak, the number of graphene layers can be estimated by using the empirical formula mentioned in Section 3.2.3.1, which is based on the peak-to-shoulder intensity ratios of graphene and its graphite starting material.[76, 292] Raman spectroscopy has the advantage over AFM in the number of layers analysis because it can provide information on the bulk scale. The thickness of graphene obtained in this way is much higher than that of AFM because more samples are used to obtain good Raman signal at bulk scale, and therefore, restacking of graphene flakes occurs.

The average number of layers of GR150 and GR50 as calculated from Raman spectroscopy analysis do not vary significantly with solvent HSP distance w.r.t. NMP or type of solvent (Figure 3.14). This aligned well with the finding of Backes *et al.*.[263] For GR50, the error bars increase with higher solvent HSP distance w.r.t. NMP. This would imply a larger deviation in graphene thickness. Besides HSP, the layer numbers for GR150 and GR50 produced in selected solvents using different exfoliation techniques (shear mixing vs. ultrasonication) are compared in Figure 3.14. Generally, GR150 exhibits lower layer number than GR50. It is evident that ultrasonication yields thinner graphene than shear mixing besides US-GR50 in IPA. The variation in graphene thickness is also smaller for ultrasonication exfoliation (as indicated by the smaller error bars). IPA:Ace is the best solvent to disperse GR50 via PEUS (2 US) to give the highest concentration of GR50 (2 US), while maintaining the similar number of layers as that obtained without PEUS (2 US), which is GR50. GR50 (2 US) in IPA exhibits the lowest number of layers as compared to that produced in IPA:Ace and EtOH:D.I.. The concentration of GR50 in EtOH:D.I. after two-minute vortex of mixing (without exfoliation) and two-minute ultrasonication from graphite (C-GR50) is even higher than that obtained from three-hour shear mixing exfoliation (GR50) (Figure B2). This leads to the possibility of EtOH:D.I. is better in dispersing graphite than the exfoliated graphene, as discussed in Section 3.4.3.2. Figure 3.14 shows the range of number of layer of C-GR50 in EtOH:D.I. is from at least 22 layers, which further proved this argument. Besides the exceptional case for GR50 in EtOH:D.I., generally, graphene produced with PEUS (2 US) exhibit lesser number of layers as compared to without.

IPA is the best solvent for exfoliating and dispersing GR150, and the number of layers for the GR150 (2 US) with optimised yield are less than 10 layers. This confirms that GR150 (2 US) in IPA can yield few-layer graphene (FLG) in bulk scale because Raman spectroscopy analysis is a bulk-scale analysis as compared to AFM. Besides IPA, IPA:Ace can also yield FLG for GR150. The Raman spectra used in Figure 3.14 are shown in Figure B12.

AFM provides direct evidence on the number of graphene layers produced and their morphologies. GR150 (2 US) in IPA has the highest concentration among all the green solvents and with low defect and number of layers. The AFM image of GR150 (2 US) in IPA in Figure 3.14 shows that the leaf-like structure (Figure 2.13, Chapter 2) is lost after applying PEUS (2 US) but its layer thickness is still maintained at around 2 nm. This thickness corresponds to five layers of graphene (taking the theoretical thickness of a monolayer graphene to be 0.34 nm). However, the thickness of monolayer graphene could be larger than the theoretical value, which can be up to 0.7 nm or more due to the presence of surface adsorbates (e.g.: adsorption of water molecules in humid air), substrate-graphene and probe-graphene interactions.[293–295]

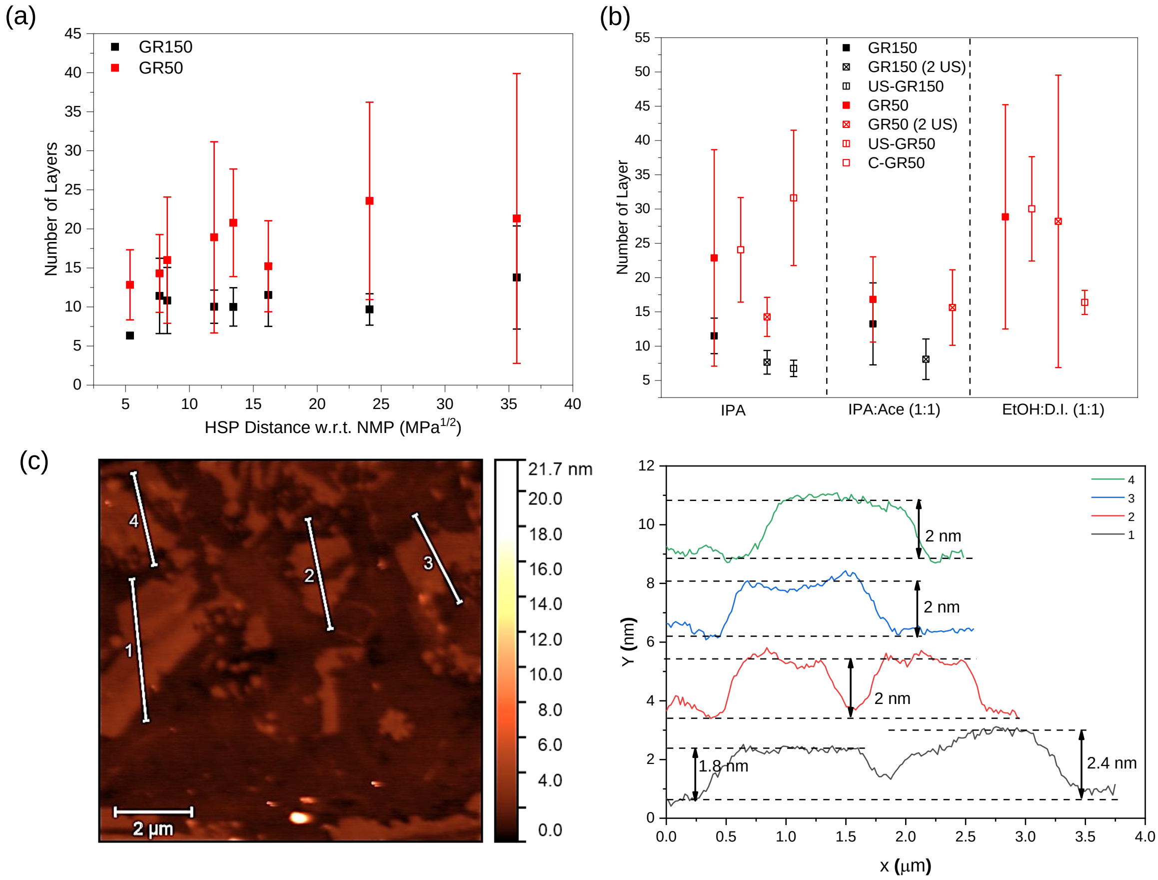

**Figure 3.14:** (a) The number of layers of GR150 and GR50 exfoliated and dispersed in the solvents listed on the x-axis, arranged in the increasing HSP distance w.r.t NMP. (b) The comparison of the number of layers of GR150 and GR50 in selected solvents, with and without PEUS (2 US). The results for graphene produced from ultrasonication (US-GR150 or US-GR50) and controlled experiment of two-minute ultrasonication from graphite (C-GR150 and C-GR50) are also shown as the comparison. Error bars are constructed from the standard deviation of measurements at a minimum of six randomly selected points on the sample. Peak fitting examples are shown in Figure B5, while the original spectra are in Figure B12. (c) The AFM image of GR150 (2 US) with line profile showing the graphene flakes thickness.

### 3.4.4.5 Stability Test

Graphene stability test was carried out by leaving the dispersion for three weeks and collect the supernatant (around top 80% of the dispersion) for analysis (Figure 3.15). The selected dispersing solvents for the stability test were solvents that could either give high concentration of graphene (e.g.: IPA, IPA:Ace, EtOH) or high increase in concentration (e.g.: IPA:Ace, EA), after applying PEUS (2 US) yield optimisation step. EA and IPA:Ace gave high concentration increase after 2 US and good stabilisation for GR50. In general, GR50 in the selected solvents are more stable than GR150. EA is the best solvent in stabilising GR50. IPA can give high concentration of GR150 and GR50, but it is poor in stabilising graphene. From the UV-Vis spectra in Figure 3.15b, the absorption peaks of GR50 and GR150 in IPA remain unchanged (no peak shift) after three weeks. This shows that the chemical composition, thickness, and lateral size of graphene that suspended in IPA after three weeks is similar as the bulk.

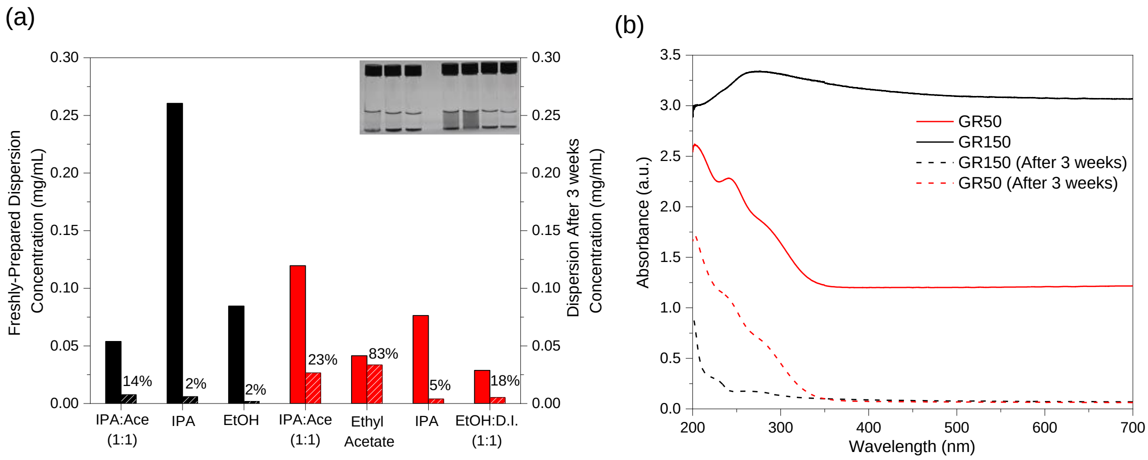

**Figure 3.15:** (a) The three-week stability test for GR150 (black) and GR50 (red) in selected solvents. The percentage of graphene left at the supernatant of the dispersion after three weeks is indicated on the bar chart. The inset shows the dispersion after three weeks with the sequence of arrangement corresponding to the solvents indicated on the x-axis. (b) UV-Vis spectra of freshly-prepared dispersions of GR150 and GR50 in IPA (solvent that gives high GR150 and GR50 concentration), in comparison to the dispersions after three weeks.

## 3.5 Conclusions

This chapter covered the study of the shear force generated by different solvents in shear mixing process, besides investigating the correlation between the solvent HSP distance w.r.t. NMP and the graphene yield/concentration. It also included the post-exfoliation ultrasonication (PEUS) method to enhance the graphene yield without functionalisation and the use of surfactants. Graphene quality assessment has been done to evaluate the oxidation and defect generation. The conclusions that can be drawn from the present study in this chapter are:

1. Shear Force Impact on Exfoliation Efficiency: Shear force emerged as one of the factors influencing the exfoliation efficiency of solvents. IPA exhibited high exfoliation efficiency partly due to its high shear force (similar to NMP).
2. Limitation of HSP w.r.t. NMP as a Universal Theory: The solvent HSP distance relative to NMP cannot serve as a universal theory for solvent selection. Its applicability varies based on the specific type of graphite or graphene and the exfoliation mechanism involved.
3. PEUS Method for Enhanced Graphene Yield: PEUS method with short ultrasonication time of two minutes demonstrated the potential to boost graphene yield or concentration up to 90 times, without generating significant defect and oxidation.
4. Effective Solvent for PEUS: IPA:Ace (1:1 vol.%) and EtOH are effective solvents for dispersing GR50 and GR150 graphene, respectively, through PEUS method.
5. Solvent Selectivity for Graphene Dispersion: EtOH:D.I. (1:1 vol.%) solvent mixture exhibited low graphene selectivity and disperses expanded graphite better than the exfoliated graphene. In contrast, IPA displayed high selectivity towards graphene.

# 4

# Beyond Graphene- Hexagonal Boron Nitride

## 4.1 Overview

Formed by layers of hexagonal planar structure of Boron (B) and Nitrogen (N), hexagonal Boron Nitride (hBN) exhibits the layered and hexagonal structures analogous to graphene. Therefore, hBN is also known as the “white graphene” (see Section 1.2.2 for more details on hBN structures and properties). The exfoliation of hBN yields BNNSs. Besides having exceptional dielectric properties, BNNSs can be integrated with graphene due to their structural similarity, making them suitable for use in modern electronic devices.[296] BNNSs can stack on top of or below graphene, creating the heterostructure. This heterostructure is typically synthesized using bottom-up techniques under controlled conditions.[297,298] While LPE is a more cost-effective method for producing BNNS-graphene, it often yields composites or blends rather than true heterostructures.[299] Although studies show that LPE can produce heterostructures as h-BN and graphene tend to stack alternately,[300] the BNNS-graphene produced by LPE in this work is referred to as a "composite" to avoid confusion. BNNS-graphene composite is useful for the application in optoelectronic devices and as photocatalyst.[301, 302] The production of BNNS-graphene in a cost-effective way using LPE is presented and discussed in this chapter. BNNS, is also widely used in the applications that require good thermal stability, mechanical strength, and chemical inertness, especially in the form of BNNS-polymer nanocomposites for biomaterials.[303]

As in the case of graphene production, LPE method is a cost-effective method for producing BNNSs. However, the ionic interaction also occurs between hBN layers, apart from the van der Waals force. This gives rise to a stronger interlayer interaction of hBN compared to that of graphene, with six times higher interlayer shear.[304]Since the exfoliation process for BNNSs involves the application of external force to overcome the interlayer van der Waals force, hBN is more difficult to be exfoliated than graphene.[304–306] The strong electrostatic force between the BNNSs also causing them to agglomerate in the solvent. Although hBN is harder to be exfoliated than graphene, it can disperse quite well in IPA solvent,[307] one of the green solvents with low boiling point and low toxicity.

Conventional strategies involving functionalisation have been used to facilitate exfoliation process by expanding the interlayers through the intercalation of functional groups, thus also known as chemical exfoliation.[308] Since most of the solvents with low toxicities and low boiling points are polar solvents, functionalisation of hBN with polar functional groups enable them to be dispersed better in polar solvents such as water, isopropanol and ethanol. However, due to its inert nature, functionalisation with polar functional groups is difficult for hBN. Here, the newly introduced PEUS method has been demonstrated, for the first time, to provide an optimum yield of hBN in IPA of up to 12 times, compared to that obtained through the normal way, hence avoiding the need for functionalisation.

# 4.2 Materials and Method

## 4.2.1 Materials

**Solvents:** 2-propanol (Sigma Aldrich, ≥99.8 %, GC grade), Acetone (Sigma Aldrich, ≥99.5 %, GC grade), Ethanol (Sigma Aldrich, ≥99.8 %, GC grade), Ethyl Acetate (Sigma Aldrich, ≥99.5 %, GC grade), Methanol (Sigma Aldrich, ≥99.9 %, HPLC grade), 1-Methyl-2-Pyrrolidinone (Sigma Aldrich, ≥99.5 %, anhydrous).

**Hexagonal Boron Nitride Powder:** BN25 and BN10 from 3M with the particle size distribution d(90) of 25 µm and 10 µm based on the specifications provided.

*Note: Hexagonal Boron Nitride Nanosheets (BNNSs) exfoliated from hBN bulk materials, BN25 and BN10, are labelled as BNNS25 and BNNS10, respectively.

## 4.2.2 Methods

### 4.2.2.1 Synthesis of BNNS and BNNS-Graphene

The shear mixing exfoliation procedures used for the synthesis of Boron Nitride Nanosheets (BNNSs) were the same as those for the exfoliation of graphite (Section 3.2.2.1). Briefly, hBN powders (BN25 or BN10) were exfoliated, with an initial concentration of the hBN dispersion of 25 mg/mL in 150 mL of solvent, under a shear mixing speed of 5000 rpm for 3 hours. To compensate for the lost in the highly volatile solvents due to evaporation, the solvents were constantly added throughout the course of the exfoliation process. After exfoliation, the BNNSs produced were separated from large hBN aggregates by centrifuging the dispersions at 500 rpm (52 RCF) for 1 hour. The speed of 500 rpm was used unless otherwise specified. The supernatant after centrifugation at 500 rpm (denoted Su_500) was taken for concentration analysis by UV-Vis spectroscopy, and for other characterisations (e.g.: Raman spectroscopy, XPS and AFM).

The shear mixing exfoliation synthesis method for BNNS-graphene was the same as BNNSs. The starting material used is a mixture of G150 graphite and BN25 powder with the weight ratio of 1:1. The concentration of the starting material in the solvent was maintained at 25 mg/mL in 150 mL of solvent, same as that used earlier for pure hBN powder exfoliation.

#### 4.2.2.2 PEUS Method for Yield Enhancement

In this Post-Exfoliation Ultrasonication (PEUS) method, the dispersion collected following the normal shear mixing exfoliation route, was sonicated in a bath ultrasonicator under a temperature of 25ºC (room temperature) for two minutes before centrifugation. This extra brief ultrasonication step under PEUS was named 2 US. The dispersion after 2 US was subsequently centrifuged at 500 rpm (52 RCF) for one hour before the supernatant was collected as the final BNNS dispersion. The BNNS dispersions produced with PEUS (2 US) are labelled as either BNNS25 (2 US) or BNNS10 (2 US), depending on which starting material used.

### 4.2.3 Characterisations

Sample preparation and characterisation procedures for Raman spectroscopy, XRD, AFM, XPS and UV-Vis spectroscopy were detailed in Section 2.2.3. The calibration curve used for UV-Vis concentration analysis based on Equation 2.1 is shown in Figure 4.1. The absorptivity, α at 300 nm wavelength is selected for the concentration calculation of hBN and BNNSs.[122, 309] Black and red graph represents BN25/BNNS25 and BN10/BNNS10, respectively.

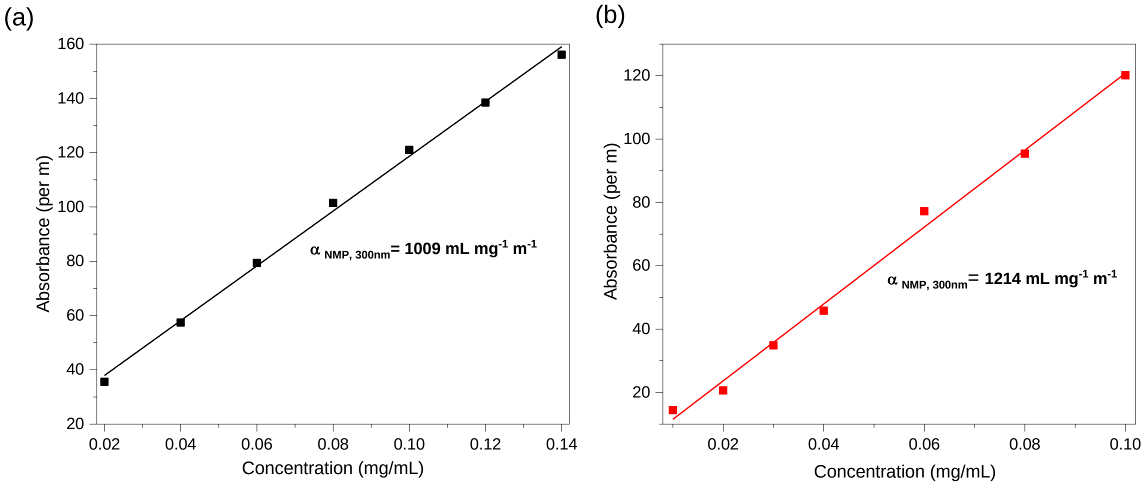

**Figure 4.1:** UV-Vis calibration curves for (a) BNNS25 and (b) BNNS10 in NMP. The absorptivity, α at the wavelength of 300nm as calculated from the gradient of the calibration curve is indicated in the figures.

*Note: Black and red graphs or data points shown in the results and discussion section represent the data for BN25/BNNS25 and BN10/BNNS10, respectively.

# 4.3 Results and Discussions

## 4.3.1 Shear Mixing Exfoliation of hBN and Yield Optimisation

### 4.3.1.1 Properties of Bulk hBN for Exfoliation

From the work on graphite exfoliation for graphene production, we have gained considerable understanding on how the inherent properties of starting materials affect the quantity and quality of the 2D materials produced. These have significant qualitative and quantitative impacts on the 2D materials produced. For hexagonal boron nitride (hBN) exfoliation, two distinct types of hBN bulk materials were used, namely, BN25 and BN10.

Figure 4.2 shows the evaluations of the hBN bulk materials from the aspect of crystallinity, BET surface area and the defect based on XRD, BET and Raman characterisations, respectively.

The XRD (002) diffraction peak from hBN is the most prominent peak indicating the preferred orientation to c-axis. It provides information on the orientation and stacking of the aromatic rings along c-axis (Figure 4.2a). This peak is commonly selected for FWHM and crystallite size analysis of hBN. The XRD peaks are indexed according to the reference from the powder diffraction file database PDF 00-034-0421. From the curve fitted to (002) diffraction peak (Figure C1), the crystallite sizes of BN25 and BN10 as calculated from the FWHM values of the peaks were found to be comparable, measuring 0.26° and 0.22°, respectively. Using the Scherrer equation with a constant (K) value of 1.3,[310] the calculated crystallite size is 31.42 nm and 37.13 nm for BN25 and BN10, respectively. The position of (002) peak is used to evaluate the d-spacing or the interlayer spacing based on Bragg's law. The interlayer spacing of BN25 is 0.33 nm, which is the same as that of BN10. A larger d-spacing implies reduced van der Waals forces within the layers. This requires less energy for exfoliation.

Both of BN25 and BN10 exhibit lower BET surface areas than G150 and G50 graphite (Figure 2.1f). This is attributed to the presence of larger electrostatic force between the layers which renders them more prone to agglomeration. Subsequent BET surface area analysis reveals that BN25 possesses three times the surface area of BN10 (Figure 4.2b). This implies more agglomeration for BN10. Since the weights of the bulk materials used for exfoliation remain constant, the effect of surface area on exfoliation becomes important in determining the amount of 2D materials produced. The surface area of the bulk materials holds implications for the surface area accessible by solvents during both the exfoliation and dispersion processes, thereby influencing the concentration of the resulting boron nitride nanosheets (BNNSs) in the dispersion. The surface area factor represents a non-chemical and non-thermodynamic influence on concentration, distinct from other factors like material polarity and surface energy. Starting materials with a larger surface areas and interlayer spacings should be able to facilitate the exfoliation process for improved yield regardless of the solvent used. In the present work, BN25 emerges as the more suitable starting material for exfoliation compared to BN10.

Other than concentration, the quality of the initial starting material (including the presence of defects and disorder), plays a crucial role in determining the quality of the final yield of the exfoliated BNNSs. Unlike graphene, the Raman spectra obtained from BN25 and BN10 only show a single intense and sharp $E_{2g}$ peak (Figure 4.2c). The FWHM of which carries information on the crystal disorder. Since the FWHM of $E_{2g}$ peak of BN10 is 0.036 smaller than that for BN25, this difference is insignificant as it is smaller than the spectra resolution of the Raman spectrum, which is 0.53cm$^{-1}$. This suggests that both starting materials possess a comparable degree of disorder.

XPS analysis in Figure 4.2d on peak fitting via CasaXPS, indicates a low degree of oxidation for both starting materials. However, both materials contain approximately 5-6% carbon contaminations (Table C1), originated from the synthesis process and atmospheric carbon exposure during XPS sample preparations.[311, 312] The Boron (B) atom tends to form strong and stable B-C bond with carbon (C) contaminant.[313] As shown in the element atomic percentage analysis, the percentage of B is 59.59% for BN25 and 59.44% for BN10, which are higher than the percentage of N. However, not all the B are bonded with nitrogen (N) to form B-N. By deconvoluting the B1s peak, around 74% and 72% of B from BN25 and BN10 respectively, are found to be bonded with N to form B-

N. The rest of Bs are bonded with oxygen (O) and C. Both BN25 and BN10 starting materials have similar elemental composition of B, N, O and C, suggesting comparable surface chemistries for these two types of BN bulk materials. The survey spectra are shown in Figure C2 and the evaluations of N1s peak of BN25 and BN10 are shown in Figure C3.

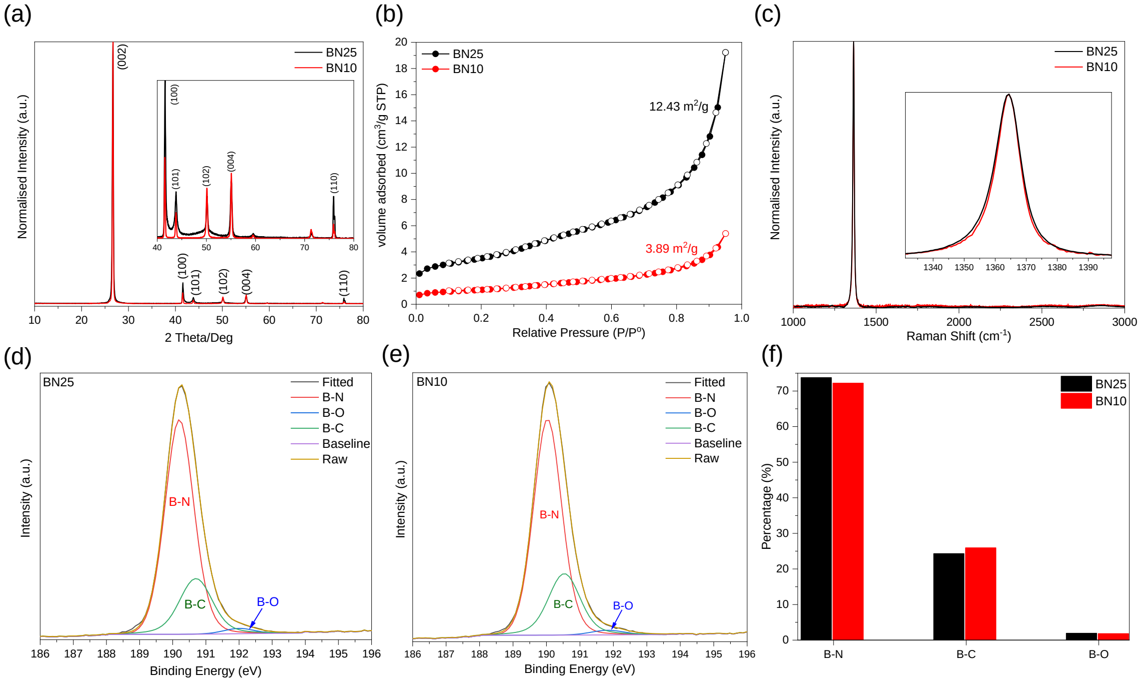

**Figure 4.2:** (a) The XRD spectra of BN25 and BN10 with the inset shows the enlarged region with small peaks beyond 40 deg. (b) BET measurement spectra and (c) Raman spectra of BN25 and BN10. XPS peak fitting/ deconvolution of B1s peak for (d) BN25 and (e) BN10. (f) Percentage of each component analysed through the fitting of B1s peak. Note: black and red represent BN25 and BN10, respectively.

### 4.3.1.2 Yield Enhancements via PEUS

From the XPS and Raman analyses of BN25 and BN10 (Figure 4.2), defect density and surface chemistry are similar for both types of BN starting materials. The primary distinguishing factor between BN25 and BN10 lies in their exposed surface areas, with BN10 demonstrating a surface area three times lower than that of BN25. This means that BN10 has three times lesser exposed surface area than BN25, available for exfoliation and dispersion of the materials in solvent. This is clearly reflected by the lower in concentration of BNNS10 as compared to BNNS25 (Figure 4.3a,b). The sequence for the solvent arrangement on the x-axis is based on the increasing order of Hansen Solubility Parameters (HSP) distance w.r.t. NMP. From the thermodynamic viewpoint, the enthalpy of mixing and exfoliation energy cost are minimised when the solvent HSP or surface tension is close to that of the material. NMP has the surface tension of 40 mJ/m$^2$ and HSP of $\delta_D$ =18MPa$^{1/2}$, $\delta_P$ =12 MPa$^{1/2}$ and $\delta_H$ =7 MPa$^{1/2}$, which is close to that of hBN.[122] Therefore, NMP is the best solvent for the exfoliation and dispersion of BNNSs. Therefore, it has been taken as the reference/ benchmark against other green solvents.

From Figure 4.3, no correlation can be observed between the concentration of BNNS dispersions and HSP distance of the solvents w.r.t NMP, for both BNNS25 and BNNS10. This implies the concentration of BNNSs is not necessarily low when the solvent HSP distance is further away from that of NMP. This shows that he efficacy of NMP as the optimal solvent for dispersing all types of BNNSs cannot be universally justified. This observation aligns well with the insights gained from Chapter 3: Section 3.4.2, where for graphene, the different types of graphene materials have different HSPs or surface energies. Therefore, the suitability of a solvent for exfoliating and dispersing a material varies with the type of the starting material used. This may be evident from the variation in trend of concentration vs. solvent HSP, with the types of BNNSs (BNNS25 in Figure 4.3a vs BNNS10 in Figure 4.3b). Beyond material-specific considerations, the determination of “best” solvent also depends on the exfoliation mechanism involved. Unfortunately, this crucial facet is overlooked in the literatures. Ironically, claims of the optimal solvent for exfoliating and dispersing 2D materials are made without due considerations to the exfoliation method employed and thus the associated mechanisms involved.

The BNNSs produced with the extra two-minute ultrasonication step introduced subsequent to shear mixing exfoliation is named as the PEUS method (Section 4.2.2.2). Accordingly, it associated two-minute ultrasonication step is denoted by “2 US”. Following the normal route in BNNSs production, NMP emerges as the superior solvent for the exfoliation and dispersion of both BNNS25 and BNNS10. Nevertheless, with the introduction of the PEUS (2 US) method, IPA and EtOH:D.I. outperform NMP for the production of BNNS25 (Figure 4.3). The solvent mixtures which are denoted as EtOH:D.I. and IPA:Ace, are with the 1:1 volume ratio. In the case of BNNS10, its concentration in EtOH:D.I. is comparable to that of NMP after PEUS (2 US) treatment. The ability of EtOH:D.I. solvent mixture to exfoliate and disperse graphene under ultrasonication has been previously established.[96] High-speed imaging with acoustic measurements has shown that in EtOH:D.I. under ultrasonication, high intensity pressure peaks (as generated from the collapse of cavitation bubbles) were formed as compared to using pure EtOH solvent.[314] The concentration of BNNS25 produced in IPA after shear mixing (without PEUS) is slightly lower than NMP but is the highest among all the green solvents. The introduction of the 2 US step in PEUS helped in dispersing the exfoliated BNNS25 after shear mixing in IPA better than the NMP. This resulted in BNNS25 (2 US) concentration in IPA higher than that in NMP. IPA has also been proven by simulations to be able to intercalate into the hBN interlayers to facilitate the exfoliation and dispersions of the layers (excellent dispersing agent).[207]

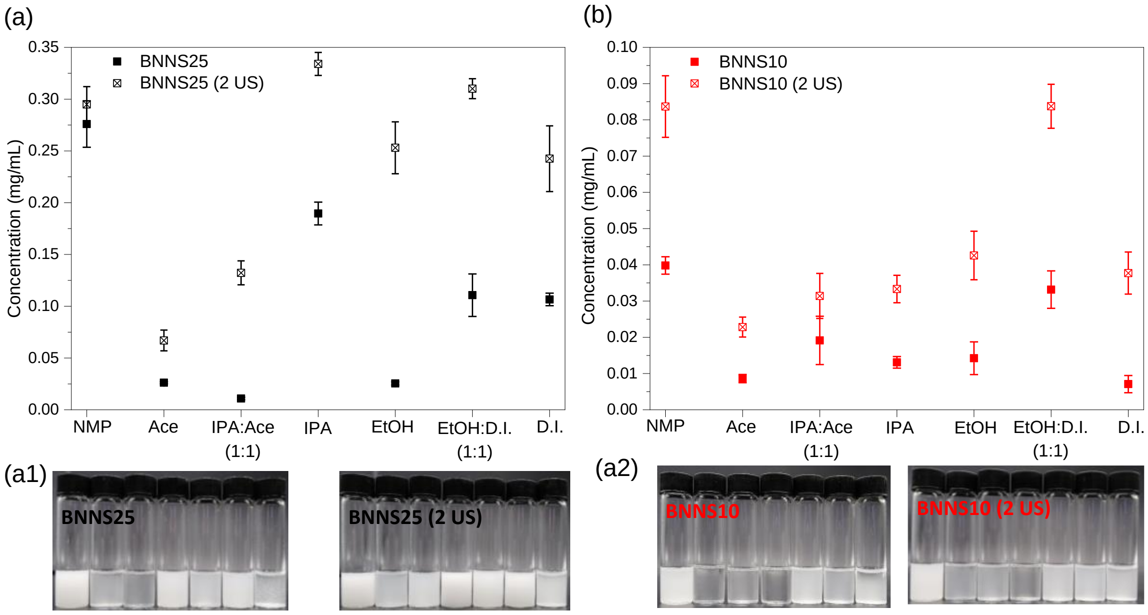

**Figure 4.3:** The concentration of (a) BNNS25 (with and without 2 US) and (b) BNNS10 (with and without 2 US) produced in the solvent media shown in x-axis. Error bars showed the standard deviation obtained through at least three sets of repeated experiments. (a1-a2) Digital images of the boron nitride nanosheets dispersions presented in (a-b), respectively, and arranged according to the solvent sequence shown in the x-axis of graphs (a) and (b).

The introduction of the 2 US step in PEUS after shear mixing has been demonstrated to enhance the concentration of BNNS in various solvents. This simple ultrasonication step after exfoliation facilitates the dispersion of the exfoliated graphene produced by shear mixing. Figure 4.4 shows the enhancement in BNNS concentration after applying the PEUS method on BNNS25 and BNNS10. The highest concentration increase for BNNS was 12 times, which was achieved by BNNS25 in IPA:Ace mixture. For graphene, the increase could be up to 90 times with the PEUS (2 US) as may be seen in Figure 3.4b. IPA:Ace mixture, IPA and EtOH are also the good solvents for dispersing graphene using PEUS method (Figure 3.4). Furthermore, stability test conducted on BNNS25 (2 US) dispersion in IPA (identified as the optimal solvent yielding the highest BNNS25 concentration) has shown a sustainable stability over a 5-months duration. Thus, the introduction of a short duration ultrasonication after shear mixing not only helps in improving the concentration of the dispersion but also enhances its long-term stability.

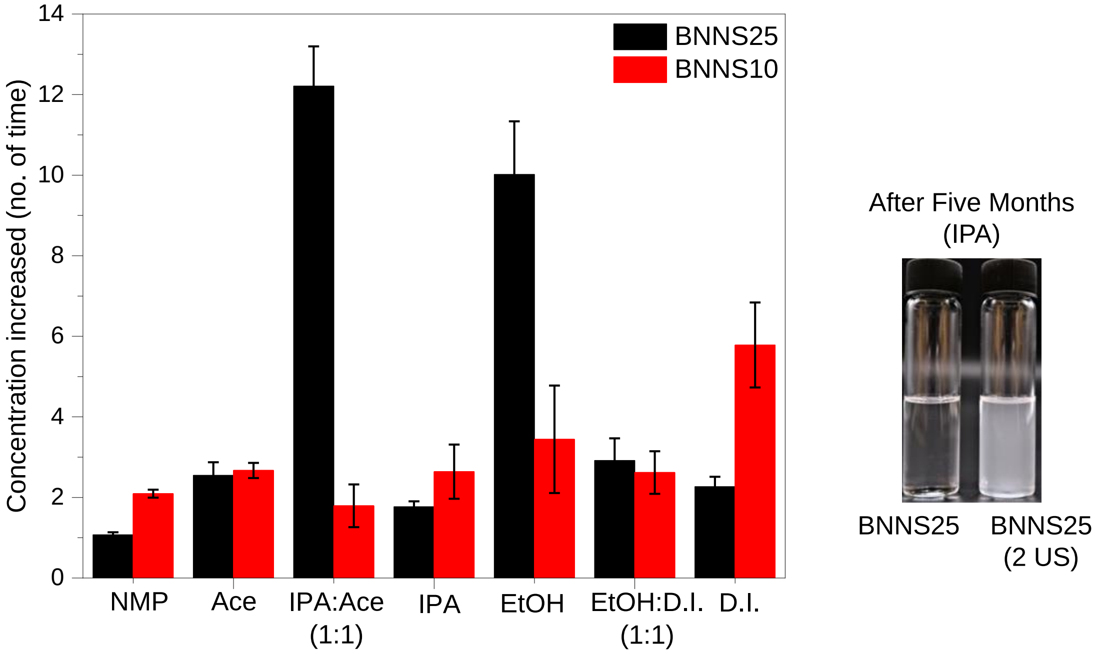

**Figure 4.4:** The number of times of concentration increase after imposing 2 US yield improvement step for BNNS25 and BNNS10. The error bars are constructed based on at least three repeated experiments. The digital image on the right shows the 5-month stability comparison between BNNS25 dispersions with and without 2 US.

## 4.3.2 Quality Assessment of BNNS Dispersions

### 4.3.2.1 UV-Vis Spectroscopy

Figure 4.5 are the UV-Vis spectra of BNNS25 and BNNS10 in green solvents. Dashed lines represent the UV-Vis spectra recorded from BNNS25 (2 US) and BNNS10 (2 US). The distinctive peak below 210 nm, specifically within the range of 203 to 206 nm, is a commonly observed feature in the UV-Vis spectra of hBN sheets, as reported in previous studies.[315, 316] Notably, for BNNS25, the appearance of a peak beyond 210 nm is exclusive to the scenarios involving exfoliation in EtOH and IPA solvents with ultrasonication. This is irrespective of whether it has been achieved through a three-hour ultrasonication or three-hour shear mixing followed by two-minute ultrasonication (2 US) under PEUS method, as shown in Figure C5 and Figure C6. This peak also persists in the diluted dispersion of BNNS25 in EtOH and IPA (Figure C7). This proves that the occurrence of this peak is independent of the concentration of BNNS25 in these solvents. The peak position shifted to lower wavelengths (but still beyond 210 nm) with the decrease in the concentration of BNNS25. The peak around 215 nm aligns well with that observed from high-pressure thermal-synthesized hBN flakes, while that around 220 nm can be observed from hBN film grown via metal-organic chemical vapour deposition (MOCVD) with high-temperature post-synthesis annealing.[317, 318] The presence of these peaks may be attributed to the structural changes induced by thermal effects during ultrasonication, as it generates heat or hot spots during the ultrasonication process.[319, 320] BNNS25 subjected to PEUS (2 US) in IPA and EtOH:D.I. demonstrates the presence of the peak at 270 nm, indicative of the preservation of the $sp^2$ structure.[321] This observation holds true for BNNS10 in IPA and EtOH as well (Figure C5).

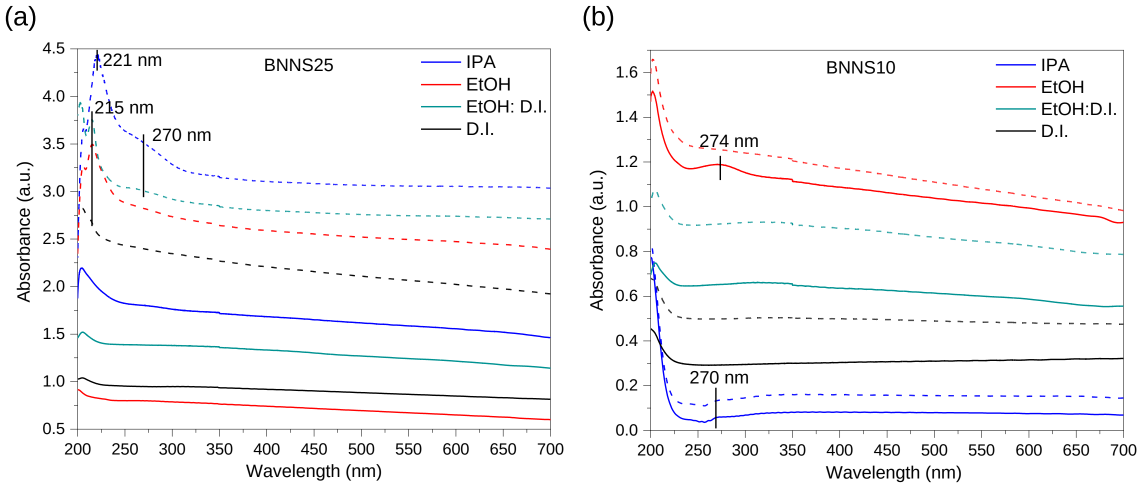

**Figure 4.5**: The UV-Vis spectra of (a) BNNS25 and (b) BNNS10. The dashed lines show the spectra of the dispersions with 2 US. Major absorption peaks are labelled.

### 4.3.2.2 Raman Spectroscopy

In contrast to the distinctive Raman fingerprint observed in graphene, the Raman spectrum of hexagonal boron nitride nanosheets (BNNSs) manifests itself solely as the peak at 1364-1365 $cm^{-1}$,[322,323] attributed to the $E_{2g}$ vibration mode of B-N. Notably, there is also an absence of the D peak and 2D peak.–In comparison to graphene, the Raman effect in hBN is notably weak owing to the far off-resonance excitation. Consequently, this hinders the extraction of information regarding thickness, strain, doping, and size from Raman spectra of hBN and poses considerable challenges. [324]

In the case of graphene, the FWHM in Raman spectroscopy provides valuable insights into the crystallite sizes and defects. However, the analysis of the size and defects from FWHM in hexagonal boron nitride (hBN) remains a challenging endeavour. The presented data in Figure 4.6a reveals that the FWHM remains constant with the exfoliation of the same type of BNNS. Considering the Raman spectra resolution of 0.53 $cm^{-1}$ with the 1800 lines/mm grating employed, the variation of less than 0.2 $cm^{-1}$ in FWHM is not significant. Nevertheless, discernible distinctions in FWHMs are observed between two distinct types of BNNS (BNNS25 and BNNS10), attributed to the differences in crystallite size as elucidated by X-ray Diffraction (XRD) analysis in Section 4.3.1.1.

Unlike graphene, where the $E_{2g}$ peak position provides information on the thickness of the material, this is not the case for hBN. Generally, there is no correlation between the $E_{2g}$ peak frequency or position and the BNNSs thickness, as indicated from the literature.[325] This observation is substantiated by the results Figure 4.6b, where almost similar $E_{2g}$ peak positions are observed across a range of exfoliation conditions and thicknesses of BNNSs, including bulk materials (BN25 and BN10) and shear mixing exfoliated BNNS, with and without using 2 US in PEUS method. Furthermore, the absence of a significant shift in the $E_{2g}$ peak positions between supernatant and sediment of the BNNS25 (2 US) dispersion, which have been left for one month, further emphasizes the lack of thickness dependence of the peak position. The raw Raman spectra are shown in Figure C8 and Figure C9.

A separate study elsewhere has shown a significant variation in $E_{2g}$ peak FWHM with BNNS thickness.[326] However, the findings from the present study suggest that $E_{2g}$ peak FWHM primarily varies with the type or size of BNNS rather than its thickness alone. The discrepancy in this finding compared to the literature may be attributed to the literature method in sorting thickness using various centrifugation speeds. At higher centrifugation speed, not only thinner but also smaller nanosheets are obtained. Hence, apart from thickness, size also influences the observed variation in FWHM in their study.

Despite the limitations associated with utilising the Raman peak for hBN property analysis, it has been reported that the $E_{2g}$ peak position is close to 1367 cm$^{-1}$ and FWHM of around 9.1 cm$^{-1}$ for a high-quality single crystal hBN. Higher frequency of $E_{2g}$ peak (~1381 cm$^{-1}$) indicates the presence of strain in the materials.[327] The increase in the $E_{2g}$ peak position upon exfoliation (Figure 4.6b) may be attributed to the strain induced by shear force and cavitation bubbles during exfoliation process.[328] Based on the qualitative Raman spectroscopy analysis on hBN and exfoliated BNNS, the FWHM and position of $E_{2g}$ peak for the exfoliated BNNS follows that of its starting bulk material. It is therefore noteworthy to mention that the characteristics of the starting bulk materials not only influence the concentration of the BNNS dispersion produced but also impact the quality of the resulting BNNS.

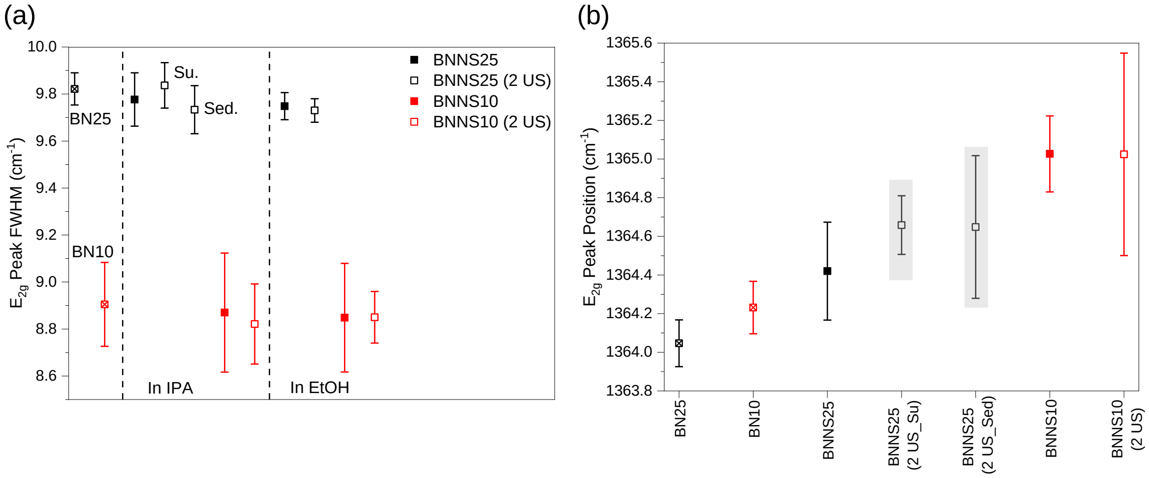

**Figure 4.6:** Raman spectroscopy analysis on the (a) FWHM and (b) peak position of $E_{2g}$ peak for BNNS25 and BNNS10, with and without 2 US. BN25 and BN10 are the bulk starting material for exfoliation to produce BNNS25 and BNNS10 respectively. Su. and Sed. are the supernatant and sediment of the dispersion left for one month. All the dispersion shown in the x-axis of peak position analysis graph in (b) are in IPA. Error bars are constructed from the standard deviation of measurements at a minimum of six randomly selected points on the sample.

### 4.3.2.3 X-Ray Photoelectron Spectroscopy (XPS)

The XPS analysis in Figure 4.7 elucidates the surface chemistry for BNNS25 in IPA upon PEUS (2 US), through the analysis on the B-N, B-O and B-C species. The analysis was done by the fitting of B1s spectrum of Boron using CasaXPS software with the reference to the established literature sources.[329, 330] BNNS25 in IPA was selected for this study owing to its highest concentration dispersion obtained using PEUS (2 US) (Figure 4.3). Chemical analysis using XPS provides information on whether the improve in concentration after 2 US is due to the surface chemical modification upon ultrasonication or physical process associated with the disperse of BNNSs through ultrasonication. Carbon presence in the unexfoliated BN powder (BN25 and BN15) was attributed to the source from atmospheric carbon contamination as explained in section 4.3.1.1, while carbon in BNNS25 (in IPA) after shear mixing exfoliation was due to unavoidable contamination from carbon impurities in the shear mixer used for graphite exfoliation. While every precaution has been taken to avoid carbon contamination including cleaning of the equipment after each exfoliation process, complete elimination of carbon contaminant was a formidable challenge in present case.

The chemical composition of BNNS25 remains mostly consistent after the introduction of the 2 US step from PEUS except for the small increase in B-N content (from 70% to 73%). This was due to the reduction in B-C and B-O species after 2 US, which could be a consequence of the removal of surface carbon and oxygen species through ultrasonication. This means that 2 US after the shear mixing exfoliation helps in dispersing the exfoliated BNNSs to increase the concentration without substantially altering their surface chemical composition. The peak fitting on the N1s spectrum of Nitrogen for the composition of N-B, N-C and N-O is shown in Figure C4 as the complimentary analysis to B1s spectrum.

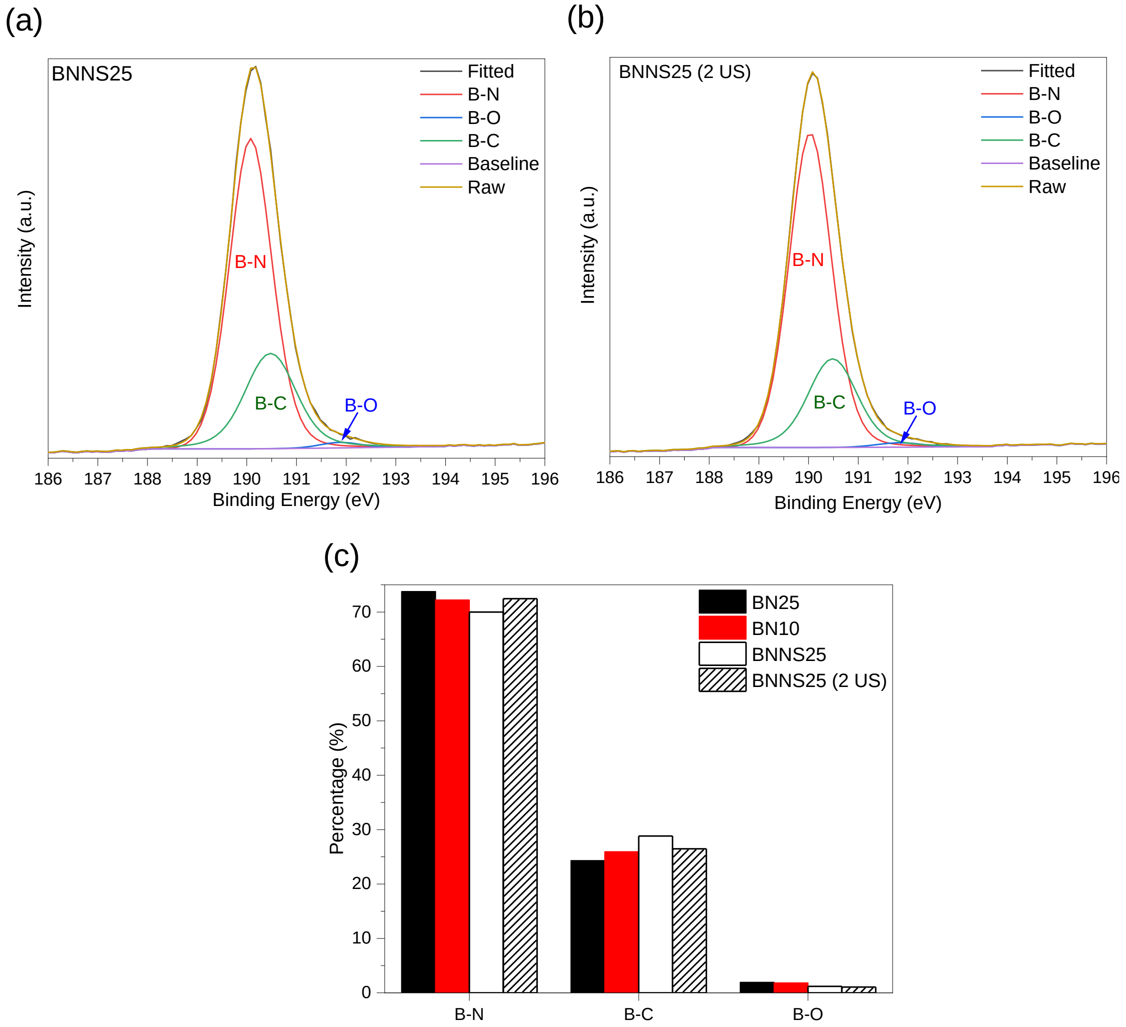

**Figure 4.7**: XPS peak fitting/ deconvolution of B1s peak for (a) BNNS25 and (b) BNNS10. (c) Percentage of each component analysed through the fitting of B1s peak. The data of BN25 and BN10 starting materials are included here for comparison.

### 4.3.2.4 Atomic Force Microscopy

Figure 4.8 presents the AFM images of BNNS25 (2 US) in IPA (the dispersion with highest concentration) and BNNS10 (2 US) in IPA. More AFM images of BNNS25 (2 US) are shown in Figure C10.

BNNS25 (2 US) exhibits larger and thinner characteristics relative to BNNS10 (2 US). The lateral dimensions of BNNS25 (2 US), measured from its longest side, are approximate two microns, whereas the lateral dimensions of BNNS10 (2 US) are less than two microns. The thickness of BNNS25 (2 US) ranges from 3 to 6 nm, while BNNS10 (2 US) can attain a thickness of up to 10 nm. Apart from the solvent and substrate effects,[331–333] it is important to note that the measured thickness is greater than the actual thickness due to flake stacking during the deposition on substrate, which is particularly notable for BNNS10 (Figure 4.8b). The measured thickness of monolayer BNNS may range from the theoretical value of 0.33 nm to 0.4 nm depending on the type of substrate and the surface water layer absorption.[334, 335]

BNNS25 are exfoliated from its bulk material (BN25) with three times more exposed surface than BN10. This implies that the former has undergone a more efficient exfoliation to yield thinner BNNSs. From the AFM images, BNNS25 sheets are in a more spherical morphology compared to the hexagonal morphology observed in BNNS10. The BNNS10 are more densely packed and stacked as those are exfoliated from the lower surface area BN10. The exfoliation from BN10 is less efficient as compared to BN25. This is also the reason behind the lower yield of BNNS10. Selecting the starting material with high total exposed surface area would yield higher concentration of thinner BNNSs.

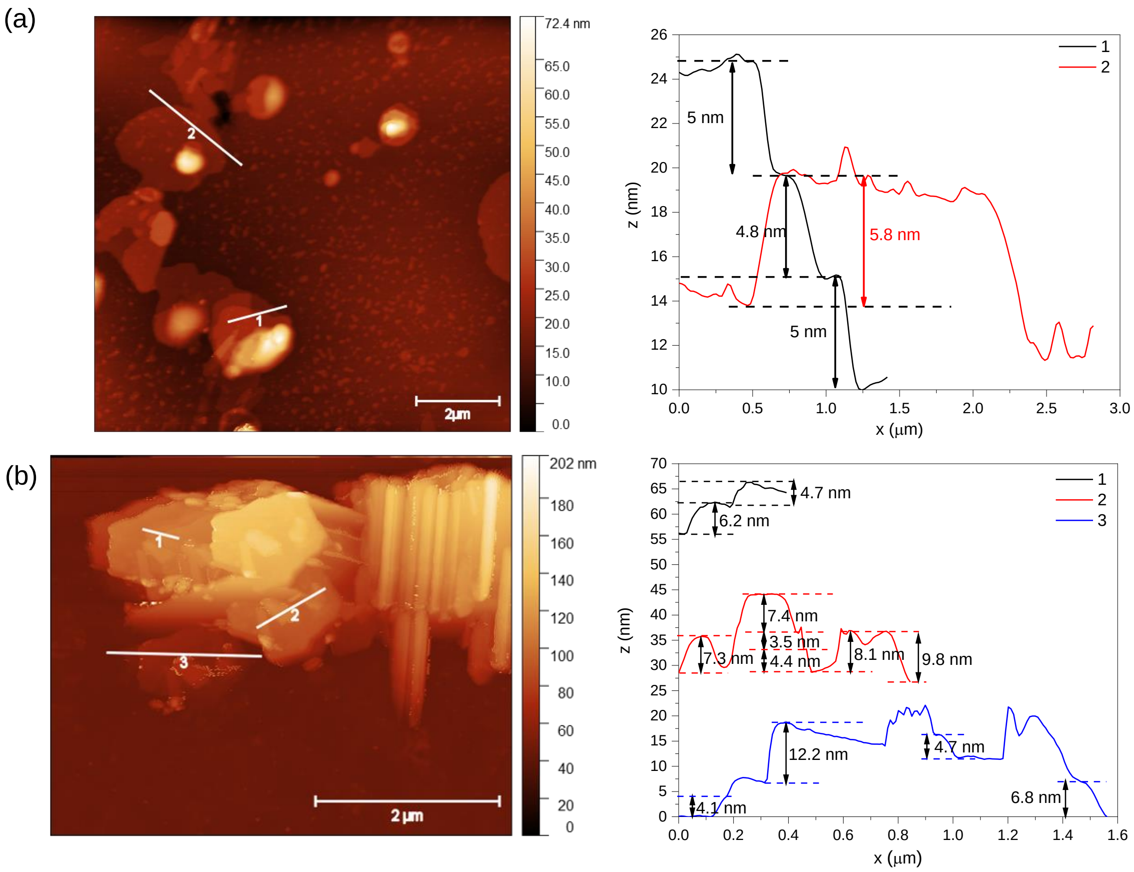

**Figure 4.8**:The AFM images of (a) BNNS25 (2 US) and (b) BNNS10 (2 US) produced in IPA, which the thickness profile shown on the right of the corresponding images. The exfoliation to produce BNNS10 (2 US) is less successful as compared to the case of BNNS25 (2 US).

### 4.3.3 BNNS-Graphene Composite

Owing to its unique electrical and optical properties, hBN-graphene composite demonstrates extensive applications like the metal-free electrocatalysts for oxygen reduction reaction of fuel cells,[336] transistors,[337] and supercapacitors.[338] Successful production of high yield graphene and BNNSs via LPE involves careful formulation of the exfoliation and dispersion solvent media and the use of PEUS method to further enhance the concentration. This drives the interest to use the state-of-art NMP solvent, together with the high performed green solvent, IPA to synthesize the BNNS-graphene composite.

Previous study elsewhere explored the liquid phase exfoliation method for hBN-graphene synthesis.[338] A multi-step procedure involves separating the exfoliation of h-BN and graphite powder in a urea/ glycerol solvent mixture with mechanical stirring. This is followed by subsequent redispersion of the exfoliated hBN and graphene into dimethylformamide (DMF) solvent. The dispersion is homogenised and purified via ultrasonication, followed by centrifugation to obtain the final hBN-graphene heterostructure flakes. Alternatively, a combination of ball milling, saturated acid mixing, high-temperature (950°C) synthesis, and ultrasonication in DMF has been employed.[339] The LPE synthesis of BNNS-graphene often involves multiple steps in harsh synthesis environment, presenting an opportunity to explore the feasibility of using the PEUS method to produce BNNS-graphene.

Figure 4.9a are the Raman spectra recorded from BNNS-graphene composite produced in various solvents. The BNNSs and graphene in BNNS-graphene are denoted as BNNS25 and GR150, respectively (Section 4.2.2.1). Efficient dispersion of both BNNS and graphene in the solvent is crucial for achieving a high yield of the BNNS-graphene in the final dispersion. The presence of the graphene is identified through major peaks which are D, G, and 2D peaks, while the presence of BNNS by the $E_{2g}$ peak. In solvents such as EtOH, no significant graphene peaks are observed, indicating predominant BNNSs production. The graphene peaks were observed with BNNS peak when NMP solvent is used. This implies that NMP is good in dispersing graphene. The solvent mixture consists of IPA and NMP in 1:1 volume ratio (denoted as IPA:NMP), is also tested for its ability to disperse both BNNS and graphene. IPA is selected to form mixture with NMP because it is the best green solvent to disperse both BNNS and graphene. Despite the prominent observation of graphene peaks, the BNNS peak remains predominant in IPA:NMP. The 2 US step in PEUS clearly helps in improving the dispersibility of graphene in IPA:NMP, as can be evident from the higher graphene G and 2D peaks in relative to without the 2 US step. The broadening of the FWHM of $E_{2g}$ peak with the 2 US process is due to the signal contribution from the D peak of graphene as a result of peak overlapping. The G peak of graphene is overlapped with $E_{2g}$ peak of BN for the BNNS-graphene in NMP. These two overlapped peaks are deconvoluted based on the Lorentzian function (Figure C11a).

The 2 US in PEUS after shear mixing exfoliation has been proven to be effective in improving the yield of pure BNNS and pure graphene in IPA, EtOH and NMP. However, this increase in concentration, which corresponds to the increase in absorbance of UV-Vis (Figure 4.9b), is not significant for BNNS-graphene. The 270 nm peak, the $\pi$ to $\pi^*$ absorption peak of BNNS and graphene, is observed for the BNNS-graphene produced in EtOH, which becomes prominent after the 2 US process. Observation of the peak at 230 nm in Figure 4.9c is also reported in the literature for oxidised graphene,[340] or graphite layers with intercalated components.[185] This can be used to explain the case of graphene intercalated-BNNS layers. The UV-Vis spectra of the dispersions with NMP are not shown here because the UV cut-off of NMP is at 285 nm, so the major absorption peaks before this cut-off wavelength cannot be observed.

It is worth emphasizing the role of 2 US in improving the yield of BNNS-graphene. IPA:NMP is good at exfoliating both BNNS and graphene but not as good in dispersing the exfoliated flakes as the pure NMP solvent. Hence, the 2 US helps in facilitating the dispersion of the flakes. Although 2 US helps in improving the concentration of BNNS or graphene in EtOH and IPA, this method does not work for BNNS-graphene in these solvents. The possible reason for this is the 2 US in EtOH and IPA is insufficient to overcome the strong stacking van der Waals forces between BNNS and graphene to disperse the BNNS-graphene. Additionally, the density of EtOH and IPA is inadequate to support the stabilised BNNS-graphene. Consequently, the materials sink as the sediment after the centrifugation and are not collected as the final product (only supernatant is collected as the final BNNS-graphene dispersion).

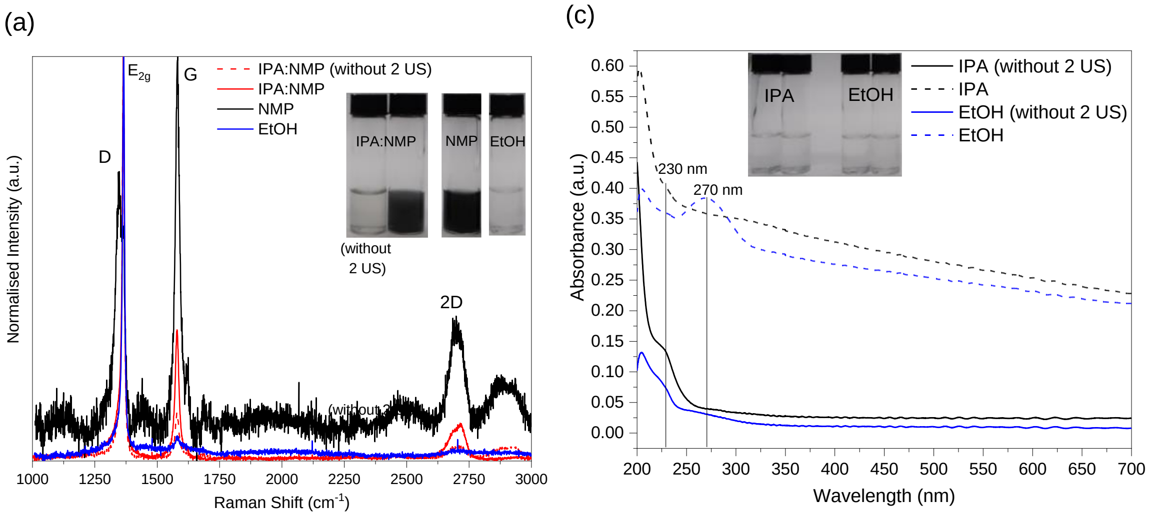

**Figure 4.9**: (a) Raman spectra of BNNS-graphene produced in different solvents and solvent mixture. $E_{2g}$ peak belongs to BNNS while D, G and 2D peaks are the peaks from graphene. The spectra are normalised to the highest peak. Inset: Digital images of BNNS-graphene dispersions. (b) The UV-Vis spectra of BNNS-graphene in IPA and EtOH, showing the BNNS and graphene absorption peaks. Inset: Digital images of BNNS-graphene dispersions in IPA and EtOH. For each set of dispersion in the same solvent, the one on the left is without 2 US. Note: All the BNNS-graphene are produced with 2 US unless otherwise specified.

# 4.4 Conclusions

Other than graphene, the PEUS method with brief 2-minutes ultrasonication (2 US) step after shear mixing exfoliation has successfully served as a simple, cost-effective, and scalable method facilitating the dispersion of BNNSs. This has led to up to 12-fold yield enhancement in IPA (compared to the yield obtained following the normal routes in shear mixing exfoliation). The thickness of the exfoliated BNNSs in IPA produced using PEUS with 2 US treatment can be down to seven layers. The quality and yield of BNNSs produced in each solvent medium is highly dependent on the type of starting material (the bulk hexagonal boron nitride) used for exfoliation. IPA and Ethanol: Deionised Water (EtOH:D.I.) solvent mixtures are the green solvents that demonstrate promising yields for both types of starting materials. Generally speaking, starting materials with higher exposed surface areas and smaller crystallite sizes tend to produce higher yields of thinner BNNSs.

Extending the efficacy of the PEUS method with 2 US to BNNS-graphene composite synthesis in IPA:NMP solvent mixture is noteworthy. The PEUS method not only enhances overall yield of the BNNS-graphene dispersion but also facilitating the dispersion of additional graphene. This breakthrough opens avenues for tailoring the IPA:NMP ratio~~.~~

# 5

# Thesis Conclusion and Future Work

## 5.1 Thesis Conclusion

At the initial stages of this research, three major challenges were identified as mentioned in Chapter 1, Section 1.5. Firstly, there was lack of a reliable method to experimentally determine the surface energies of the starting materials. Secondly, there was also no reliable method to independently study the exfoliation efficiency and dispersibility of 2D materials in green solvents. Lastly, there was no direct method to enhance the yields of 2D materials in green solvents without the use of surfactants, functionalisation, or dispersants.

These challenges were solved as the research progressed. Firstly, by the introduction of the NMP and green solvents for the redispersion of the exfoliated graphene. This redispersion technique allows the "deconvolution" of the combined contribution from exfoliation efficiency and dispersibility to the overall graphene yield. The key finding from this deconvolution process has led to the crucial insight into the exfoliation efficiency of green solvents. These green solvents, particularly IPA, have been found to have high exfoliation efficiencies and are capable of producing graphene at concentrations as high as or even higher than that of the widely recognised NMP solvent. The graphite surface energy analysis and shear force simulation results have unravelled the reason behind the high exfoliation efficiency of IPA. The main hindrance to achieving high graphene yield by using green solvents has been attributed to low graphene dispersibility. To overcome this issue, a simple yet effective yield optimisation method has been devised for yield enhancement negating the need for surfactants/ dispersants or functionalisation. This method involves the imposition of a brief ultrasonication step as short as two minutes after exfoliation, or the so-called Post Exfoliation Ultrasonication (PEUS) method. This results in a remarkable increase in graphene yield of up to 90 times, specifically in IPA solvent, with minimal defects generation. Interestingly, when applied to the exfoliation of hexagonal boron nitride, a 12-fold increase in the yield of the exfoliated boron nitride nanosheets was achieved in IPA solvent.

Since the choice of an effective solvent for exfoliation depends on the graphite surface energy, in this research, the surface energy of graphite used for the exfoliation was determined and evaluated using Washburn method, considering both the polar and non-polar components of the surface energy. This information is of paramount importance for the selection of a suitable solvent with the desired surface tension for exfoliating specific graphite types and other layered materials.

The efforts spent in this work have led to several areas of future research. One key area is the development of a universal solvent selection theory to provide a guidance on solvent selection for the production of different 2D materials or production of graphene from different graphite materials by shear mixing exfoliation. Additionally, when considering the low toxicity and low boiling point of green solvents, there is potential for designing solvent recovery and reuse systems to facilitate the scale-up and continuous production of 2D materials. Lastly, the solvent study and evaluation techniques developed for graphene and hexagonal boron nitride nanosheets could be extended to the sustainable production and property tuning of other 2D materials, such as molybdenum disulphide

($MoS_2$) and tungsten disulphide ($WS_2$). These future works would potentially lead to a low cost, large scale, and sustainable production of 2D material dispersions or 2D material inks for substrate printing technology in the fabrications of sensors and energy devices.

## 5.2 Future Work

### 5.2.1 Enhancing Result Validation and Improving Characterisation Technique

Despite extensive studies aimed at understanding the solvent parameters and factors influencing graphene yield and quality, further research is needed to validate the findings and address remaining gaps.

In this work, the surface energy of graphite was measured to investigate solvent parameters affecting the graphite-solvent interaction during exfoliation. However, the surface energy of graphene has not yet been measured. Since dispersibility is governed by the graphene-solvent interaction, measuring graphene's surface energy would provide valuable insights into the solvent parameters that dictate graphene dispersibility.

Regarding graphene quality characterisation, additional AFM images should be collected to enable statistical analysis of the thickness and lateral dimensions of graphene produced from different solvents or exfoliation techniques. Moreover, conducting Raman measurements on well-dispersed individual flakes on a substrate, rather than aggregated graphene, will yield more accurate data in identifying the types of defects present. Transmission electron microscopy (TEM) can also serve as a complementary technique to further investigate defects and determine graphene thickness.

### 5.2.2 Theoretical Model for Solvent Selection

My future research aspiration is to create a model for the design of green solvents with low boiling points and low toxicity for exfoliating and storing of graphene and other 2D materials. The existing models in literature focus on the selection of solvents by matching their surface tensions with the surface energy of graphene. These models neglect other key factors like the types of starting material used for exfoliation and other properties of solvent media, for example, viscosity. Additionally, the present models for solvent selection mainly concern the overall yield of graphene, without addressing the effectiveness of the solvent in exfoliation (exfoliation efficiency) and the ability of the solvent to disperse the exfoliated material (dispersibility). There is, therefore, a need for a new model which includes the contributions from these two factors to the overall yield of graphene in the final dispersion.

In this research, a technique to experimentally study the exfoliation efficiency and dispersibility of graphene in a series of solvents and solvent mixtures was developed. This lays the groundwork for a more robust theoretical models incorporating the criteria for selecting solvents based on experimentally determined exfoliation efficiencies and dispersibilities. These models should prove useful in identifying the suitable green solvents for each step of the exfoliation and dispersion processes in LPE. To enhance the current database of solvent properties which are related to exfoliation efficiency and dispersibility, a broader range of solvents and types of graphite or graphene materials should be included in the future. The initial findings from the present work suggest that the ratio of polar to dispersive components of the solvent plays a critical role in determining the exfoliation efficiency (Section 2.4.3). However, more detailed work and experimental data are necessary to establish this claim.

An experimental analysis of the impacts of viscosity and surface tension on exfoliation efficiency and dispersibility, based on shear mixing exfoliation for two distinct graphite types is presented in Figure 5.1. Besides the commonly mentioned surface tension and solubility parameters, viscosity emerges as an important factor affecting the shear forces in LPE. This is the key determinant of the exfoliation efficiency in shear mixing.

The shaded regions in the Figure 5.1 represent the "preferential" regions for solvent selection. It can be noticed from the figure that higher solvent viscosity within these shaded regions favour both exfoliation and dispersion of both graphene types. However, the construction of a reliable theoretical model should include more experimental data, especially within these shaded regions. Similarly, for surface tension, a greater number of data points within the shaded regions are required for the selection of suitable solvents with the correct surface tension for efficient exfoliation and dispersion of graphene.

Figure 5.1c1&d1 provide the magnified views of the regions between surface tensions of 21.5 to 24 mN/m. This range corresponds to the surface tension of most of the low boiling point green solvents such as isopropanol, ethanol, acetone, ethyl acetate, etc. For additional data points, one needs to include more solvents or solvent mixtures to tune the viscosity and surface tension values to cover the range of interest.

This proposed solvent selection method could be extended to accommodate other types of 2D materials. Additionally, this model serves as a valuable tool for identifying optimal solvents for exfoliating and dispersing graphene derived from various waste graphite sources, such as waste batteries, as well as animal and plant-derived waste.[44] By improving solvent selection, this approach can help lower the production costs of graphene while enhancing the sustainability of its production life cycle.

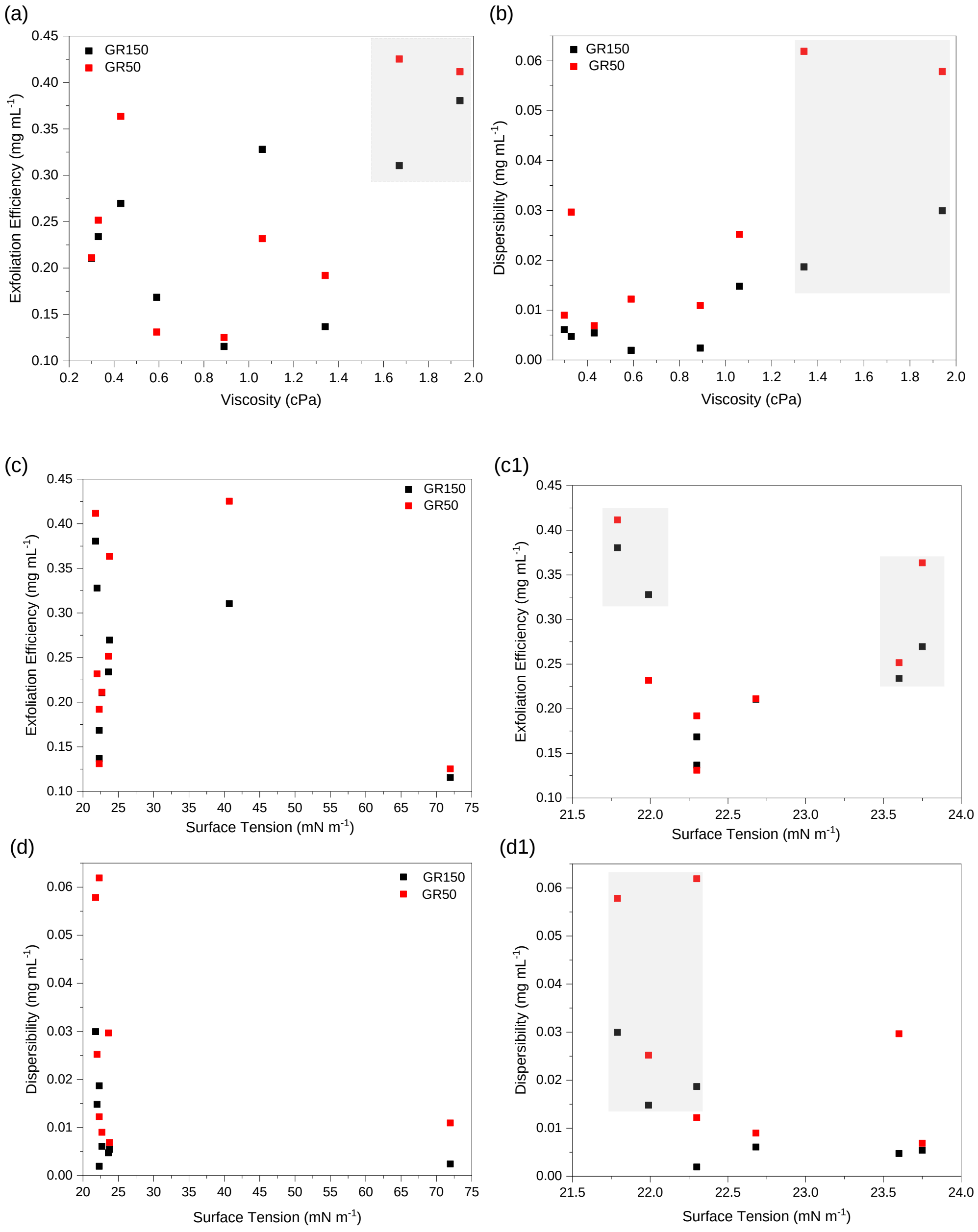

**Figure 5.1:** (a) Exfoliation efficiency and (b) graphene dispersibility of solvents with different viscosities. (c) Exfoliation efficiency and (d) graphene dispersibility of solvents with different surface tension. (c1 and d1) are the enlarged of (c and d) respectively, focusing on the low surface tension region. The data are obtained from two different types of graphene, GR150 and GR50, exfoliated from different types of graphite. Shaded regions are the regions with recommended solvent viscosity or surface tension range for achieving high exfoliation efficiency and dispersibility.

### 5.2.3 Solvent and Material Recovery System

Using green solvents with low boiling points and low toxicities has several advantages; these solvents can be easily evaporated, recovered, and reused for subsequent graphene exfoliation processes. Additionally, the graphite aggregates that remain unexfoliated or partially exfoliated can be removed as sediment by centrifugation after the exfoliation, and can be reused in subsequent exfoliations, thus contributing to an increase in graphene yield.

This material recovery and reuse protocol was tested at the lab-scale for three continuous exfoliations using IPA as solvent (Figure 5.2a). 90% of the solvent from first exfoliation was successfully recovered using rotary evaporator. This recovered solvent was then used for at least two more exfoliations. By recycling the graphite aggregates left over from past exfoliation processes, a yield increase of up to 0.5% per exfoliation run was achieved. The post-exfoliation ultrasonication technique as reported in Section 3.2.2.2, was employed to enhance the yield. Notably, this material recovery and reuse system outperformed the yield increase by other methods reported elsewhere in the literature, using the same graphite starting material and water-surfactant as the solvent. [76] As mentioned earlier, a higher yield increase of 0.5% per exfoliation run was achieved compared to only 0.15% reported in the literature.

Exfoliating graphene from recycled graphite aggregates is more efficient compared to from fresh graphite because these aggregates have already partially exfoliated and smaller in sizes. This leads to an increase in the yield for each subsequent exfoliation run to be greater than the one before, as evident from Figure 5.2a. Besides yield, the quality of the graphene produced from recycled graphite is a key concern in graphene production. Raman spectroscopy analysis has shed some lights on the crystal defects and lattice disorders of the graphene. Generally, graphene produced from subsequent recycling shows a wider distribution in size and quality (broader error bars in Figure 5.2b&c). The FWHM of the G peak in the Raman spectrum reflects graphene crystal disorder, with the greater disorder reflected by larger G Peak FWHM. The graphene produced after second recycling exhibits higher disorder than the graphene produced from the fresh graphite and from the first recycling (or second exfoliation) (Figure 5.2b). The $I_D/I_{D'}$ intensity ratio decreases from the first recycling process signifies a reduction in size. A low $I_D/I_{D'}$ ratio around 3.5 indicates edge defects, commonly seen in small-sized graphite with a high density of exposed edges.[220] Raman spectroscopy analysis reveals more defective graphene is produced from recycled graphite aggregates. While this is undesirable for certain applications, it can be advantageous to applications requiring slightly defective properties, such as for catalysis.

This lab-scale methodology has the potential of scaling up to industrial level. It offers a continuous solvent recovery and materials recycling route for the sustainable graphene and 2D materials production while minimising waste at the same time. All of these benefits demand for an efficient and innovative design of high-yield industrial graphene production infrastructure.

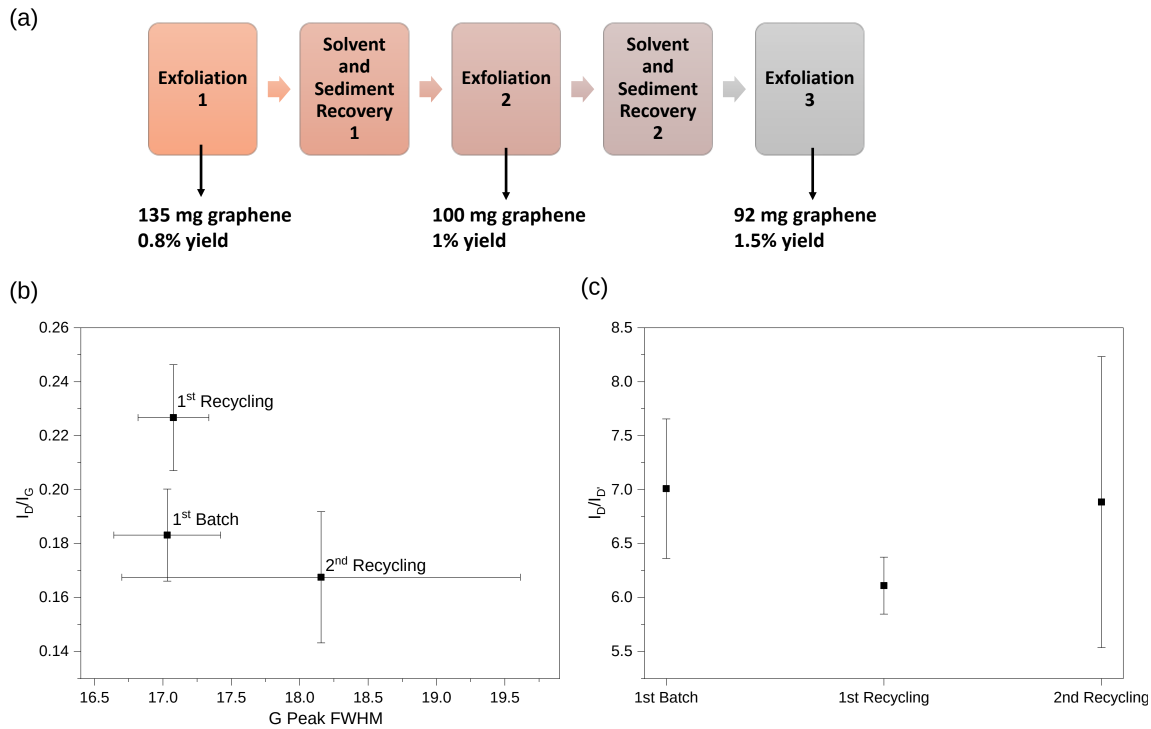

**Figure 5.2**: (a) Schematic of a lab-scale system for solvent and material recovery during graphene production, with indicated graphene mass produced and total yield achieved after each exfoliation stage. (b,c) Raman spectroscopy analysis comparing defect and lattice disorder in graphene produced from fresh graphite (first batch) to that produced from recycled graphite aggregates, including second and third recycling stages. Error bars represent standard deviation from Raman spectra data at six randomly selected points.

### 5.2.4 Sustainable Production of Other Two-Dimensional Material Dispersions with Bandgap Tuning

LPE is a versatile and cost-effective method for producing 2D materials. In the present research, the shear mixing, which is one of the techniques from LPE, has been used to produce graphene and hexagonal boron nitride nanosheets (BNNSs). To improve the dispersibility of these exfoliated materials in green solvents, a brief PEUS method was introduced right after the exfoliation. This shear mixing-PEUS method has proven to be effective in enhancing the dispersion of exfoliated graphene and BNNSs in green solvents. This approach has the potential extending its applications to other 2D materials like $MoS_2$ and $WS_2$. The resulting dispersions obtained are compatible with the printing technologies on substrates, thus suitable for electronic and other energy device applications.

$MoS_2$ and $WS_2$ are notable materials with applications in optoelectronic devices such as transistors and photodetectors.[341, 342] $MoS_2$, in particular, exhibits excellent properties for photocatalysis.[343] Acetone and IPA have been identified as the effective green solvents for LPE of $MoS_2$.[344] Here, $MoS_2$ exfoliation using various green solvents, including acetone and IPA, have been investigated as a preliminary study of the proposed future work. Unexpectedly, the as-produced $MoS_2$ dispersions using the shear mixing-PEUS exfoliation method exhibits different colours in different solvent media (Figure 5.3a). This phenomenon is interesting as the $MoS_2$ nanosheets dispersions produced via LPE from the previous works were typically reported as black dispersions in NMP,[122] and clear or dark-green colour in IPA.[345] The observed difference in colour is attributed to the variations in the bandgaps of the $MoS_2$ nanosheets due to the variations in their size and thickness. UV-Vis absorption analysis performed on the $MoS_2$ nanosheets show absorption peaks of below 260 nm for $MoS_2$ nanosheets produced in IPA, EtOH and D.I. (Figure 5.3b,b1). These absorption peaks occur at much lower wavelengths than typically reported in the literatures, which is beyond 400 nm.[346, 347] Another interesting finding involves the colour change of $MoS_2$ nanosheets in NMP dispersion, transitioning from dark green to light yellow when stored in a dark environment (Figure 5.3a). The colour reverts from light yellow back to dark green when the dispersion was reintroduced to light. To the best of my knowledge, this phenomenon has not been reported elsewhere to date. This unique property of the $MoS_2$ nanosheets in NMP might find its way into applications in advanced photonic devices.

Instead of just focusing on the solvent properties that influence the yield of 2D materials, as is commonly done for graphene, the initial results on $MoS_2$ and $WS_2$ exfoliation suggest an exciting prospect for investigating how solvent properties specifically might impact the thickness and size of nanosheets produced via LPE. This is particularly relevant for the case of $MoS_2$ nanosheets. Understanding the solvent's role in determining nanosheet thickness and size becomes a powerful tool for tuning the fundamental properties of materials like $MoS_2$ for specific applications. This approach allows for the fine-tuning of bandgap and other optical and electronic properties of the materials, thus presenting an efficient means of customising material behaviour simply by selecting the appropriate solvent for LPE. Moreover, the dispersions of $MoS_2$ or $WS_2$ nanosheets can be integrated with other 2D materials, such as graphene. This opens the whole possibility of creating composite dispersions that combine the unique properties of different materials for specific applications.

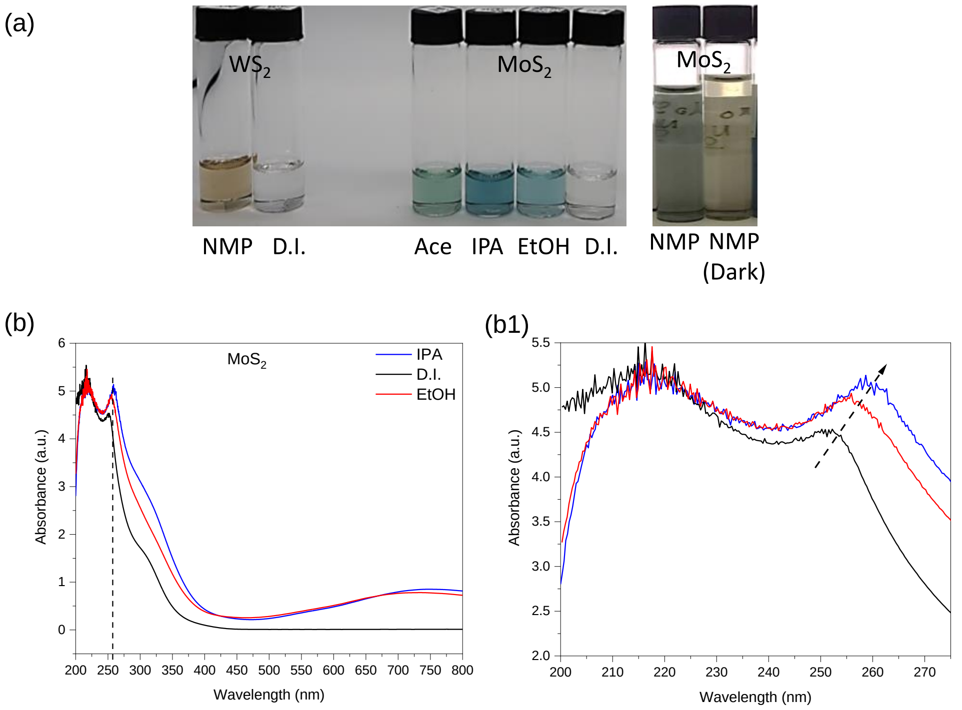

**Figure 5.3:** (a) Digital images of $WS_2$ and $MoS_2$ dispersions in different solvents. The $MoS_2$ dispersion that stored in the dark are labelled as NMP (dark). (b) The UV-Vis spectra of $MoS_2$ produced in different green solvents, highlighting the detailed absorption peaks region in (b1).

### 5.2.5 Substrate Printing of the Green Solvent-Based 2D Materials Ink for Device Applications

In my research, I have developed a sustainable, scalable and simple method for the surfactant-free, high-yield production of graphene in green solvents, particularly IPA. The achievement is advantageous in facilitating easy printing of graphene or 2D materials on substrates for applications in electronic and energy conversion devices.

The primary advantage of using green solvents as a replacement for toxic solvents in printing processes is their non-toxicity, which allows for safer handling during large-scale printing operations. Moreover, the use of green solvents significantly reduces the environmental impact, from their usage through to disposal. For battery devices, the utilisation of green solvents with low boiling points is impactful in terms of energy saving during the printing process. The solvent, having a low boiling point, can be easily evaporated at lower temperatures, leading to significant energy savings. The reported study shows that using solvents with lower boiling points, such as dimethylformamide (DMF) over NMP, can result in up to four times less energy consumption for drying the electrodes of Li-ion batteries.[348] Another advantage of using the green solvent-based 2D materials ink for substrate printing is its concentration can be adjusted by simply evaporating the solvent at low temperatures. This is particularly beneficial for sensors requiring high material concentration for improved substrate contact.[349]

The low surface tension of green solvents like IPA and ethanol contributes to enhanced wettability during substrate printing. This property is advantageous as it promotes uniform spreading of the ink, ensuring precision in the printing process. Notably, avoiding the use of surfactants in 2D material ink is essential in applications where high electrical conductivity is a critical property, as surfactants are non-conductive. Therefore, the surfactant-free synthesis route of high-yield graphene in IPA has the potential in its applications as conductive catalyst support on the catalyst coated membrane in polymer electrolyte membrane fuel cells (PEMFCs). In fuel cell technology, high electrical conductivity and surface area of the catalyst support are key properties for effective electrocatalysis.

Considering the economic aspect, the primary concern in using graphene and other 2D materials for electronic and energy devices is the performance-to-cost ratio. The high yield 2D materials ink, produced through a cost-effective route, plays a crucial role in reducing production costs and thereby promoting the potential widespread adoption of these materials in electronic, photonic and energy devices.

# Appendix A

## Supporting Information for Chapter 2

## A.1 Concentration Analysis by UV-Vis Spectroscopy

### A.1.1 Graphene Concentration without Redispersion

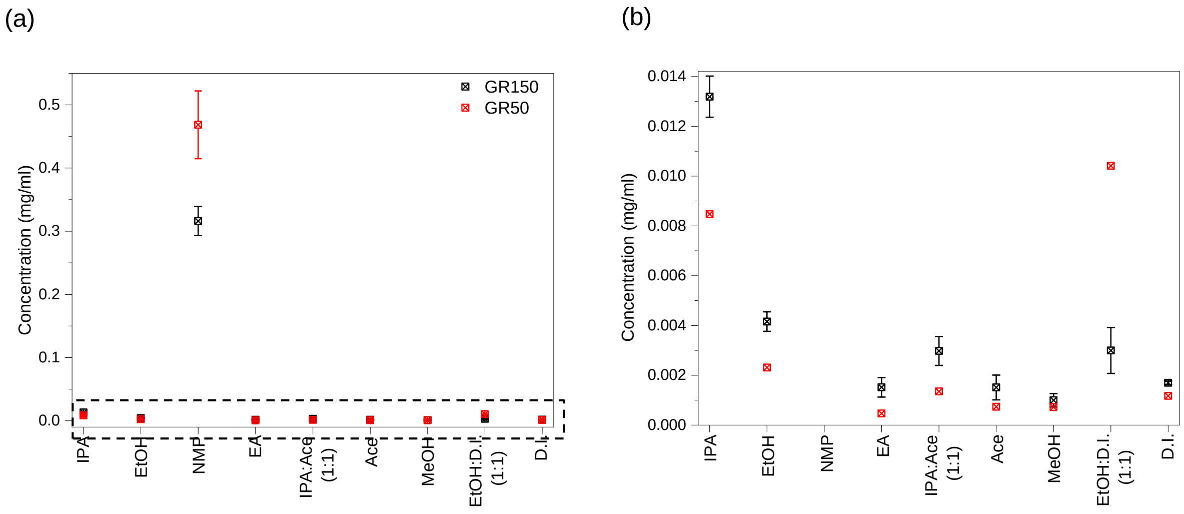

**Figure A1:** (a) and (b) Concentrations of as produced GR150 and GR50 in different solvents. (b)'Close-up' of the concentration of GR150 and GR50 in green solvents shown in the highlighted region in (a).

### A.1.2 Graphene Concentration After NMP and Green Solvent Redispersion (NMP-R and GS-R)

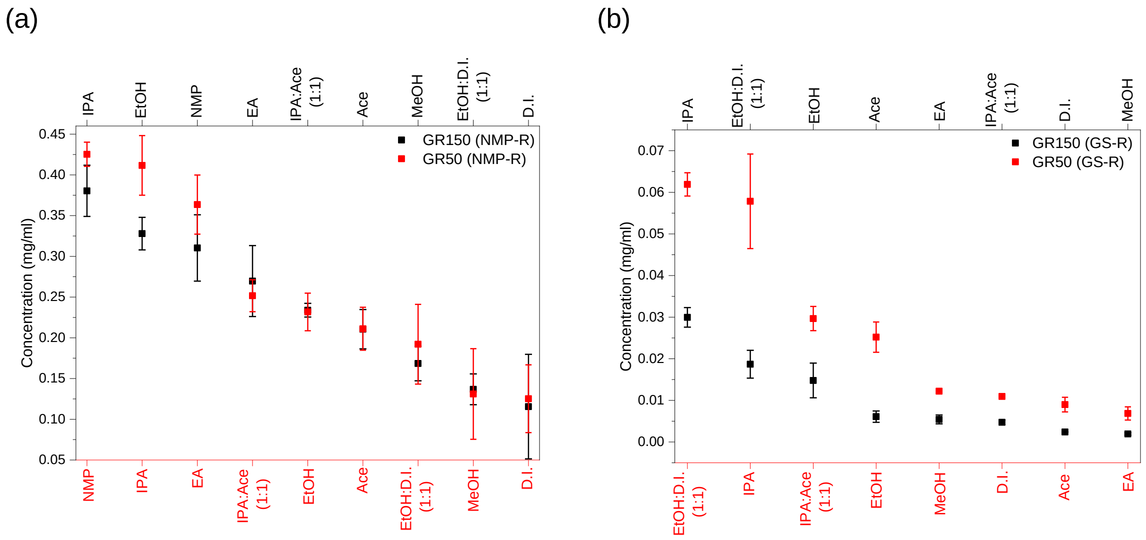

**Figure A2**: Concentration of GR150 and GR50 after redispersion in (a) NMP (NMP-R) and (b) green solvents (GS-R). The solvents shown in x-axis are arranged in decreasing order of (a) concentration/exfoliation efficiency and (b) concentration/dispersibility.

## A.2 Interfacial Contact Angle Measurement and Surface Energy Analysis

### A.2.1 Interfacial Contact Angle

The viscosity, surface tension, and density used for the contact angle calculation in Equation 2.2 were obtained from KRUSS instrument database apart from the solvent mixtures of EtOH:D.I (1:1) and IPA:Ace (1:1) which were taken from the literature as referenced:

**Table A1:** Surface tension viscosity and density values for used test liquids.

| Solvents (Test Liquid) | Surface Tension [mN/m] | Density [g/mL] | Viscosity [mPa·s] |
|---|---|---|---|
| IPA | 23.0 | 0.7860 | 1.960 |
| EtOH:D.I. (1:1) | 22.3 [1] | 0.7895 [2] | 1.341 [3] |
| EtOH | 22.3 | 0.7858 | 1.100 |
| Ace | 25.2 | 0.7910 | 0.295 |
| NMP | 40.4 | 1.0280 | 1.661 |
| IPA:Ace (1:1) | 20.3 [4] | 0.7808 [5] | 0.308 [6] |
| D.I. | 72.3 | 0.9970 | 0.900 |

## References:

1. **Ethanol-Water Mixture Surface Tension**, Datasheet from "Dortmund Data Bank (DDB) – Thermophysical Properties Edition 2014" in SpringerMaterials (https://materials.springer.com/thermophysical/docs/msft_c11c174), J. Gmehling, Editor., Springer-Verlag Berlin Heidelberg & DDBST GmbH, Oldenburg, Germany.

2. **Ethanol-Water Density**, Datasheet from "Dortmund Data Bank (DDB) – Thermophysical Properties Edition 2014" in SpringerMaterials (https://materials.springer.com/thermophysical/docs/ve1_c11c174), J. Gmehling, Editor., Springer-Verlag Berlin Heidelberg & DDBST GmbH, Oldenburg, Germany.

3. **Ethanol-Water Mixture Viscosity**, Datasheet from "Dortmund Data Bank (DDB) – Thermophysical Properties Edition 2014" in SpringerMaterials (https://materials.springer.com/thermophysical/docs/vism_c11c174), J. Gmehling, Editor., Springer-Verlag Berlin Heidelberg & DDBST GmbH, Oldenburg, Germany.

4. **Binary Mixtures**, Wohlfarth, C. and B. Wohlfarth, Datasheet from Landolt-Börnstein - Group IV Physical Chemistry · Volume 16: "Surface Tension of Pure Liquids and Binary Liquid Mixtures" in SpringerMaterials (https://doi.org/10.1007/10560191_4), M.D. Lechner, Editor., Springer-Verlag Berlin Heidelberg.

5. **Acetone-2-Propanol Density**: Datasheet from "Dortmund Data Bank (DDB) – Thermophysical Properties Edition 2014" in SpringerMaterials (https://materials.springer.com/thermophysical/docs/ve1_c4c95), J. Gmehling, Editor., Springer-Verlag Berlin Heidelberg & DDBST GmbH, Oldenburg, Germany.

6. **Acetone-2-Propanol Mixture Viscosity**: Datasheet from "Dortmund Data Bank (DDB) – Thermophysical Properties Edition 2014" in SpringerMaterials (https://materials.springer.com/thermophysical/docs/vism_c4c95), J. Gmehling, Editor., Springer-Verlag Berlin Heidelberg & DDBST GmbH, Oldenburg, Germany.

## A.2.2 Graphite Surface Energy: OWRK model

The surface energies of G150 and G50 graphite were calculated using Owens-Wendt-Rabel & Kaelble model (OWRK) equation:

$$\frac{\sigma_l(\cos\theta+1)}{2(\sqrt{\sigma_l^d})} = (\sqrt{\sigma_s^p})\frac{\sqrt{\sigma_l^p}}{\sqrt{\sigma_l^d}} + \sqrt{\sigma_s^d} \qquad \text{(Eq. A1)}$$

$\sigma_l$ [mN/m] is the overall surface tension of liquid/solvent; $\sigma_s^d$ is the dispersive component of the graphite surface energy; $\sigma_l^d$ is the surface tension of liquid/solvent; $\sigma_s^p$ is the polar component of graphite surface energy; $\sigma_l^d$ is the liquid surface tension; $\theta$ (deg) is the interfacial contact angle between graphite and liquid.

By plotting the linear graph of

$$\frac{\sigma_l(\cos\theta+1)}{2(\sqrt{\sigma_l^d})} \quad \text{against} \quad \frac{\sqrt{\sigma_l^p}}{\sqrt{\sigma_l^d}}$$

as shown in Figure A3, the overall surface energy of graphite, $\sigma_s$ can be estimated from the slope and y-intercept of the graph, which gives the value for $\sqrt{\sigma_s^p}$ and $\sqrt{\sigma_s^d}$ , respectively.

The equation used for calculating the surface energy is:

$$\sigma_s = \sigma_s^p + \sigma_s^d \qquad \text{(Eq. A2)}$$

The overall surface energy of both G150 and G50 graphite ($\sigma_{G150}$ and $\sigma_{G50}$) were calculated as follows:

$$\sigma_{G150} = \sigma_{G150}^p + \sigma_{G150}^d = \left(\sqrt{\sigma_{G150}^p}\right)^2 + \left(\sqrt{\sigma_{G150}^d}\right)^2$$

$$= (2.969)^2 + (3.260)^2 = \mathbf{19.441\ mN/m}$$

$$\sigma_{G50} = \sigma_{G50}^{p} + \sigma_{G50}^{d} = \left(\sqrt{\sigma_{G50}^{p}}\right)^2 + \left(\sqrt{\sigma_{G50}^{d}}\right)^2$$

$$= (3.079)^2 + (3.802)^2 = \mathbf{23.930\ mN/m}$$

The values used for polar and dispersive components of solvent surface tension for graphite surface energy calculation are listed as follows:

**Table A2:** Estimated polar and dispersive surface tension component of the test liquids.

| Solvents | Polar Surface Tension | Dispersive Surface Tension |
|---|---|---|
| EtOH | 4.4 | 19.3 |
| D.I. | 51 | 21.8 |
| Ace | 16.5 | 6.8 |
| NMP | 11.58 | 29.21 |
| IPA | 3.5 | 19.5 |

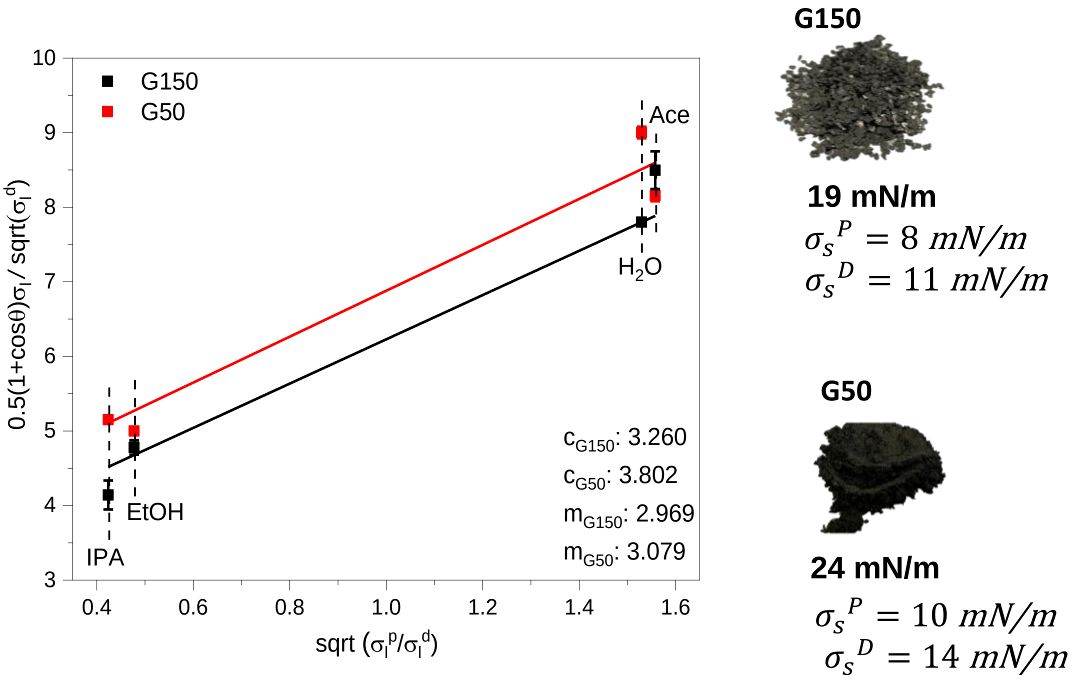

**Figure A3:** Graph plotting for surface energy calculation based on OWRK equation. The digital pictures of G150 and G50 graphite are shown, along with the calculated surface energies. $\sigma_s{}^P$ and $\sigma_s{}^D$ are the polar and dispersive components of the graphite surface energy, respectively.

# A.3 UV-Vis Spectra of GR150 and GR50

## A.3.1 UV-Vis Spectra Before and After Green Solvent Redispersion (GS-R)

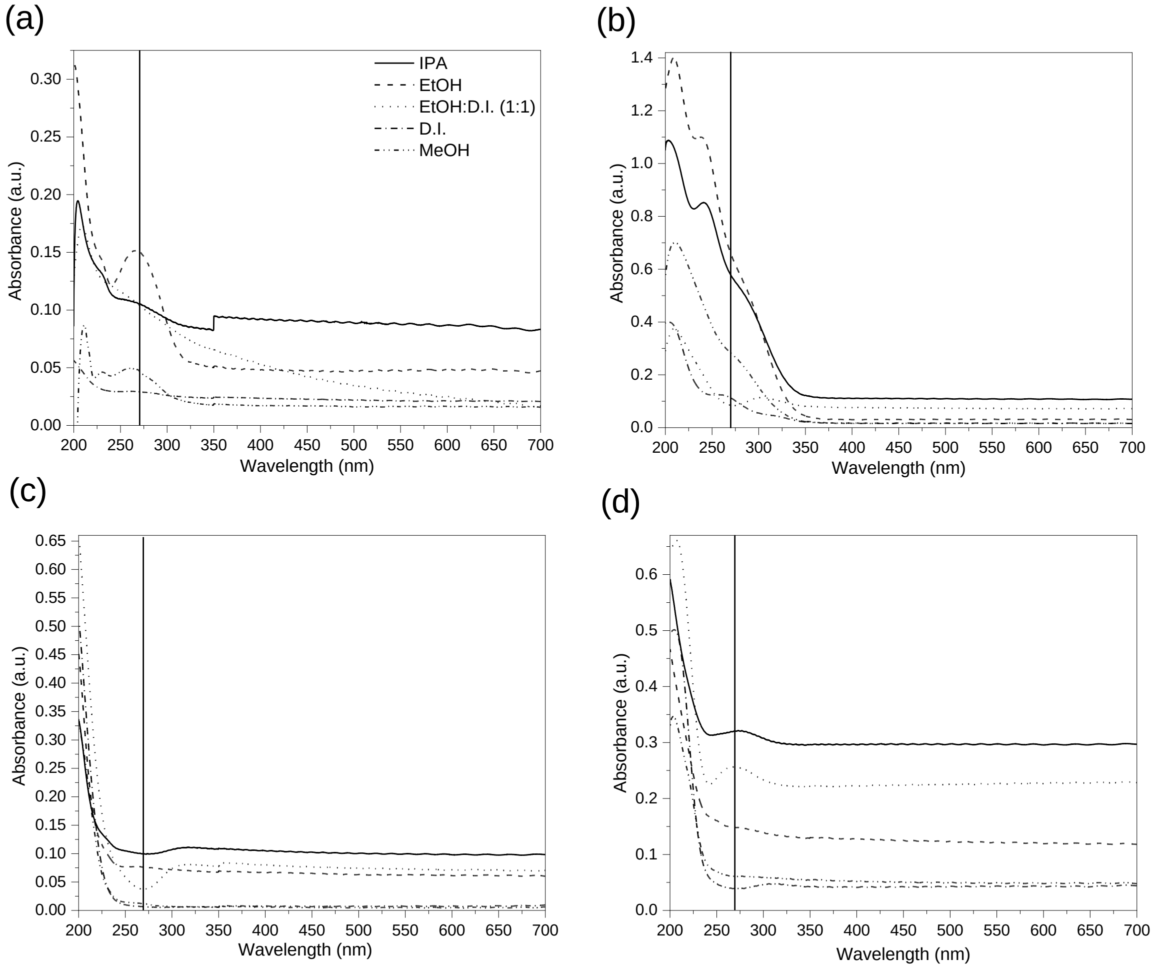

**Figure A4:** UV- Vis spectra of (a) GR150, (b) GR50, (c) GR150 (GS-R) and (d) GR50 (GS-R). The π-π* absorption peak position at 270 nm is indicated by the vertical lines in the graphs, which is the typical absorption wavelength for pristine graphene and is depending on the dispersing solvent medium used.

# A.3.2 UV-Vis Cut-Off Wavelength

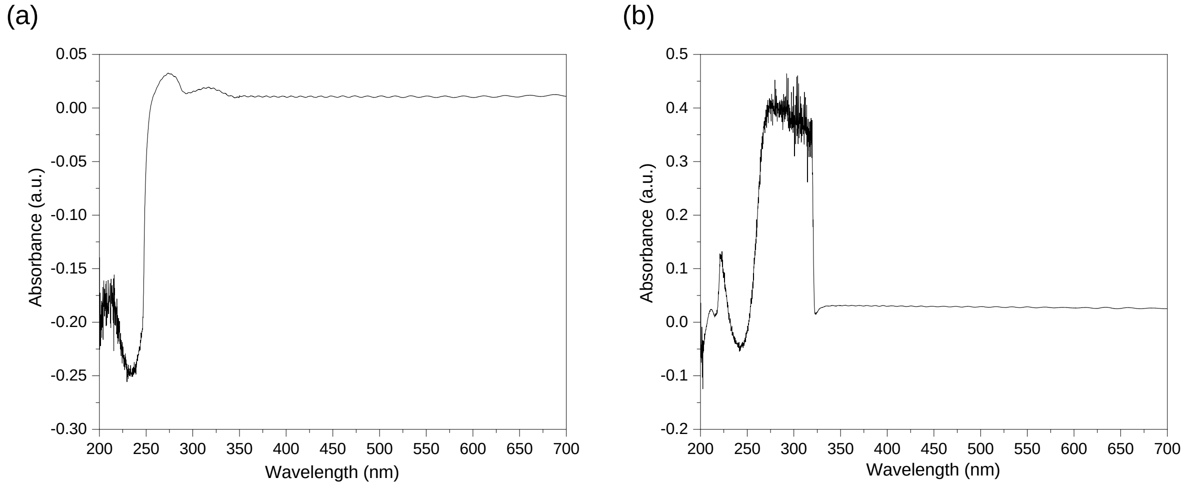

**Figure A5:** UV- Vis spectra of GR50 in (a) ethyl acetate and (b) acetone. The UV-vis cut-off wavelength for ethyl acetate and acetone is 260 nm and 330 nm respectively. The graphene signature absorption peaks at the wavelength between 230 and 270 nm are not clearly seen if the measurement is taken in these solvents with the UV-vis cut-off wavelength beyond the wavelength of these absorption peaks.

# A.4 Raman spectroscopy of graphene with and without NMP-Redispersion (NMP-R)

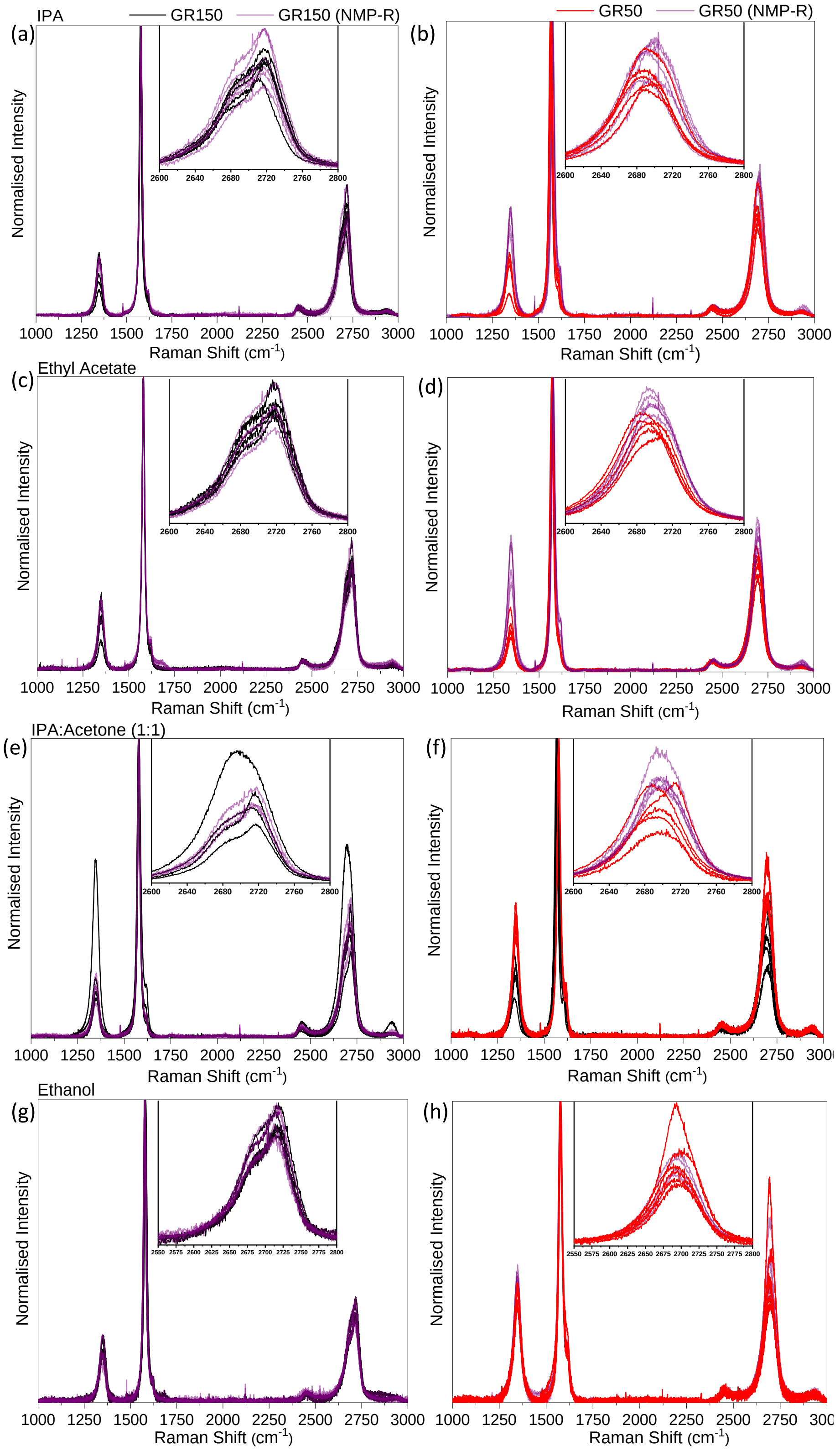

**Figure A6:** Comparison of GR150 and GR50 Raman spectra without NMP-R (GR150 black, GR50 red), with the spectra acquired with NMP-R (purple). The Raman spectra were normalised against the G peak. The 2D peaks are shown in the inset of each graph; a) GR150 exfoliated in IPA, b) GR50 exfoliated in IPA, c) GR150 exfoliated in ethyl acetate, d) GR50 exfoliated in ethyl acetate, e) GR150 exfoliated in IPA:acetone (1:1). f) GR50 exfoliated in IPA:acetone, g) GR150 exfoliated in ethanol and h) GR50 exfoliated in ethanol.

## A.5 Raman Spectroscopy of IPA-Exfoliated and NMP-Exfoliated GR150 vs. Commercial Graphene

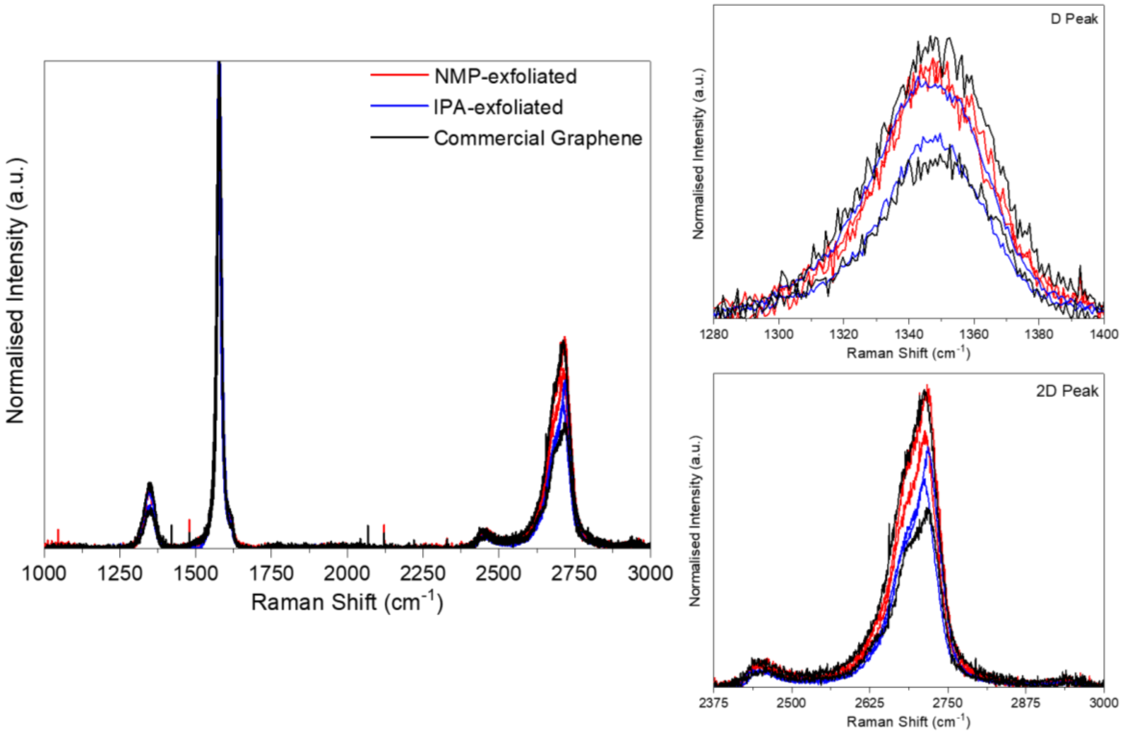

**Figure A7:** Raman spectra of GR150 exfoliated in IPA and NMP, and that of commercial graphene. The spectra were normalised to the highest intensity G peak. The enlarged region of D peak and 2D peak are also shown to qualitatively compare the graphene defect and thickness based on D and 2D peak, respectively.

# A.6 Atomic Force Microscopy of IPA-Exfoliated GR150 Redispersed in NMP (NMP-R)

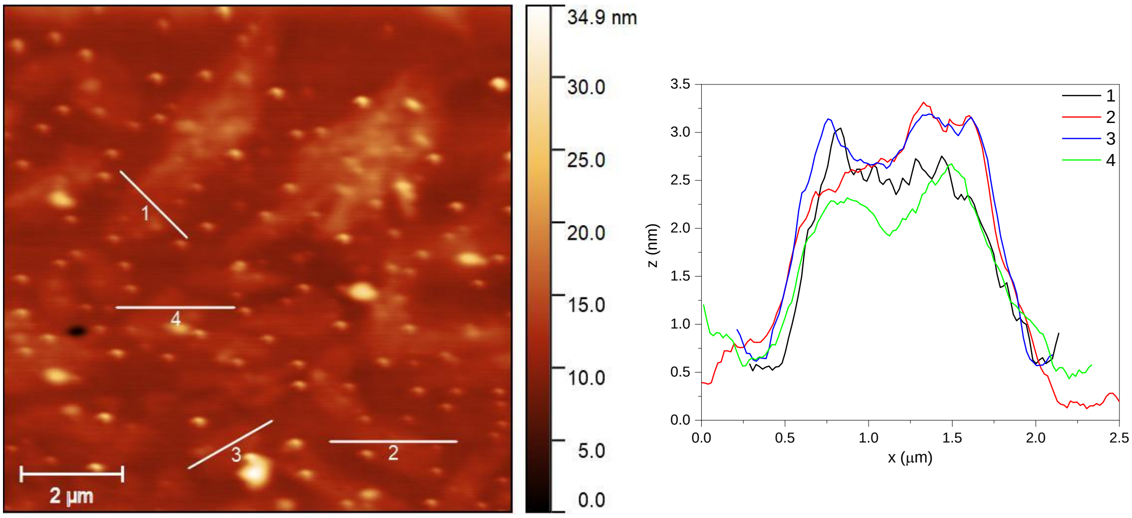

**Figure A8:** Atomic Force Microscopy (AFM) image and the thickness profile of IPA-exfoliated GR150, redispersed in NMP (NMP-R). The “spots” on the AFM image are the residual NMP solvent. GR150 graphene retained its leaf-like structure morphology with the thickness less than 10 layers after redispersion in NMP proved the ability of NMP to disperse graphene while retaining its original thickness and morphology after exfoliation.

# Appendix B

## Supporting Information for Chapter 3

## B.1 UV-Vis Spectra of the Dispersions Produced by Shear Mixing and Ultrasonication Exfoliations

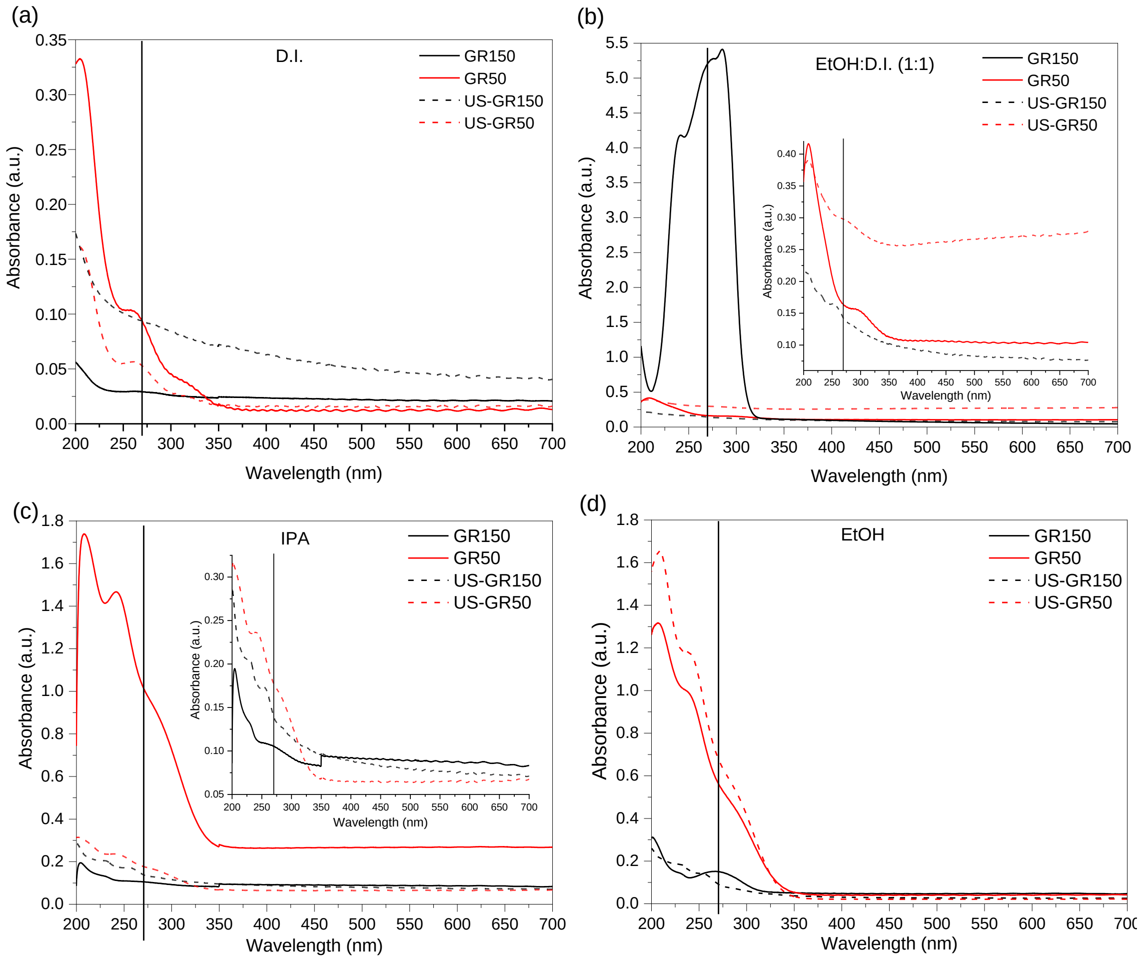

**Figure B1**: The comparison of UV-Vis spectra of GR150 and GR50 produced with 3-hour shear mixing and 3-hour ultrasonication (indicated by "US-"). The solvent media used to exfoliate and disperse the materials are indicated in the graphs. π-π* absorption peak position at 270 nm (indicated by the vertical lines drawn in the graphs) is the typical absorption wavelength for pristine graphene. The shifting of the absorption peak position from 270 nm is used to indicate the oxidation of graphene.

# B.2 UV-Vis Spectra of the Dispersions Produced with and without PEUS (2 US)

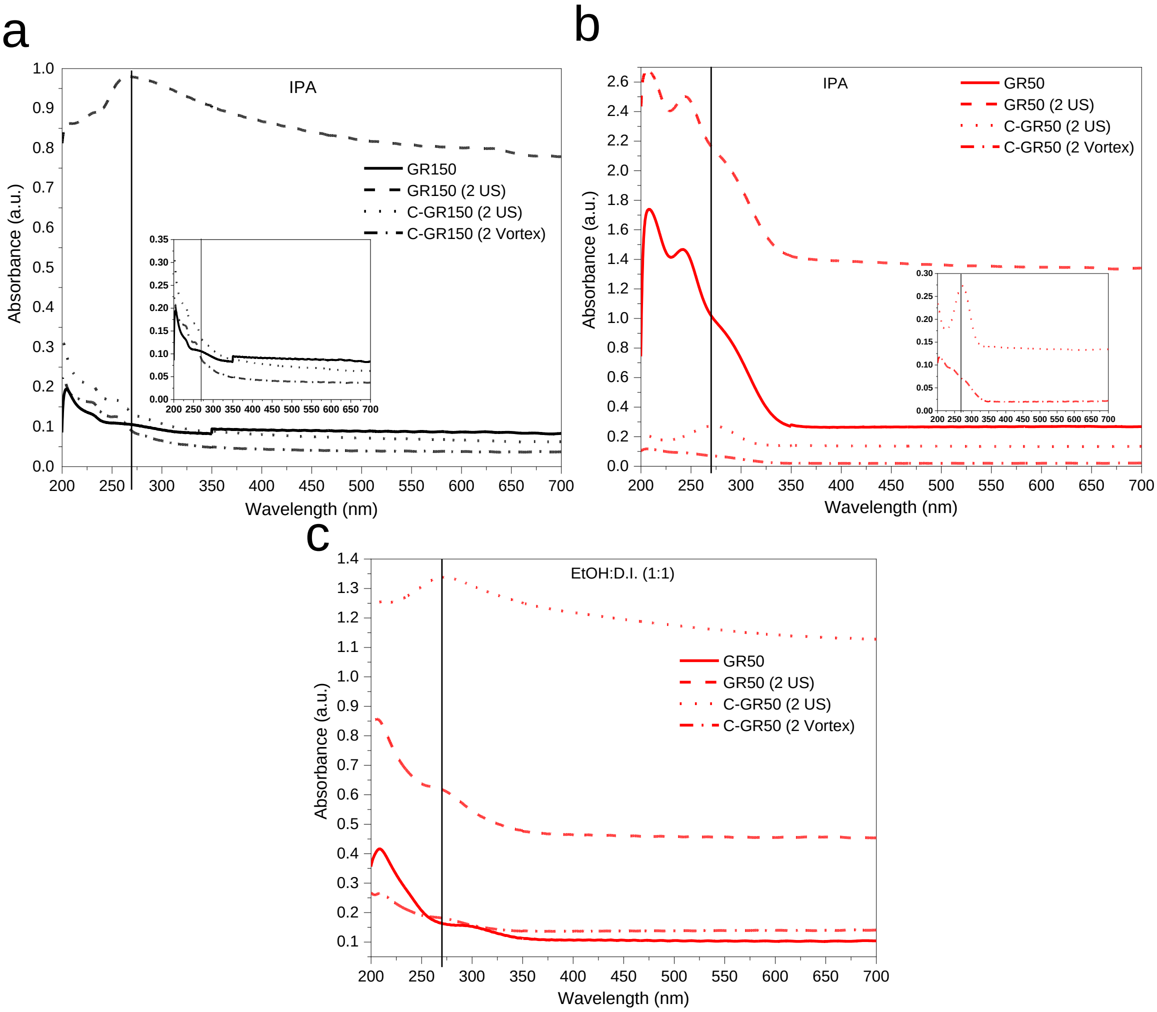

**Figure B2:** The comparison of UV-Vis spectra of GR150 and GR50 produced with and without PEUS (2 US). The spectra obtained through 2-min ultrasonication directly from the graphite starting materials without shear mixing exfoliation (C-GR150 or C-GR50) are also shown as the controlled reference. The solvent media used to exfoliate and disperse the materials are indicated in the graphs. π-π* absorption peak position at 270 nm (indicated by the vertical lines drawn in the graphs) is the typical absorption wavelength for pristine graphene. The shifting of the absorption peak position from 270 nm is used to indicate the oxidation of graphene.

# B.3 UV-Vis Spectra of the Dispersions Produced from Shear Mixing with PEUS (2 US) and 2 US directly from Graphite (the Control Experiment)

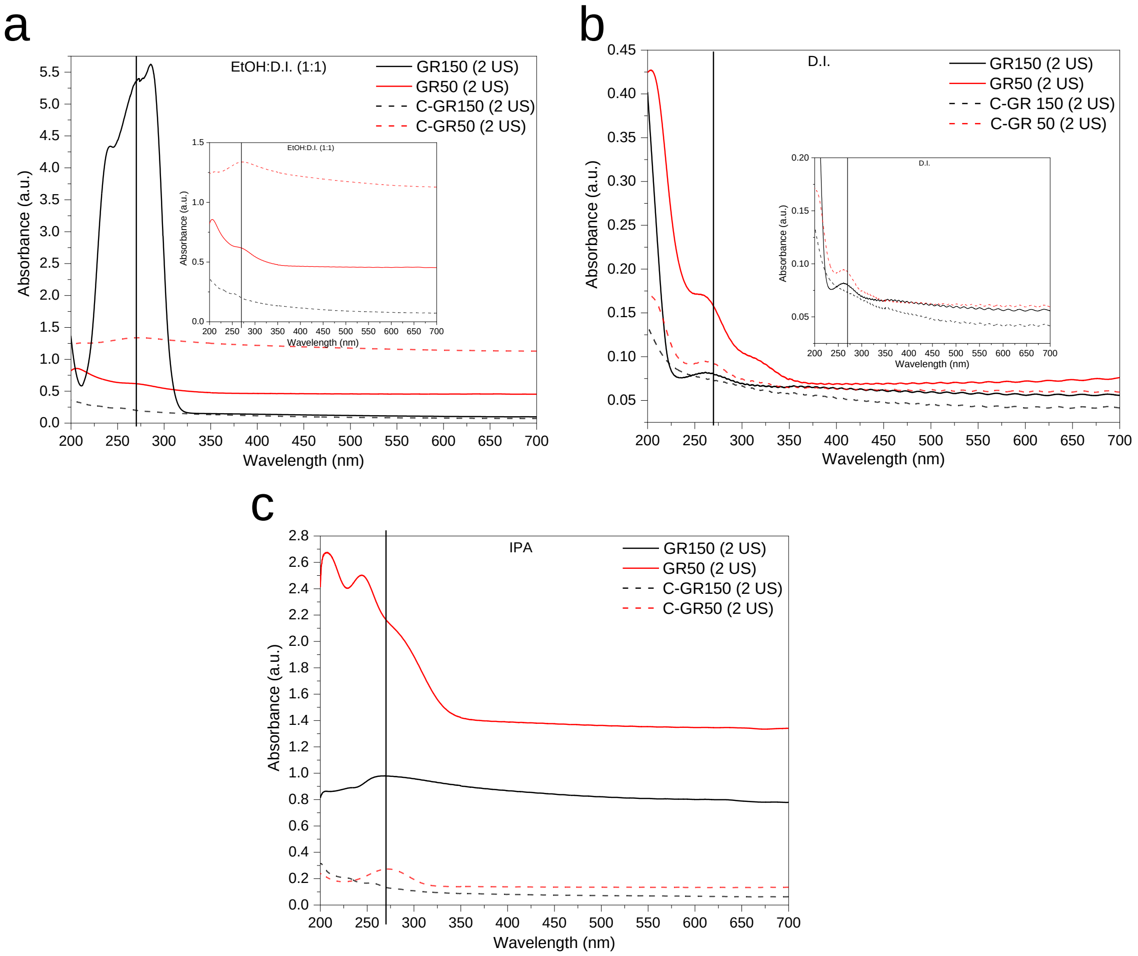

**Figure B3**: The comparison of UV-Vis spectra of GR150 and GR50 produced from three-hour shear mixing followed by two-minute ultrasonication PEUS (2 US), with the concentration obtained through two-minute ultrasonication directly from the graphite starting materials (C-GR150 or C-GR50) in (a) EtOH:D.I. (1:1), (b) D.I. and (c) IPA solvents. π-π* absorption peak position at 270 nm (indicated by the vertical lines in the graphs) is the typical absorption wavelength for pristine graphene.

# B.4 The Effect of the Temperatures of PEUS and Centrifugation

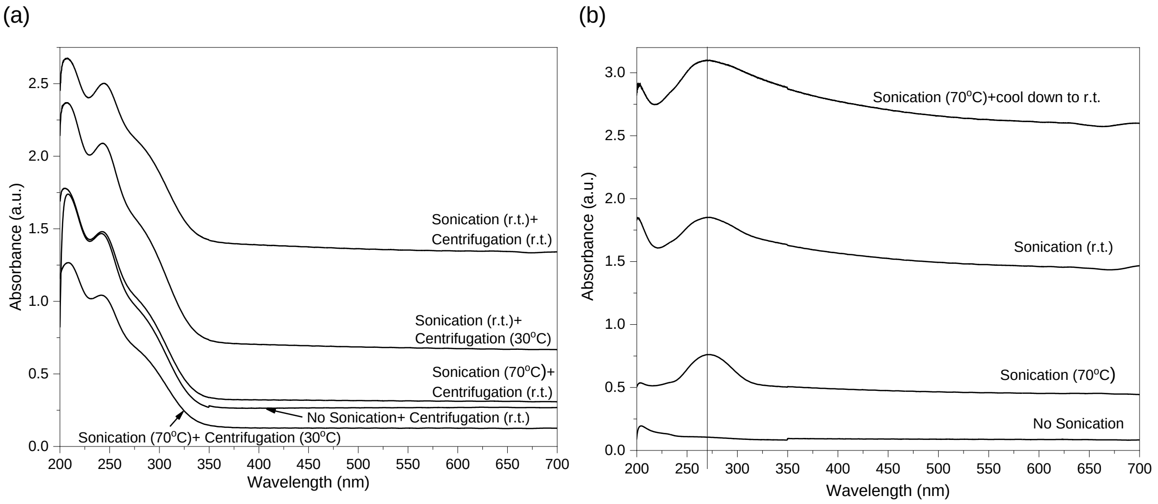

**Figure B4**: The UV-Vis spectra of (a) GR50 and (b) GR150 exfoliated and dispersed in IPA. The absorbance (concentration) changes significantly with the sonication (PEUS) and centrifugation temperature.

# B.5 Raman Defect Analysis under Different Post-Exfoliation Ultrasonication (PEUS) Temperature

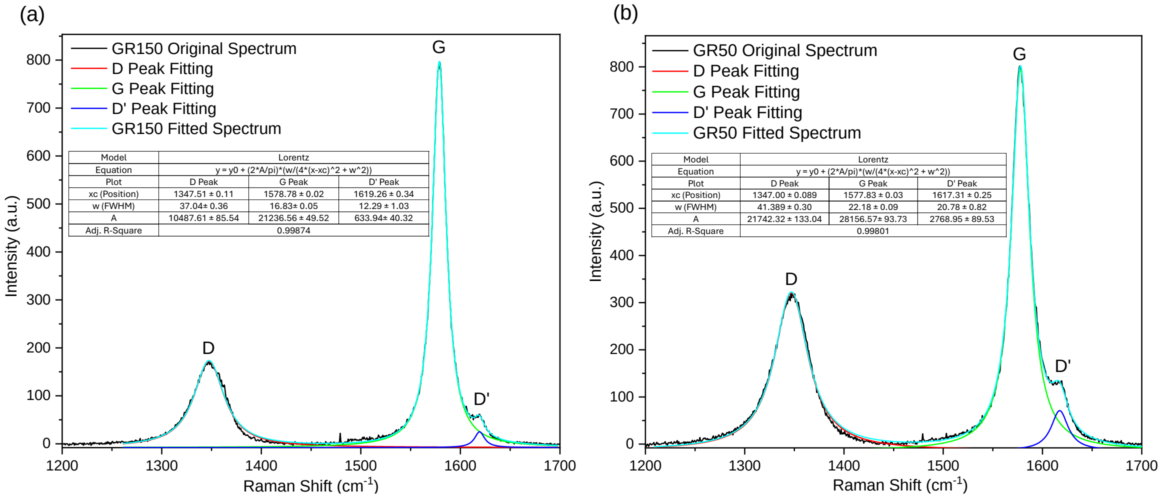

| Model | Lorentz | | |
|---|---|---|---|
| Equation | y = y0 + (2*A/pi)*(w/(4*(x-xc)^2 + w^2)) | | |
| Plot | D Peak | G Peak | D' Peak |
| xc (Position) | 1347.51 ± 0.11 | 1578.78 ± 0.02 | 1619.26 ± 0.34 |
| w (FWHM) | 37.04± 0.36 | 16.83± 0.05 | 12.29 ± 1.03 |
| A | 10487.61 ± 85.54 | 21236.56 ± 49.52 | 633.94± 40.32 |
| Adj. R-Square | 0.99874 | | |

| Model | Lorentz | | |
|---|---|---|---|
| Equation | y = y0 + (2*A/pi)*(w/(4*(x-xc)^2 + w^2)) | | |
| Plot | D Peak | G Peak | D' Peak |
| xc (Position) | 1347.00 ± 0.089 | 1577.83 ± 0.03 | 1617.31 ± 0.25 |
| w (FWHM) | 41.389 ± 0.30 | 22.18 ± 0.09 | 20.78 ± 0.82 |
| A | 21742.32 ± 133.04 | 28156.57± 93.73 | 2768.95 ± 89.53 |
| Adj. R-Square | 0.99801 | | |

**Figure B5:** Representative peak fitting on the Raman spectra of (a) GR150 and (b) GR50. Peak fitting was performed using a Lorentzian function for the D, G, and D' peaks. The intensities and FWHM of these fitted peaks were used to analyse graphene defects.

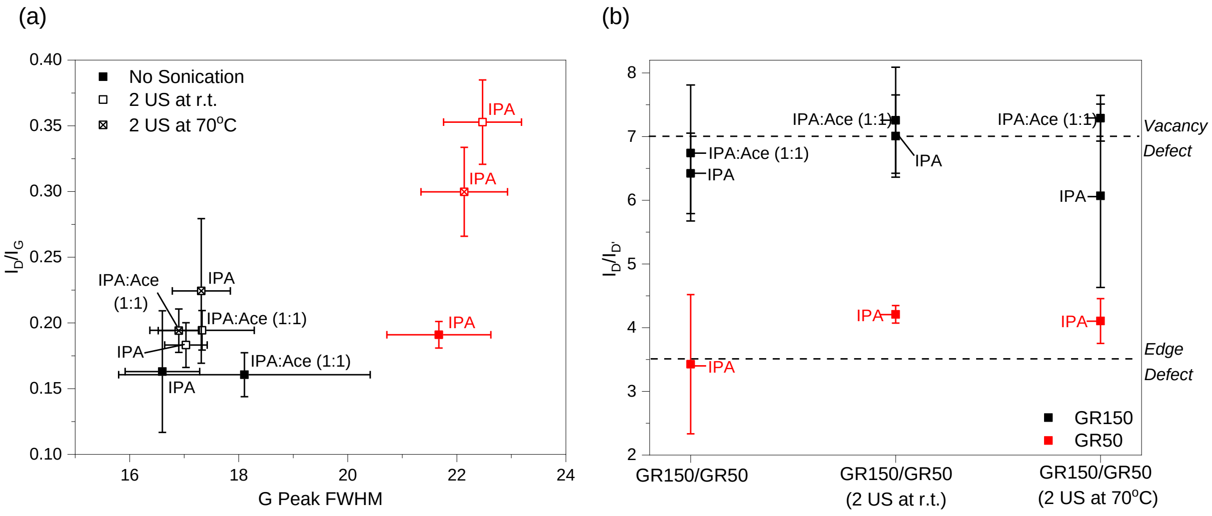

**Figure B6:** (a) The defect density ($I_D/I_G$) and crystal disorder (G peak FWHM), and (b) the type of defect ($I_D/I_{D'}$) analysis through Raman Spectroscopy on GR150 and GR50 obtained at different PEUS (2 US) temperatures.

# B.6 XPS Analysis on Graphite and Graphene

**Table B1**: The XPS analysis on the atomic percentage of $sp^2$, $sp^3$, $\pi$-$\pi$* and oxygen groups in selected graphite/graphene.

| | $sp^2$ | $sp^3$ | C=O | C-O | O-C=O | $\pi$-$\pi$* |
|---|---|---|---|---|---|---|
| G150 | 82.28 | 7.71 | 3.03 | 1.15 | 0.92 | 4.88 |
| GR150 IPA | 66.22 | 20.24 | 5.00 | 2.88 | 1.68 | 3.98 |
| GR150 (2 US) IPA | 73.24 | 17.19 | 4.14 | 1.36 | 0.50 | 3.58 |
| G50 | 72.64 | 15.38 | 3.17 | 0 | 1.28 | 4.49 |
| GR50 IPA | 77.21 | 12.63 | 5.37 | 0.97 | 0.76 | 3.07 |
| GR50(2 US) IPA | 73.58 | 17.74 | 6.34 | 0.77 | 0.21 | 1.36 |

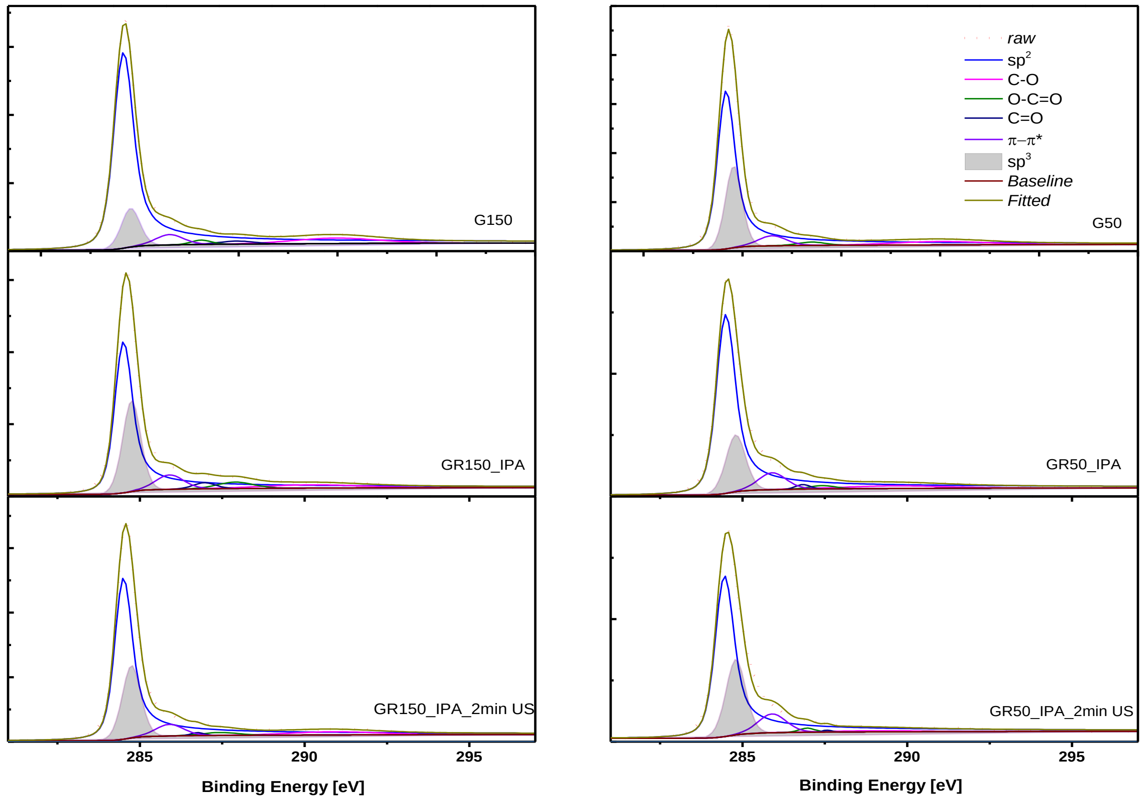

**Figure B7**: XPS peak fitting/ deconvolution of carbon C1s peaks for graphite starting materials (G150 and G50), and graphene (GR150 and GR50) in IPA.

# B.7 The Effect of the Concentration on the UV-Vis Absorption Peaks

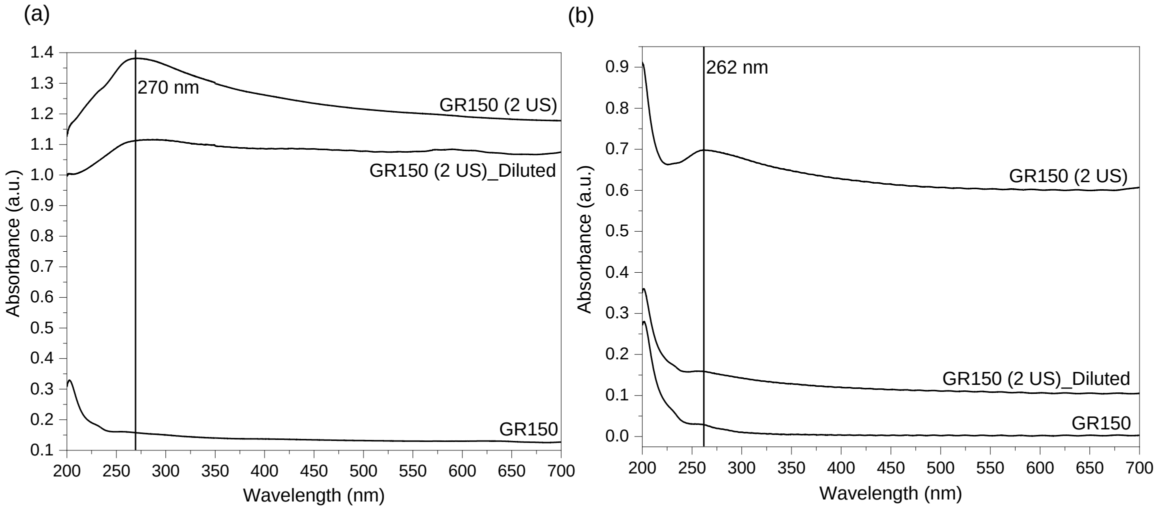

**Figure B8**: The UV-Vis spectra of GR150 exfoliated and dispersed in IPA obtained from (a) 500 rpm centrifugation speed and (b) 2500 rpm centrifugation speed. The ratio between the adsorption peak (marked with the line) and the plateau region beyond 600 nm changes with concentration.

# B.8 The Raman Spectra

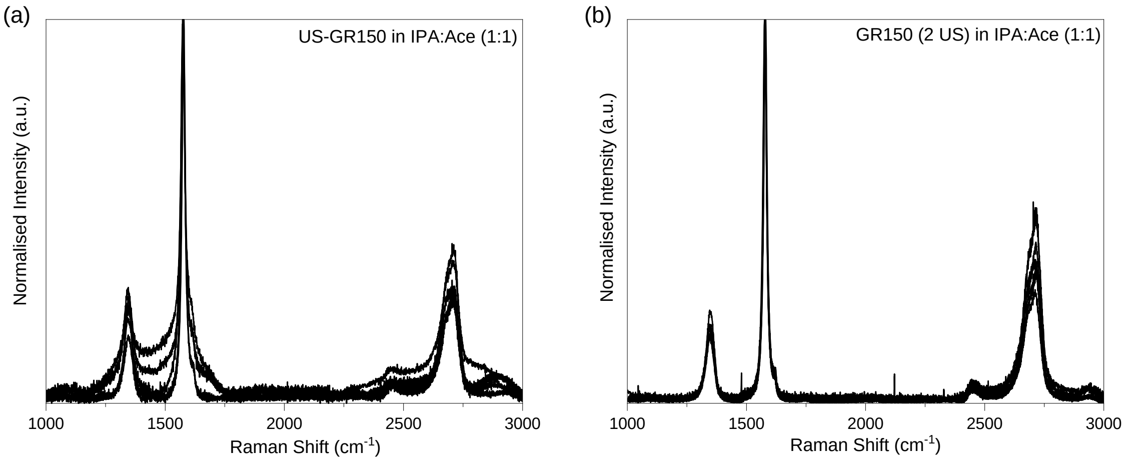

**Figure B9**: The stacked Raman spectra for GR150 obtained in IPA:Ace (1:1) and from the exfoliation process specified in the graph. These spectra are background-subtracted and normalised against the highest peak. These are the raw spectra used for part of the process-data in fig. 3.11.

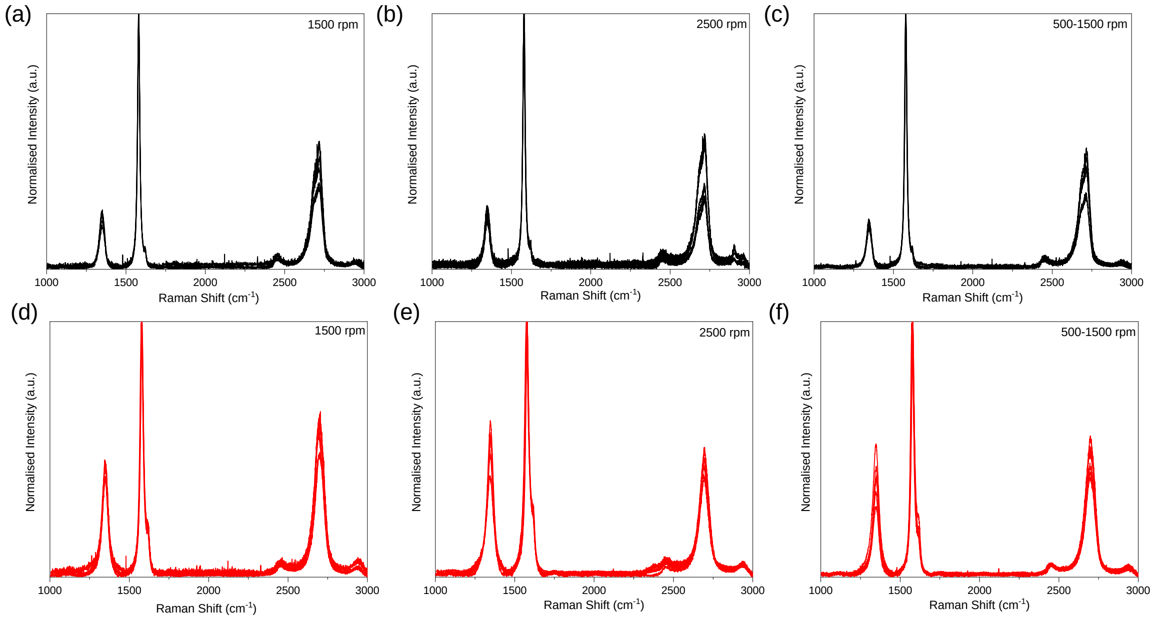

**Figure B10**: The stacked Raman spectra for GR150 and GR50 obtained in IPA solvent and from the centrifugation speed specified in the graph. 500-1500 rpm is the graphene obtained at 1500 rpm centrifugation, following the 500 rpm centrifugation. These spectra are background-subtracted and normalised against the highest peak. These are the raw spectra used for the process-data in fig. 3.13a and 3.13c.

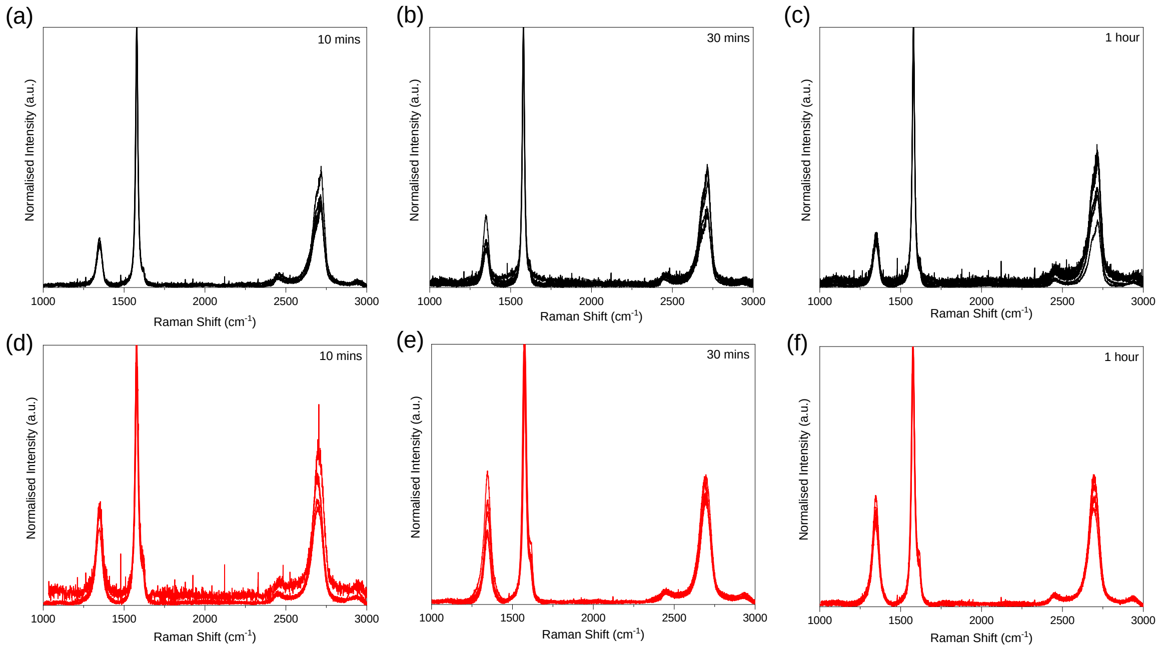

**Figure B11**: The stacked Raman spectra for GR150 and GR50 obtained in IPA solvent, with different post-exfoliation ultrasonication time specified in the graph. These spectra are background-subtracted and normalised against the highest peak. These are the raw spectra used for the process-data in fig. 3.13b and 3.13d.

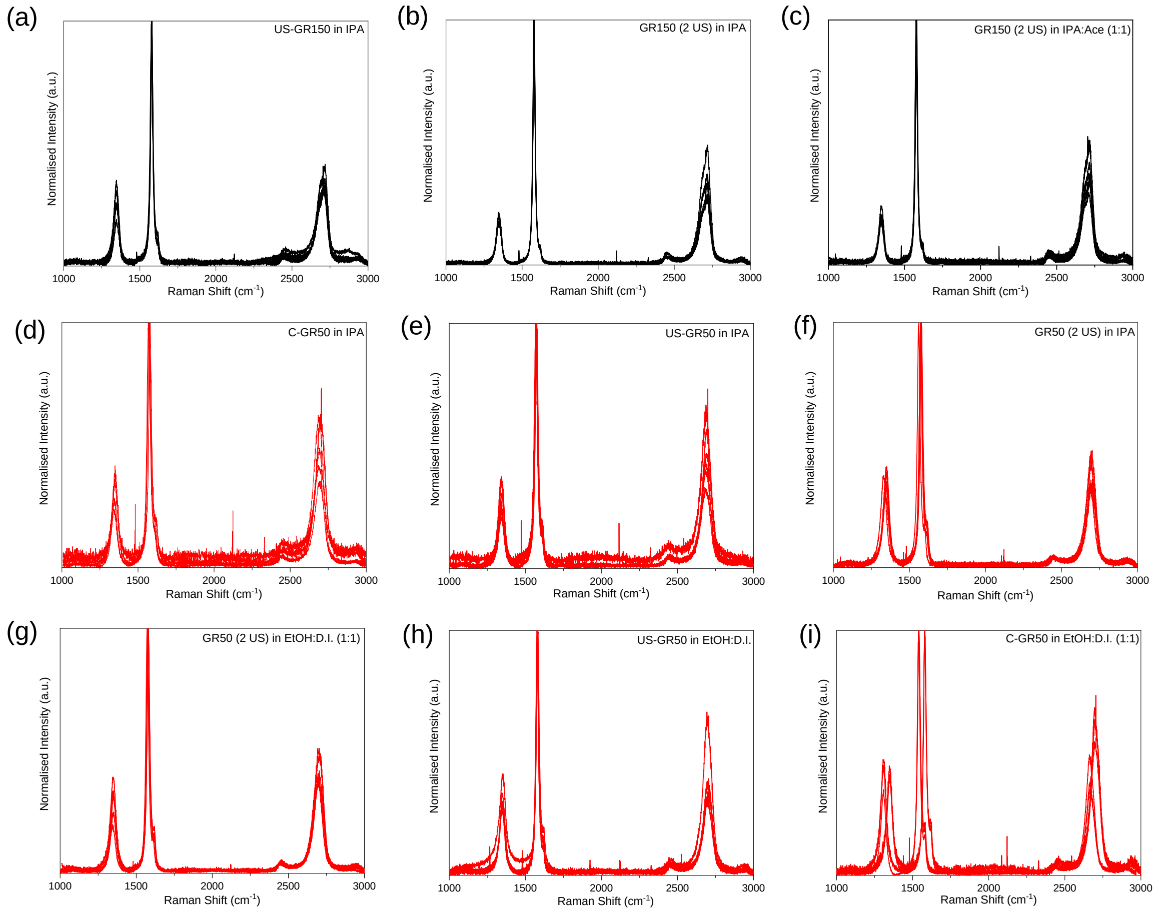

**Figure B12:** The stacked Raman spectra for GR150 and GR50 obtained in the solvent and from the exfoliation process specified in the graph. These spectra are background-subtracted and normalised against the highest peak. These are the raw spectra used for the process-data in fig. 3.14.

# Appendix C

## Supporting Information for Chapter 4

## C.1 X-Ray Diffraction Peak Analysis

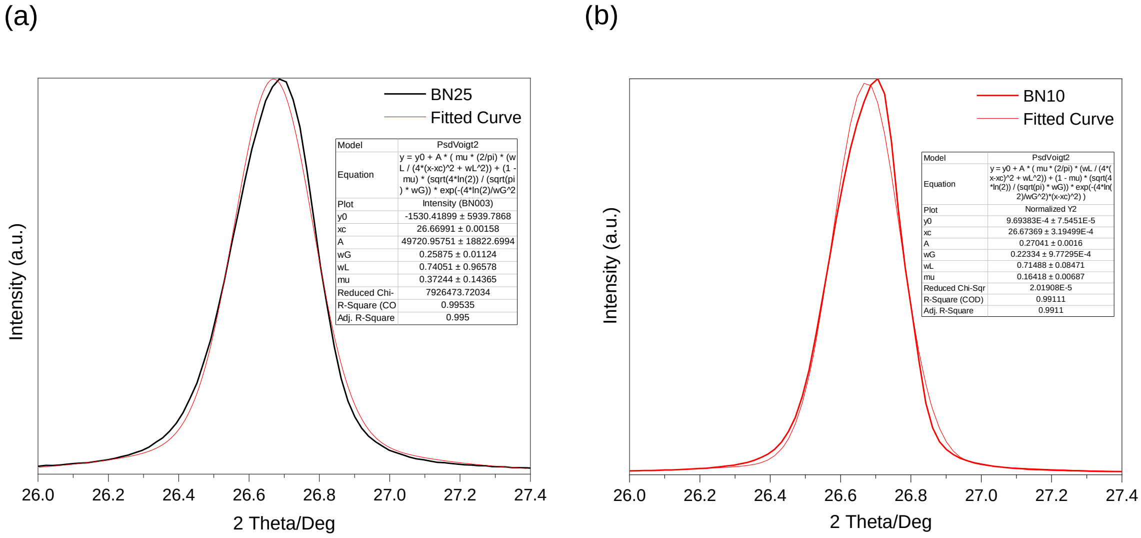

| | |
|---|---|
| Model | PsdVoigt2 |
| Equation | y = y0 + A * ( mu * (2/pi) * (wL / (4*(x-xc)^2 + wL^2)) + (1 - mu) * (sqrt(4*ln(2)) / (sqrt(pi) * wG)) * exp(-(4*ln(2)/wG^2 |
| Plot | Intensity (BN003) |
| y0 | -1530.41899 ± 5939.7868 |
| xc | 26.66991 ± 0.00158 |
| A | 49720.95751 ± 18822.6994 |
| wG | 0.25875 ± 0.01124 |
| wL | 0.74051 ± 0.96578 |
| mu | 0.37244 ± 0.14365 |
| Reduced Chi- | 7926473.72034 |
| R-Square (CO | 0.99535 |
| Adj. R-Square | 0.995 |

| | |
|---|---|
| Model | PsdVoigt2 |
| Equation | y = y0 + A * ( mu * (2/pi) * (wL / (4*(x-xc)^2 + wL^2)) + (1 - mu) * (sqrt(4*ln(2)) / (sqrt(pi) * wG)) * exp(-(4*ln(2)/wG^2)*(x-xc)^2) ) |
| Plot | Normalized Y2 |
| y0 | 9.69383E-4 ± 7.5451E-5 |
| xc | 26.67369 ± 3.19499E-4 |
| A | 0.27041 ± 0.0016 |
| wG | 0.22334 ± 9.77295E-4 |
| wL | 0.71488 ± 0.08471 |
| mu | 0.16418 ± 0.00687 |
| Reduced Chi-Sqr | 2.01908E-5 |
| R-Square (COD) | 0.99111 |
| Adj. R-Square | 0.9911 |

**Figure C1:** The fitting of XRD (002) peak of (a) BN25 and (b) BN10. The fitting is done using the model that gives the R-square value closest to 1, which is the Pseudo Voigt function. The Full Width at Half Maximum (FWHM) and peak position of (002) peak are used to calculate the crystallite size and d-spacing (interlayer spacing) respectively.

# C.2 X-Ray Photoelectron Spectroscopy

**Table C1**: The atomic percent of each element analysed from the XPS spectra of each sample.

| **Samples** | **B1s (atomic %)** | **N1s (atomic %)** | **C1s (atomic %)** | **O1s (atomic %)** |
|---|---|---|---|---|
| BN25 | 50.59 | 42.08 | 5.1 | 2.23 |
| BN10 | 50.44 | 41.76 | 5.96 | 1.84 |
| BNNS25 | 45.38 | 36.33 | 16.54 | 1.74 |
| BNNS25 (2 US) | 47.71 | 38.31 | 12.25 | 1.72 |

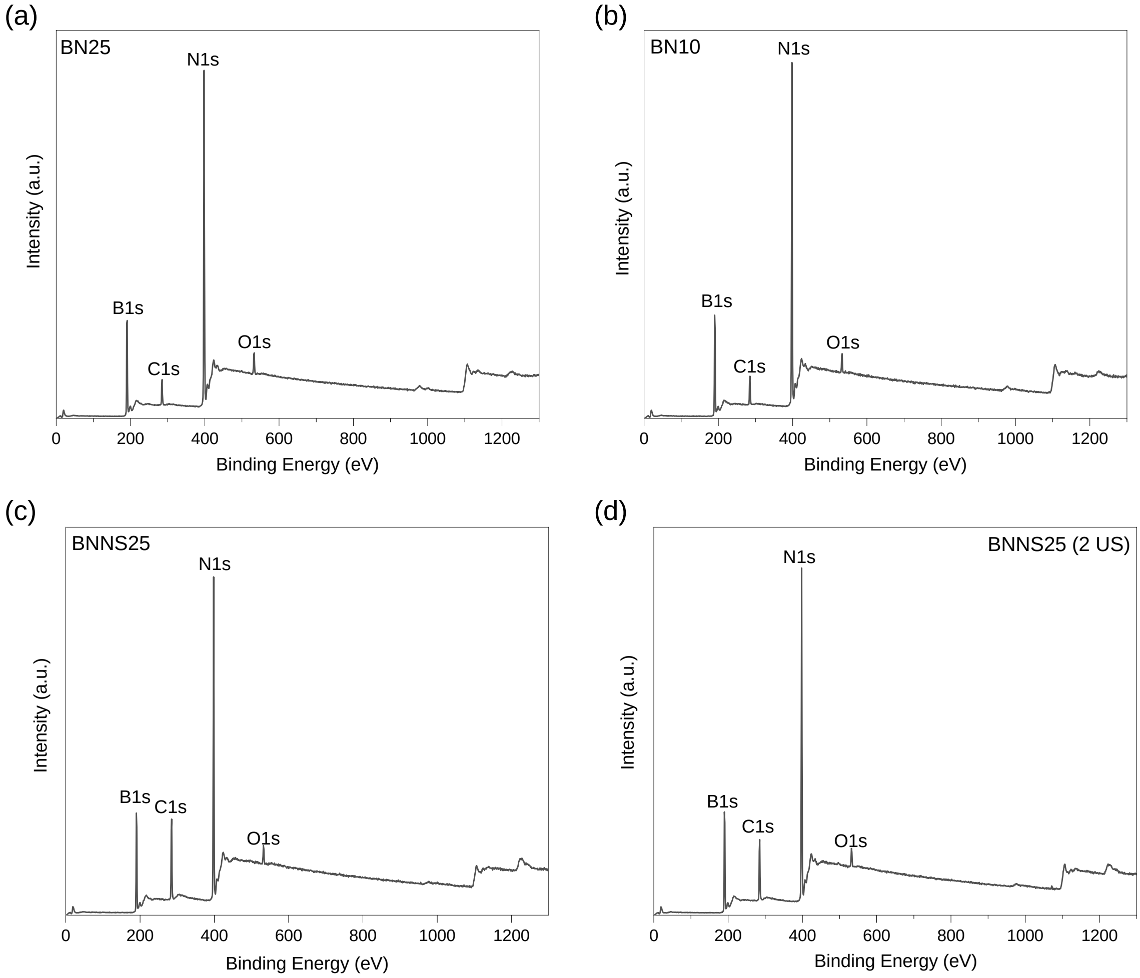

**Figure C2**: XPS survey spectra of (a) BN25, (b) BN10, (c) BNNS25 and (d) BNNS25 (2 US).

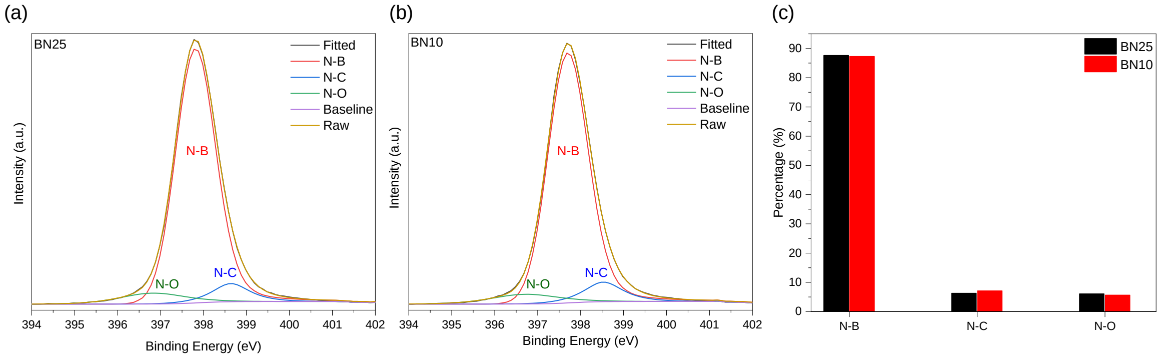

**Figure C3:** XPS peak fitting/ deconvolution of N1s peak for (a) BN25 and (b) BN10. (c) Percentage of each components analysed through the fitting of N1s peak.

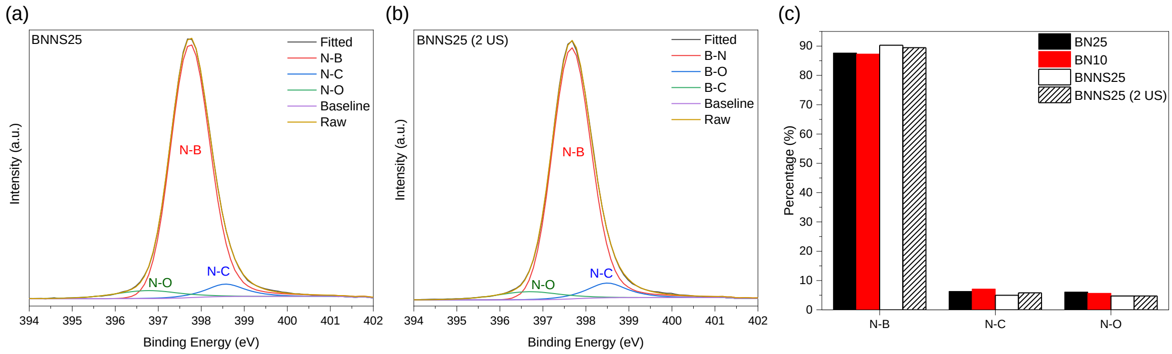

**Figure C4:** XPS peak fitting/ deconvolution of N1s peak for (a) BNNS25 and (b) BNNS25 (2 US). (c) Percentage of each components analysed through the fitting of N1s peak. The data for raw bulk hBN  materials used for exfoliation (BN25 and BN10) are also shown for comparison.

# C.3 UV-Vis Spectrometry

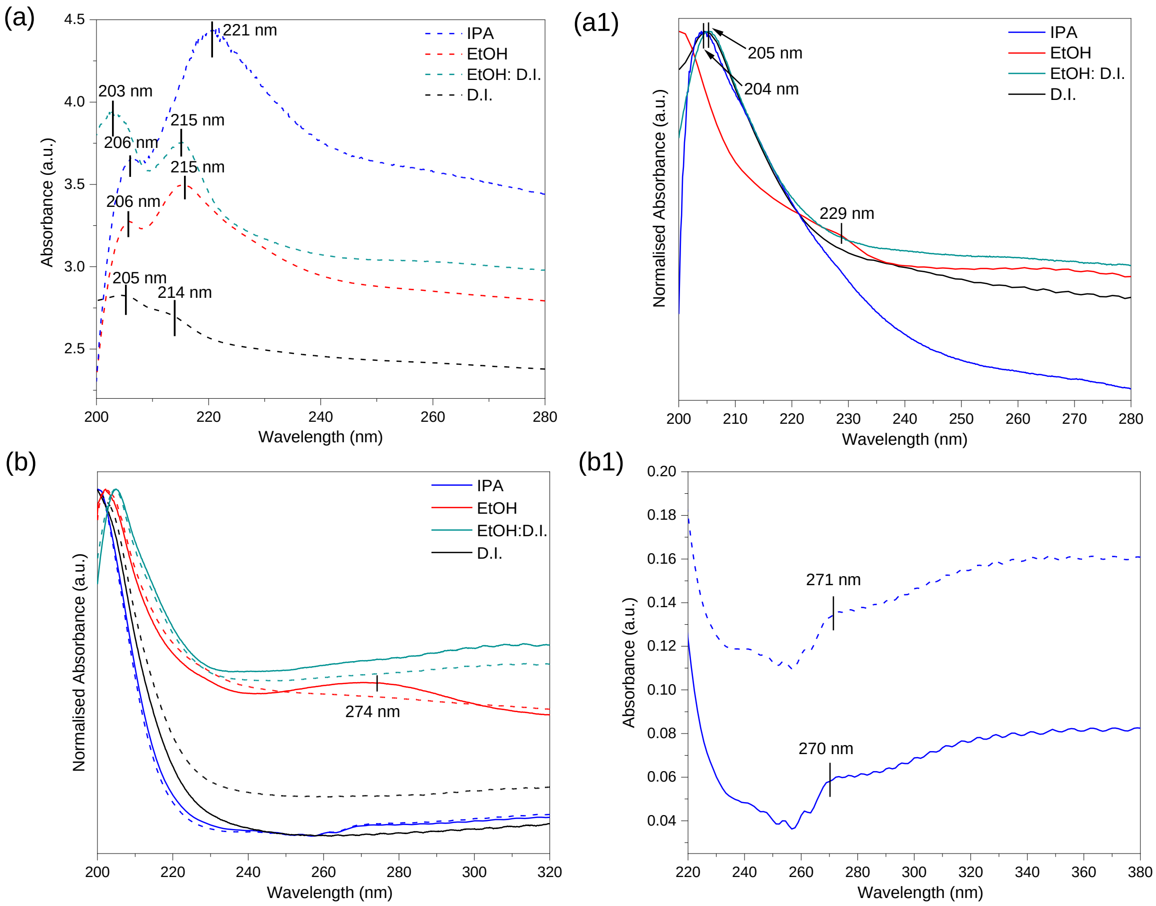

**Figure C5**: UV-Vis spectra of (a& a1) BNNS25 and (b& b1) BNNS10 produced in different solvents focusing on the shorter wavelength region that showed the main BNNS absorption peaks. Spectra with dashed lines are spectra obtained from dispersions with 2 US. The BNNS absorption peaks beyond 210 nm mainly occur only for the BNNS25 with 2 US (a), besides for BNNS25 in EtOH (a1). BNNS10 in EtOH (without 2 US) and in IPA (both with and without 2 US) showed the π-π* absorption peak around 270 nm.

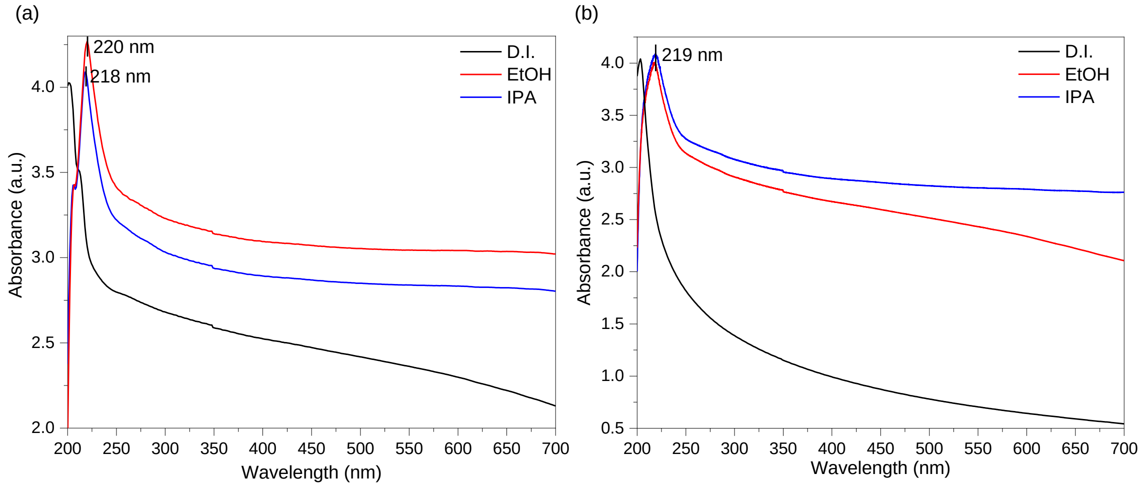

**Figure C6:** The UV-Vis spectra of (a) BNNS25 and (b) BNNS10 produced by 3-hour ultrasonication exfoliation. Both BNNS25 and BNNS10 produced in EtOH and IPA show absorption peak around 220 nm, besides BNNS produced in D.I..

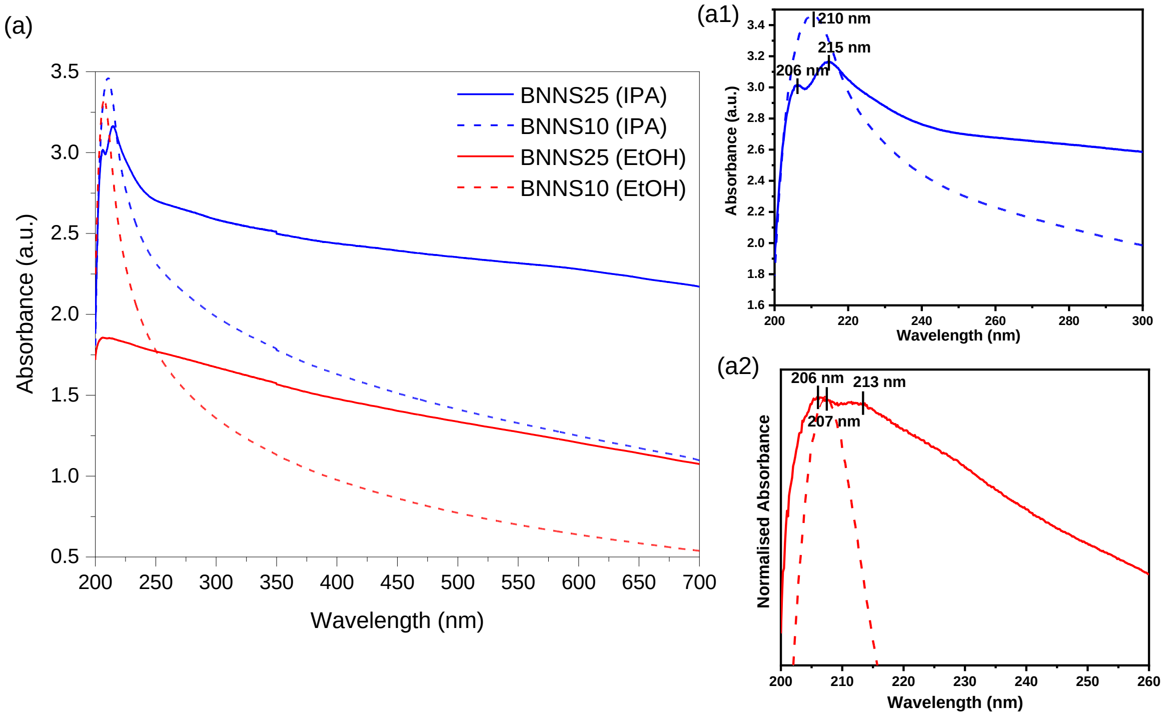

**Figure C7**: (a) The UV-Vis spectra of diluted BNNS25 and BNNS10 dispersion produced by 3-hour ultrasonication exfoliation. The absorption peak beyond 210 nm occurs for both BNNS25 and BNNS10 produced in EtOH and IPA (besides BNNS10 in EtOH), despite of the dilution. This shows that the occurrence of this absorption peak is not concentration dependent, but it shifted to the shorter wavelength upon dilution. Fig. C6 shows the spectra without the dilution.

# C.4 Raman Spectroscopy of Hexagonal Boron Nitride Nanosheets (BNNS)

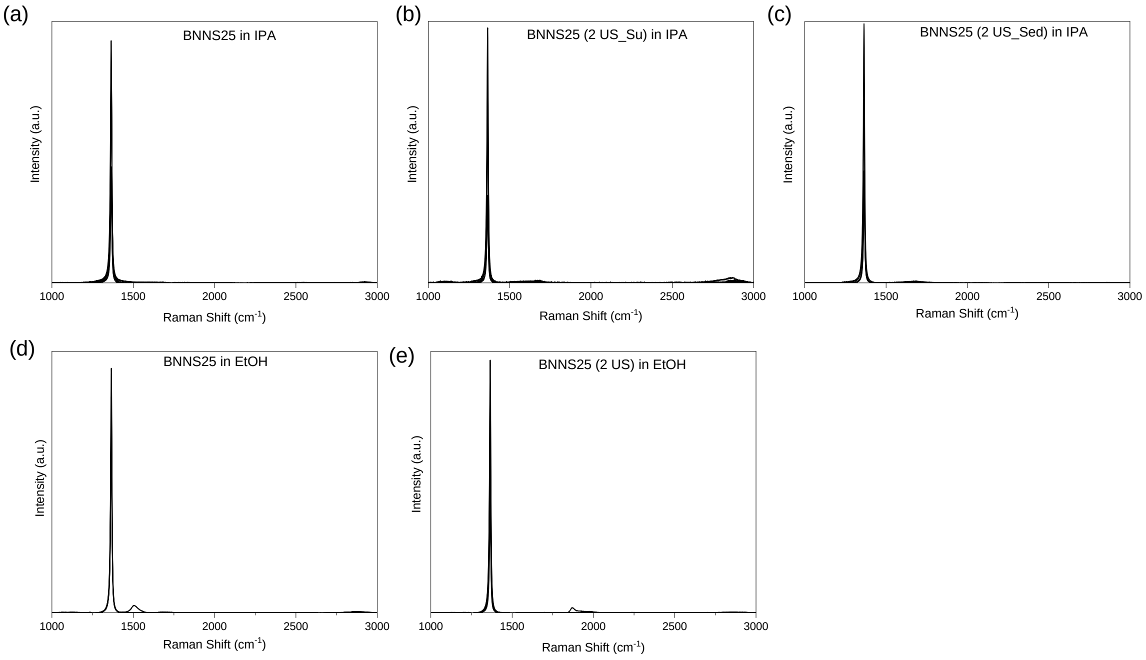

**Figure C8:** (a-e) The Raman spectra of BNNS25, with and without 2-min ultrasonication (2 US) in IPA and EtOH.

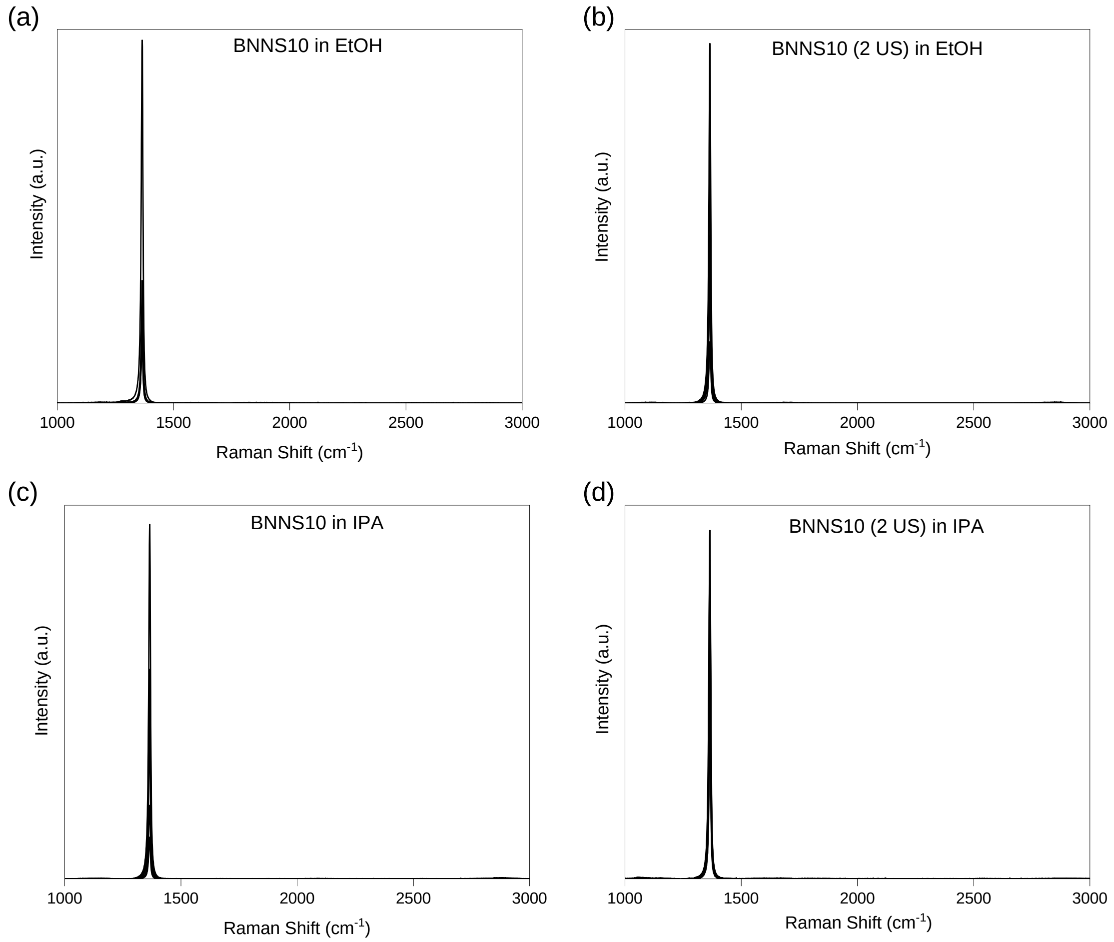

**Figure C9**: (a-d) The Raman spectra of BNNS10, with and without 2-min ultrasonication (2 US) in IPA and EtOH.

## C.5 Atomic Force Microscopy (AFM)

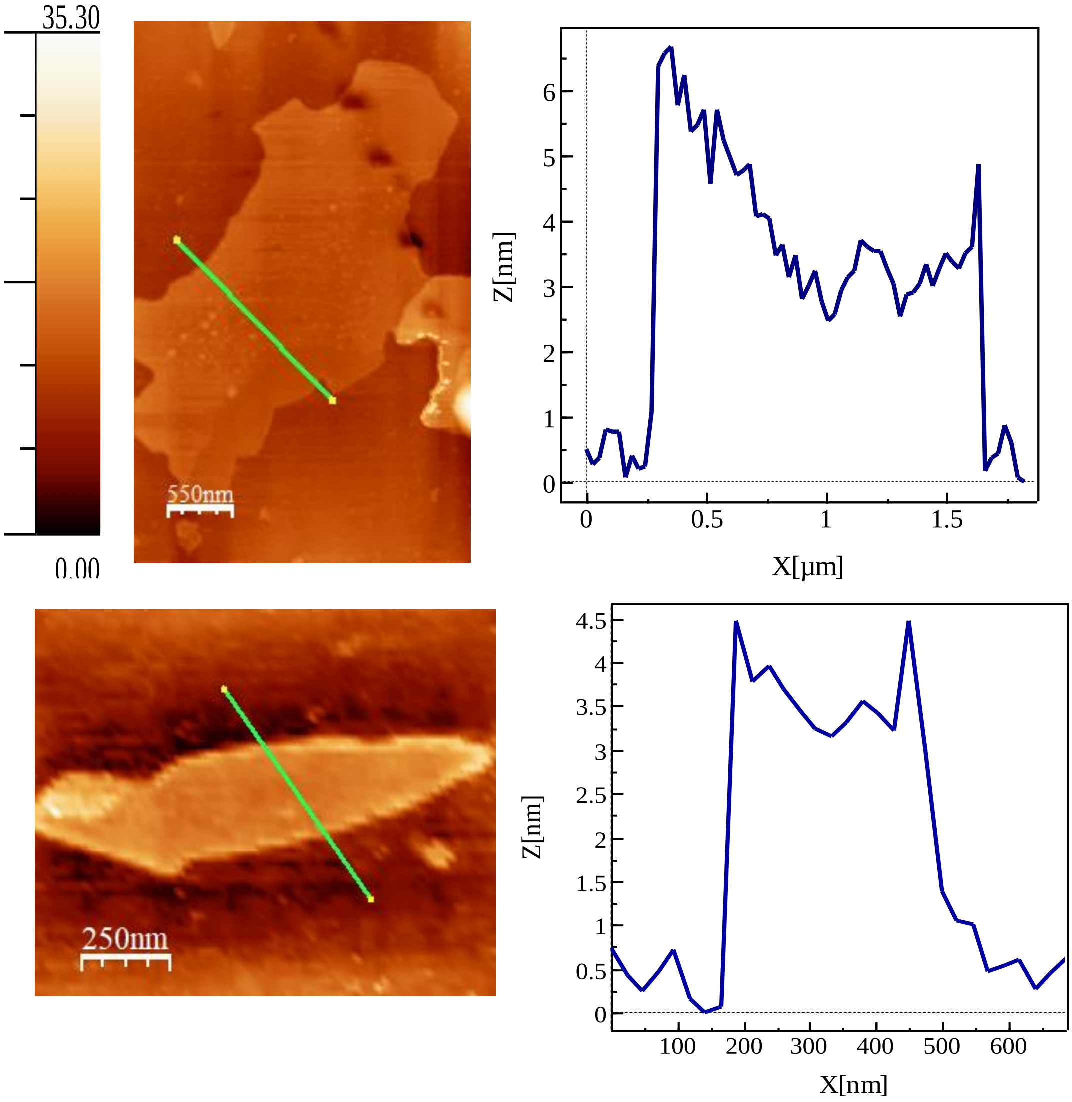

**Figure C10**: The additional AFM images and thickness profiles of BNNS25 (2 US) in IPA.

## C.6 Raman Spectroscopy of BNNS-Graphene

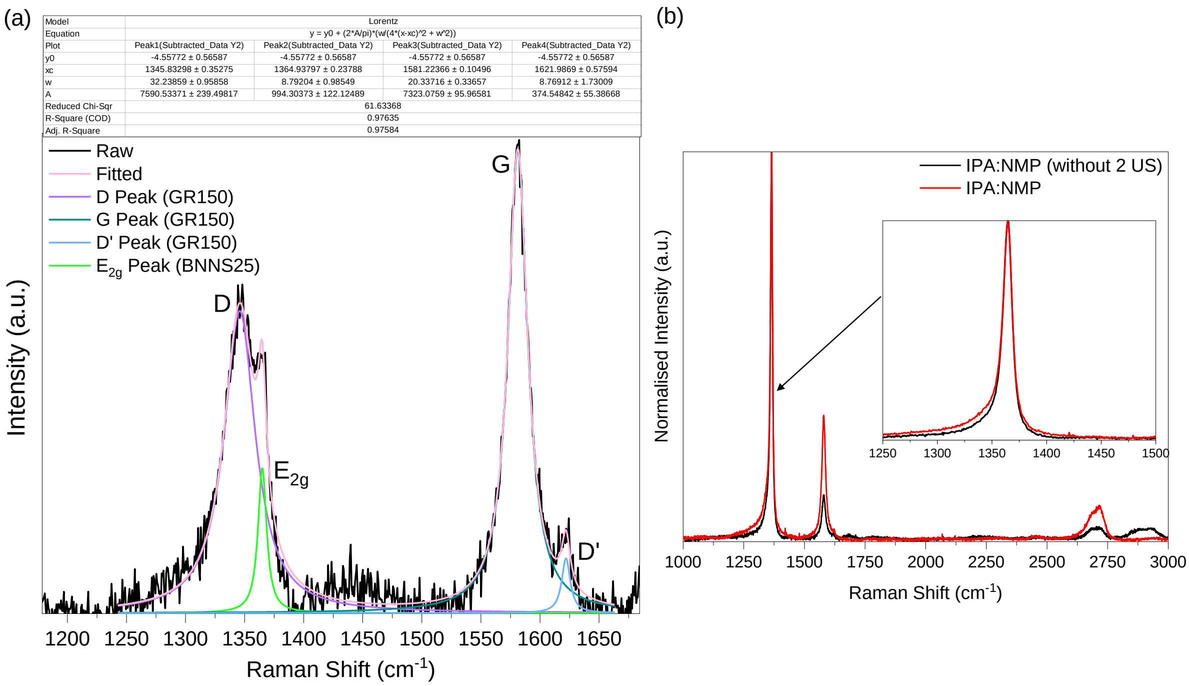

| Model | Lorentz | | | |
|---|---|---|---|---|
| Equation | y = y0 + (2*A/pi)*(w/(4*(x-xc)^2 + w^2)) | | | |
| Plot | Peak1(Subtracted_Data Y2) | Peak2(Subtracted_Data Y2) | Peak3(Subtracted_Data Y2) | Peak4(Subtracted_Data Y2) |
| y0 | -4.55772 ± 0.56587 | -4.55772 ± 0.56587 | -4.55772 ± 0.56587 | -4.55772 ± 0.56587 |
| xc | 1345.83298 ± 0.35275 | 1364.93797 ± 0.23788 | 1581.22366 ± 0.10496 | 1621.9869 ± 0.57594 |
| w | 32.23859 ± 0.95858 | 8.79204 ± 0.98549 | 20.33716 ± 0.33657 | 8.76912 ± 1.73009 |
| A | 7590.53371 ± 239.49817 | 994.30373 ± 122.12489 | 7323.0759 ± 95.96581 | 374.54842 ± 55.38668 |
| Reduced Chi-Sqr | 61.63368 | | | |
| R-Square (COD) | 0.97635 | | | |
| Adj. R-Square | 0.97584 | | | |

**Figure C11:** (a) The fitting and deconvolution of the overlapped BNNS (BNNS25) and graphene (GR150) peaks in BNNS-graphene sample (produced in NMP) using Lorentzian function. (b) The comparison of BNNS-graphene produced in IPA:NMP (1:1) with and without 2 US. The spectra are normalised to the highest $E_{2g}$ peak of BNNS. The BNNS-graphene produced with 2 US shows higher graphene peaks.

# References

1. Parviz, D. *et al.* Challenges in Liquid-Phase Exfoliation, Processing, and Assembly of Pristine Graphene. *Advanced Materials* (2016) doi:10.1002/adma.201601889.
2. Coleman, J. N. Liquid-phase exfoliation of nanotubes and graphene. *Adv Funct Mater* (2009) doi:10.1002/adfm.200901640.
3. Ng, K. L. *et al.* Direct Evidence of the Exfoliation Efficiency and Graphene Dispersibility of Green Solvents toward Sustainable Graphene Production. *ACS Sustain Chem Eng* (2023) doi:10.1021/acssuschemeng.2c03594.
4. Zheng, W. & Lee, L. Y. S. Beyond sonication: Advanced exfoliation methods for scalable production of 2D materials. *Matter* 5, 515–545 (2022).
5. Shen, J. *et al.* Liquid Phase Exfoliation of Two-Dimensional Materials by Directly Probing and Matching Surface Tension Components. *Nano Lett* 15, 5449–5454 (2015).
6. O'Neill, A., Khan, U., Nirmalraj, P. N., Boland, J. & Coleman, J. N. Graphene dispersion and exfoliation in low boiling point solvents. *Journal of Physical Chemistry C* (2011) doi:10.1021/jp110942e.
7. Sumdani, M. G., Islam, M. R., Yahaya, A. N. A. & Safie, S. I. Recent advances of the graphite exfoliation processes and structural modification of graphene: a review. *Journal of Nanoparticle Research* 23, 253 (2021).
8. Le, T., Oh, Y., Kim, H. & Yoon, H. Exfoliation of 2D Materials for Energy and Environmental Applications. *Chemistry – A European Journal* 26, 6360–6401 (2020).
9. Kumar, N. *et al.* Top-down synthesis of graphene: A comprehensive review. *FlatChem* 27, 100224 (2021).
10. Khan, U. *et al.* Size selection of dispersed, exfoliated graphene flakes by controlled centrifugation. *Carbon N Y* (2012) doi:10.1016/j.carbon.2011.09.001.
11. Backes, C. *et al.* Production of highly monolayer enriched dispersions of liquid-exfoliated nanosheets by liquid cascade centrifugation. *ACS Nano* (2016) doi:10.1021/acsnano.5b07228.
12. *Inorganic Two-Dimensional Nanomaterials*. (Royal Society of Chemistry, Cambridge, 2017). doi:10.1039/9781788010306.

13. Iacopi, F., Boeckl, J. J. & Jagadish, C. *2D Materials*. (Academic Press is an imprint of Elsevier, Cambridge, MA, 2016).

14. Kamble, G. S. *2D Functional Nanomaterials : Synthesis, Characterization, and Applications*. (Wiley-VCH, Weinheim, Germany, 2022). doi:10.1002/9783527823963.

15. Chakroborty, Subhendu. *2D Nanomaterials : Synthesis, Properties, and Applications.* (John Wiley & Sons, Inc., Newark, 2024).

16. Franck, M., Dabrowski, J., Schubert, M. A., Wenger, C. & Lukosius, M. Towards the Growth of Hexagonal Boron Nitride on Ge(001)/Si Substrates by Chemical Vapor Deposition. *Nanomaterials (Basel)* 12, 3260 (2022).

17. Zhu, Z. *et al.* Hexagonal Boron Nitride Thick Film Grown on a Sapphire Substrate via Low-Pressure Chemical Vapor Deposition. *Cryst Growth Des* 23, 7662–7668 (2023).

18. He, Y., Andrade, A. F., Ménard-Moyon, C. & Bianco, A. Biocompatible 2D Materials via Liquid Phase Exfoliation. *Advanced materials (Weinheim)* 36, e2310999-n/a (2024).

19. Hu, C.-X., Shin, Y., Read, O. & Casiraghi, C. Dispersant-assisted liquid-phase exfoliation of 2D materials beyond graphene. *Nanoscale* 13, 46–484 (2021).

20. Zhao, M., Casiraghi, C. & Parvez, K. Electrochemical exfoliation of 2D materials beyond graphene. *Chem Soc Rev* 53, 336–364 (2024).

21. Chen, H., Jiang, D., Yang, Z. & Dai, S. Engineering Nanostructured Interfaces of Hexagonal Boron Nitride-Based Materials for Enhanced Catalysis. *Acc Chem Res* 56, 52–65 (2023).

22. Zhang, G., Zhao, Y. & Sun, J. Design and fabrication of a large-range graphene/hexagonal boron nitride heterostructure based pressure sensor with poly(methyl methacrylate) substrate. *Review of scientific instruments* 93, 015009–015009 (2022).

23. Hwang, J. H. *et al.* Nanoscale layer of a minimized defect area of graphene and hexagonal boron nitride on copper for excellent anti-corrosion activity. *Nanotechnology* 33, 55601 (2022).

24. Zhao, Y., Wu, X., Yang, J. & Zeng, X. C. Oxidation of a two-dimensional hexagonal boron nitride monolayer: a first-principles study. *Phys Chem Chem Phys* 14, 5545–5550 (2012).

25. Das, S. *2D Materials for Electronics, Sensors and Devices : Synthesis, Characterization, Fabrication and Application*. (Elsevier, Amsterdam, Netherlands, 2022).

26. Novoselov, K. S. *et al.* Electric Field Effect in Atomically Thin Carbon Films. *Science (American Association for the Advancement of Science)* 306, 666–669 (2004).
27. Kumar, N. *et al.* Top-down synthesis of graphene: A comprehensive review. *FlatChem* 27, 100224 (2021).
28. Kauling, A. P. *et al.* The Worldwide Graphene Flake Production. *Advanced Materials* 30, (2018).
29. Zhang, X. *et al.* Raman characterization of AB-and ABC-stacked few-layer graphene by interlayer shear modes. *Carbon N Y* 99, 118–122 (2016).
30. Subramaniam, R. T. *Graphene : Fabrication, Properties and Applications*. (Springer Nature Singapore Pte Ltd, Singapore, 2023). doi:10.1007/978-981-99-1206-3.
31. Zhang, J. *Chemically Derived Graphene : Functionalization, Properties and Applications*. (Royal Society of Chemistry, Cambridge, 2018).
32. Takahashi, K., Imamura, M., Yamamoto, I. & Azuma, J. Thickness dependent band structure of α-bismuthene grown on epitaxial graphene. *Journal of physics. Condensed matter* 34, 235502 (2022).
33. Li, H. *et al.* Thickness-dependent magnetotransport: from multilayer graphene to few-layer graphene. *Carbon (New York)* 124, 193–200 (2017).
34. Kat͡snelʹson, M. I. (Mikhail I. *The Physics of Graphene*. (Cambridge University Press, Cambridge, 2020).
35. Ferrari, A. C. & Basko, D. M. Raman spectroscopy as a versatile tool for studying the properties of graphene. *Nature Nanotechnology* Preprint at https://doi.org/10.1038/nnano.2013.46 (2013).
36. Novoselov, K. S. *et al.* Electronic properties of graphene. in *Physica Status Solidi (B) Basic Research* vol. 244 4106–4111 (2007).
37. Mak, K. F., Sfeir, M. Y., Misewich, J. A. & Heinz, T. F. evolution of electronic structure in few-layer graphene revealed by optical spectroscopy. *Proceedings of the National Academy of Sciences - PNAS* 107, 14999–15004 (2010).
38. Zhang, R. *et al.* In-Situ Growth of High-Quality Customized Monolayer Graphene Structures for Optoelectronics. *Adv Funct Mater* 32, n/a (2022).
39. Romagnoli, M. *et al.* Graphene-based integrated photonics for next-generation datacom and telecom. *Nat Rev Mater* 3, 392–414 (2018).
40. Das, S. *2D Materials for Electronics, Sensors and Devices : Synthesis, Characterization, Fabrication and Application*. (Elsevier, Amsterdam, Netherlands, 2022).

41. Yang, Y. *et al.* Electrochemical exfoliation of graphene-like two-dimensional nanomaterials. *Nanoscale* 11, 16–33 (2019).

42. Wu, W., Zhang, C. & Hou, S. Electrochemical exfoliation of graphene and graphene-analogous 2D nanosheets. *J Mater Sci* 52, 10649–10660 (2017).

43. Chakroborty, Subhendu. *2D Nanomaterials : Synthesis, Properties, and Applications.* (John Wiley & Sons, Inc., Newark, 2024).

44. Munuera, J., Britnell, L., Santoro, C., Cuéllar-Franca, R. & Casiraghi, C. A review on sustainable production of graphene and related life cycle assessment. *2D Materials* vol. 9 Preprint at https://doi.org/10.1088/2053-1583/ac3f23 (2022).

45. Paton, K. R. *et al.* Scalable production of large quantities of defect-free few-layer graphene by shear exfoliation in liquids. *Nat Mater* (2014) doi:10.1038/nmat3944.

46. Park, Y. & Hyun, S. Vibrational Characteristics of Two-Dimensional Composite Structures of Hexagonal Boron Nitride and Graphene. *Journal of the Korean Physical Society* 75, 569–576 (2019).

47. *Hexagonal Boron Nitride*. (Elsevier, 2024). doi:10.1016/C2022-0-00394-9.

48. Cassabois, G., Valvin, P. & Gil, B. Hexagonal boron nitride is an indirect bandgap semiconductor. *Nat Photonics* 10, 262–266 (2016).

49. Yuan, C. *et al.* Modulating the thermal conductivity in hexagonal boron nitride via controlled boron isotope concentration. *Commun Phys* 2, (2019).

50. Robinson, Z. R., Schmucker, S. W., McCreary, K. M. & Cobas, E. D. Chemical Vapor Deposition of Two-Dimensional Crystals. in *Handbook of Crystal Growth: Thin Films and Epitaxy: Second Edition* vol. 3 785–833 (Elsevier Inc., 2015).

51. Tian, X. *et al.* Shear-Assisted Production of Few-Layer Boron Nitride Nanosheets by Supercritical CO2 Exfoliation and Its Use for Thermally Conductive Epoxy Composites. *Sci Rep* 7, (2017).

52. Liu, Z. *et al.* Challenges and solutions in surface engineering and assembly of boron nitride nanosheets. *Materials Today* 44, 194–210 (2021).

53. Wang, Z. *et al.* Functionalization of boron nitride nanosheets by diazonium salt for preparation of nanocomposites with high-density polyethylene. *Polym Compos* 40, 2346–2356 (2019).

54. Songfeng, E., Liu, J., Zhao, R., Ning, D. & Lu, Z. Formation Mechanisms of Hexagonal Boron Nitride Nanosheets in Solvothermal Exfoliation. *Langmuir* (2023) doi:10.1021/acs.langmuir.2c03049.

55. Zhu, W. *et al.* Controlled Gas Exfoliation of Boron Nitride into Few-Layered Nanosheets. *Angewandte Chemie International Edition* 55, 10766–10770 (2016).

56. Tian, R. *et al.* Efficient exfoliation and functionalization of hexagonal boron nitride using recyclable ionic liquid crystal for thermal management applications. *Chemical Engineering Journal* 446, 137255 (2022).

57. Wen, W. *et al.* Recent advances in emerging 2D nanomaterials for biosensing and bioimaging applications. *Materials Today* vol. 21 164–177 Preprint at https://doi.org/10.1016/j.mattod.2017.09.001 (2018).

58. An, L. *et al.* Hexagonal boron nitride nanosheets: Preparation, heat transport property and application as thermally conductive fillers. *Prog Mater Sci* 138, 101154 (2023).

59. Gu, S., Chandra Mallick, B., Hsieh, C.-T., Gandomi, Y. A. & Zhang, R.-S. Hexagonal boron nitride nanosheets as metal-free electrochemical catalysts for oxygen reduction reactions. *Ceram Int* 48, 9506–9517 (2022).

60. Wang, N., Yang, G., Wang, H., Sun, R. & Wong, C.-P. Visible Light-Responsive Photocatalytic Activity of Boron Nitride Incorporated Composites. *Front Chem* 6, (2018).

61. Wu, W. *et al.* Thermally conductive composites based on hexagonal boron nitride nanosheets for thermal management: Fundamentals to applications. *Compos Part A Appl Sci Manuf* 169, 107533 (2023).

62. Li, L. *et al.* Research Progress of the Liquid-Phase Exfoliation and Stable Dispersion Mechanism and Method of Graphene. *Frontiers in Materials* Preprint at https://doi.org/10.3389/fmats.2019.00325 (2019).

63. Deokar, G., Jin, J., Schwingenschlögl, U. & Costa, P. M. F. J. Chemical vapor deposition-grown nitrogen-doped graphene's synthesis, characterization and applications. *npj 2D Materials and Applications* Preprint at https://doi.org/10.1038/s41699-022-00287-8 (2022).

64. Chen, D. *et al.* Programmed electrochemical exfoliation of graphite to high quality graphene. *Chemical Communications* (2019) doi:10.1039/c9cc00393b.

65. Kidambi, P. R. *et al.* Observing graphene grow: Catalyst-graphene interactions during scalable graphene growth on polycrystalline copper. *Nano Lett* (2013) doi:10.1021/nl4023572.

66. Weatherup, R. S., Dlubak, B. & Hofmann, S. Kinetic control of catalytic CVD for high-quality graphene at low temperatures. *ACS Nano* (2012) doi:10.1021/nn303674g.

67. Ani, M. H. *et al.* A critical review on the contributions of chemical and physical factors toward the nucleation and growth of large-area graphene. *Journal of Materials Science* Preprint at https://doi.org/10.1007/s10853-018-1994-0 (2018).

68. Chen, K., Shi, L., Zhang, Y. & Liu, Z. Scalable chemical-vapour-deposition growth of three-dimensional graphene materials towards energy-related

applications. *Chemical Society Reviews* Preprint at https://doi.org/10.1039/c7cs00852j (2018).

69. Zhang, Y. *et al.* Comparison of graphene growth on single-crystalline and polycrystalline Ni by chemical vapor deposition. *Journal of Physical Chemistry Letters* (2010) doi:10.1021/jz1011466.

70. Kolesnichenko, I. V., Goloverda, G. Z. & Kolesnichenko, V. L. A Versatile Method of Ambient-Temperature Solvent Removal. *Org Process Res Dev* (2020) doi:10.1021/acs.oprd.9b00368.

71. Yi, M. & Shen, Z. A review on mechanical exfoliation for the scalable production of graphene. *Journal of Materials Chemistry A* Preprint at https://doi.org/10.1039/c5ta00252d (2015).

72. Baig, Z. *et al.* Investigation of tip sonication effects on structural quality of graphene nanoplatelets (GNPs) for superior solvent dispersion. *Ultrason Sonochem* (2018) doi:10.1016/j.ultsonch.2018.03.007.

73. Tran, T. S., Park, S. J., Yoo, S. S., Lee, T. R. & Kim, T. Y. High shear-induced exfoliation of graphite into high quality graphene by Taylor-Couette flow. *RSC Adv* (2016) doi:10.1039/c5ra22273g.

74. Biccai, S. *et al.* Exfoliation of 2D materials by high shear mixing. *2d Mater* (2019) doi:10.1088/2053-1583/aae7e3.

75. Vashisth, V., Nigam, K. D. P. & Kumar, V. Design and development of high shear mixers: Fundamentals, applications and recent progress. *Chem Eng Sci* (2021) doi:10.1016/j.ces.2020.116296.

76. Paton, K. R. *et al.* Scalable production of large quantities of defect-free few-layer graphene by shear exfoliation in liquids. *Nat Mater* (2014) doi:10.1038/nmat3944.

77. Yi, M. & Shen, Z. A review on mechanical exfoliation for the scalable production of graphene. *Journal of Materials Chemistry A* Preprint at https://doi.org/10.1039/c5ta00252d (2015).

78. Hernandez, Y., Lotya, M., Rickard, D., Bergin, S. D. & Coleman, J. N. Measurement of multicomponent solubility parameters for graphene facilitates solvent discovery. *Langmuir* (2010) doi:10.1021/la903188a.

79. Fernandes, J., Nemala, S. S., De Bellis, G. & Capasso, A. Green Solvents for the Liquid Phase Exfoliation Production of Graphene: The Promising Case of Cyrene. *Frontiers in Chemistry* Preprint at https://doi.org/10.3389/fchem.2022.878799 (2022).

80. Hernandez, Y. *et al.* High-yield production of graphene by liquid-phase exfoliation of graphite. *Nat Nanotechnol* (2008) doi:10.1038/nnano.2008.215.

81. Coleman, J. N. Liquid-phase exfoliation of nanotubes and graphene. *Adv Funct Mater* (2009) doi:10.1002/adfm.200901640.

82. Gibbs, J. W. & Tyndall, J. *On the Equilibrium of Heterogeneous Substances : First [-Second] Part*. (Published by the Academy, [New Haven, 1874). doi:10.5479/sil.421748.39088007099781.

83. Peter Atkins and Julio de Paula. *Physical Chemistry*. (Oxford University Press, Oxford, 2014).

84. Sedehi, H. R. R. & Khordad, R. Entropy and specific heat of graphene at low and high temperatures under an external magnetic field. *Solid State Commun* 313, 113911 (2020).

85. Hernandez, Y. *et al.* High-yield production of graphene by liquid-phase exfoliation of graphite. *Nat Nanotechnol* (2008) doi:10.1038/nnano.2008.215.

86. Varrla, E. *et al.* Turbulence-assisted shear exfoliation of graphene using household detergent and a kitchen blender. *Nanoscale* (2014) doi:10.1039/c4nr03560g.

87. Morton, J. A. *et al.* An eco-friendly solution for liquid phase exfoliation of graphite under optimised ultrasonication conditions. *Carbon N Y* (2023) doi:10.1016/j.carbon.2022.12.070.

88. Yang, X. *et al.* Efficient exfoliation to MoS2 nanosheets by salt-assisted refluxing and ultrasonication with photocatalytic application. *Mater Lett* (2019) doi:10.1016/j.matlet.2019.126596.

89. Diasio, M. A. & Green, D. L. The Effect of Solvent Viscosity on Production of Few-layer Graphene from Liquid-phase Exfoliation of Graphite. *MRS Adv* 4, pp241-247 (2019).

90. Zhang, B. & Chen, T. Study of ultrasonic dispersion of graphene nanoplatelets. *Materials* (2019) doi:10.3390/ma12111757.

91. Ishikawa, M. *et al.* Atomic-scale peeling of graphene. *Applied Physics Express* (2012) doi:10.1143/APEX.5.065102.

92. Backes, C. *et al.* Equipartition of Energy Defines the Size-Thickness Relationship in Liquid-Exfoliated Nanosheets. *ACS Nano* (2019) doi:10.1021/acsnano.9b02234.

93. Stafford, J., Patapas, A., Uzo, N., Matar, O. K. & Petit, C. Towards scale-up of graphene production via nonoxidizing liquid exfoliation methods. *AIChE Journal* 64, 3246–3276 (2018).

94. Lund, S. *et al.* Fast high-shear exfoliation of natural flake graphite with temperature control and high yield. *Carbon N Y* (2021) doi:10.1016/j.carbon.2020.11.094.

95. Tyurnina, A. V. *et al.* Ultrasonic exfoliation of graphene in water: A key parameter study. *Carbon N Y* (2020) doi:10.1016/j.carbon.2020.06.029.

96. Gu, X. *et al.* Method of ultrasound-assisted liquid-phase exfoliation to prepare graphene. *Ultrason Sonochem* (2019) doi:10.1016/j.ultsonch.2019.104630.

97. Pollet, B. G. & Kocha, S. S. Using Ultrasound to Effectively Homogenise Catalyst Inks: Is this Approach Still Acceptable? Recommendations on the use of ultrasound for mixing catalyst inks. *Johnson Matthey Technology Review* (2022) doi:10.1595/205651321X16196162869695.

98. Turner, P., Hodnett, M., Dorey, R. & Carey, J. D. Controlled Sonication as a Route to in-situ Graphene Flake Size Control. *Sci Rep* (2019) doi:10.1038/s41598-019-45059-5.

99. Mellado, C., Figueroa, T., Baez, R., Meléndrez, M. & Fernández, K. Effects of probe and bath ultrasonic treatments on graphene oxide structure. *Mater Today Chem* (2019) doi:10.1016/j.mtchem.2019.04.006.

100. Sethurajaperumal, A. & Varrla, E. High-Quality and Efficient Liquid-Phase Exfoliation of Few-Layered Graphene by Natural Surfactant. *ACS Sustain Chem Eng* (2022) doi:10.1021/acssuschemeng.2c03742.

101. Utomo, A., Baker, M. & Pacek, A. W. The effect of stator geometry on the flow pattern and energy dissipation rate in a rotor-stator mixer. *Chemical Engineering Research and Design* (2009) doi:10.1016/j.cherd.2008.12.011.

102. Biccai, S. *et al.* Exfoliation of 2D materials by high shear mixing. *2d Mater* (2019) doi:10.1088/2053-1583/aae7e3.

103. Varrla, E. *et al.* Turbulence-assisted shear exfoliation of graphene using household detergent and a kitchen blender. *Nanoscale* (2014) doi:10.1039/c4nr03560g.

104. Liu, L., Shen, Z., Yi, M., Zhang, X. & Ma, S. A green, rapid and size-controlled production of high-quality graphene sheets by hydrodynamic forces. *RSC Adv* (2014) doi:10.1039/c4ra05635c.

105. Utomo, A. T., Baker, M. & Pacek, A. W. Flow pattern, periodicity and energy dissipation in a batch rotor–stator mixer. *Chemical Engineering Research and Design* 86, 1397–1409 (2008).

106. Qin, H. *et al.* Effect of Stator Geometry on the Emulsification and Extraction in the Inline Single-Row Blade-Screen High Shear Mixer. *Ind Eng Chem Res* (2017) doi:10.1021/acs.iecr.7b01362.

107. Gacka, E., Majchrzycki, Ł., Marciniak, B. & Lewandowska-Andralojc, A. Effect of graphene oxide flakes size and number of layers on photocatalytic hydrogen production. *Sci Rep* (2021) doi:10.1038/s41598-021-95464-y.

108. Khan, U. *et al.* Size selection of dispersed, exfoliated graphene flakes by controlled centrifugation. *Carbon N Y* (2012) doi:10.1016/j.carbon.2011.09.001.

109. Gacka, E., Majchrzycki, Ł., Marciniak, B. & Lewandowska-Andralojc, A. Effect of graphene oxide flakes size and number of layers on photocatalytic hydrogen production. *Sci Rep* 11, 15969 (2021).

110. Cui, X., Zhang, C., Hao, R. & Hou, Y. Liquid-phase exfoliation, functionalization and applications of graphene. *Nanoscale* Preprint at https://doi.org/10.1039/c1nr10127g (2011).

111. On the Effect of the Internal Friction of Fluids on the Motion of Pendulums. in *Mathematical and Physical Papers* 1–10 (Cambridge University Press, 2009). doi:10.1017/CBO9780511702266.002.

112. Zhang, X., Tran, S. & Gray-Weale, A. Hydrodynamic Drag on Diffusing Nanoparticles for Size Determination. *The Journal of Physical Chemistry C* 120, 21888–21896 (2016).

113. Kuang, Y., Song, S., Huang, J. & Sun, X. Separation of colloidal two dimensional materials by density gradient ultracentrifugation. *J Solid State Chem* 224, 120–126 (2015).

114. Qin, J., Wang, X., Jiang, Q. & Cao, M. Optimizing Dispersion, Exfoliation, Synthesis, and Device Fabrication of Inorganic Nanomaterials Using Hansen Solubility Parameters. *ChemPhysChem* Preprint at https://doi.org/10.1002/cphc.201900110 (2019).

115. Ma, H. & Shen, Z. Exfoliation of graphene nanosheets in aqueous media. *Ceramics International* Preprint at https://doi.org/10.1016/j.ceramint.2020.05.314 (2020).

116. Venkatram, S., Kim, C., Chandrasekaran, A. & Ramprasad, R. Critical Assessment of the Hildebrand and Hansen Solubility Parameters for Polymers. *J Chem Inf Model* (2019) doi:10.1021/acs.jcim.9b00656.

117. Koenhen, D. M. & Smolders, C. A. The determination of solubility parameters of solvents and polymers by means of correlations with other physical quantities. *J Appl Polym Sci* (1975) doi:10.1002/app.1975.070190423.

118. Lin, H. -M & Nash, R. A. An experimental method for determining the hildebrand solubility parameter of organic nonelectrolytes. *J Pharm Sci* (1993) doi:10.1002/jps.2600821001.

119. Li, C. & Strachan, A. Cohesive energy density and solubility parameter evolution during the curing of thermoset. *Polymer (Guildf)* (2018) doi:10.1016/j.polymer.2017.12.002.

120. Fink, J. K. *Reactive Polymers: Fundamentals and Applications*. *Reactive Polymers: Fundamentals and Applications A Concise Guide to Industrial Polymers* (2017). doi:10.1016/C2017-0-01641-5.

121. Liang, K. Y. & Yang, W. D. Prediction the concentration of graphite direct exfoliation by liquid solution with solubility parameters map. *AIP Adv* (2018) doi:10.1063/1.5005498.

122. Coleman, J. N. *et al.* Two-dimensional nanosheets produced by liquid exfoliation of layered materials. *Science (1979)* (2011) doi:10.1126/science.1194975.

123. Coleman, J. N. Liquid exfoliation of defect-free graphene. *Acc Chem Res* (2013) doi:10.1021/ar300009f.

124. Louwerse, M. J. *et al.* Revisiting Hansen Solubility Parameters by Including Thermodynamics. *ChemPhysChem* (2017) doi:10.1002/cphc.201700408.

125. Venkatram, S., Kim, C., Chandrasekaran, A. & Ramprasad, R. Critical Assessment of the Hildebrand and Hansen Solubility Parameters for Polymers. *J Chem Inf Model* (2019) doi:10.1021/acs.jcim.9b00656.

126. Cao, J. K., Zhou, D. F. & Zhang, Y. B. Improvements in the surface tension measurement using the capillary rise method and its application to water under external magnetic fields. *J Mol Liq* (2023) doi:10.1016/j.molliq.2023.121988.

127. Patterson, R. E. & Ross, S. The pendent-drop method to determine surface or interfacial tensions. *Surf Sci* (1979) doi:10.1016/0039-6028(79)90112-2.

128. Berry, J. D., Neeson, M. J., Dagastine, R. R., Chan, D. Y. C. & Tabor, R. F. Measurement of surface and interfacial tension using pendant drop tensiometry. *Journal of Colloid and Interface Science* Preprint at https://doi.org/10.1016/j.jcis.2015.05.012 (2015).

129. Yu, W. & Hou, W. Correlations of surface free energy and solubility parameters for solid substances. *J Colloid Interface Sci* (2019) doi:10.1016/j.jcis.2019.02.074.

130. Kaelble, D. H. Dispersion-Polar Surface Tension Properties of Organic Solids. *J Adhes* (1970) doi:10.1080/0021846708544582.

131. Owens, D. K. & Wendt, R. C. Estimation of the surface free energy of polymers. *J Appl Polym Sci* (1969) doi:10.1002/app.1969.070130815.

132. Blanks, R. F. & Prausnitz, J. M. Thermodynamics of polymer solubility in polar and nonpolar systems. *Industrial and Engineering Chemistry Fundamentals* (1964) doi:10.1021/i160009a001.

133. MOOSA, A. A. & ABED, M. S. Graphene preparation and graphite exfoliation. *Turkish Journal of Chemistry* Preprint at https://doi.org/10.3906/kim-2101-19 (2021).

134. Kozbial, A. *et al.* Study on the surface energy of graphene by contact angle measurements. *Langmuir* (2014) doi:10.1021/la5018328.

135. Rafiee, J. *et al.* Wetting transparency of graphene. *Nat Mater* (2012) doi:10.1038/nmat3228.

136. Chibowski, E. & Holysz, L. Use of the Washburn Equation for Surface Free Energy Determination. *Langmuir* (1992) doi:10.1021/la00038a066.

137. Salavagione, H. J. *et al.* Identification of high performance solvents for the sustainable processing of graphene. *Green Chemistry* (2017) doi:10.1039/c7gc00112f.

138. Shen, J. *et al.* Liquid Phase Exfoliation of Two-Dimensional Materials by Directly Probing and Matching Surface Tension Components. *Nano Lett* (2015) doi:10.1021/acs.nanolett.5b01842.

139. Washburn, E. W. The dynamics of capillary flow. *Physical Review* (1921) doi:10.1103/PhysRev.17.273.

140. Washburn, E. W. The dynamics of capillary flow. *Physical Review* (1921) doi:10.1103/PhysRev.17.273.

141. Zubar, T. I. *et al.* Method of surface energy investigation by lateral AFM: application to control growth mechanism of nanostructured NiFe films. *Sci Rep* (2020) doi:10.1038/s41598-020-71416-w.

142. Lamprou, D. A. *et al.* A comparative study of surface energy data from atomic force microscopy and from contact angle goniometry. *Appl Surf Sci* (2010) doi:10.1016/j.apsusc.2010.03.064.

143. Otyepková, E. *et al.* Surface properties of MoS2 probed by inverse gas chromatography and their impact on electrocatalytic properties. *Nanoscale* (2017) doi:10.1039/c7nr07342a.

144. Lee, S. Y., Lee, J. H., Kim, Y. H., Mahajan, R. L. & Park, S. J. Surface energetics of graphene oxide and reduced graphene oxide determined by inverse gas chromatographic technique at infinite dilution at room temperature. *J Colloid Interface Sci* (2022) doi:10.1016/j.jcis.2022.07.183.

145. Yu, J. *et al.* Inverse gas chromatography as a method for determination of surface properties of binding materials. in *IOP Conference Series: Materials Science and Engineering* (2017). doi:10.1088/1757-899X/242/1/012001.

146. Xu, Y., Cao, H., Xue, Y., Li, B. & Cai, W. Liquid-phase exfoliation of graphene: An overview on exfoliation media, techniques, and challenges. *Nanomaterials* Preprint at https://doi.org/10.3390/nano8110942 (2018).

147. Li, L. *et al.* Research Progress of the Liquid-Phase Exfoliation and Stable Dispersion Mechanism and Method of Graphene. *Frontiers in Materials* Preprint at https://doi.org/10.3389/fmats.2019.00325 (2019).

148. Mori, F., Kubouchi, M. & Arao, Y. Effect of graphite structures on the productivity and quality of few-layer graphene in liquid-phase exfoliation. *J Mater Sci* (2018) doi:10.1007/s10853-018-2538-3.

149. Sukumaran, S. S., Jinesh, K. B. & Gopchandran, K. G. Liquid phase exfoliated graphene for electronic applications. *Mater Res Express* 4, 095017 (2017).

150. Amiri, A., Naraghi, M., Ahmadi, G., Soleymaniha, M. & Shanbedi, M. A review on liquid-phase exfoliation for scalable production of pure graphene, wrinkled, crumpled and functionalized graphene and challenges. *FlatChem* 8, 40–71 (2018).

151. Mori, F., Kubouchi, M. & Arao, Y. Effect of graphite structures on the productivity and quality of few-layer graphene in liquid-phase exfoliation. *J Mater Sci* (2018) doi:10.1007/s10853-018-2538-3.

152. Silva, L. I., Mirabella, D. A., Pablo Tomba, J. & Riccardi, C. C. Optimizing graphene production in ultrasonic devices. *Ultrasonics* (2020) doi:10.1016/j.ultras.2019.105989.

153. Parviz, D. *et al.* Challenges in Liquid-Phase Exfoliation, Processing, and Assembly of Pristine Graphene. *Advanced Materials* (2016) doi:10.1002/adma.201601889.

154. Hernandez, Y., Lotya, M., Rickard, D., Bergin, S. D. & Coleman, J. N. Measurement of multicomponent solubility parameters for graphene facilitates solvent discovery. *Langmuir* (2010) doi:10.1021/la903188a.

155. Niu, L. *et al.* Production of Two-Dimensional Nanomaterials via Liquid-Based Direct Exfoliation. *Small* (2016) doi:10.1002/smll.201502207.

156. Rohman, N., Mohiuddin, T. & Al-Ruqeishi, M. S. Surface free energy of graphene-based coatings and its component elements. *Inorg Chem Commun* 153, 110855 (2023).

157. Lee, S.-Y., Lee, J.-H., Kim, Y.-H., Mahajan, R. L. & Park, S.-J. Surface energetics of graphene oxide and reduced graphene oxide determined by inverse gas chromatographic technique at infinite dilution at room temperature. *J Colloid Interface Sci* 628, 758–768 (2022).

158. Saeed, M., Alshammari, Y., Majeed, S. A. & Al-Nasrallah, E. Chemical Vapour Deposition of Graphene—Synthesis, Characterisation, and Applications: A Review. *Molecules* Preprint at https://doi.org/10.3390/molecules25173856 (2020).

159. Capello, C., Fischer, U. & Hungerbühler, K. What is a green solvent? A comprehensive framework for the environmental assessment of solvents. *Green Chemistry* (2007) doi:10.1039/b617536h.

160. Byrne, F. P. *et al.* Tools and techniques for solvent selection: green solvent selection guides. *Sustainable Chemical Processes* (2016) doi:10.1186/s40508-016-0051-z.
161. Johnson, D. W., Dobson, B. P. & Coleman, K. S. A manufacturing perspective on graphene dispersions. *Current Opinion in Colloid and Interface Science* Preprint at https://doi.org/10.1016/j.cocis.2015.11.004 (2015).
162. Bhoria, R. Enhancing Liquid Phase Exfoliation of Graphene in Organic Solvents with Additives. in *Graphene and its derivatives - Synthesis and applications [Working Title]* (2019). doi:10.5772/intechopen.81462.
163. O'Neill, A., Khan, U., Nirmalraj, P. N., Boland, J. & Coleman, J. N. Graphene dispersion and exfoliation in low boiling point solvents. *Journal of Physical Chemistry C* (2011) doi:10.1021/jp110942e.
164. Ma, J. *et al.* Exfoliating two-dimensional materials into few layers via optimized environmentally-friendly ternary solvents. *Nanotechnology* (2020) doi:10.1088/1361-6528/ab4a43.
165. Yi, M., Shen, Z., Zhang, X. & Ma, S. Achieving concentrated graphene dispersions in water/acetone mixtures by the strategy of tailoring Hansen solubility parameters. *J Phys D Appl Phys* (2013) doi:10.1088/0022-3727/46/2/025301.
166. Liu, W. W., Xia, B. Y., Wang, X. X. & Wang, J. N. Exfoliation and dispersion of graphene in ethanol-water mixtures. *Front Mater Sci* (2012) doi:10.1007/s11706-012-0166-4.
167. Cai, L. *et al.* Exfoliation and stabilization mechanism of graphene in carbon dioxide expanded organic solvents: Molecular dynamics simulations. *Physical Chemistry Chemical Physics* (2020) doi:10.1039/c9cp05924e.
168. Yi, M., Shen, Z., Zhang, X. & Ma, S. Achieving concentrated graphene dispersions in water/acetone mixtures by the strategy of tailoring Hansen solubility parameters. *J Phys D Appl Phys* (2013) doi:10.1088/0022-3727/46/2/025301.
169. Goldie, S. J. *et al.* Identification of Graphene Dispersion Agents through Molecular Fingerprints. *ACS Nano* (2022) doi:10.1021/acsnano.2c04406.
170. Sethurajaperumal, A. & Varrla, E. High-Quality and Efficient Liquid-Phase Exfoliation of Few-Layered Graphene by Natural Surfactant. *ACS Sustain Chem Eng* (2022) doi:10.1021/acssuschemeng.2c03742.
171. Tyurnina, A. V. *et al.* Effects of green solvents and surfactants on the characteristics of few-layer graphene produced by dual-frequency ultrasonic liquid phase exfoliation technique. *Carbon N Y* (2023) doi:10.1016/j.carbon.2023.01.062.

172. Griffin, A. *et al.* Effect of Surfactant Choice and Concentration on the Dimensions and Yield of Liquid-Phase-Exfoliated Nanosheets. *Chemistry of Materials* (2020) doi:10.1021/acs.chemmater.9b04684.

173. Zhang, X. *et al.* Dispersion of graphene in ethanol using a simple solvent exchange method. *Chemical Communications* (2010) doi:10.1039/c0cc02688c.

174. Li, J. *et al.* A simple route towards high-concentration surfactant-free graphene dispersions. *Carbon* Preprint at https://doi.org/10.1016/j.carbon.2012.03.011 (2012).

175. Cheng, Z. L., Kong, Y. C., Fan, L. & Liu, Z. Ultrasound-assisted Li+/Na+ co-intercalated exfoliation of graphite into few-layer graphene. *Ultrason Sonochem* (2020) doi:10.1016/j.ultsonch.2020.105108.

176. Yang, R. *et al.* High-yield production of mono- or few-layer transition metal dichalcogenide nanosheets by an electrochemical lithium ion intercalation-based exfoliation method. *Nature Protocols* Preprint at https://doi.org/10.1038/s41596-021-00643-w (2022).

177. Cheng, Z. L., Kong, Y. C. & Liu, Z. Li+/Na+ Co-Assisted Hydrothermal Exfoliation for Graphite into Few-Layer Graphene Nanosheets and Their Excellent Friction-Reducing Performance. *ACS Sustain Chem Eng* (2019) doi:10.1021/acssuschemeng.9b05060.

178. Raksha, E. V. *et al.* Morphology and Structure of Carbon Nanoparticles Generated from Graphite Nitrate Co-intercalation Compound. Effect of Sonication Regime. in *Springer Proceedings in Materials* (2020). doi:10.1007/978-3-030-45120-2_4.

179. Lee, H., Choi, J. Il, Park, J., Jang, S. S. & Lee, S. W. Role of anions on electrochemical exfoliation of graphite into graphene in aqueous acids. *Carbon N Y* (2020) doi:10.1016/j.carbon.2020.06.044.

180. Biranje, P. M., Patwardhan, A. W., Joshi, J. B. & Dasgupta, K. Exfoliated graphene and its derivatives from liquid phase and their role in performance enhancement of epoxy matrix composite. *Composites Part A: Applied Science and Manufacturing* Preprint at https://doi.org/10.1016/j.compositesa.2022.106886 (2022).

181. Yang, F. *et al.* Detonation exfoliated mechanism of graphene-like MoS2 prepared by the intercalation-detonation method and promising exfoliation for 2D materials. *Appl Surf Sci* (2020) doi:10.1016/j.apsusc.2020.145867.

182. Huang, L. *et al.* Salt-Assisted Synthesis of 2D Materials. *Advanced Functional Materials* Preprint at https://doi.org/10.1002/adfm.201908486 (2020).

183. Liang, B. *et al.* Organic salt-assisted liquid-phase shear exfoliation of expanded graphite into graphene nanosheets. *Journal of Materiomics* (2021) doi:10.1016/j.jmat.2021.03.007.

184. Jalalabadi, T., Wu, J., Moghtaderi, B., Sharma, N. & Allen, J. A new approach to turbostratic carbon production via thermal salt-assisted treatment of graphite. *Fuel* (2023) doi:10.1016/j.fuel.2023.128489.

185. Wang, S., Wang, C. & Ji, X. Towards understanding the salt-intercalation exfoliation of graphite into graphene. *RSC Adv* (2017) doi:10.1039/c7ra07489a.

186. Li, J., Yan, H., Dang, D., Wei, W. & Meng, L. Salt and water co-assisted exfoliation of graphite in organic solvent for efficient and large scale production of high-quality graphene. *J Colloid Interface Sci* (2019) doi:10.1016/j.jcis.2018.09.094.

187. Yang, X. *et al.* Efficient exfoliation to MoS2 nanosheets by salt-assisted refluxing and ultrasonication with photocatalytic application. *Mater Lett* (2019) doi:10.1016/j.matlet.2019.126596.

188. He, K., Zhang, Z. Y. & Zhang, F. S. Synthesis of graphene and recovery of lithium from lithiated graphite of spent Li-ion battery. *Waste Management* (2021) doi:10.1016/j.wasman.2021.01.017.

189. Van Hao, N. *et al.* Facile synthesis of graphene oxide from graphite rods of recycled batteries by solution plasma exfoliation for removing Pb from water. *RSC Adv* (2020) doi:10.1039/d0ra07723b.

190. Lotya, M. *et al.* Liquid phase production of graphene by exfoliation of graphite in surfactant/water solutions. *J Am Chem Soc* (2009) doi:10.1021/ja807449u.

191. Heard, K. W. J. *et al.* Initial Studies Directed toward the Rational Design of Aqueous Graphene Dispersants. *ACS Omega* (2019) doi:10.1021/acsomega.8b03147.

192. Lavin-Lopez, M. P., Valverde, J. L., Sanchez-Silva, L. & Romero, A. Solvent-Based Exfoliation via Sonication of Graphitic Materials for Graphene Manufacture. *Industrial and Engineering Chemistry Research* Preprint at https://doi.org/10.1021/acs.iecr.5b03502 (2016).

193. Tambe, P., Sharma, A., Kulkarni, H. & Panda, B. Surfactant assisted dispersion of graphene in aqueous solution using mixed surfactants. *Mater Today Proc* (2022) doi:10.1016/j.matpr.2021.11.173.

194. Letoffé, A. *et al.* Functionalization and exfoliation of graphite with low temperature pulse plasma in distilled water. *Physical Chemistry Chemical Physics* (2022) doi:10.1039/d1cp04826k.

195. Varrla, E. *et al.* Large-scale production of size-controlled MoS2 nanosheets by shear exfoliation. *Chemistry of Materials* (2015) doi:10.1021/cm5044864.

196. Hu, C. X., Shin, Y., Read, O. & Casiraghi, C. Dispersant-assisted liquid-phase exfoliation of 2D materials beyond graphene. *Nanoscale* Preprint at https://doi.org/10.1039/d0nr05514j (2021).

197. Gupta, D., Chauhan, V. & Kumar, R. A comprehensive review on synthesis and applications of molybdenum disulfide (MoS2) material: Past and recent developments. *Inorganic Chemistry Communications* Preprint at https://doi.org/10.1016/j.inoche.2020.108200 (2020).

198. Roy, S. *et al.* Structure, Properties and Applications of Two-Dimensional Hexagonal Boron Nitride. *Advanced Materials* Preprint at https://doi.org/10.1002/adma.202101589 (2021).

199. Orts Mercadillo, V. *et al.* Electrically Conductive 2D Material Coatings for Flexible and Stretchable Electronics: A Comparative Review of Graphenes and MXenes. *Advanced Functional Materials* Preprint at https://doi.org/10.1002/adfm.202204772 (2022).

200. De-Mello, G. B. *et al.* Surfactant-exfoliated 2D molybdenum disulphide (2D-MoS2): The role of surfactant upon the hydrogen evolution reaction. *RSC Adv* (2017) doi:10.1039/c7ra05085b.

201. Zhu, M. *et al.* High yield and concentration exfoliation of defect-free 2D nanosheets via gentle water freezing-thawing approach and stabilization with PVP. *Mater Res Express* (2019) doi:10.1088/2053-1591/ab2de3.

202. Wang, J., Ma, F. & Sun, M. Graphene, hexagonal boron nitride, and their heterostructures: properties and applications. *RSC Advances* Preprint at https://doi.org/10.1039/c7ra00260b (2017).

203. Yankowitz, M., Xue, J. & Leroy, B. J. Graphene on hexagonal boron nitride. *Journal of Physics Condensed Matter* Preprint at https://doi.org/10.1088/0953-8984/26/30/303201 (2014).

204. Wu, W. *et al.* Thermally conductive composites based on hexagonal boron nitride nanosheets for thermal management: Fundamentals to applications. *Composites Part A: Applied Science and Manufacturing* Preprint at https://doi.org/10.1016/j.compositesa.2023.107533 (2023).

205. Li, Y., Zhang, W., Guo, B. & Datta, D. Interlayer shear of nanomaterials: Graphene–graphene, boron nitride–boron nitride and graphene–boron nitride. *Acta Mechanica Solida Sinica* (2017) doi:10.1016/j.camss.2017.05.002.

206. Shang, J., Xue, F., Fan, C. & Ding, E. Preparation of few layers hexagonal boron nitride nanosheets via high-pressure homogenization. *Mater Lett* (2016) doi:10.1016/j.matlet.2016.05.154.

207. Mukhopadhyay, T. K. & Datta, A. Deciphering the role of solvents in the liquid phase exfoliation of hexagonal boron nitride: A molecular dynamics simulation study. *Journal of Physical Chemistry C* (2017) doi:10.1021/acs.jpcc.6b09446.

208. Songfeng, E., Liu, J., Zhao, R., Ning, D. & Lu, Z. Formation Mechanisms of Hexagonal Boron Nitride Nanosheets in Solvothermal Exfoliation. *Langmuir* (2023) doi:10.1021/acs.langmuir.2c03049.

209. Yang, G., Wang, H., Wang, N., Sun, R. & Wong, C. P. Hydrothermal exfoliation for two-dimension boron nitride nanosheets. in *Proceedings - Electronic Components and Technology Conference* (2018). doi:10.1109/ECTC.2018.00217.

210. Ng, K. L. *et al.* Direct Evidence of the Exfoliation Efficiency and Graphene Dispersibility of Green Solvents toward Sustainable Graphene Production. *ACS Sustain Chem Eng* (2023) doi:10.1021/acssuschemeng.2c03594.

211. *Principles and Techniques of Biochemistry and Molecular Biology*. (Cambridge University Press, 2005). doi:10.1017/CBO9780511813412.

212. *Handbook of Ultrasonics and Sonochemistry*. (Springer Singapore, Singapore, 2016). doi:10.1007/978-981-287-278-4.

213. Gu, X. *et al.* Method of ultrasound-assisted liquid-phase exfoliation to prepare graphene. *Ultrason Sonochem* (2019) doi:10.1016/j.ultsonch.2019.104630.

214. Childs, P. R. N. Vorticity and Rotation. in *Rotating Flow* 53–79 (Elsevier, 2011). doi:10.1016/B978-0-12-382098-3.00003-2.

215. Ferrari, A. & Robertson, J. Interpretation of Raman spectra of disordered and amorphous carbon. *Phys Rev B Condens Matter Mater Phys* (2000) doi:10.1103/PhysRevB.61.14095.

216. Nagyte, V. *et al.* Raman fingerprints of graphene produced by anodic electrochemical exfoliation. *Nano Lett* (2020) doi:10.1021/acs.nanolett.0c00332.

217. Dubale, A. A. *et al.* The synergetic effect of graphene on Cu2O nanowire arrays as a highly efficient hydrogen evolution photocathode in water splitting. *J Mater Chem A Mater* (2014) doi:10.1039/c4ta03464c.

218. King, A. A. K. *et al.* A new raman metric for the characterisation of graphene oxide and its derivatives. *Sci Rep* (2016) doi:10.1038/srep19491.

219. Bracamonte, M. V., Lacconi, G. I., Urreta, S. E. & Foa Torres, L. E. F. On the nature of defects in liquid-phase exfoliated graphene. *Journal of Physical Chemistry C* (2014) doi:10.1021/jp501930a.

220. Eckmann, A. *et al.* Probing the nature of defects in graphene by Raman spectroscopy. *Nano Lett* (2012) doi:10.1021/nl300901a.

221. Cançado, L. G. *et al.* Quantifying defects in graphene via Raman spectroscopy at different excitation energies. *Nano Lett* (2011) doi:10.1021/nl201432g.

222. Urade, A. R., Lahiri, I. & Suresh, K. S. Graphene Properties, Synthesis and Applications: A Review. *JOM* Preprint at https://doi.org/10.1007/s11837-022-05505-8 (2023).

223. Anusuya, T., Pathak, D. K., Kumar, R. & Kumar, V. Deconvolution and quantification of defect types from the first order Raman spectra of graphene oxide derivatives. *FlatChem* (2022) doi:10.1016/j.flatc.2022.100422.

224. Eigler, S., Dotzer, C. & Hirsch, A. Visualization of defect densities in reduced graphene oxide. *Carbon N Y* (2012) doi:10.1016/j.carbon.2012.03.039.

225. Ferrari, A. C. Raman spectroscopy of graphene and graphite: Disorder, electron-phonon coupling, doping and nonadiabatic effects. *Solid State Commun* (2007) doi:10.1016/j.ssc.2007.03.052.

226. Cançado, L. G., Pimenta, M. A., Neves, B. R. A., Dantas, M. S. S. & Jorio, A. Influence of the atomic structure on the Raman spectra of graphite edges. *Phys Rev Lett* (2004) doi:10.1103/PhysRevLett.93.247401.

227. Backes, C. *et al.* Spectroscopic metrics allow in situ measurement of mean size and thickness of liquid-exfoliated few-layer graphene nanosheets. *Nanoscale* (2016) doi:10.1039/c5nr08047a.

228. Cayambe, M. *et al.* Dispersion of graphene in ethanol by sonication. *Mater Today Proc* 37, 4027–4030 (2021).

229. Read, O. *et al.* Insights into the exfoliation mechanism of pyrene-assisted liquid phase exfoliation of graphene from lateral size-thickness characterisation. *Carbon N Y* 186, 550–559 (2022).

230. Ojrzynska, M. *et al.* Study of optical properties of graphene flakes and its derivatives in aqueous solutions. *Opt Express* (2020) doi:10.1364/oe.382523.

231. Yi, M., Shen, Z., Zhang, X. & Ma, S. Achieving concentrated graphene dispersions in water/acetone mixtures by the strategy of tailoring Hansen solubility parameters. *J Phys D Appl Phys* (2013) doi:10.1088/0022-3727/46/2/025301.

232. Stafford, J. *et al.* Real-time monitoring and hydrodynamic scaling of shear exfoliated graphene. *2d Mater* (2021) doi:10.1088/2053-1583/abdf2f.

233. Zhao, S. *et al.* Green and High-Efficiency Production of Graphene by Tannic Acid-Assisted Exfoliation of Graphite in Water. *ACS Sustain Chem Eng* (2018) doi:10.1021/acssuschemeng.8b00497.

234. Tung, T. T. *et al.* Graphene Oxide-Assisted Liquid Phase Exfoliation of Graphite into Graphene for Highly Conductive Film and Electromechanical Sensors. *ACS Appl Mater Interfaces* (2016) doi:10.1021/acsami.6b04872.

235. Lund, S. *et al.* Fast high-shear exfoliation of natural flake graphite with temperature control and high yield. *Carbon N Y* (2021) doi:10.1016/j.carbon.2020.11.094.

236. Kozhemyakina, N. V. *et al.* Effect of the structure and morphology of natural, synthetic and post-processed graphites on their dispersibility and electronic properties. *Fullerenes Nanotubes and Carbon Nanostructures* (2013) doi:10.1080/1536383X.2012.702162.

237. Alzakia, F. I., Sun, W., Pennycook, S. J. & Tan, S. C. Introducing Normalized Centrifugation for a More Accurate Thermodynamic Analysis of Molybdenum Disulfide Dispersions: A Study on Mixed Solvents of Alcohols and Amines with Water. *ACS Appl Mater Interfaces* (2020) doi:10.1021/acsami.9b14510.

238. Xu, Y., Cao, H., Xue, Y., Li, B. & Cai, W. Liquid-phase exfoliation of graphene: An overview on exfoliation media, techniques, and challenges. *Nanomaterials* Preprint at https://doi.org/10.3390/nano8110942 (2018).

239. Backes, C. *et al.* Spectroscopic metrics allow in situ measurement of mean size and thickness of liquid-exfoliated few-layer graphene nanosheets. *Nanoscale* (2016) doi:10.1039/c5nr08047a.

240. Tene, T. *et al.* Optical properties of graphene oxide. *Front Chem* 11, (2023).

241. Uran, S., Alhani, A. & Silva, C. Study of ultraviolet-visible light absorbance of exfoliated graphite forms. *AIP Adv* (2017) doi:10.1063/1.4979607.

242. Wang, M. *et al.* Surface Tension Components Ratio: An Efficient Parameter for Direct Liquid Phase Exfoliation. *ACS Appl Mater Interfaces* (2017) doi:10.1021/acsami.6b16578.

243. Gupta, A., Arunachalam, V. & Vasudevan, S. Liquid-Phase Exfoliation of MoS2 Nanosheets: The Critical Role of Trace Water. *Journal of Physical Chemistry Letters* (2016) doi:10.1021/acs.jpclett.6b02405.

244. Wan, Q., Wang, H., Li, S. & Wang, J. Efficient liquid-phase exfoliation of few-layer graphene in aqueous 1, 1, 3, 3-tetramethylurea solution. *J Colloid Interface Sci* (2018) doi:10.1016/j.jcis.2018.04.110.

245. Yi, M., Shen, Z., Ma, S. & Zhang, X. A mixed-solvent strategy for facile and green preparation of graphene by liquid-phase exfoliation of graphite. *Journal of Nanoparticle Research* (2012) doi:10.1007/s11051-012-1003-5.

246. Uran, S., Alhani, A. & Silva, C. Study of ultraviolet-visible light absorbance of exfoliated graphite forms. *AIP Adv* (2017) doi:10.1063/1.4979607.

247. Yoon, J. C. *et al.* Graphitization with Suppressed Carbon Loss for High-Quality Reduced Graphene Oxide. *ACS Nano* (2021) doi:10.1021/acsnano.1c02178.

248. *CRC Handbook of Chemistry and Physics*. (CRC Press, 2019).

249. Reichardt, C. & Welton, T. *Solvents and Solvent Effects in Organic Chemistry*. (Wiley, 2010). doi:10.1002/9783527632220.

250. Bracamonte, M. V., Lacconi, G. I., Urreta, S. E. & Foa Torres, L. E. F. On the nature of defects in liquid-phase exfoliated graphene. *Journal of Physical Chemistry C* (2014) doi:10.1021/jp501930a.

251. Eckmann, A., Felten, A., Verzhbitskiy, I., Davey, R. & Casiraghi, C. Raman study on defective graphene: Effect of the excitation energy, type, and amount of defects. *Phys Rev B* 88, 035426 (2013).

252. Eckmann, A. *et al.* Probing the nature of defects in graphene by Raman spectroscopy. *Nano Lett* (2012) doi:10.1021/nl300901a.

253. Ferguson, A., Harvey, A., Godwin, I. J., Bergin, S. D. & Coleman, J. N. The dependence of the measured surface energy of graphene on nanosheet size. *2d Mater* 4, 015040 (2016).

254. Kozbial, A. *et al.* Study on the Surface Energy of Graphene by Contact Angle Measurements. *Langmuir* 30, 8598–8606 (2014).

255. Coleman, J. N. *et al.* Two-dimensional nanosheets produced by liquid exfoliation of layered materials. *Science (1979)* (2011) doi:10.1126/science.1194975.

256. Ogilvie, S. P. *et al.* Considerations for spectroscopy of liquid-exfoliated 2D materials: emerging photoluminescence of N-methyl-2-pyrrolidone. *Sci Rep* 7, 16706 (2017).

257. Hansen, C. M. *Hansen Solubility Parameters A User's Handbook. CRC Press* (2013).

258. Salavagione, H. J. *et al.* Identification of high performance solvents for the sustainable processing of graphene. *Green Chemistry* (2017) doi:10.1039/c7gc00112f.

259. Hatazawa, T., Kagami, J. & Kawaguchi, T. Friction torque of cylindrical roller thrust bearings in bingham fluid -comparison of the calculated results with experimental ones-. *Tribology Series* Preprint at https://doi.org/10.1016/s0167-8922(00)80129-7 (2000).

260. George, H. F. & Qureshi, F. Newton's Law of Viscosity, Newtonian and Non-Newtonian Fluids. in *Encyclopedia of Tribology* (2013). doi:10.1007/978-0-387-92897-5_143.

261. Schnerr, G. H. & Sauer, J. Physical and Numerical Modeling of Unsteady Cavitation Dynamics. *4th International Conference on Multiphase Flow* (2001).

262. Wang, W. *et al.* Highly Efficient Production of Graphene by an Ultrasound Coupled with a Shear Mixer in Supercritical CO2. *Ind Eng Chem Res* (2018) doi:10.1021/acs.iecr.8b04113.

263. Backes, C. *et al.* Equipartition of Energy Defines the Size-Thickness Relationship in Liquid-Exfoliated Nanosheets. *ACS Nano* (2019) doi:10.1021/acsnano.9b02234.

264. Ding, J. H., Zhao, H. R. & Yu, H. Bin. A water-based green approach to large-scale production of aqueous compatible graphene nanoplatelets. *Sci Rep* (2018) doi:10.1038/s41598-018-23859-5.

265. Niu, L. *et al.* Production of Two-Dimensional Nanomaterials via Liquid-Based Direct Exfoliation. *Small* (2016) doi:10.1002/smll.201502207.

266. Telkhozhayeva, M. *et al.* Higher Ultrasonic Frequency Liquid Phase Exfoliation Leads to Larger and Monolayer to Few-Layer Flakes of 2D Layered Materials. *Langmuir* (2021) doi:10.1021/acs.langmuir.0c03668.

267. Skaltsas, T., Ke, X., Bittencourt, C. & Tagmatarchis, N. Ultrasonication induces oxygenated species and defects onto exfoliated graphene. *Journal of Physical Chemistry C* (2013) doi:10.1021/jp4057048.

268. Cheng, Q., Debnath, S., Gregan, E. & Byrne, H. J. Ultrasound-Assisted swnts dispersion: Effects of sonication parameters and solvent properties. *Journal of Physical Chemistry C* (2010) doi:10.1021/jp101431h.

269. Yau, H. C., Bayazit, M. K., Steinke, J. H. G. & Shaffer, M. S. P. Sonochemical degradation of N-methylpyrrolidone and its influence on single walled carbon nanotube dispersion. *Chemical Communications* (2015) doi:10.1039/c5cc06526g.

270. Morton, J. A. *et al.* Effect of Temperature and Acoustic Pressure During Ultrasound Liquid-Phase Processing of Graphite in Water. *JOM* (2021) doi:10.1007/s11837-021-04910-9.

271. Fauzi, F., Azizi, F., Musawwa, M. M. & Dwandaru, W. S. B. Synthesis and Characterisations of Reduced Graphene Oxide Prepared by Microwave Irradiation with Sonication. *Journal of Physical Science* (2021) doi:10.21315/jps2021.32.2.1.

272. Morton, J. A. *et al.* An eco-friendly solution for liquid phase exfoliation of graphite under optimised ultrasonication conditions. *Carbon N Y* (2023) doi:10.1016/j.carbon.2022.12.070.

273. Nonomura, Y., Morita, Y., Deguchi, S. & Mukai, S. A. Anomalously stable dispersions of graphite in water/acetone mixtures. *J Colloid Interface Sci* (2010) doi:10.1016/j.jcis.2010.02.029.

274. Kim, J. *et al.* Direct exfoliation and dispersion of two-dimensional materials in pure water via temperature control. *Nat Commun* (2015) doi:10.1038/ncomms9294.

275. Morton, J. A. *et al.* Effect of Temperature and Acoustic Pressure During Ultrasound Liquid-Phase Processing of Graphite in Water. *JOM* (2021) doi:10.1007/s11837-021-04910-9.

276. Lund, S. *et al.* Fast high-shear exfoliation of natural flake graphite with temperature control and high yield. *Carbon N Y* (2021) doi:10.1016/j.carbon.2020.11.094.

277. Gomez, C. V. *et al.* Structural and Electronic Properties of Graphene Oxide for Different Degree of Oxidation1. *Mater Today Proc* 3, 796–802 (2016).

278. Sreeprasad, T. S. & Berry, V. How Do the Electrical Properties of Graphene Change with its Functionalization? *Small* 9, 341–350 (2013).

279. Blume, R. *et al.* Characterizing Graphitic Carbon with X-ray Photoelectron Spectroscopy: A Step-by-Step Approach. *ChemCatChem* 7, 2871–2881 (2015).

280. Theodosiou, A., Spencer, B. F., Counsell, J. & Jones, A. N. An XPS/UPS study of the surface/near-surface bonding in nuclear grade graphites: A comparison of monatomic and cluster depth-profiling techniques. *Appl Surf Sci* 508, 144764 (2020).

281. Kovtun, A. *et al.* Accurate chemical analysis of oxygenated graphene-based materials using X-ray photoelectron spectroscopy. *Carbon N Y* 143, 268–275 (2019).

282. Skaltsas, T., Ke, X., Bittencourt, C. & Tagmatarchis, N. Ultrasonication induces oxygenated species and defects onto exfoliated graphene. *Journal of Physical Chemistry C* (2013) doi:10.1021/jp4057048.

283. Dan, H. *et al.* Mechanism of sonication time on structure and adsorption properties of 3D peanut shell/graphene oxide aerogel. *Science of the Total Environment* (2020) doi:10.1016/j.scitotenv.2020.139983.

284. Lai, Q., Zhu, S., Luo, X., Zou, M. & Huang, S. Ultraviolet-visible spectroscopy of graphene oxides. *AIP Adv* (2012) doi:10.1063/1.4747817.

285. Backes, C. *et al.* Spectroscopic metrics allow in situ measurement of mean size and thickness of liquid-exfoliated few-layer graphene nanosheets. *Nanoscale* (2016) doi:10.1039/c5nr08047a.

286. Gopinath, S. C. B. *et al.* Characterization of reduced graphene oxide obtained from vacuum-assisted low-temperature exfoliated graphite. *Microsystem Technologies* (2018) doi:10.1007/s00542-018-3921-3.

287. Kaniyoor, A. & Ramaprabhu, S. A Raman spectroscopic investigation of graphite oxide derived graphene. *AIP Adv* (2012) doi:10.1063/1.4756995.

288. Dong, L. *et al.* A non-dispersion strategy for large-scale production of ultra-high concentration graphene slurries in water. *Nat Commun* (2018) doi:10.1038/s41467-017-02580-3.

289. Papageorgiou, D. G., Kinloch, I. A. & Young, R. J. Mechanical properties of graphene and graphene-based nanocomposites. *Progress in Materials Science* Preprint at https://doi.org/10.1016/j.pmatsci.2017.07.004 (2017).

290. Khan, U., O’Neill, A., Lotya, M., De, S. & Coleman, J. N. High-concentration solvent exfoliation of graphene. *Small* (2010) doi:10.1002/smll.200902066.

291. Malard, L. M., Pimenta, M. A., Dresselhaus, G. & Dresselhaus, M. S. Raman spectroscopy in graphene. *Physics Reports* Preprint at https://doi.org/10.1016/j.physrep.2009.02.003 (2009).

292. Yoon, D. *et al.* Variations in the Raman spectrum as a function of the number of graphene layers. *Journal of the Korean Physical Society* (2009) doi:10.3938/jkps.55.1299.

293. Shearer, C. J., Slattery, A. D., Stapleton, A. J., Shapter, J. G. & Gibson, C. T. Accurate thickness measurement of graphene. *Nanotechnology* (2016) doi:10.1088/0957-4484/27/12/125704.

294. Lee, H. & Park, J. Y. Height determination of single-layer graphene on mica at controlled humidity using atomic force microscopy. *Review of Scientific Instruments* (2019) doi:10.1063/1.5098483.

295. Vázquez de Parga, A. L. & Miranda, R. Scanning tunneling microscopy (STM) of graphene. in *Graphene: Properties, Preparation, Characterization and Applications, Second Edition* (2021). doi:10.1016/B978-0-08-102848-3.00007-4.

296. Wang, L., Pu, Y., Soh, A. K., Shi, Y. & Liu, S. Layers dependent dielectric properties of two dimensional hexagonal boron nitridenanosheets. *AIP Adv* (2016) doi:10.1063/1.4973566.

297. Juma, I. G., Kim, G., Jariwala, D. & Behura, S. K. Direct growth of hexagonal boron nitride on non-metallic substrates and its heterostructures with graphene. *iScience* 24, 103374 (2021).

298. Wu, Q. *et al.* In situ chemical vapor deposition of graphene and hexagonal boron nitride heterostructures. *Current Applied Physics* 16, 1175–1191 (2016).

299. Wang, J., Ma, F. & Sun, M. Graphene, hexagonal boron nitride, and their heterostructures: properties and applications. *RSC Advances* Preprint at https://doi.org/10.1039/c7ra00260b (2017).

300. Gao, G. *et al.* Artificially Stacked Atomic Layers: Toward New van der Waals Solids. *Nano Lett* 12, 3518–3525 (2012).

301. Gomes, P. V. R. *et al.* Layered graphene/hexagonal boron nitride nanosheets (Gr/h-BNNs) applied to the CO2 photoconversion into methanol. *Appl Mater Today* (2022) doi:10.1016/j.apmt.2022.101605.

302. Güler, Ö., Güler, S. H. & Taşkin, M. The production of graphene-boron nitride nanosheet heterostructures via liquid phase exfoliation assisted by a milling process. *Bulletin of Materials Science* (2019) doi:10.1007/s12034-018-1703-2.

303. Rasul, M. G., Kiziltas, A., Arfaei, B. & Shahbazian-Yassar, R. 2D boron nitride nanosheets for polymer composite materials. *npj 2D Materials and Applications* Preprint at https://doi.org/10.1038/s41699-021-00231-2 (2021).

304. Li, Y., Zhang, W., Guo, B. & Datta, D. Interlayer shear of nanomaterials: Graphene–graphene, boron nitride–boron nitride and graphene–boron nitride. *Acta Mechanica Solida Sinica* (2017) doi:10.1016/j.camss.2017.05.002.

305. Jung, J. H., Park, C. H. & Ihm, J. A Rigorous Method of Calculating Exfoliation Energies from First Principles. *Nano Lett* (2018) doi:10.1021/acs.nanolett.7b04201.

306. Gautam, C. & Chelliah, S. Methods of hexagonal boron nitride exfoliation and its functionalization: Covalent and non-covalent approaches. *RSC Advances* Preprint at https://doi.org/10.1039/d1ra05727h (2021).

307. Mukhopadhyay, T. K. & Datta, A. Deciphering the role of solvents in the liquid phase exfoliation of hexagonal boron nitride: A molecular dynamics simulation study. *Journal of Physical Chemistry C* (2017) doi:10.1021/acs.jpcc.6b09446.

308. Gautam, C. & Chelliah, S. Methods of hexagonal boron nitride exfoliation and its functionalization: Covalent and non-covalent approaches. *RSC Advances* Preprint at https://doi.org/10.1039/d1ra05727h (2021).

309. Ye, H. *et al.* Liquid-Phase Exfoliation of Hexagonal Boron Nitride into Boron Nitride Nanosheets in Common Organic Solvents with Hyperbranched Polyethylene as Stabilizer. *Macromol Chem Phys* (2018) doi:10.1002/macp.201700482.

310. Ali, M. & Abdala, A. Large scale synthesis of hexagonal boron nitride nanosheets and their use in thermally conductive polyethylene nanocomposites. *Int J Energy Res* (2022) doi:10.1002/er.7149.

311. Maestre, C., Toury, B., Steyer, P., Garnier, V. & Journet, C. Hexagonal boron nitride: A review on selfstanding crystals synthesis towards 2D nanosheets. *JPhys Materials* (2021) doi:10.1088/2515-7639/ac2b87.

312. Comini, N., Huthwelker, T., Diulus, J. T., Osterwalder, J. & Novotny, Z. Factors influencing surface carbon contamination in ambient-pressure x-ray photoelectron spectroscopy experiments. *Journal of Vacuum Science & Technology A: Vacuum, Surfaces, and Films* (2021) doi:10.1116/6.0001013.

313. Knochel, P. & Molander, G. A. *Comprehensive Organic Synthesis: Second Edition*. *Comprehensive Organic Synthesis: Second Edition* (2014). doi:10.1016/C2011-1-05331-6.

314. Morton, J. A. *et al.* An eco-friendly solution for liquid phase exfoliation of graphite under optimised ultrasonication conditions. *Carbon N Y* (2023) doi:10.1016/j.carbon.2022.12.070.

315. Khan, A. F., Brownson, D. A. C., Foster, C. W., Smith, G. C. & Banks, C. E. Surfactant exfoliated 2D hexagonal Boron Nitride (2D-hBN) explored as a potential electrochemical sensor for dopamine: Surfactants significantly influence sensor capabilities. *Analyst* (2017) doi:10.1039/c7an00323d.

316. Song, L. *et al.* Large scale growth and characterization of atomic hexagonal boron nitride layers. *Nano Lett* (2010) doi:10.1021/nl1022139.

317. Singh, B. *et al.* Nanostructured Boron Nitride with High Water Dispersibility for Boron Neutron Capture Therapy. *Sci Rep* (2016) doi:10.1038/srep35535.

318. Lee, S. H. *et al.* Improvements in structural and optical properties of wafer-scale hexagonal boron nitride film by post-growth annealing. *Sci Rep* (2019) doi:10.1038/s41598-019-47093-9.

319. Roberts, Z. A., Son, S. F. & Rhoads, J. F. Direct observations of ultrasonically generated hot spots in polymer composite energetic materials. *Combust Flame* (2022) doi:10.1016/j.combustflame.2021.111704.

320. Kumar, K., Srivastav, S. & Sharanagat, V. S. Ultrasound assisted extraction (UAE) of bioactive compounds from fruit and vegetable processing by-products: A review. *Ultrasonics Sonochemistry* Preprint at https://doi.org/10.1016/j.ultsonch.2020.105325 (2021).

321. Kotsidi, M. *et al.* Graphene nanoplatelets and other 2D-materials as protective means against the fading of coloured inks, dyes and paints. *Nanoscale* (2023) doi:10.1039/d2nr05795f.

322. Rivera, M., Velázquez, R., Aldalbahi, A., Zhou, A. F. & Feng, P. High Operating Temperature and Low Power Consumption Boron Nitride Nanosheets Based Broadband UV Photodetector. *Sci Rep* 7, 42973 (2017).

323. Nie, X. *et al.* Co-Solvent Exfoliation of Hexagonal Boron Nitride: Effect of Raw Bulk Boron Nitride Size and Co-Solvent Composition. *Nanomaterials* 10, 1035 (2020).

324. Ling, J. *et al.* Vibrational Imaging and Quantification of Two-Dimensional Hexagonal Boron Nitride with Stimulated Raman Scattering. *ACS Nano* (2019) doi:10.1021/acsnano.9b06337.

325. Cai, Q. *et al.* Raman signature and phonon dispersion of atomically thin boron nitride. *Nanoscale* (2017) doi:10.1039/c6nr09312d.

326. Griffin, A. *et al.* Spectroscopic Size and Thickness Metrics for Liquid-Exfoliated h -BN. *Chemistry of Materials* (2018) doi:10.1021/acs.chemmater.7b05188.

327. Singh, B. *et al.* Nanostructured Boron Nitride with High Water Dispersibility for Boron Neutron Capture Therapy. *Sci Rep* (2016) doi:10.1038/srep35535.

328. Gorbachev, R. V. *et al.* Hunting for monolayer boron nitride: Optical and raman signatures. *Small* (2011) doi:10.1002/smll.201001628.

329. Wang, Q. W., Li, J., Lin, J. Y. & Jiang, H. X. Probing the surface oxidation process in hexagonal boron nitride epilayers. *AIP Adv* (2020) doi:10.1063/1.5134993.

330. Liu, Q. *et al.* Porous Hexagonal Boron Nitride Sheets: Effect of Hydroxyl and Secondary Amino Groups on Photocatalytic Hydrogen Evolution. *ACS Appl Nano Mater* (2018) doi:10.1021/acsanm.8b00867.

331. Bu, T. *et al.* Thickness measurements of graphene oxide flakes using atomic force microscopy: results of an international interlaboratory comparison. *Nanotechnology* (2023) doi:10.1088/1361-6528/acbf58.

332. Shearer, C. J., Slattery, A. D., Stapleton, A. J., Shapter, J. G. & Gibson, C. T. Accurate thickness measurement of graphene. *Nanotechnology* (2016) doi:10.1088/0957-4484/27/12/125704.

333. Crovetto, A. *et al.* Nondestructive Thickness Mapping of Wafer-Scale Hexagonal Boron Nitride Down to a Monolayer. *ACS Appl Mater Interfaces* (2018) doi:10.1021/acsami.8b08609.

334. Crovetto, A. *et al.* Nondestructive Thickness Mapping of Wafer-Scale Hexagonal Boron Nitride Down to a Monolayer. *ACS Appl Mater Interfaces* (2018) doi:10.1021/acsami.8b08609.

335. Zhang, S., Chen, W., Cheng, W., Liang, R. & Xu, J. Thickness identification of 2D hexagonal boron nitride thin flakes by optical imaging in dry transfer method. *Mater Res Express* (2019) doi:10.1088/2053-1591/ab15e4.

336. Rastogi, P. K. *et al.* Graphene-hBN non-van der Waals vertical heterostructures for four- electron oxygen reduction reaction. *Physical Chemistry Chemical Physics* (2019) doi:10.1039/c8cp06155f.

337. Wang, J., Ma, F. & Sun, M. Graphene, hexagonal boron nitride, and their heterostructures: properties and applications. *RSC Advances* Preprint at https://doi.org/10.1039/c7ra00260b (2017).

338. Zheng, X. *et al.* Liquid Phase Exfoliated Hexagonal Boron Nitride/Graphene Heterostructure Based Electrode Toward Asymmetric Supercapacitor Application. *Front Chem* (2019) doi:10.3389/fchem.2019.00544.

339. Güler, Ö., Güler, S. H. & Taşkin, M. The production of graphene-boron nitride nanosheet heterostructures via liquid phase exfoliation assisted by a milling process. *Bulletin of Materials Science* (2019) doi:10.1007/s12034-018-1703-2.

340. Emiru, T. F. & Ayele, D. W. Controlled synthesis, characterization and reduction of graphene oxide: A convenient method for large scale production. *Egyptian Journal of Basic and Applied Sciences* (2017) doi:10.1016/j.ejbas.2016.11.002.

341. Ortiz, W. *et al.* Two-dimensional tungsten disulfide nanosheets and their application in self-powered photodetectors with ultra-high sensitivity and stability. *Vacuum* (2022) doi:10.1016/j.vacuum.2022.111092.

342. Zou, L. R. *et al.* Research progress of optoelectronic devices based on two-dimensional MoS2 materials. *Rare Metals* Preprint at https://doi.org/10.1007/s12598-022-02113-y (2023).

343. Rahman, A., Jennings, J. R., Tan, A. L. & Khan, M. M. Molybdenum Disulfide-Based Nanomaterials for Visible-Light-Induced Photocatalysis. *ACS Omega* Preprint at https://doi.org/10.1021/acsomega.2c01314 (2022).

344. Liu, Y. & Li, R. Study on ultrasound-assisted liquid-phase exfoliation for preparing graphene-like molybdenum disulfide nanosheets. *Ultrason Sonochem* (2020) doi:10.1016/j.ultsonch.2019.104923.

345. Liu, H. *et al.* Production of mono- to few-layer MoS2 nanosheets in isopropanol by a salt-assisted direct liquid-phase exfoliation method. *J Colloid Interface Sci* (2018) doi:10.1016/j.jcis.2018.01.023.

346. Sharma, R. *et al.* A Facile Liquid-Phase, Solvent-Dependent Exfoliation of Large Scale MoS2 Nanosheets and Study of Their Photoconductive Behaviour for UV-Photodetector Application. *ChemistrySelect* (2021) doi:10.1002/slct.202102439.

347. Lukianov, M. Y. *et al.* Photoluminescence of Two-Dimensional MoS2 Nanosheets Produced by Liquid Exfoliation. *Nanomaterials* (2023) doi:10.3390/nano13131982.

348. Sliz, R. *et al.* Suitable Cathode NMP Replacement for Efficient Sustainable Printed Li-Ion Batteries. *ACS Appl Energy Mater* 5, 4047–4058 (2022).

349. Fenech-Salerno, B., Holicky, M., Yao, C., Cass, A. E. G. & Torrisi, F. A sprayed graphene transistor platform for rapid and low-cost chemical sensing. *Nanoscale* (2023) doi:10.1039/d2nr05838c.